The Differential Regulation of Adult Neural Stem Cells by Beclin1 and Atg5

Alena Kalinina

Thesis submitted to the University of Ottawa

in partial fulfillment of the requirements for the

Doctor of Philosophy degree in Cellular and Molecular Medicine

Department of Cellular and Molecular Medicine

Cellular and Molecular Medicine Program

Faculty of Medicine

University of Ottawa

2024

© Alena Kalinina, Ottawa, Canada, 2024

Dedicated to my dear grandparents

Stepanov Vasily Vasilyevich and Romashova Ludmila Nefedovna.

Thank you for the life you gave me.

ABSTRACT

Adult hippocampal neurogenesis is orchestrated by neural stem cell (NSC) activity. Some associations exist between autophagy and neurogenesis, yet much remains unknown about autophagic regulation of adult neurogenesis. This thesis interrogates the requirement and role of Beclin1 and Atg5, two regulators of autophagy, in the formation of adult hippocampal neurons.

To examine adult brain NSCs, the experiments presented in the first objective of this thesis test the ability to isolate adult NSCs using flow cytometry and a DNA-binding dye, DyeCycleViolet. While adult NSCs could not be isolated from the adult neurogenic niches using this methodology, it was effective in isolating endothelial cells. This provided valuable insight on the use of DNA-binding dyes and a new method for isolation of brain endothelial cells.

The next objective determines the role of Beclin1 in adult NSCs and their progeny using an inducible model. Beclin1 loss in Nestin-expressing hippocampal NSCs resulted in reduced proliferation, autophagy, and adult neurogenesis within one month. Single-cell RNA sequencing and other methods illuminated that loss of Beclin1 resulted in mitosis reduction, disrupted mitotic regulation of chromatin maintenance, and induction of DNA damage.

The final objective first tests whether Beclin1 loss results in similar deficits within GLAST-expressing NSCs and progeny. This model mirrored neurogenesis deficits and requirement of Beclin1 in mitosis and DNA maintenance. Next, to test whether this phenotype occurs with other autophagy proteins, Atg5 was removed from GLAST NSCs. This resulted in reduced autophagy and a transient decrease in neurons in the absence of any effect on NSC proliferation. Thus, proliferation deficits are unique to Beclin1 loss and do not underlie reduced adult hippocampal neurogenesis after Atg5 removal. This work demonstrates a novel discovery of mitosis regulation in adult NSCs by Beclin1, and individual roles of Beclin1 and Atg5 in neurogenesis.

TABLE OF CONTENTS

LIST OF FIGURES AND TABLES

Chapter 1

Chapter 2

Chapter 3

LIST OF ABBREVIATIONS

SGZ – subgranular zone

NSCs – neural stem cells

qNSCs – quiescent NSCs

aNSCs – activated NSCs

NPCs – neural progenitor cells

NSPCs – neural stem and progenitor cells

GL – granule layer

ML – molecular layer

IHC - immunohistochemistry

scRNA-seq – single-cell RNA sequensing

SVZ – subventricular zone

GLAST - glutamate aspartate transporter 1

Sox2 - SRY (sex determining region Y)-box 2

GFAP – glial fibrillary acidic protein

AldoC – aldolase C

CD133 – cluster of differentiation 133

CD15 – cluster of differentiation 15

ABC transporter - ATP-binding cassette transporter

prNSCs – primed NSCs

EGFR – endothelial growth factor receptor

Mcm2 – mini-chromosome maintenance complex 2

PCNA – proliferating nuclear cell antigen

EdU - 5-Ethynyl-2′-deoxyuridine

BrdU - 5-bromo-2'-deoxyuridine

Ascl1 - achaete-scute homolog 1

CFP – cyan fluorescent protein

eGFP – enhanced green fluorescent protein

eYFP – enhanced yellow fluorescent protein

Hopx – homeodomain protein X

OXPHOS - oxidative phosphorylation

Sox9 - SRY (sex determining region Y)-box 9

Blbp - brain lipid-binding protein

Notch - neurogenic locus notch homolog protein

CDKs – cyclin-dependent kinases

CKIs – cyclin-dependent kinase inhibitors

ROS – reactive oxygen species

Chk1 – checkpoint kinase 1

Mad2 - mitotic arrest deficient gene 2

Bub1R - budding uninhibited by benzimidazoles 1

Nek - NIMA-related kinases

ɣH2AX - H2A histone family member X phosphorylated ser139

DAPI - 4′,6-diamidino-2-phenylindole

IdU - 5-Iodo-2 -deoxyuridine

CldU - 5-Chloro-2′-deoxyuridine

Fucci2a - Fluorescent Ubiquitination-based Cell Cycle Indicator

DCV - DyeCycleViolet

BDNF - brain-derived neurotrophic factor

FGF2 - fibroblast growth factor 2

IGF1 - insulin-like growth factor 1

VEGF - vascular endothelial growth factor

Wnt - Wingless and Int-1

DG – dentate gyrus

APC – anaphase promoting complex

NFI – nuclear factor I

PI3P/ PtdIns[3]P - phosphatidylinositol 3-phosphate

ULK1 - Unc-51-like kinase 1

FIP200 - focal adhesion kinase family interacting protein of 200 kD

PI3KC3 - class III phosphatidylinositol PI3-kinase complexes 1

Vps34 - vacuolar protein sorting protein 34

Vps15 - vacuolar protein sorting protein 15

Ndp52 - nuclear dot protein 52

Tbk1 - Neighbor of BRCA1 Gene 1 Protein

GABARAP - Gamma-aminobutyric acid receptor-associated protein

LC3 - microtubule-associated proteins light chain 3

BH3 - Bcl-2 homology 3 domain

Bcl-2 - B-cell lymphoma-2 protein

Bcl-xl - B-cell lymphoma-extra large protein

ECD - Evolutionarily Conserved Domain

CCD – coiled-coil domain

UVRAG - UV radiation resistance-associated gene

Bif1 - Bax-interacting factor 1

CamkII - Calcium–calmodulin (CaM)-dependent protein kinase II

Ampk - AMP-activated protein kinase

BARA - β-sheet-α-helix repeats domain

Dapk - Death-associated protein kinase

Hmgb1/2 - high mobility group box 1/2

Pink1 – PTEN induced kinase 1

Rab - Ras-associated binding protein

Nef – negative regulatory factor

Rack1 - Receptor For Activated C Kinase 1

miRNA – micro-RNA

FADD - FAS-associated death domain protein

Sod1 - superoxide dismutase type 1

FoxO3 - Forkhead box O3 protein

CD31 – cluster of differentiation 31

CD45 – cluster of differentiation 45

VP – verapamil

FTC – fumitremorgin C

vWF - vonWillebrand factor

SP – side population

WT – wild-type

DqNSCs – dormant qNSCs

Top2a – topoisomerase 2a

CCE – cell cycle exit

Calb2 – calbindin 2

Dbi - diazepam binding inhibitor

ApoE – apolipoprotein E

SAC – spindle assembly checkpoint

Dynll1 - Dynein Light Chain LC8-Type 1

DCX – doublecortin

NeuN – neuronal nuclear antigen

DEGs- differentially expressed genes

Pclaf - PCNA Clamp Associated Factor

Nptn - neuroplastin

Ttc28 – Tetratricopeptide Repeat Domain 28

MAPT – microtubule associated protein TAU

Atg proteins – autophagy proteins

CHAPTER 1: INTRODUCTION

1. Adult hippocampal neurogenesis.

Adult hippocampal neurogenesis refers to the life-long addition of new functional neurons in the adult mammalian hippocampus, including humans[1–5]. The neurogenic niche of the hippocampus is located at the border of the subgranular zone (SGZ) and the hilus within the dentate gyrus (DG; Figure 1A). It maintains the continuous creation of adult-born neurons via dynamic fate shifts of quiescent neural stem cells (qNSCs) that give rise to activated NSCs (aNSCs)[6].

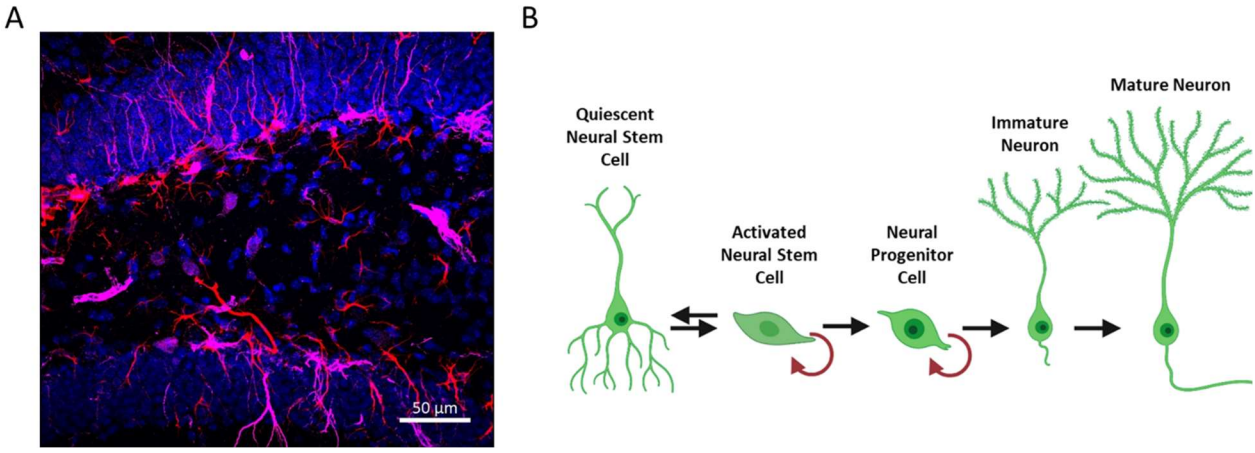

Figure 1. A) The dentate gyrus of the hippocampus labeled with a nuclear cell marker (blue), adult neural stem cells labeled with Nesin (violet) and GFAP (red); B) Graphical representation of adult hippocampal neurogenesis. GL – granule layer, SGZ – subgranular zone layer. The graphical representation in B was created with BioRender.com.

Hippocampal q/aNSCs are complex multipotent stem cells with self-renewal capacity that produce neural progenitor cells (NPCs), immature, and mature neurons (Figure 1B). As these cells transition into different stages, they express unique proteins[8,10] which allow the minutiae of neurogenesis to be studied throughout the whole lineage. These markers have been instrumental in identifying the intrinsic cell-autonomous programs, as well as extrinsic paracrine/juxtracrine signals that govern adult hippocampal neurogenesis[12,14,16,99]. Recent studies have propelled metabolism and autophagy to the forefront of investigations of cell-autonomous processes that have a critical role in adult neurogenesis through regulation of different cell types[19,21,24,28]. The work completed in this thesis, adds to this growing field by determining the role of autophagy

proteins Beclin1 and Atg5 in regulation of adult hippocampal neural stem and progenitor cells (NSPCs) and their progeny.

a. Unique signatures of adult NSCs

For years the research community was puzzled by adult NSCs hypothesizing that that they are a multipotent type of astrocyte. However, more recent advancements in methods beyond use of immunohistochemistry (IHC), such as single-cell RNA sequencing (scRNA-seq), have shown adult NSCs distinct from astrocytes[26]. The adult NSCs are the direct continuation of the stem cells residing locally during embryonic development that over time acquire a highly quiescent state[29,30]. Their multipotency in the adult mouse brain is still contested, however there are several reports of progeny besides neurons, including astrocytes[88] in the SGZ and oligodendrocytes in the subventricular zone (SVZ)[33]. The common proteins used to detect NSCs via *in situ* IHC include glial fibrillary acidic protein (GFAP), glutamate aspartate transporter (GLAST), Nestin, SRY (sex determining region Y)-box 2 (Sox2), and aldolase C (AldoC)[8]. They can also be detected or purified live *ex vivo* by targeting membrane proteins such as cluster of differentiation 133 (CD133)[36,58] or 15 (CD15)[38]. The ability to specifically detect NSCs for imaging or genetic manipulation is extremely valuable in order to help elucidate the functional roles of various proteins and pathways in the process of adult neurogenesis.

b. qNSCs versus aNSCs

NSCs exist on a relative continuum of quiescence that has been described in a lot of detail in the last 7 years owing it largely to scRNA-seq technologies[40,42]. Recent research in NSCs has illuminated cell activities that underlie the process of NSC priming and activation. These are directly reflected in levels of expression or various proteins, such as AldoC[44], GLAST[16,36], and GFAP[58] which are found in qNSCs and primed NSCs (prNSCs) with unlimited self-renewal

capacity. These cells represent the majority of the adult NSC population. On the other hand, Sox2[46] and Nestin[16,99] are expressed in neurogenic cells with a limited self-renewal capacity, which includes some qNSCs, aNSCs, as well as early NPCs. The aNSCs and NPCs can also be identified through their expression of proliferation markers, for example endothelial growth factor receptor (EGFR)[36,38], Ki67[48], mini-chromosome maintenance protein 2 (Mcm2)[50], or proliferating cell nuclear antigen (PCNA)[50]. Similarly these cells can be identified through their ability to incorporate synthetic DNA bases such as 5-Ethynyl-2′-deoxyuridine (EdU)[52] and 5-bromo-2'-deoxyuridine (BrdU)[54] that are interwoven into the cell′s DNA during S phase of the cell cycle. Lastly, proliferating NSCs can be additionally labeled using achaete-scute homolog 1 (Ascl1)[56], as it is mainly restricted to cells undergoing activation with more limited expression in NPCs. Together this research demonstrates the possibility to distinguish aNSCs from qNSCs using a variety of markers, however it remains very difficult to tease aNSCs apart from NPCs.

c. aNSCs versus NPCs

The main issue with not being able to tell aNSCs apart from NPCs is that, at least transcriptionally, when these cells progress far enough in their cell cycle they lose their stemness features and expression of genes that are seen in qNSCs[6,36,59]. This largely owes to many NSC markers being, in fact, related to metabolism during periods of high reliance on glycogenesis instead of oxidative phosphorylation (OXPHOS) etc[6,59]. ScRNA-seq significantly enhanced our ability to separate NSCs from NPCs beginning with a comprehensive examination of NSC transitional states. Using a NestinCFP (cyan fluorescent protein) reporter mouse, research showed a separation between qNSCs, aNSCs and NPCs based on downregulation of AldoC and homeodomain protein X (Hopx) as the NSCs become primed and activated[6]. The NPCs are known to express no quiescence markers, however, they may still express markers like Nestin or Sox2, albeit, they also express

Tbr2 and Eomes that are not expressed by the NSCs[7]. In addition, aNSCs and NPCs show SRY (sex determining region Y)-box 9 (Sox9)[61,63] and neurogenic locus notch homolog protein (Notch)[65,67] expression that fluctuates along the differentiation continuum. Lastly the early and late NPCs have been identified, which differ in expression of neural fate markers such as doublecortin (DCX) and NeuN[6,36,69]. The difficulty in identifying these separate population reflects the dispersed and heterogeneous nature of hippocampal NSCs and NPCs that is difficult to assess, even with such high-resolution analysis as scRNA-seq. This may call for the development of additional methods that can divide the heterogeneous NSCs and NPCs when assessing their transcriptional profiles.

d. Methods to manipulate adult NSPCs *in vivo*, *ex vivo*, and *in vitro*

The first examination of NSCs *in vivo* was limited to postmortem methods in which markers allow for their identification in the dentate gyrus as described above. These genes were then targeted to generate conditional and inducible knockout mouse models[8,10,71]. The most widely used mouse models target the NSCs and/or NPCs and rely on such promoters as GFAP[14], Nestin[99], GLAST[12,16], brain lipid-binding protein (Blbp)[73], or Ascl1[75]. The differences between the targeted populations are based in the fact that the different proteins are expressed at slightly distinct timepoints of a stem cell′s life. For example GFAP is more highly expressed in cells during quiescence, whereas Ascl1 is expressed in an activated and ready-to-proliferate cells[36,42]. In the case of conditional Cre-lox mouse models, when the promoter is first expressed it allows for activation of the Cre enzyme in order to induce a fluorescent tag and/or modify or remove a protein of interest that has been floxed[77]. Since most of these promoters are based on proteins expressed during embryogenesis, manipulation of the cells and their progeny during embryogenesis produces a confound for studies that need to observe effects of different regulators of neurogenesis specifically in adulthood[8,92].

For this reason, the inducible mouse models have become much more popular as they allow for temporal and spatial control of transgenes. Using the Cre-lox system, administration of tamoxifen and fusion of a modified estrogen receptor to Cre allows for recombination in specific cells and their progeny at any point in animal's life by changing the experimental timing[80]. A similar but slightly more limited way of targeting neurogenic cells in the dentate gyrus is through the use of viruses. Viruses have differential tropism for distinct cell types, and certain ones have been shown to only infect NSCs, NPCs, neurons, or some combination of the above[8,82,84]. Specificity of a virus can be further improved either by utilizing tendencies for naturally high affinities for certain cell types (such as retroviruses for proliferating cells), or by engineering them to contain fragments that allow for silencing of fluorescent signal should an unintended cell type be infected[8,82,84].

Identification of adult NSC-type cells in the culture dish first occurred in 1992 with Reynolds and Weiss describing a protocol to isolate and expand the cells directly from the adult mouse brain. The cells were subsequently induced with growth factors, such as fibroblast growth factor (FGF) and epidermal growth factor (EGF)[86], and allowed to grow in an incubator. These cultures form neurospheres form a round structure of expanded cells that can be used to assess proliferation of NSPCs. Additionally the differentiation potential of these cells can be determined through further digestion and treatment with other appropriate factors[89]. The neurosphere assay has been used widely and has become a very vital tool in studying adult hippocampal neurogenesis[89,90,93]. However, care must be taken when interpreting results from this system as its validity is sensitive to cell seeding concentrations, contamination, and other important variables[94] and should be combined with *in vivo* methods.

Flow cytometry is another useful tool to study NSPCs and neurogenesis by utilizing *ex vivo* processing of cells derived directly from brain neurogenic areas or expanded cultures. Generic

markers of the neuronal lineage can be also used in flow cytometry paradigms that involve fixed cells, however, generally preference is given to staining protocols that can be used directly on live cells due to less processing steps and, therefore, larger sample yield. A limitation for the use of flow cytometry is the small number of available membrane markers that can be combined with live cell flow cytometry protocols. For example, only a few membrane markers are available to study live NSPCs *ex vivo* and include a combination of stemness markers like cluster of differentiation 133 (CD133) or cluster of differentiation 15 (CD15) with proliferation markers such as the endothelial growth factor receptor (EGFR)[58,60]. To expand the ability to isolate live cells from the brain, methods are also being borrowed from other areas of biology. Specifically, the use of cell-permeable DNA dyes promised the ability to assess cell cycle and purify the stem cell population on the basis of DNA content, and dye expulsion, respectively. However, to date the use of cell-permeable DNA-binding dyes, such as DyeCycle Violet in the adult brain to study cell cycle resulted in inadequate resolution[60]. In addition to cell cycle analysis, the use of cell permeable dyes has never been tested for isolation of quiescent NSCs, despite being highly utilized in quiescent cancer cells due to their ability to expel dyes via ATP-binding cassette (ABC) transporter membrane channels[97,100,101].

The analyses of cells captured in their *in vivo* and *ex vivo* states have drastically improved over the last 10 years from simple colorimetric flow cytometry to single cell- or nucleus- RNA sequencing. In these paradigms, cells are directly extracted from neurogenic regions, digested, and processed one-by-one to obtain transcriptomes for each individual cell. The methods and work examining the first few dozens of scRNA-seq studies in adult neurogenic niches, including the dentate gyrus, the SVZ, and the thalamus are summarized in my published review appended to this thesis[7]. This

work has largely enriched our understanding of the neurogenic process at the level of transcriptional changes and allowed to easily separate populations of cells never seen before.

Overall, this brief summary highlights the large variety of methods for targeting and manipulation of NSPCs from *in situ* fluorescence methods to scRNA-seq. In addition, many of these methods are continuously refined to achieve the best of each worlds, specifically, the ecological validity of *in vivo* and the rigor of *in vitro* models.

2. Cell cycle dynamics and regulation

The cell cycle is a multifaceted process that drives proliferation and, hence, all multicellular life. It is fairly well conserved across animals and tissues and has been described in detail for many model organisms[103,106,124]. Only some of cell cycle characteristics of adult NSPCs have been described *in vivo* since it remains difficult to study the biochemistry of cell cycle dynamics and individual players directly in the brain. As such, much of the data reported on cell cycle in other models currently only theoretically apply to adult neurogenesis and only a few studies directly assess some mechanisms. For instance, it is known that adult qNSCs are continuously maintaining the G0 phase and rarely enter the cell cycle[108]. It is also known that adult NPCs in the dentate gyrus divide only once every day[110]. The timing of G2[112] and S[114] phase can also vary, with the length of S phase reducing as the cells get close to the differentiation tipping point. Therefore, the G1, S, G2, and M cell cycle phases of adult aNSCs and NPCs range on average from 12 to 25 hours with the S-phase normally lasting around 5 to 12 hours. The process of the cell cycle is regulated by the coordinated activation and inhibition of cyclins A/B/E, cycling-dependent kinases (CDKs), such as CDK1, and cyclin-dependent kinase inhibitors (CKIs), such as p21 (Cdkn1a) or p16 (Cdkn2a) most of which have been manipulated in the adult brain[116,118,120,122]. While cyclin-dependent kinases and kinase inhibitors are somewhat stable and not rate-limiting during cell cycle

progression, the cyclins are reliant on protein synthesis and targeted degradation, including via autophagy-related processes[186].

a. Interphase and S phase

Once primed, NSCs enter interphase 1, or G1 phase, a growth phase that ensures cell's preparedness for chromosome duplication prior to S-phase entry (Figure 2). The G1 phase is important for a cell's decision to commit to cell cycle or withdraw, and is reliant on the dynamics of cyclins and CDKs, as well as extracellular signals[124]. Specifically, at this step, the D-cyclins associate with CDK4 and 6 to inhibit retinoblastoma protein and enhance E2F activity which mediates transition to S phase. In S-phase the DNA of the cell is replicated. This process is accompanied by association of cyclin E and cyclin A with CDK2 to inhibit transcription of genes governed by E2F. Later, cyclin A associates with CDK1 to mediate transition into interphase 2, or G2, the second growth phase which prepares the cell for mitosis.

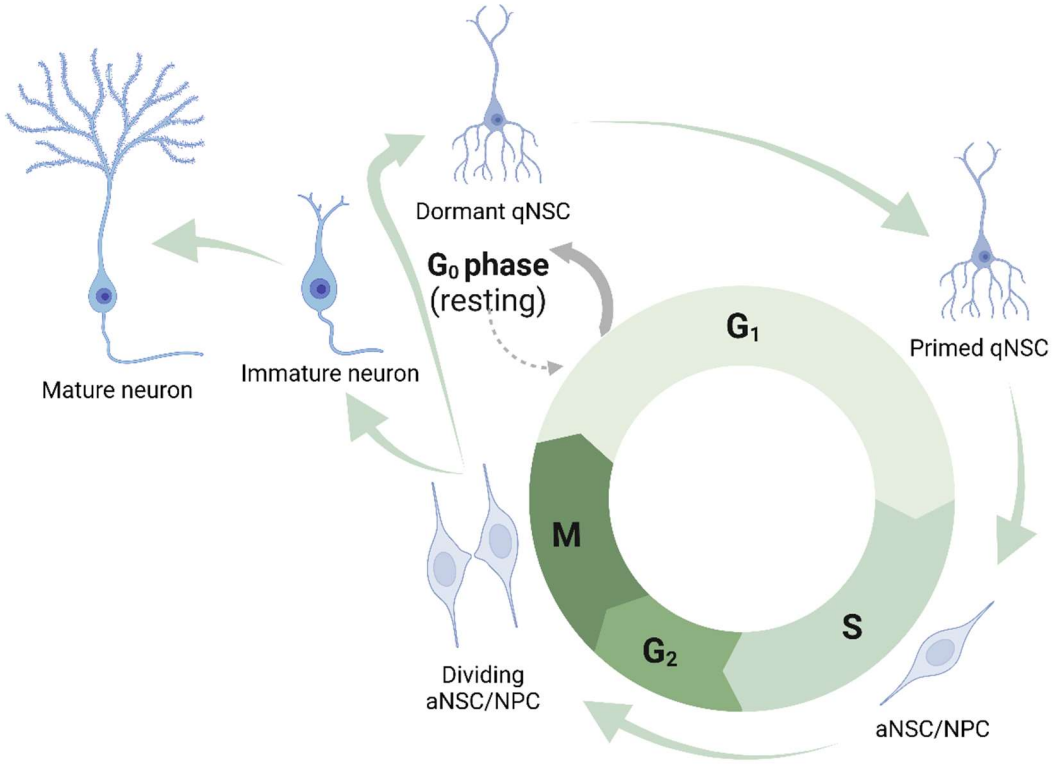

Figure 2. Depiction of hippocampal neurogenic cells passing through cell cycle stages. The graphical representation was created with BioRender.com.

b. M phase

The M phase commences once cyclin B binds to CDK1 to form the mitosis promoting factor and restructure the cell in preparation for cytokinesis[106,124]. The full mitotic process consists of multiple stages: prophase, prometaphase, metaphase, anaphase, telophase, and cytokinesis. In prophase, the centrioles separate and nuclear membrane begins dissolving[106,124]. In prometaphase, centrioles align at the opposite poles and the nuclear lamina is dispersed, while in metaphase the chromosomes attached to spindle fibers align on the metaphase plate. This is followed by anaphase in which the two sister chromatids are separated and pulled to the opposite poles. The nuclear membrane is regenerated in telophase around the separated chromosomes. Lastly, in cytokinesis a midbody ring pinches the double-nucleated cell along the metaphase plate forming two cells[125].

Once the cells divide and exit mitosis cyclin B is targeted for degradation, and they either enter G1 phase or prepare to complete the cell cycle again[110]. It is also possible for cells to undergo multiple consequent mitoses instead of repeating the cell cycle. The time before aNSCs and NPCs differentiate is one of the critical periods of adult neurogenesis representing a bottleneck that kills most of the proliferating population through apoptotic signaling[127]. Given the natural pro-apoptotic tendencies of aNSCs and NPCs exiting the cell cycle, quality checks are in place to help the NSPCs survive.

c. Cell cycle quality control and what happens when things go awry

The cells that commit to cell cycle have a natural ability to quality control various parameters necessary for its successful completion[106,124]. In order to do this, cells activate specific molecular cascades that result in suspension of cyclin activity and entry into a checkpoint, or a pause state,

until the underlying issue can be resolved[103]. If the abnormality is too great, it may be immediately lethal or can cause changes to cell cycle progression and cell fate. Checkpoint activity can also be lost if certain protein deficiencies are present, such as inactive p21 and loss of G1 checkpoint[129], aiding to cycling abnormalities and passage of unfavorable characteristics to daughter cells[49,131,133]. The types of abnormalities that can be passed down to daughter cells within both defective interphase and M phase are discussed below. Notable is that these phenomena have not been investigated within the context of NSCs/NPCs and remain to be studied in the future.

In interphase G1 and G2, cell rounding and size quality checkpoints can be observed slowing the cell cycle progression until any issues are resolved. Accordingly, the proposed sensors of this are ribosomal mass and translational activity, as well as cell geometry[103]. DNA damage responses are easily triggered during cell cycle progression due to the importance of inheriting undamaged and unmutated copies of DNA. Chromosomal damage can be detected at any point in interphase, which arrests the cell cycle and triggers a checkpoint until resolved. DNA damage response can result from metabolic challenges and toxic metabolites (e.g., reactive oxygen species (ROS), telomeric instability, overexpression of oncogenes, or DNA replication/synthesis errors[103]. During cell cycle the DNA damage response cascade is governed either by p53 or checkpoint kinase 1 (Chk1) directing DNA repair, apoptosis, and other cell decisions[136,138].

During M phase, deficient cells can become arrested and unresolved damage can either result in mitotic catastrophe and cell death or mitotic slippage and passage of dysfunctional traits such as aneuploidy[133,140,142]. However, the cell has only a limited amount of quality control in place during M phase and there are a variety of errors that can occur. For instance, cells undergo a mitotic spindle checkpoint that is orchestrated by mitotic arrest deficient gene 2 (Mad2) protein and budding uninhibited by benzimidazoles protein 1 (Bub1R)[142]. However, errors can occur if the

spindles aren't attached to kinetochores or attached to wrong sites (merotelic attachments, no tension) which results in the halting of mitosis and prevention of anaphase entry. Spindle defects can however be corrected under the activity of Polo, Aurora, and NIMA-related kinase (Nek)[103,144,146]. Mitotic deficiencies can also be caused by midbody ring remnants, inappropriate mitochondrial content, unresolved replicative stress, and other factors[49,72,125]. If found, DNA damage is not repaired during mitosis and does not trigger any checkpoints, and can either be tagged for subsequent repair or trigger cellular senescence or cell death[49]. In addition, DNA damage can be directly caused by mitotic deficiencies such as prometaphase arrest resulting in H2A histone family member X ser139 phosphorylated (ɣH2AX) foci[49,133,138,149]. The cells can also fail during anaphase, telophase or cytokinesis if lagging chromosomes are produced due to unresolved merotelic attachment of the kinetochore and the microtubules, which ultimately results in DNA damage[49,151]. The cells that failed prophase or metaphase progression do exit mitosis and enter G1 phase unless they die. This type of mitotic slippage results in further DNA damage accumulation[49]. In the case of a failed chromosome segregation, cells may not always show DNA damage and rather demonstrate micronuclei and aneuploidy, which in turn do give rise to de novo DNA damage[49,153]. It is not surprising that the negative DNA damage loop is sustained during and after S-phase or mitotic aberrations: the same machinery that directs DNA synthesis during S phase and maintains the genome during mitosis and cytokinesis is needed for repair and continued DNA health[138,155].

d. Limitation in analysis of cell cycle in adult NSPCs *in vivo*

One of the reasons less is known about the regulation of cell cycle phases and the dynamic processes that occur in adult NSPCs is that the methods of assessing the cell cycle *in situ* or *ex vivo* suspensions remain a nearly insurmountable challenge within the field. Indeed, only a few *in*

situ/ex vivo methods have been developed where cells from mouse dentate gyrus can be directly analyzed in terms of cell cycle position.

The best current method to analyze cell cycle position in *ex vivo* cells is by treating the mice with EdU and later staining the fixed DG cell suspension with an EdU cocktail and a DNA-binding dye like 4′,6-diamidino-2-phenylindole (DAPI)[157]. EdU is preferable to BrdU, as it doesn't require additional processing steps and is gentler on cells than other types of synthetic DNA base stains which necessitate DNA denaturation[159]. Although other fluorescence-based protocol has been developed to parse NSCs and NPCs into different cell cycle stages, there utility has been very limited. For example, one method utilizes multiple injections with synthetic DNA bases like BrdU, EdU, 5-Iodo-2 -deoxyuridine (IdU), or 5-Chloro-2′-deoxyuridine (CldU) at various times to determine cell cycle stages based on timing of the chemical introduced and the phenotype of its incorporation into chromatin[57]. This method, unsurprisingly, relies on access to relatively powerful microscopy which has likely limited its use[162]. Similarly, one of these synthetic DNA bases can be used to track proliferating cells and followed by fixation for flow cytometry in combination with a DNA-binding dye which would allow to visualize cells in S and M phases[157,164,166,168]. This protocol (also known as horseshoe analysis) has been used to a limited extent in the field of adult neurogenesis[166]. With some modification, it is possible to use the horseshoe analysis in combination with antibodies to phenotype the cycling cells to a limited extent. Cell-permeable DNA dyes can also be used separately to study the cell cycle of live cells, however, have been only been used to a limited extent in *ex vivo* adult SVZ cells[60]. The development of the Fluorescent Ubiquitination-based Cell Cycle Indicator (Fucci2a) mice that have a fluorescent reporter for cell cycle position which can be combined with most fluorescence-relevant protocols raised a lot of hope to provide a novel method to visualize cell cycle dynamics[170]. However, the use of these mice

is limited likely due to the time required for mouse breeding and requirement of high-resolution single cell imaging. In other fields of study, scRNA-seq has improved the ability to separate cells, however, no studies have shown the ability to isolate the proliferating neurogenic cells by cell cycle stages through analyzing their unique dynamics. Thus, this remains to be a challenge for the field to either develop these methodologies further or create methods that could allow for cells to be analyzed in different stages of their cell cycle easily.

3. The complex landscape of neurogenic regulation.

The cell cycle is one aspect of intrinsic regulation of neurogenesis, however, there is growing appreciation for others. The intrinsic, or cell-autonomous, regulators of neurogenesis can be defined as those produced directly by the cell for regulating its own activity. In contrast extrinsic regulators include paracrine or juxtracrine signals, or any other chemical or event that reliably governs their behavior. Both types of regulators are paramount in the life of adult neuronal cells.

a. Cell-extrinsic regulation of neurogenesis

The specialized microenvironment of the hippocampal neurogenic niche provides a variety of extrinsic signals for the maintenance of qNSCs and aNSCs in order to modulate rates of neurogenesis according to the organism′s biological and cognitive demands[172]. This microenvironment encapsulates functional vasculature, as well as neighboring endothelial cells, microglia, astrocytes, and neurons. NSCs have a great ability to sense local signals due to their physical contact with blood vessels, synapses, as well as astrocytes[174,176,178]. This physical contact is possible due to paracrine and juxtracrine exchange of information in the form of growth factors, morphogens, hormones, and neurotransmitters[67,83,172,180]. Accordingly, the cues released to NSCs and NPCs modulate their quiescence, activation, and proliferation, highlighting their importance in state shifts. A few well known paracrine molecules that affect NSC and NPC behaviors include

brain-derived neurotrophic factor (BDNF), fibroblast growth factor 2 (FGF2), insulin-like growth factor 1 (IGF1), and vascular endothelial growth factor (VEGF)[172]. Other important players determining neurogenesis and neuronal morphogenesis include: 1) bone morphogenic factors released by adult granule cells and NSCs[183]; 2) Notch, released by NSCs to communicate with astrocytes[79]; 3) Wingless and Int-1 (Wnt) proteins released by astrocytes and granule neurons[187], and; 4) sonic hedgehog derived from mossy cells in the hilus[188]. These players highlight the dynamic range of signals that modulate the within-niche communications between NSCs, NPCs, and neurons to self-regulate rates of neurogenesis. Additionally, they show that the signals are necessary to regulate quiescence, activation and proliferation of NSCs through Notch, Wnt, and many others[190] which come from local astrocytes to a large extent. These factors and contact with non-neuronal cell populations add to the complexity and challenge of studying adult hippocampal neurogenesis *in vivo* and *in vitro*.

b. Cell-autonomous regulation of neurogenesis

Beyond extrinsic regulators there are hundreds of other molecules that help maintain quiescence of NSCs, cell cycle entry, and differentiation of NPCs into neurons. This includes different cell pathways and processes that aid in direct regulation of cell dynamics. Some recently discovered intrinsic regulators or embryonic and postnatal neurogenesis in the SVZ and DG involve metabolic pathways, such as mitochondrial respiration which has been shown to affect NSC proliferation and also determine differentiation outcomes of progeny[21,192,194]. Similarly, the proteasome can intrinsically regulate proliferation of embryonic NSCs and ultimately neurogenesis by changing the availability of different cyclins during the cell cycle, with anaphase-promoting complex (APC) pushing cells into anaphase[196], a notion that remains to be explored in adult neurogenic niches. Other pathways are known to particularly enhance neural fate choices by regulating a myriad of

genes relevant for cell's differentiation, such as the nuclear factor I (NFI) family of transcription factors, that modulate aNSC and NPC activity at mitotic exit with pro-neuronal tendencies[198,200]. Lastly, some autophagy proteins, but not others, have been shown very important for the process of neurogenesis and neuron survival[24,27,39]. Together these findings only begin to encapsulate the complex picture of neurogenesis regulation inside the cytosol of neurogenic cells.

4. Autophagy proteins and their role in neurogenesis.

It is very clear that metabolism determines a lot of behaviors of adult NSCs and NPCs. Indeed, the number of studies examining metabolism-related anabolic processes such as mitochondrial respiration, glycolysis, function of the proteasome, and fatty acid synthesis has become high in the recent years[21,36,40]. It is no surprise, since these various pathways are often found failing heavily in neurodegenerative diseases and are of paramount interest to the research community[204,206,208]. Another metabolic process that has been shyly studied by several labs over the course of a few decades is autophagy, a large network of proteins working together to keep away debris and provide substrates for the cell's life[19,206,210,212]. In this thesis, the roles of Beclin1 and Atg5 autophagy proteins in adult hippocampal neurogenesis will be evaluated and discussed.

a. The autophagy machinery

The autophagy pathway was described fairly recently, and in 2016 this discovery left Yoshinori Ohsumi with a Nobel Prize in Medicine[213]. This important process is responsible for collection, destruction and recycling of various cellular products such as misfolded/damaged proteins, organelles, and can be involved in intensive cell restructuring during proliferation and differentiation[144,186,206,212]. The types of canonical autophagy include macroautophagy, microautophagy, and chaperone-mediated autophagy[177]. Non-canonical autophagy pathways include LC3-associated phagocytosis; Beclin1-independent autophagy; autophagosomes forming

from multiple phagophores and pathogen-specific modification; autophagy-associated unconventional protein secretion; and defective ribosomal products-containing autophagosome-rich blebs, most of which are yet to be examined in the naive adult brain[177,214]. For the purposes of this work, macroautophagy will hereafter be referred to as autophagy.

The process of autophagy has multiple stages as shown in Figure 3. It begins with a signal, such as presence of cell stressor like nutrient deprivation, hypoxia or other changes to metabolism and has been described in detail elsewhere[215]. These changes result in the initiation of the formation of phagosome double membranes at the endoplasmic reticulum using phosphatidylinositol 3-phosphate (PI3P) as a substrate. This process is governed by the Unc-51-like kinase 1 (ULK1) complex consisting of ULK1/2, Atg13, focal adhesion kinase family interacting protein of 200 kD (FIP200), and Atg101, and the PI3KC3 complex 1 (class III phosphatidylinositol (PI)3-kinase complex 1) that contains vacuolar protein sorting proteins 15 and 34 (Vps15 and Vps34), Atg14L, and Beclin1. Beclin1 is a scaffold of PI3KC3 complex 1 and controls its lipid kinase activity. Throughout the formation of the phagophore, cargo destined for the autophagy pathway is transported to the site of phagophore expansion, commonly via ubiquitin, sequestosome 1 (p62), optineurin, parkin, nuclear dot protein 52 (Ndp52), TANK-binding kinase 1 (Tbk1), Neighbor of BRCA1 gene 1 protein (Nbr1), gamma-aminobutyric acid receptor-associated proteins (GABARAPs) or other autophagy adaptors[216]. The continuous expansion of the phagophore is governed by the Atg12 conjugation system that contains Atg12, Atg10, Atg5, Atg7, Atg16, and Atg5 and involves cleavage and lipidation of microtubule-associated proteins light-chain 3 (LC3)-I. Lastly, the Atg8 conjugation system that comprises Atg3, Atg7, and Atg4 and lipidated LC3-II (LC3-II) proteins mediate the closure and maturation of the autophagosome. Once the autophagosome is mature, it fuses with lysosomes to create a highly acidic autolysosome which

degrades and releases its contents. The released contents can be used to replenish the cells substrates for various functions and repair or participate in the exocytic pathway by releasing the contents into extracellular environment. Since this thesis examines the role of Beclin1 and Atg5 in adult neurogenesis, both proteins are specifically reviewed below.

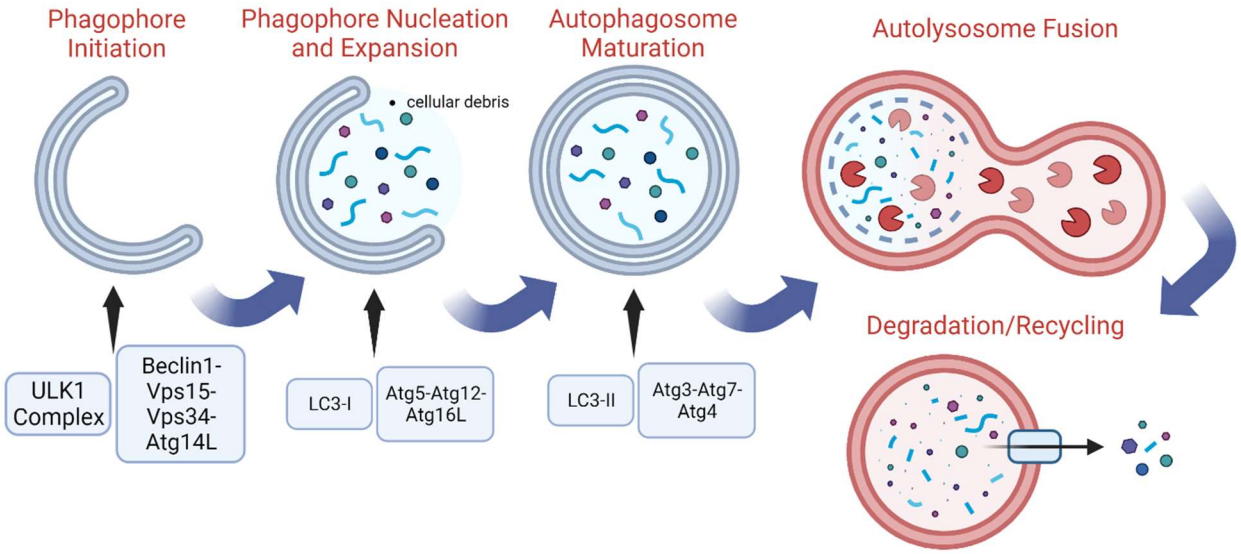

Figure 3. A graphical representation of the stages of autophagy and key autophagic machinery. The graphical representation was created with BioRender.com.

b. Beclin1

Beclin1 is one, if not the most, interesting autophagy protein. This gene and its products are regulated at the epigenetic, transcriptional, post-transcriptional, and post-translational mechanisms allowing for rapid manipulation of its levels in the cytoplasm[217]. Beclin1 is often bound to cell death regulator B-cell lymphoma-2 (Bcl2) protein and B-cell lymphoma-extra large (Bcl-xl) protein via its Bcl-2 homology 3 (BH3) domain, putting the autophagy pathway at the interplay of cell adaptation and death[218]. Beclin1 also contains the evolutionarily conserved domain (ECD) which enables phospatidylinositol-3 kinase class III (PtdIns3KC3, i.e., Vps34) binding, and the coiled-coil (CCD) domain which is used to bind Beclin1 into large homo-oligomers. The oligomerization process is necessary for downstream recruitment of the Atgs as well as allows for

partnerships with proteins like UV radiation resistance-associated gene (UVRAG) protein, Rubicon, and Bax-interacting factor 1 (Bif1)[76,218]. The N-terminal domain binds Calcium–calmodulin (CaM)-dependent protein kinase II (CamkII), AMP-activated protein kinase (Ampk), and Ulk1. The β-sheet-α-helix repeats (BARA) domain interacts with Akt1, EGFR, and Ampk[218]. Interestingly, many more binding partners have been described for Beclin1 without a determined binding site, including death-associated protein kinase 1 (Dapk), high mobility group box 1 (Hmgb1), Survivin, PTEN induced kinase 1 (Pink1), Ras-associated binding protein (Rab), negative regulatory factor (Nef), and other regulators of membrane trafficking, cell death, and proliferation[205,218,219].

The main role of Beclin1 is in the regulation of the key component of the phagophore, PtdIns[3]P lipid molecules by recruiting PI3KC3-dependent processes. This makes Beclin1′s functional implication for cell′s life dramatic. Phosphoinositides such as PI3P are paramount for the functioning of the cell as a part of various cellular membranes and allowing for intracellular communication via effector proteins where they modulate cell adaptation, stress, DNA damage, apoptosis, senescence, and metabolism cascades[220–222]. Multiple complexes have been described that contain Beclin1 and regulate these lipids, including PI3KC complex 1 discussed above. In contrast to the PI3KC complex 1 which begins the process of autophagy, there is complex 2, which includes UVRAG instead of Atg14L[76]. This complex is involved in the initiation of the endosome pathway which shares a lot of homology with the autophagy pathway and is difficult to parse from the effects of Beclin1-dependent autophagy without direct manipulation of Beclin1 domains or specific binding partners.

Other than Beclin1′s autophagy functions, Beclin1 is also involved in endocytic trafficking and exo/phagocytosis which also rely on its lipid kinase regulator activity[35,223,224]. In addition, Beclin1

can localize to kinetochores during proliferation[225] and to DNA at sites of DNA damage[226–228]. Recently Beclin1 was also described as a part of a complex containing Vps15, UVRAG, Vps34, and Bif1 that aids the cell in cytokinesis[229] via endocytic mechanisms. This is worthy of mentioning since this complex may be particularly relevant in dividing NSPCs participating in adult hippocampal neurogenesis. In summary, although Beclin1 participates in many different cellular events, they are all linked with the same need for active membrane restructuring or trafficking of membrane components and rely on Beclin1′s lipid kinase activity[17], while the binding partners determine specific cellular localization and particular function.

c. Atg5

While autophagy persists in some cases of Beclin1 loss[218], the Atg5 protein has been shown indispensable during canonical autophagy[230]. Atg5 protein is part of the core Atg12 conjugation machinery, and its ubiquitin-like conjugation activity is what drives phagophore membrane elongation and maturation[20,231]. In complex with Atg12, Atg5 also facilitates the fusion of the autophagosome with the lysosome in the final steps of autophagy[177]. When *Atg5* is knocked out it almost always results in a complete inhibition of autophagic vesicle formation[232], making it a common target for autophagy removal. The Atg5 protein has Ubiquitin-A and -B ubiquitin-binding domains, however, little else is known about this protein due to difficulty of isolation and processing[233,234]. A binding partner of the Atg5 protein, Receptor for Activated C Kinase 1 (Rack1), has been described as an autophagy initiator in stressful conditions and its deletion leads to a reduction in the autophagy pathway activity[233]. Together these studies highlight the importance of Atg5 in several processes.

The Atg5 protein is similarly promiscuous to Beclin1 and also has many functions that lie outside of the autophagy pathway[20,177]. Calplain1[20] and microRNA miR181a[235] have been shown to

directly affect the activity of the autophagy pathway by binding to Atg5. Atg5 or Atg5 calplain-cleaved fragments have been shown to bind FAS-associated death domain protein (FADD), Bcl-2 and Bcl-xl apoptosis-related proteins[20], a process that was also observed with Beclin1 and drives pro-apoptotic signaling upon cleavage of the autophagy proteins into fragments[236,237]. Atg5 has other roles in cell apoptosis via regulation of cytochrome C, caspase 8, and cathepsin B/K secretion[175]. The most explored autophagy-independent role of Atg5 in the cell is in innate immunity via pathogen presentation[238–240]. Others include adipogenesis[241] and interferon signaling[242]. Therefore, while Beclin1 exerts its function via promoting lipid kinase activity, Atg5 mostly affects the various processes described above via its ubiquitin-like activity. As a consequence, outside of autophagy, both proteins are heavily involved in mechanisms underlying cell adaptation, cell-to-cell signaling via extracellular release of components, and antigen/receptor presentation[175,230].

d. The functional roles of autophagy

Differential roles of autophagy have been described at lengths in many cell types, tissues, and some animal models. It is widely accepted that autophagy prevents premature aging and lack of autophagy has been related to damaged organelles and protein aggregates accumulating inside cells in different models[40,177,206,215,243,244]. As such, the main role of autophagy is removal and recycling of materials inside the cell such that the damaged cell components don't cause issues and the cell is also constantly provided with energy substrates. However, the roles of autophagy are deeper than simply cell clearance and recycling[175,177,189]. Indeed, the roles of autophagy in specific contexts and cell processes remain contested or, at best, unclear.

Some of the more controversial roles of autophagy lie within hypothesized roles for autophagy in regulation of the cell cycle, particularly in mitosis and genome maintenance. Specifically, novel

findings are emerging that autophagy aids substantially in chromosome segregation via the interaction with the cohesin complex[189]. The mitochondrial content and localization are important during mitosis and are maintained via sufficient rates of mitophagy such that the most competent and healthy mitochondria are passed down to progeny[189,245]. In addition, autophagy directly mediates mitosis progression via doryphagy that targets centriolar satellites for degradation as well as indirectly by controlling the presence of lysosomes that mediate telomere dynamics during mitosis[189,246]. Cell rounding and spindle orientation are also indirectly supported by the autophagic process. The above notions are supported largely by autophagy protein deletion studies *in vitro*, which resulted in spindle and centrosome defects, inhibition of doryphagy, chromosomal segregation and instability resulting in DNA damage, as well as accumulation of midbody remnants[189,227,247]. As such, autophagic machinery may also be important for DNA damage repair. As mentioned earlier in this introduction, autophagy indirectly supports DNA health by mediating a healthy cell cycle and preventing metabolic stressors and aneuploidy[189,248]. It also indirectly supports DNA repair via the degradation of ribosomes and mRNA and increasing nucleotide substrates[177]. DNA damage is also recognized by the autophagic machinery which is followed by DNA repair induction[199]. Lastly, the DNA damage response activates autophagy through Ampk signaling[249], however, autophagic activation in response to DNA damage has also been related to senescence-like phenotypes[250]. In sum, the autophagy pathway is involved in a number of processes that guide many aspects of the cell's life.

5. Examination of autophagy protein removal in neurogenesis.

In the field of neurogenesis, the role of different autophagy proteins has been tested mainly in the context of embryonic and early postnatal neurogenesis as reviewed briefly below and in more detail by our lab and others[19,212]. Although inducible models have been developed to modify

autophagy during adult neurogenesis, the functional role of autophagy and specific mechanisms by which the autophagic machinery modifies adult neurogenesis remain elusive. This is likely due to the plethora of non-autophagic functions of autophagy proteins as described above. Additionally, there is likely a differential reliance on autophagic processes based on cell type and cellular context in which they are tested. Thus, examining the role of autophagy in neurogenesis creates a challenging endeavor when teasing apart roles of the various autophagy proteins in the process of neurogenesis which involves multiple cell types drastically different from one another in potency, state, and fate.

a. Role of autophagy during embryonic neurogenesis

It is well known that some autophagy proteins are necessary for proper embryogenesis and neonatal development in naïve conditions as shown by homozygous knockouts of Atg7[251], Atg12[252], and Atg16L[253] which result in neonatal death. Similarly, full knockout of Atg5 in mice results in neonatal death as it is important in the regulation of neonatal starvation[22]. On the other hand, full knockout of Beclin1 in mice proves lethal in the embryo[18], suggesting that there are no mechanisms or proteins to compensate for Beclin1′s loss. These studies highlight heterogeneity as the hallmark of autophagy-deficient phenotypes where very different results may be seen based on autophagy protein in question as well as the context in which autophagy is being manipulated. Moreover, these findings created a need for conditional autophagy-specific knockout models to specifically test the required for different autophagic proteins in neurogenesis.

Four publications using cell-specific (conditional) embryonic knockouts of different autophagic proteins from GFAP-expressing NSCs and their progeny have proposed autophagic proteins are essential regulators of adult neurogenesis. The first report described the conditional ablation of FIP200 from GFAP+ NSCs and their subsequent progeny at embryonic day 10.5[28]. FIP200 is a

component of the autophagy initiation complex and is required for the induction of phagophore formation[254]. Removal of FIP200-depdendent autophagy resulted in fewer NSCs, NPCs, immature, and mature neurons in the SVZ/olfactory bulb and the dentate gyrus when assessed up to 4 weeks postnatally. Subsequently in 2016, this research group demonstrated that the FIP200-mediated decrease in neurogenesis was unique to the GFAP-FIP200 model, since knockout of either Atg16L or Atg7, which are required for autophagosome elongation, did not impact adult neurogenesis[255]. In contrast to the other models, FIP200-null GFAP-positive NSCs and progeny accumulated p62, aberrant mitochondria, decreased superoxide dismutase type 1 (Sod1) levels, and increased ROS, highlighting the importance of autophagy-dependent cellular homeostasis in hippocampal neurogenesis. Additionally, the Guan laboratory began examining autophagy-dependent and autophagy-independent effects of autophagy protein loss. FIP200-dependent NSC maintenance and p62 accumulation were due to non-canonical autophagy-independent functions of FIP200 which were required cell-autonomously[256]. On the other hand, the differentiation of NPCs was dependent on non-cell-autonomous roles of FIP200 in microglia[32]. Importantly, these findings illustrated the variability of unique phenotypes produced by deletions of autophagic proteins from hippocampal NSCs and that the cumulative effect of autophagy protein loss can be attributed to both autophagy-dependent and -independent mechanisms.

b. Adult models of autophagy protein deletion

To clarify the role of autophagy in adult hippocampal neurogenesis, four studies have investigated phenotypes that arise from deletions of autophagic and autophagy-related proteins in adult NSCs and NPCs. In 2016 our lab first published using a retroviral approach to ablate Atg5 in NPCs, and showed that removal of Atg5-dependent autophagy decreased neurogenesis by inhibiting the maturation and survival of immature DCX-expressing neurons[24]. In 2018, Schäffner et al. used

inducible methods to remove the autophagy-related protein Forkhead box O3 (FoxO3) from GLAST-expressing NSPCs and reported that this interfered with synaptic development of neurons and reduced their long-term survival in an autophagy-dependent manner[39]. Specifically, FoxO3 exerted direct transcriptional control on the autophagy network which then regulated protein degradation in NSPCs[257]. Also in 2018, Jung et al used an inducible model of Atg7 deletion from adult hippocampal Nestin-expressing NSPCs and progeny and observed that Atg7 was not required for hippocampal neurogenesis in naïve conditions, but was required for Atg7-dependent autophagic death during exposure to chronic emotional stress[27]. In contrast, most recently in 2023, Atg7 was removed from embryonic and postnatal Nestin-expressing NSPCs and their progeny, which resulted in severe changes to dentate gyrus morphogenesis via mechanisms related to quiescence and protein aggregate accumulation[258]. Thus, together these studies suggest that autophagy has an effect on adult hippocampal neurogenesis that is dependent on the type of autophagy protein, the neurogenic cell type, and the animal′s experience. These findings therefore also highlight the need for work to continue to elucidate the role of different members of the autophagy pathway within the complex architecture of adult neurogenesis.

6. Hypotheses

The primary goal of this PhD project is to determine the roles of Beclin1 and Atg5 in adult hippocampal neurogenesis. The main hypotheses of these studies are: 1) Beclin1 and Atg5 loss results in decreased neurogenesis; 2) Beclin1 and Atg5 regulate neurogenesis via distinct mechanisms. This dissertation consists of three data chapters:

Chapter 2 is a published article (Kalinina et al., 2021) tested the hypothesis that DNA-binding dyes can provide a method for isolation of live adult NSC in the dentate gyrus and subventricular zone.

Chapter 3 is a submitted manuscript (Kalinina et al., 2024) testing the hypothesis that Beclin1 is required for adult hippocampal neurogenesis.

Chapter 4 is being prepared for submission and is testing the hypothesis that Beclin1 and Atg5 have similar roles in the regulation of adult neurogenesis.

CHAPTER 2:

Isolation of the side population from neurogenic niches enriches for endothelial cells

Published Manuscript

PlosOne

Contributions of co-authors

Kalinina A. performed all *in vivo* (unless stated otherwise), *in vitro* and *ex vivo* experiments, managed experimental design, analysis and interpretation of data and writing of the manuscript

Gnyra C. performed initial titration experiments

Xue Y. maintained animal breeding and housing

Tang V. assisted with design of flow cytometry experiments

Lagace D.C. Contributed to the design, analysis, interpretation of results and writing of the manuscript

Isolation of the side population from neurogenic niches enriches for endothelial cells

Alena Kalinina[1], Catherine Gnyra[1], Vera Tang[2], Yingben Xue[1], and Diane Lagace[1]*

1. Department of Cellular and Molecular Medicine, Neuroscience Program, Ottawa Hospital Research Institute, Brain and Mind Research Institute, University of Ottawa, Ottawa, Canada
2. University of Ottawa Flow Cytometry and Virometry Core Facility, Ottawa, Ontario, Canada.

*Corresponding author

E-mail: diane.lagace@uottawa.ca

Abstract

In stem cell research, DNA-binding dyes offer the ability to purify live stem cells using flow cytometry as they form a low-fluorescence side population due to the activity of ABC transporters. Adult neural stem cells exist within the lateral ventricle and dentate gyrus of the adult brain yet the ability of DNA-binding dyes to identify these adult stem cells as side populations remains untested. The following experiments utilize the efflux of a DNA-binding dye, Vyrbant DyeCycle Violet (DCV), to isolate *bona fide* side populations in the mouse dentate gyrus and subventricular zone (SVZ), and test their sensitivity to ABC transporter inhibitors. A distinct side population was found in both the adult lateral ventricle and dentate gyrus using DCV fluorescence and forward scatter instead of the conventional dual fluorescence approach. These side populations responded strongly to inhibition with the ABC transporter antagonists, verapamil and fumitremorgin C. The majority of the cells residing in the side populations of dentate gyrus and SVZ were characterized by their expression of CD31. Additionally, at least 90% of all CD31+ cells found in the dentate gyrus and SVZ were negative for the hematopoietic marker CD45, leading to the hypothesis that the CD31+ cells in the side population were endothelial. These findings, therefore, suggest that the side population analysis provides an efficient method to purify CD31-expressing endothelial cells, but not adult neural stem cells.

Keywords: neurogenesis; DNA dyes; side population; dentate gyrus; subventricular zone; ABC transporter inhibitors; adult neural stem cells; endothelial cells

Introduction

DNA-binding dyes have been perpetually used in flow cytometry and fluorescence-activated cell-sorting (FACS) paradigms to identify cancer stem cells (1,2). This has included the use of dyes such as Hoechst 33342 (3,4) and, more recently, Vybrant DyeCycleViolet (DCV), which is less toxic to stem cells (8–10). In these assays, live stem cells are identified as a side population that has low dual fluorescence intensity in both blue- and red-shifted spectra due to the activity of ABC transporters, which can efflux the DNA-binding dyes. In contrast, cells that do not have ABC transporters will accumulate the dye and show higher fluorescence. Since ABC transporters have been identified in stem cells from a large variety of tissues (8), this method has extended to be used routinely to isolate various types of stem cells.

Neural stem cells (NSCs) within the subventricular zone (SVZ) of the lateral ventricle and the subgranular zone of the dentate gyrus can develop into functional mature neurons in the adult brain. There is interest in harvesting cells from these regions in order to understand how NSCs and their progeny contribute to brain function in health and disease and could be harnessed for cell-based brain repair (9,10). The isolation of neural stem cells (NSCs) has been a challenge in the field due to many reasons. These include the relatively small numbers of NSCs, the multiple subtypes of NSCs, and lack of a highly specific surface marker for identification and isolation by FACS (9,11). Classically, flow cytometry paradigms utilized low expression of PNA (peanut agglutinin) and HAS (heat stable antigen), or high expression of Notch, LewisX (cluster of differentiation-15, CD15) and EGFR (early growth response factor) surface markers to identify neural stem cells (12–15). More recent methods have made additional significant advances in identification and enrichment of subpopulations of NSCs using multi-parameter FACS, inducible transgenic mice models (13), or single-cell transcriptional analyses (16–19). However, these

methodologies are time- and cost-intensive, which has led our lab and others to investigate the use of DNA-binding dyes as a simpler and more efficient method for identification and purification of NSCs

Many have identified an ABC transporter-dependent side population with an NSC identity in cells isolated from neurospheres that were derived from primary embryonic neural or postnatal/adult SVZ tissue (3,12,20). In contrast, NSCs isolated *ex vivo* in cells freshly harvested from embryonic or early postnatal SVZ (postnatal day 2) brain tissue are not found in the side population (3,12,20). Instead of NSCs, endothelial and microglial cells were comprising the side population identified in *ex vivo* preparations of developing SVZ (3). This finding is not surprising as, endothelial and microglial cells along with pericytes and astrocytes, form and maintain the blood brain barrier (21–23). Accordingly, one of the main roles of endothelial cells is in brain homeostasis, which relies on the function of the ABC transporters (23).

This raises the question of whether NSC-containing side populations can be identified from *ex vivo* primary adult mouse dentate gyrus and SVZ tissue. To answer this question, we optimized the detection and phenotyping of the side population using flow cytometry and the DNA-binding dye, DCV, in live single-cell suspensions from the young adult mouse dentate gyrus and SVZ. The data shows that an ABCG2/B1-dependent side population can be identified in the neurogenic niches that is enriched for CD31-expressing endothelial cells but not NSCs.

Materials and Methods

Animals

This study was carried out in strict accordance with the recommendations in the Guidelines of the Canadian Council on Animal Care and all efforts were made to minimize suffering. The animal care protocol was approval by the University of Ottawa Animal Care Committee (Protocol CMM-1150). Fifty six male and female two to three months old C57bl/6J background mice were used for all experiments. Animals were group housed in standard laboratory cages and kept on a 12-hour night/day cycle with *ad libitum* access to food and water.

Tissue collection and digestion

Mice were deeply anesthetized with euthanyl (90 mg/kg) and the brains were quickly placed in ice-cold artificial cerebrospinal fluid (aCSF, pH = 7.4) prepared in miliQ water with 124mM NaCl, 5mM KCl, 1.3 mM MgCl2·6H2O, 2mM CaCl2·2H2O, 26mM NaHCO3, and 1X penicillin-streptomycin (10,000 U/mL; ThermoFisher) and sterilized using stericup and steritop filtration set (Millipore). Dentate gyrus and SVZ were microdissected using SteREO Discovery V8 microscope (Zeiss) following previously published protocols (24,25).

Tissue was digested according to protocols described previously (26,27). First, the tissue was gently broken up using small surgical scissors then incubated on shaker (30 minutes, 37ºC) in 500uL of digestion media, containing 20 U/mL papain (Worthington Biochemicals), 12 mM EDTA (Invitrogen) in DMEM:F12 (Invitrogen). Following incubation, Resuspension media (0.05 mg/mL DNase1 (Roche) with 10% fetal bovine serum (Wisent Bioproducts) in DMEM:F12) was added to each tube, triturated 10X with a P1000 micropipette, and incubated for five minutes at RT. Suspension was then transferred in Percoll media, consisting of 19.8% Percoll (GE Healthcare Life Sciences), 2.2% 10X PBS (Wisent Bioproducts) in Resuspension media. Cells were then spun

down (500 x g, 13 minutes, 4ºC), the supernatant was removed. For each experiment, cells from multiple mice were pooled into one dentate gyrus sample and one SVZ sample, and were resuspended in phenol-free DMEM:F12. Live cells were counted on Countess automated cell counter (ThermoFisher Scientific) using 0.4% Trypan blue (Invitrogen) at a concentration of 1:2 and suspended in phenol-free DMEM:F12 medium at a concentration of 10^6/mL.

Staining and drug treatments

To generate negative, single-stained, and all-stained samples, an average of eight mice was used per experiment. After splitting cells based on staining conditions, Vybrant DyeCycle Violet Ready Flow™ Reagent (Invitrogen) was added to cells in phenol-free DMEM:F12 medium and incubated at 37ºC in a 5% CO2 cell culture chamber (Forma Series II Water Jacket; ThermoFisher Scientific) for 30 minutes. The concentration of DCV was tested at both 1X and 2X, and based on these experiments (Fig S1), all future experiments used the concentration of 2X, or 160uL in 10^6 cells/ml. For experiments involving ABC transporter inhibition, fumitremorgin C (FTC; Sigma) and (±) verapamil hydrochloride (VP; Sigma) were added to unwashed cells at final concentrations of 10uM and 50uM, respectively, after DCV incubation and kept in the same conditions for additional 30 minutes. Cells were then kept on ice in dark until sort, and 7-Amino-Actinomycin D (7AAD, 40 ug/ml, Sigma) was added to cell suspensions 10 minutes before analysis for dead cell discrimination. For experiments determining the identity of the side population, CD31 antibody conjugated to allophycocyanin (APC), BD Biosciences, BioLegend), was added to cells in DMEM:F12 at final concentration of 1:50 (28) and incubated on ice in the dark for 30 minutes before DCV incubation, which followed the same workflow as discussed above. For supplementary experiment, CD45 antibody conjugated to fluorescein isothiocyanate (FITC) was

co-incubated together with APC anti-CD31 on ice at a concentration of 1:500 for 30 minutes. Antibodies, dyes, and drugs used for all experiments are listed in Table 1.

Table 1. Reagents used for tissue processing and DCV assay.

Reagents	Company	Catalogue #	Final Concentration
Vybrant DyeCycle Violet Ready Flow™ Reagent	Invitrogen	R37172	160 uL/ml
APC anti-mouse CD31	BioLegend	102409	1:50
FITC anti-mouse CD45	BioLegend	147709	1:500
7AAD	Sigma	A9400-1MG	1 ug/ml
Fumitremorgin C	Sigma	F9054-250UG	10uM
(+/-) Verapamil Hydrochloride	Sigma	V4629-1G	50uM
Papain suspension	Cedarlane	LS003126	20 U/ml
Percoll	Sigma	17-0891-02	22% v/v
Trypan Blue	Invitrogen	T10282	1:1 (0.2%)

Cell lines

Two cancer cell lines, U-2OS (ATCC, osteosarcoma) and A2780 S (17, ovarian cancer), were generously provided by Dr. Laura Trickle-Mulcahy and Dr. Barbara Vanderhyden, respectively. Cells were grown in DMEM/10%FBS until minimum 75% confluency was reached. Cells were detached from flasks in 5mM EDTA for 20 minutes at 37ºC in a cell culture incubator, then triturated and washed several times with 1X PBS before cell count and DCV staining, which followed the same procedure as staining in primary brain cells.

Flow cytometry

All flow cytometry experiments were performed using BD LSRFortessa^{TM} flow cytometer (BD Biosciences) in the Flow Cytometry and Virometry Core at the University of Ottawa, Faculty of Medicine. Unstained and single-stained controls were used to set up laser parameters and gating for all-stained samples. First, cell debris and doublets were excluded based on FSC and SSC parameters, and then 7AAD+ dead cells were removed from analyses. Following this, all samples

were collected under 405nm laser with 450/50 and 660/20 bandpass filters. DCV+ populations could only be resolved with optimal excitation of the samples (Fig S1). 7AAD signal was collected under the 561nm laser with a 670/30 filter. APC-CD31 fluorescence was collected using the 640nm laser with a 660/20 bandpass filter without compensation. FITC-CD45 signal was collected using the 488 laser with a 530-30 bandpass filter without compensation. Single-stained controls were used to identify and gate CD31+ and CD31- cells. The side population fidelity of DCV+ cells was determined by comparison to FTC- and VP-treated samples. The number of live single cells analyzed in all-stained samples averaged 160±20k live single cells for all experiments. The full entirety of the samples was not run in the experiments since it is reported that at least 25k live single cells is an optimal number for this analysis, thus, other experimenters may be able to collect more live single cells from the same number of mice that is reported in this study.

Data analysis

FlowJo software (BD Biosciences) and GraphPad Prism 8 (GraphPad Software) were used to analyze and visualize all flow cytometry data. All average values are reported as mean ± standard error. All relevant data are within the manuscript and its Supporting files.

Results

Primary cells isolated from the dentate gyrus and SVZ contain multiple populations with side population properties

We used the Vybrant DyeCycle Violet Ready Flow Reagent™ (Invitrogen) to test the presence of a side population that was able to efflux the DNA-dye. Primary live cells harvested from the dissected neurogenic regions of the dentate gyrus and SVZ showed heterogeneous populations of DCV-stained cells as demonstrated by variable DNA content (Fig 1A and 1B). In both the dentate gyrus and SVZ populations there was a large population of cells with low DCV fluorescence that

appeared in the lower left corner of dual fluorescence DCV-Blue/DCV-Red plots (Fig 1A and 1B). These cells in the lower corner resembled effluxing cells, which were absent in the negative control U2OS cell line (Fig 1C) that has been previously reported to not contain a side population (30,31). In the cell suspensions from the dentate gyrus and SVZ it was difficult to distinguish the side population from the continuous main population using the red and blue dual fluorescence of DCV. Therefore, a forward scatter parameter (cell size) was added for the remainder of our analyses to observe the cell heterogeneity together with DCV fluorescence (Fig 1D-F). The size/DCV-Blue plots of dentate and SVZ cells reveal multiple low-fluorescence cell populations that appeared to be effluxing DCV, which we labeled as the tentative side population (Fig 1D and 1E). As expected the DCV-stained live U2OS control cells showed no low-fluorescence cell populations (Fig 1F), highlighting the lack of side population in this culture system.

Side populations in primary dentate gyrus and SVZ are responsive to ABC transporter inhibition

To further identify the side population of the adult neural cells, fumitremorgin C (FTC) and verapamil (VP) were used to inhibit the activity of ABCG2 and ABCB1 transporters, which are known to prevent the efflux of DCV (6,32). Primary dentate gyrus cells located in the labeled tentative SP area in the size-DCV-blue plot, showed a population of cells that was reduced from 3.39% to 0.37% after addition of ABC-transporter antagonists (Fig 2A, 2D). Similarly, primary SVZ cells located in the tentative SP area responded to the inhibitor treatment with a reduction of the population from 0.71% to 0.22% after treatment (Fig 2B, 2E). To confirm specificity of ABC transporter inhibitors, the A2780 S cell line was used as a positive control for VP- and FTC-sensitive side population cells (2,7,33). As predicted, A2780 S cells had a very distinct side

population in standard dual-fluorescence plots that was reduced from 7.97% to 1.51% after treatment (Fig 2C, 2F).

Examination of all performed experiments revealed that the size of dentate gyrus and SVZ side populations was reproducible between experimental days. Specifically, the average size of the dentate gyrus side population from 5 experiments was 3.82±0.26% of all live singlets, with 4050±1099 SP cells analyzed per sample. Similarly, the average size of the SVZ side population from 3 experiments was SVZ of 1.48±0.47% of all live singlets and contained 3328±1817 live single cells per sample. Overall, these data suggest that primary dentate gyrus and SVZ cells contain a reproducible population of cells that possesses side population properties and effluxes DNA-binding dyes via ABC transporters, and that can be clearly visualized through measuring cell size together with the fluorescence of the DNA-binding dye.

The dentate gyrus and SVZ side populations comprise CD31+ endothelial cells

We hypothesized that the side population may have endothelial cell identity, as have been previously identified in *ex vivo* early postnatal SVZ cells (3). This hypothesis was tested using the surface marker for endothelial cells, cluster of differentiation 31 (CD31) to identify them among the dentate gyrus cell types. As shown in Fig3, CD31 expressing (CD31+) endothelial cells represented 5.96% of all cells in the dissected adult dentate gyrus (Fig 3C) and 3.07% of all cells in the dissected adult SVZ (Fig 3F). Analysis of three experiments revealed that CD31+ cells in the dentate gyrus averaged 6.35±0.37% of all live singlets and comprised 13197±2141 live single cells per sample. CD31+ cells from the SVZ were on average 3.93± 0.58% of all live singlets, and contained 6738± 974 live single cells per sample. All other cells, including the adult neural stem cells, were labeled as CD31-negative (CD31-) main population. CD31- cells from the dentate gyrus did not contain the majority of side population, as shown by the size-DCV-Blue plot (Fig

3B). On the contrary, CD31+ cells were heterogeneous in size and DNA content but mostly exhibited a homogenous low DCV fluorescence (Fig 3E). In fact, 75.48% of SP cells in the dentate were CD31+ cells (Fig 3D). Similarly, for the SVZ, CD31- cells from the SVZ did not contain the majority of side population cells (Fig 3C), while CD31+ cells occupied this area (Fig 3F) and represented 52.65% of the side population (Fig 3G).

Since CD31 is also a marker of hematopoietic cells, we examined whether CD31+ cells co-expressed CD45, a ubiquitous cell antigen expressed on the surface of hematopoietic cells, including monocytes (34,35), and which has been used in flow cytometry together with CD31 to exclude blood cells (28,36). We found that CD45+ cells accounted for 4.80% of all live cells from the dentate gyrus (Fig S2 B), and 6.43% in the SVZ (Fig S 2E). The distribution of CD45+ cells among the CD31+ cells represented a small fraction of all CD31+ cells. Specifically, 5.54% of CD31+ cells in dentate gyrus were positive for CD45 (S2 C Fig), and 9.87% in SVZ (S2 F Fig). Thus, the fairly small overlap in CD31 and CD45 markers suggests that the vast majority of the CD31-expressing DCV-effluxing cells in the side populations of the SVZ and DG are endothelial cells rather than blood cells.

Discussion

This series of experiments was used to examine whether a side population can be identified in primary cells of the dentate gyrus and SVZ using DCV, a live-cell-permeable DNA-binding dye, in flow cytometry. We identified a side population that effluxes DCV that was best visualized through measuring cell size together with the fluorescence of the DNA-binding dye. These cells represent the *bona fide* side population that responds to the inhibition with ABC transporter antagonists, verapamil and fumitremorgin C. In both the dentate gyrus and SVZ cells, the side population of the neurogenic regions is enriched with CD31-expressing endothelial cells.

CD31-expressing endothelial cells are enriched within the side population of ex vivo neurogenic extracts

Our data support that within the young adult dentate gyrus and SVZ, CD31+ cells are the major cell cluster in the side population that responded to ABC transporter inhibition. Approximately 75% of dentate gyrus SP cells and 53% of SVZ SP cells were positive for CD31. More than 90% of all CD31+ cells found in the dentate gyrus and SVZ were negative for the hematopoietic marker CD45, leading us to hypothesize that these CD31+ cells are endothelial cells, and not CD31+ hematopoietic cells.

Additional support for our interpretation that the CD31+ cells are endothelial, comes from converging lines of indirect evidence from different studies. For example, data from single-cell RNA sequencing studies show few to no blood cells in *ex vivo* samples collected from naive adult dentate gyrus and SVZ tissue (19,37,38). Primary adult cerebral endothelial cells show high ABC transporter protein levels (39), and single-cell RNA sequencing datasets from the human and mouse brain demonstrate that endothelial cells strongly express ABC transporter mRNA (40,41). Lastly, the results of Mouthon et al. (3) show that the side population of early postnatal SVZ

identified by Hoechst 33342 contains a majority of cells that express the endothelial cell marker CD31 and vonWillebrand factor (vWF), and do not contain NSC markers (e.g., CD133) or the pan-hematopoietic marker CD45. Together these data strongly suggest that the side population from the SVZ and dentate gyrus identified by DCV fluorescence and cell size are likely to be endothelial cells, and future studies could extend this finding when performing more extensive downstream cell analysis.

Requirements for optimization of side population assay

This study also showed that optimization of some parameters is required for accurate side population analysis. The optimization of the DCV dilution (Fig. S1) was done in order to avoid use of low or excess concentrations of DNA-binding dyes that can lead to the false identification of low-fluorescence cells as belonging to the side population (32), as non-effluxing cells in side and main populations are often continuous. Ensuring proper excitation with optimal voltage parameters for primary brain cells (S Fig. 1C, F) is also important to capture full heterogeneity of their DNA content. In addition, the usefulness of the relative cell size parameter (FSC) cannot be understated when locating very small side populations, such as those in the dentate gyrus and SVZ. The incorporation of the ABC transporter inhibitors further allows for more precise, higher resolution identification of the *bona fide* side population. This is demonstrated by the strong evidence of efflux within the side populations of dentate gyrus and SVZ cells, with 89% and 69% cells inhibited by verapamil and fumitremorgin C, respectively, which may be due to the fact that our inhibitions do not include the ABCC family of transporters. Overall, our findings show that the dentate gyrus and SVZ side populations were reproducible and modest in size and responded to verapamil and fumitremorgin C treatment but could only be identified while gating on DNA content together with relative cell size.

Using SP assay to detect NSCs

The CD31+ cells represented a fairly small population of total live single cells in the dentate gyrus and SVZ, however, most of the cells within the side population area were positive for CD31. A small fraction of around 25% of dentate gyrus and 48% SVZ side population cells did not express CD31. We hypothesize that these CD31- cells are not NSCs but may be microglial cells, as previously reported in the side populations of SVZ (3), which remains to be confirmed in future work. Moreover, even if these cells are NSCs, given the majority of cells are CD31+ endothelial cells, our data shows that the side population assay would not be efficient for the isolation of NSCs. This is in direct contrast to the efficiency of the side population assay to detect NSCs from cultured embryonic and adult cells from the SVZ niche (3,12). Such discrepancies may point to biological differences in cultured and uncultured neurogenic cell niches, which has been suggested to be due to hypoxic conditions of neurosphere cultures (3,12). Independent of the cause of these differences, our findings and the work of others support that the identification of NSCs is limited to NSCs cultured *in vitro*. Additionally, we conclude that the use of DCV and analysis of the side population from *ex vivo* cell preparations from the neurogenic regions of the adult brain provides an inexpensive method to study effluxing perivascular cells.

Acknowledgements

We would like to thank all members of the Lagace lab for continued valued. We thank Vera A. Tang, the operations manager of the uOttawa Flow Cytometry and Virometry Core Facility for critical feedback and assistance with data collection.

Figures and figure legends

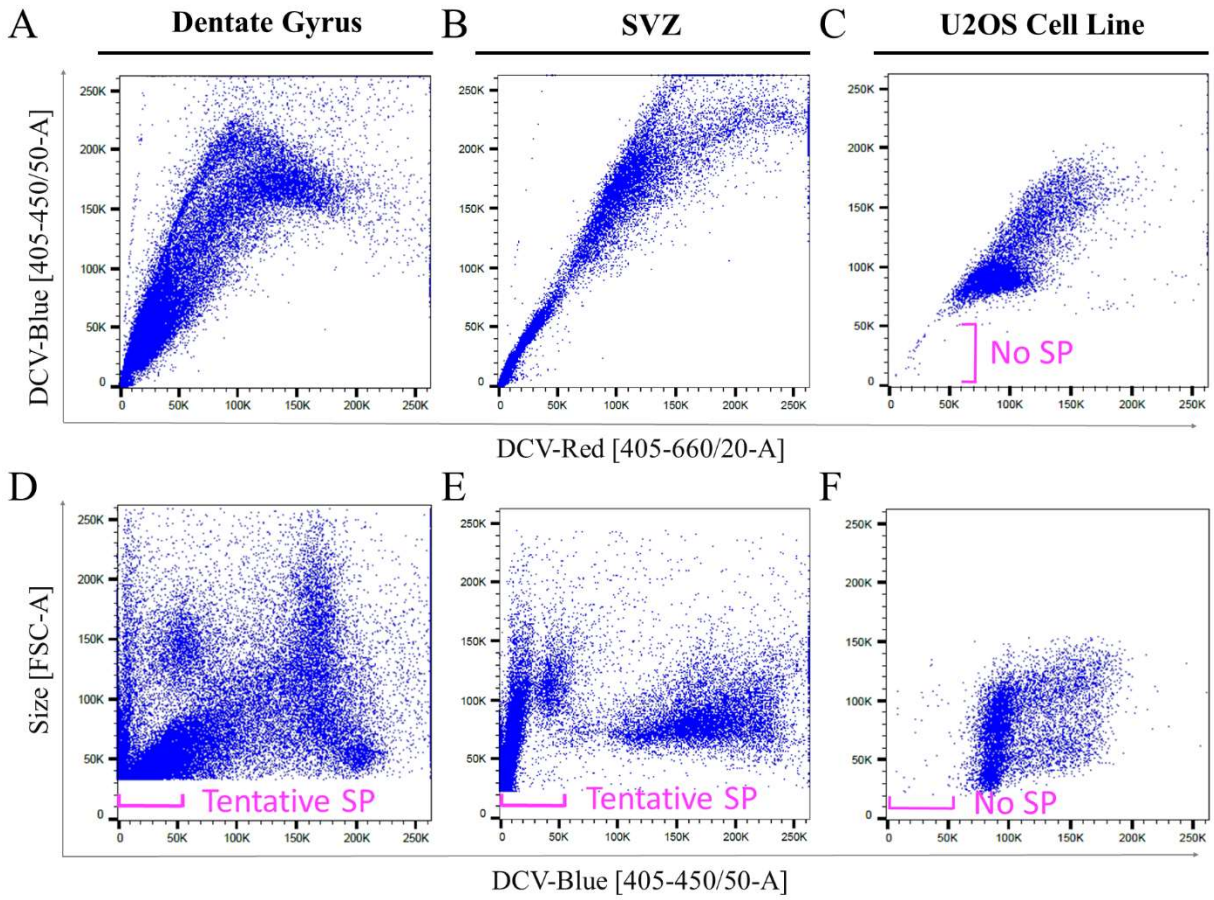

Fig 1. DCV identifies heterogeneous cell populations in primary neurogenic brain cells. Cell heterogeneity is illustrated in dual fluorescence DCV-Red vs DCV-Blue plots with adult cells isolated from the dentate gyrus (A), SVZ (B), as well as control cultured U2OS cells (C) that do not have a side population. Forward scatter (size) and DCV-Blue combined plots for dentate gyrus (D) and SVZ (E) show multiple low-fluorescence populations that could be bona fide side populations (labeled as Tentative SP), whereas, U2OS cells (F) show a few scattered cells that are debris and nuclear fragments. Plots A and D are representative plots based on samples pooled from two male and ten female mice. Plots B and E representative plots based on samples pooled from two male and seven female mice.

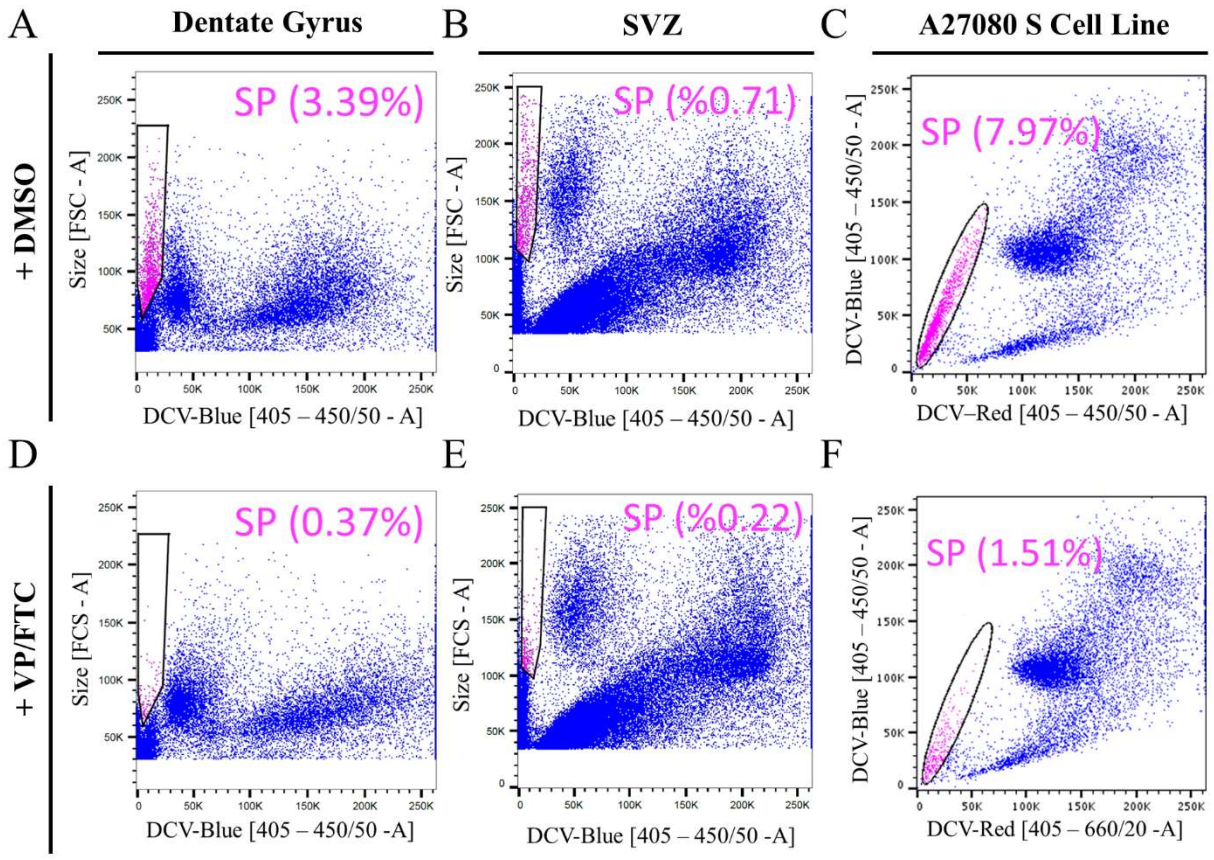

Fig 2. ABC transporter antagonists (VP and FTC) inhibit the side population phenotype of primary adult dentate gyrus and SVZ cells. Fluorescence/size plots for dentate gyrus (A) and SVZ (B) show the side population (SP, pink) and percentage of cells in the SP in the absence (A, B) and presence of VP and FTC (D, E) which significantly reduced the side population. A2780 S cell line, a positive control, shows a large side population in dual fluorescence plots (C) and nearly complete removal (F) of the effluxing side population by addition of inhibitors. Plots A and D were based on samples pooled from five male and three female mice. Plots B and E are based on samples pooled from six female mice.

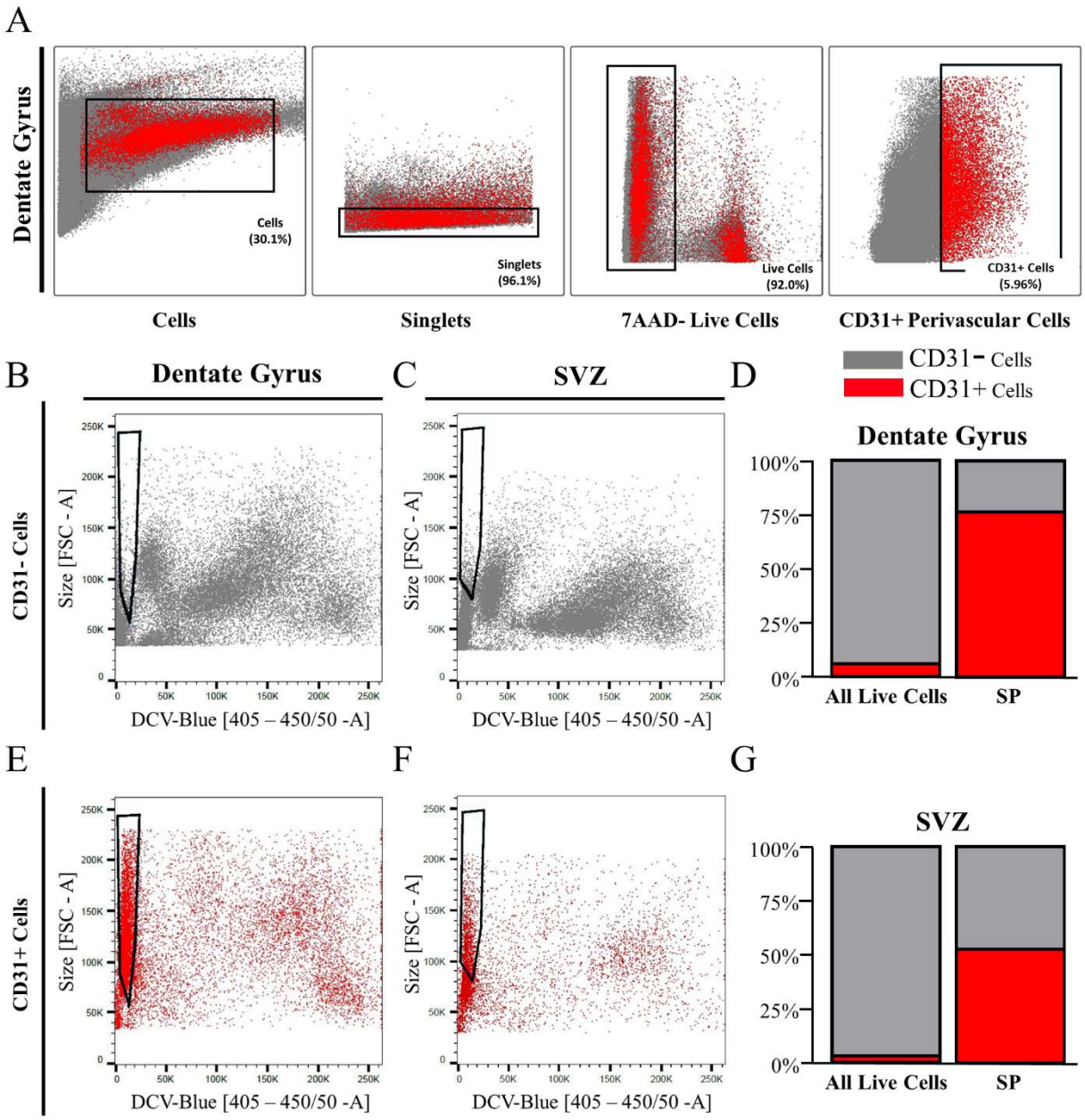

Fig 3. The side population phenotype of adult primary dentate gyrus and SVZ cells is mainly composed of endothelial cells. Gating of CD31+ cells (red) apart from the main population (grey) in the dentate gyrus (A) is shown as an example. The CD31-negative cells are a heterogeneous population in the dentate gyrus (B) and SVZ (C) and do not contain the DNA-dye-effluxing side population. Alternatively, CD31-positive cells localize to the side population area make up a large

portion of the SP in primary dentate gyrus (D, E) and SVZ cells (F, G). Plots B and E are based on samples pooled from five male and four female mice. Plots C and F are based on samples pooled from seven male mice.

References

1. Wu C-P, Zhou L, Xie M, Du H-D, Tian J, Sun S, et al. Identification of Cancer Stem-Like Side Population Cells in Purified Primary Cultured Human Laryngeal Squamous Cell Carcinoma Epithelia. PLOS ONE. 2013 Jun 11;8(6):e65750.

2. Boesch M, Zeimet AG, Fiegl H, Wolf B, Huber J, Klocker H, et al. High prevalence of side population in human cancer cell lines. Oncoscience. 2016;3(3–4):85–7.

3. Mouthon M-A, Fouchet P, Mathieu C, Sii-Felice K, Etienne O, Lages CS, et al. Neural stem cells from mouse forebrain are contained in a population distinct from the "side population." J Neurochem. 2006 11-01;99(3):807–17.

4. Salcido CD, Larochelle A, Taylor BJ, Dunbar CE, Varticovski L. Molecular characterisation of side population cells with cancer stem cell-like characteristics in small-cell lung cancer. Br J Cancer. 2010 May;102(11):1636–44.

5. Telford WG. Stem Cell Identification by DyeCycle Violet Side Population Analysis. In: Helgason CD, Miller CL, editors. Basic Cell Culture Protocols [Internet]. Totowa, NJ: Humana Press; 2013 [cited 2020 Jul 14]. p. 163–79. (Methods in Molecular Biology). Available from: https://doi.org/10.1007/978-1-62703-128-8_11

6. Telford WG, Bradford J, Godfrey W, Robey RW, Bates SE. Side population analysis using a violet-excited cell-permeable DNA binding dye. Stem Cells Dayt Ohio. 2007 Apr;25(4):1029–36.

7. Boesch M, Wolf D, Sopper S. Optimized Stem Cell Detection Using the DyeCycle-Triggered Side Population Phenotype [Internet]. Vol. 2016, Stem Cells International. Hindawi; 2015 [cited 2020 Jul 15]. p. e1652389. Available from: https://www.hindawi.com/journals/sci/2016/1652389/

8. Zhou S, Schuetz JD, Bunting KD, Colapietro A-M, Sampath J, Morris JJ, et al. The ABC transporter Bcrp1/ABCG2 is expressed in a wide variety of stem cells and is a molecular determinant of the side-population phenotype. Nat Med. 2001 Sep;7(9):1028–34.

9. Bond AM, Ming G, Song H. Ontogeny of adult neural stem cells in the mammalian brain. In: Current Topics in Developmental Biology [Internet]. Elsevier; 2020 [cited 2021 Mar 2]. p. S0070215320301241. Available from: https://linkinghub.elsevier.com/retrieve/pii/S0070215320301241

10. Denoth-Lippuner A, Jessberger S. Formation and integration of new neurons in the adult hippocampus. Nat Rev Neurosci. 2021 Apr;22(4):223–36.

11. Chaker Z, Codega P, Doetsch F. A mosaic world: puzzles revealed by adult neural stem cell heterogeneity. WIREs Dev Biol. 2016;5(6):640–58.

12. Kim M, Morshead CM. Distinct populations of forebrain neural stem and progenitor cells can be isolated using side-population analysis. J Neurosci Off J Soc Neurosci. 2003 Nov 19;23(33):10703–9.

13. Pastrana E, Cheng L-C, Doetsch F. Simultaneous prospective purification of adult subventricular zone neural stem cells and their progeny. Proc Natl Acad Sci. 2009 Apr 14;106(15):6387–92.

14. Rietze RL, Valcanis H, Brooker GF, Thomas T, Voss AK, Bartlett PF. Purification of a pluripotent neural stem cell from the adult mouse brain. Nature. 2001 Aug;412(6848):736–9.

15. Murayama A, Matsuzaki Y, Kawaguchi A, Shimazaki T, Okano H. Flow cytometric analysis of neural stem cells in the developing and adult mouse brain. J Neurosci Res. 2002;69(6):837–47.

16. Hochgerner H, Zeisel A, Lönnerberg P, Linnarsson S. Conserved properties of dentate gyrus neurogenesis across postnatal development revealed by single-cell RNA sequencing. Nat Neurosci. 2018 Feb;21(2):290–9.

17. Shin J, Berg DA, Zhu Y, Shin JY, Song J, Bonaguidi MA, et al. Single-Cell RNA-Seq with Waterfall Reveals Molecular Cascades underlying Adult Neurogenesis. Cell Stem Cell. 2015;17(3):360–72.

18. Dulken BW, Leeman DS, Boutet SC, Hebestreit K, Brunet A. Single-Cell Transcriptomic Analysis Defines Heterogeneity and Transcriptional Dynamics in the Adult Neural Stem Cell Lineage. Cell Rep. 2017 Jan 17;18(3):777–90.

19. Artegiani B, Lyubimova A, Muraro M, van Es JH, van Oudenaarden A, Clevers H. A Single-Cell RNA Sequencing Study Reveals Cellular and Molecular Dynamics of the Hippocampal Neurogenic Niche. Cell Rep. 2017 Dec;21(11):3271–84.

20. Hulspas R, Quesenberry PJ. Characterization of neurosphere cell phenotypes by flow cytometry. Cytometry. 2000;40(3):245–50.

21. Giannoni P, Badaut J, Dargazanli C, De Maudave AF, Klement W, Costalat V, et al. The pericyte–glia interface at the blood–brain barrier. Clin Sci. 2018 Feb 14;132(3):361–74.

22. Ayloo S, Gu C. Transcytosis at the blood–brain barrier. Curr Opin Neurobiol. 2019 Aug 1;57:32–8.

23. Mahringer A, Fricker G. ABC transporters at the blood–brain barrier. Expert Opin Drug Metab Toxicol. 2016 May 3;12(5):499–508.

24. Walker TL, Kempermann G. One Mouse, Two Cultures: Isolation and Culture of Adult Neural Stem Cells from the Two Neurogenic Zones of Individual Mice. J Vis Exp JoVE [Internet]. 2014 Feb 25 [cited 2020 Oct 15];(84). Available from: https://www.ncbi.nlm.nih.gov/pmc/articles/PMC4131911/

25. Hagihara H, Toyama K, Yamasaki N, Miyakawa T. Dissection of Hippocampal Dentate Gyrus from Adult Mouse. J Vis Exp JoVE [Internet]. 2009 Nov 17 [cited 2020 Oct 15];(33). Available from: https://www.ncbi.nlm.nih.gov/pmc/articles/PMC3142893/

26. Kannangara TS, Carter A, Xue Y, Dhaliwal JS, Béïque J-C, Lagace DC. Excitable Adult-Generated GABAergic Neurons Acquire Functional Innervation in the Cortex after Stroke. Stem Cell Rep. 2018 Dec 11;11(6):1327–36.

27. Babu H, Claasen J-H, Kannan S, Rünker AE, Palmer T, Kempermann G. A Protocol for Isolation and Enriched Monolayer Cultivation of Neural Precursor Cells from Mouse Dentate Gyrus. Front Neurosci [Internet]. 2011 Jul 14 [cited 2020 Oct 30];5. Available from: https://www.ncbi.nlm.nih.gov/pmc/articles/PMC3140691/

28. Crouch EE, Doetsch F. FACS isolation of endothelial cells and pericytes from mouse brain microregions. Nat Protoc. 2018 Apr;13(4):738–51.

29. Shaw TJ, Senterman MK, Dawson K, Crane CA, Vanderhyden BC. Characterization of intraperitoneal, orthotopic, and metastatic xenograft models of human ovarian cancer. Mol Ther. 2004 Dec;10(6):1032–42.

30. Tang Q-L, Liang Y, Xie X-B, Yin J-Q, Zou C-Y, Zhao Z-Q, et al. Enrichment of osteosarcoma stem cells by chemotherapy. Chin J Cancer. 2011 Jun;30(6):426–32.

31. Murase M, Kano M, Tsukahara T, Takahashi A, Torigoe T, Kawaguchi S, et al. Side population cells have the characteristics of cancer stem-like cells/cancer-initiating cells in bone sarcomas. Br J Cancer. 2009 Oct;101(8):1425–32.

32. Golebiewska A, Brons NHC, Bjerkvig R, Niclou SP. Critical Appraisal of the Side Population Assay in Stem Cell and Cancer Stem Cell Research. Cell Stem Cell. 2011 Feb 4;8(2):136–47.

33. Boesch M, Zeimet AG, Reimer D, Schmidt S, Gastl G, Parson W, et al. The side population of ovarian cancer cells defines a heterogeneous compartment exhibiting stem cell characteristics. Oncotarget. 2014 Jun 1;5(16):7027–39.

34. Penninger JM, Irie-Sasaki J, Sasaki T, Oliveira-dos-Santos AJ. CD45: new jobs for an old acquaintance. Nat Immunol. 2001 May;2(5):389–96.

35. Thomas ML. The Leukocyte Common Antigen Family. Annu Rev Immunol. 1989 Apr 1;7(1):339–69.

36. Yousef H, Czupalla CJ, Lee D, Butcher EC, Wyss-Coray T. Papain-based Single Cell Isolation of Primary Murine Brain Endothelial Cells Using Flow Cytometry. Bio-Protoc. 2018 Nov 20;8(22):e3091.

37. Xie XP, Laks DR, Sun D, Poran A, Laughney AM, Wang Z, et al. High-resolution mouse subventricular zone stem-cell niche transcriptome reveals features of lineage, anatomy, and aging. Proc Natl Acad Sci. 2020 Dec 8;117(49):31448–58.

38. Chen X, Cao S, Wang Y, Li M, Guo Y, Ye Y, et al. Single-Cell Profiling Resolved Transcriptional Alterations and Lineage Dynamics of Subventricular Zone after Mild Traumatic Brain Injury. bioRxiv. 2021 May 31;2021.05.31.446381.

39. Warren MS, Zerangue N, Woodford K, Roberts LM, Tate EH, Feng B, et al. Comparative gene expression profiles of ABC transporters in brain microvessel endothelial cells and brain in five species including human. Pharmacol Res. 2009 Jun 1;59(6):404–13.

40. Song HW, Foreman KL, Gastfriend BD, Kuo JS, Palecek SP, Shusta EV. Transcriptomic comparison of human and mouse brain microvessels. Sci Rep. 2020 Jul 23;10(1):12358.

41. Kiss T, Nyúl-Tóth Á, Balasubramanian P, Tarantini S, Ahire C, DelFavero J, et al. Single-cell RNA sequencing identifies senescent cerebromicrovascular endothelial cells in the aged mouse brain. GeroScience. 2020 Mar 31;42(2):429–44.

Supplemental information

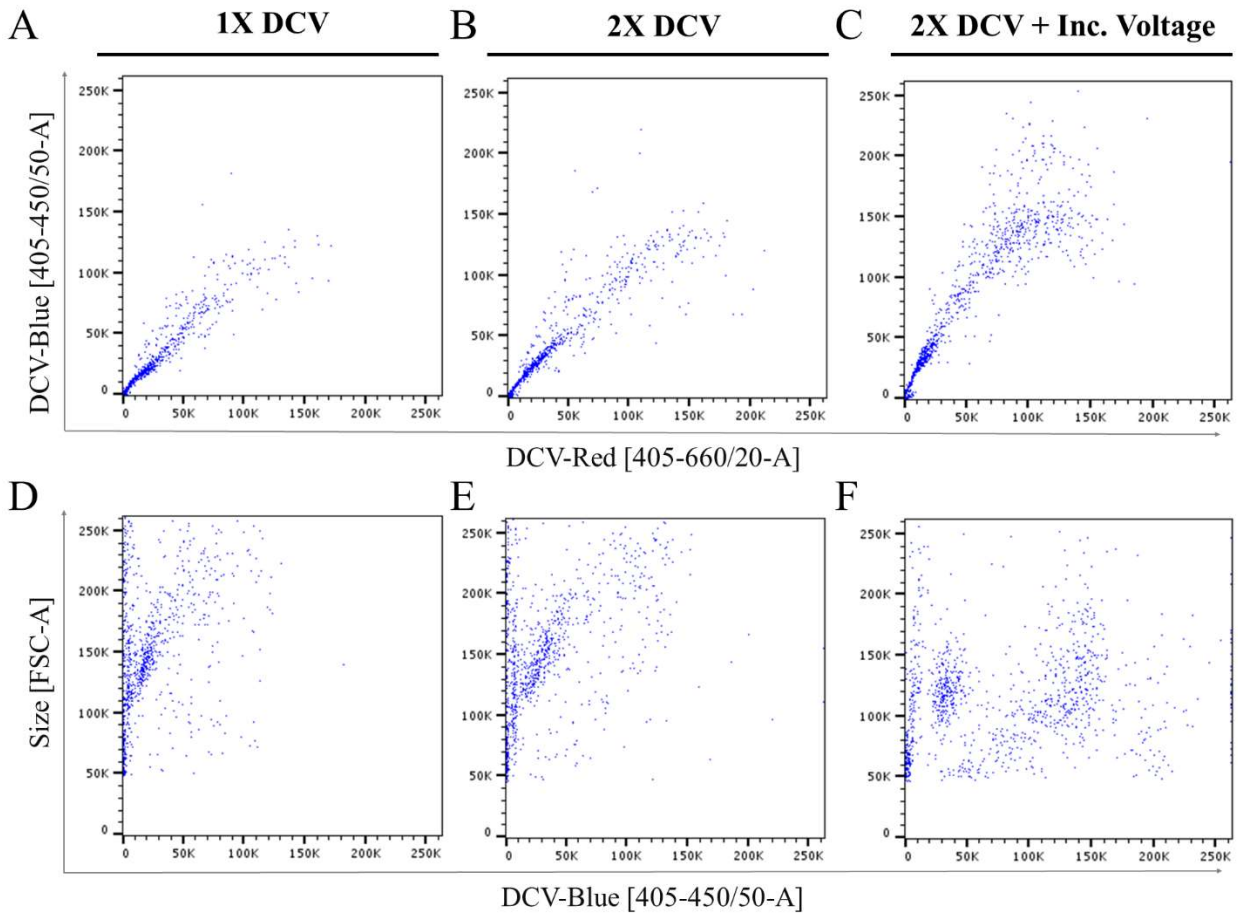

S 1 Fig. The titration of the DCV reagent in adult dentate gyrus cells. DCV staining testing 1X (A,D) or 2X DCV (B, E, C, F), as well as varying degrees of voltage for the 2X DCV concentration (B, E vs. C, F) as shown in dual fluorescence plots (A-C) and DCV-Blue/size plots (D-F). These results suggested 2X DCV with optimal excitation (C, F) was sufficient to distinguish the heterogeneous populations. Plots A, B, D, and E were generated from samples of pooled nine female mice. Plot C and F were generated from pooled samples of five male and three female mice, 2.5k cells are shown.

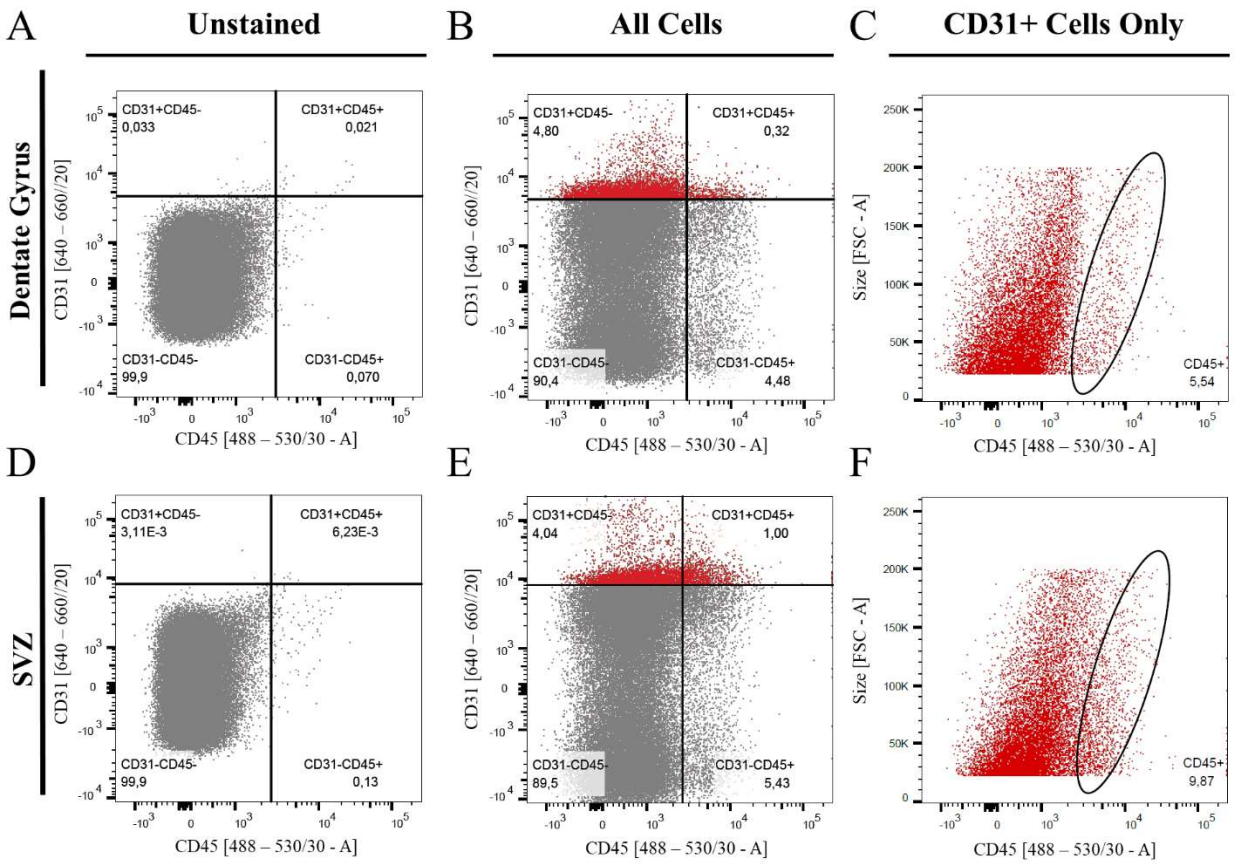

S 2 Fig. Characterization of CD31-expresing cells. CD31 and CD45 staining in the dentate gyrus (A – unstained, B – all-stained) and the SVZ (D – unstained, E – all-stained) show little co-expression of CD31 and CD45 in the main populations (B and E, respectively) with only a small proportion of CD31+ cells expressing CD45 (C and F). These plots are generated based on pooled samples from five male and three female mice, 50k cells are shown.

CHAPTER 3:

Mitotic Activity and DNA Maintenance of Adult Neural Stem Cells is Regulated by Beclin1

In submission

Contributions of co-authors

Alena K. performed all *in vivo* (unless stated otherwise), *in vitro* and *ex vivo* experiments, managed experimental design, analysis and interpretation of data and writing the manuscript

Dhaliwal J. performed all virus preparation and injections, contributed to tissue collection and IHC experiments

Xue Y. maintained the breeding and housing of mice, and assisted with tamoxifen treatments

Vaculik M. performed quantification of virus-infected puncta

McCambley M. performed quantification of virus-infected puncta

Fong B.C. and Cook D. contributed to sc-RNAseq analyses

Slack R.S. provided valuable input for manuscript preparation

Lagace D.C. contributed to the design, analysis, interpretation of results and writing the manuscript

Mitotic Activity and DNA Maintenance of Adult Neural Stem Cells is Regulated by Beclin1

Kalinina A.[1], Dhaliwal J.[3], Xue Y.[1,2], Vaculik M.[1], McCambley M.[1], Fong B.C., Cook D.[4], Slack R.S. [1,2], & Lagace D.C. [1,2,*]

[1]Department of Cellular and Molecular Medicine, Faculty of Medicine; University of Ottawa; Ottawa, ON, K1H 8M5; Canada.

[2]Brain and Mind Research Institute, Department of Neuroscience, Faculty of Medicine, University of Ottawa; Ottawa, ON, K1H 8M5; Canada.

[3]Hospital for Sick Children; University of Toronto; Toronto, ON, M5G 1X8; Canada.

[4]Ottawa Hospital Research Institute; Ottawa, ON, K1Y 4E9: Canada

*Correspondence: dlagace@uottawa.ca

SUMMARY

Beclin1 is a known tumor suppressor gene and can regulate cell proliferation under pathological conditions. Whether Beclin1 has a role in regulating proliferation in physiological conditions remains unknown. Here, through the creation of an inducible transgenic mouse that removes Beclin1 from adult NSPCs and their progeny we uncovered that Beclin1 is required cell-autonomously to sustain proliferating NSCPs *in vivo* and *ex vivo*. Flow cytometry analysis and single-cell RNA-sequencing show that Beclin1 reduces the proportion of mitotic cells. Additionally, scRNA-seq analysis of proliferating cells resolved by stage of cell cycle highlights Beclin1-null cells have a distinct differential developmental trajectory accompanied by the downregulation of genes involved in chromosomal maintenance and upregulation of cell stress genes upon cell cycle exit. These effects align with DNA damage in Beclin1-null cells and ultimately result in the generation of less adult-born granular neurons. Together these data identify Beclin1 as a novel regulator of the mitosis in the NSPCs.

KEY WORDS: Beclin1, autophagy, adult neurogenesis, hippocampus, proliferation, adult neural stem cells, mitosis

INTRODUCTION

Beclin1 (Atg6) is a scaffold protein that has well-established roles in the regulation of autophagy[1,2], endocytosis[3,4], and phagocytosis[5,6]. There is also a growing appreciation that Beclin1 is multifunctional and can regulate proliferation within the field of oncology where it has been characterized as a tumor suppressor. For example, in aggressive breast cancer cells, knockdown of Beclin1 suppresses proliferation by regulating the cell cycle and apoptosis[7]. Similarly, in colorectal and HeLa cells Beclin1 deficiency increases genomic instability[8–10], and disrupts chromatin dynamics during mitosis resulting in deficient proliferation[10]. Whether Beclin1 regulates proliferation under normal physiological conditions remains largely unknown.

The examination of the role in Beclin1 has been mainly studied in the embryonic and early stages of development. Homozygous Beclin1 knockout mice are embryonic lethal in early stages of development and heterozygous Beclin1 knockout mice are viable but have significant increases in tumorgenicity[11] as well as a reduction in neurogenesis in the olfactory bulb[12]. Conditional Beclin1 mouse models have further shown that loss of Beclin1 in keratinocytes is lethal due to dampened expansion of the embryonic epidermis[4], while loss of Beclin1 in select neurons during development leads to severe neurodegeneration and premature death[13]. Together this body of literature suggests that Beclin1 may be necessary for proliferation *in vivo* under physiological conditions. To test this hypothesis, we specifically explore the requirement of Beclin1 within the neural stem and progenitor cells (NSPCs) that develop into adult granule neurons within the hippocampus of the adult brain.

Our findings reveal that Beclin1 is required during adult neurogenesis through its role in mitosis and chromatin stability. Specifically, through the creation of the conditional inducible Beclin1

knockout mouse, Beclin1 removal from adult nestin-expressing cells and their progeny resulted in a significant cell-autonomous reduction in the proliferation of NSPCs. The combination of flow cytometry and single-cell RNA sequencing (scRNA-seq) data independently highlighted that Beclin1 loss reduced proliferation by directly impeding cell mitosis. The ability to resolve the states of proliferating NSPCs, as well as cells exiting the cell cycle identified that Beclin1-null mitotic cells have a distinct differential developmental trajectory accompanied by changes in key players that regulate mitosis and differentiation, and directly modify genes impeding proliferation. Specifically, mitotic cells downregulate genes involved in chromosomal maintenance and upregulate cell stress genes upon cell cycle exit. These deficits are accompanied by DNA damage in Beclin1-null cells which ultimately decreased their survival and led to a reduction in the generation of adult-born neurons.

RESULTS

Loss of Beclin1 reduces proliferation cell-autonomously

To conditionally remove Beclin1 from adult nestin-expressing NSPCs and progeny, we created a Beclin1 Nestin-inducible transgenic mouse model (hereafter referred to as Beclin1 nKO; NestinCreER^{T2}:R26R-eYFP: Beclin1$^{flox/flox}$) and littermate control wild-type (WT) mice (NestinCreER^{T2}:R26R -eYFP: fBeclin1$^{WT/WT}$). The recombined (YFP+) cells in the Beclin1 nKO mice were confirmed to have a significant reduction in the amount of Beclin1, as shown by the quantification of Beclin1 puncta in fixed brain sections (Fig 1A,B), as well as western blot detection of Beclin1 protein from YFP cells purified using fluorescence-activated cell sorting (FACS) (Fig 1C). To further test if the Beclin1-null cells had a reduction in autophagy, Beclin1 nKO and WT mice were injected with a Cherry-EGFP-LC3 retrovirus, using our published *in vivo* methodology to identify autolyosomes[14]. Quantification of the number of autolysosomes (mCherry+ puncta) revealed a significant reduction in autolysosomes in Beclin1-null cells in the Beclin1 nKO mice compared to control cells in the WT mice (Fig S1 A,B), supporting that the Beclin1-null cells had a significant reduction in autophagy.

We next assessed proliferation in the Beclin1 nKO compared to WT mice. To label the slowly dividing activated NSCs (aNSCs) and rapidly dividing NPCs[15–18], two weeks after the injection of tamoxifen (14 dpi), the mice were treated with multiple injections of EdU (5-ethynyl-2′-deoxyuridine) two hours apart and perfused two hours after the last injection[19]. EdU incorporation showed a significant genotype-dependent decrease in the proportion of proliferating (YFP+Edu+) Beclin1-null cells (Fig 1D, E). Additionally, the proportion of aNSCs, identified by their expression of EdU and a stem cell marker, Sox2[20–22], showed a significant decrease in Beclin1-

null aNSCs (Fig 1D, F). This decrease in the proportion of aNSCs was not associated with an increase in the proportion of Beclin1-null quiescent NSCs (qNSCs), as there were no significant differences in the proportion of qNSCs between the Beclin1 and WT mice (Fig S2A, B). These findings suggest that Beclin1 reduces the proliferation of both aNSCs and NPCs.

To examine if Beclin1 removal perturbs the number of aNSCs and NPCs actively cycling or exiting cell cycle, Beclin1 nKO and WT mice were treated with multiple injections of EdU (5-ethynyl-2′-deoxyuridine) two hours apart and the mice were perfused 24 hours after the first injection[19]. Beclin1 nKO mice had a significant reduction in the proportion of cells that were actively cycling as measured by the YFP+EdU+ cells that expressed Ki67 (Fig 1G, H). Additionally, Beclin1 nKO mice had a significant increase in the proportion of EdU+ cells exiting the cell cycle (EdU+Ki67-), with an average of 36% of EdU-labeled Beclin1-null cells leaving cell cycle in a 24-hour period compared to only 14% of WT cells (Fig 1G, I). Together these data support the notion loss of Beclin1 reduces proliferation in the actively cycling aNSCs and NPCs.

To begin to determine if the reduction in proliferation in the Beclin1-null cells was due to a cell-autonomous mechanism the *in vitro* neurosphere assay was performed using cultures obtained from the dentate gyrus of Beclin1 nKO and WT adult mice. Both the number and size of the primary YFP+ spheres were significantly reduced in the Beclin1 nKO compared to WT mice (Fig 1J-L). To further examine the dynamics of cell division of daughter cells in Beclin1-null cells we performed live cell imaging of WT and Beclin1-null DG cells in monolayer culture conditions. WT cells produced healthy progeny as observed by their maintained proliferation and a high survival rate throughout the imaging period and continued up to 11 generations (Fig 1M, N). In contrast, Beclin1-null cells showed increased cell death over time and could not produce daughter cells after 8 generations. This was accompanied by a significant 25% reduction in the maximum

number of divisions that could be carried out by Beclin1-null compared to WT cells (Fig 1O). In addition, WT and Beclin1-null cells that successfully underwent mitosis were not different in latency to enter next mitosis (Fig 1P) suggesting that Beclin1 removal does not perturb cell abscission or entry into next cell cycle. Overall, these data support Beclin1 is required in the regulation of NSPC proliferation.

ScRNAseq analysis highlights altered mitotic dynamics of Beclin1-nell cells.

To gain insights into the cellular mechanisms underlying the disruption proliferation and increased cell death in the Beclin1 nKO mice, we dissected and collected single YFP+ WT and Beclin1-null cells by FACS and subjected them to the 10x Genomics single cell RNA sequencing (scRNAseq). As expected, examination of the WT and Beclin1-null cells revealed the lineage of recombined nestin-expressing neurogenic cells and their progeny formed the largest group of related cells (Fig 2A). In addition to these cells, there were three other small groups of cells that are known to express nestin, including pericytes[23], endothelial cells (EC)[23], and myelin-forming oligodendrocyte (MFOL) precursor cells[24].

Analysis of the neuronal lineage of the WT and Beclin1 nKO samples allowed for the resolution of 9 different cell types in the neurogenic lineage (Fig 2B). The qNSCs were detected by Aldoc, Hopx, and other quiescence genes[25] (Fig 2C-E). They were divided into dormant qNSCs (DqNSCs) and primed qNSCs (PqNSCs), with the PqNSCs having higher expression of genes such as Btg1 and FOS[26]. Using the transient expression of cell cycle markers, the proliferating NPCs and NSCs were divided into cells in S phase and G2/M phases (hereafter, M phase) of the cell cycle (Fig 2C). S phase cells were marked by genes such as Ascl1, Mcm2, and cyclin D2 (Ccnd2), while M phase cells were positive for Top2a, Hmgb2/n2, and Mki67 (Fig 2C-E). There

was also a group of cells that were exiting cell cycle (CCE) marked by a large reduction in Pcna[27] and rise of early differentiation markers (Fig 2C-E). The remaining non-cycling neurogenic cells consisted of four clusters of neurons. They included three groups of immature neurons labeled IN1-3 that had decreasing expression of immature neuron markers Eomes, Tubb3, and Dcx (Fig 2C-E). The last group of neurons was labeled as mature neurons based on relative increase in expression of mature neuron markers such as Calb2 (Fig 2C-E). Examination of the proportion of these 9 cell types showed the highest change in the proportion of cells in M phase with a 2-fold reduction in the Beclin1-null mice compared to WT mice (Fig 2F). These results led us to hypothesize that Beclin1-null cells have abnormal cell cycle dynamics that mediated the reduction in proliferation.

Beclin1 nKO mice have fewer mitotic cells *ex vivo* and *in vitro*.

To test if the loss of Beclin1 altered the proportion of cells in the different stages of the cell-cycle, we performed an *ex vivo* cell cycle assay[28,29]. Specifically, 14 dpi WT and Beclin1 nKO mice were injected with 4 injections of EdU two hours apart, then 24 hours after first injection single cells were obtained from the DG. Cells underwent flow cytometry analysis to measure EdU incorporation and DNA content in order to identify cells in S phase, as well as M phase. This assay revealed a significant decrease in the percentage of total mitotic cells in the DG of Beclin1 nKO mice (Fig 3A, B). This reduction in mitotic cells was accompanied by no significant change in the percent of cells in the S phase of the cell cycle (Fig 3A, C). These results therefore verify the scRNAseq results and corroborate the loss of Beclin1-null mitotic cells.

To further test if the cell-autonomous reduction in neurosphere formation in Beclin1 nKO mice is accompanied also by a reduction in cells in M phase, we made neurospheres from the DGs of 14

dpi WT and Beclin1 nKO animals and performed an *in vitro* pulse-chase with EdU (Fig 3D). Similar to our *ex vivo* results (Fig 3A-C), the percent of mitotic cells was significantly reduced (Fig 3D, E) in the absence of change in the percent of cells in S-phase (Fig 3F). Together all these data the cell-autonomous reduction in proliferation of Beclin1-null cells is accompanied by altered progression through mitosis stage of the cell cycle.

Beclin1-null prophase/prometaphase cells are fewer in number and diverge upon cell cycle exit.

To explore mechanisms by which loss of Beclin1 impedes mitosis, we resolved the states of proliferating cells identified by our scRNAseq analysis that were in S/M phase or exiting the cell cycle (groups 3-5 in Fig 3B). This revealed eight clusters of cells including: aNSCs; NSCs and NPCs in S phase of the cell cycle; cells in early and late M phase; and 3 groups of cells exiting the cell cycle (Fig 4A, B). To establish the cell cycle status of the proliferating clusters, we used Seurat's cell cycle scoring algorithm that approximates cell cycle identity as being in G1, G2/M or S-phase based on the expression of known S and M cell cycle genes[30]. The scoring for G1 phase identity aligned with CC1-CC3, whereas the proliferative early/late M cells and S NSCs/NPCs aligned with G2/M and S cells. Additionally, the Seurat cell cycle analysis also validated the reduction in proportion of Beclin1-null cells in the G2/M and S phase (Fig 4A, B, E). Cells in the S phase of the cell cycle divided into NSCs and NPCs (Fig 4A, B).

We further subdivided NSPCs into groups based on their respective stages along the activation-differentiation continuum using expression of known markers. The aNSC subcluster was positive for activation markers Ascl1 and Dbi and NSC markers Aldoc and Apoe (Fig 4D, E). The aNSCs represent a transition state between the PqNSCs and S phase NSCs as they are also positive for S

phase markers like Mcm genes and Pcna. The aNSCs did not include cells in M phase, as shown by the absence of M phase markers. Between the Beclin1-null and WT cells there was a similar proportion in aNSCs (Fig 4F). The S-phase NSCs had decreased expression of Apoe, Dbi and Ascl1 NSC markers compared to early aNSCs, whereas these genes were completely downregulated in the S-phase NPCs (Fig 4D, E). There was no difference in proportion of S phase NSCs between Beclin1-null and WT cells, yet a prominent decline in the proportion of S phase NPCs (Fig 4F).

Cells in M phase separated into early M and Late M phases, but NSCs and NPCs could not be distinguished from each other (Fig 4A, B). Early M phase cells expressed more prophase, prometaphase, and spindle assembly checkpoint (SAC) genes such as Spc25, Incenp, and Nuf2 (Fig. 4E, G). The Late M cells were expressing SAC, metaphase and anaphase genes like Cdc25c, Cdc20, and Dynll1 (Fig. 4E, G). Compared to WT, Beclin1-null cells had a striking reduction in the proportion of early M phase cells, however, there was no difference in the percentage of cells in late M phase (Fig 4F). This suggests that the cell cycle perturbation in the NSPCs following Beclin1 removal may involve inadequate prophase/prometaphase maintenance.

Lastly, this analysis allowed for the identification of three clusters of cells exiting the cell cycle (Fig 4A, B, CCE 1-3). The differences between CCE1-CCE3 represented early progeny on a continuum of expression of neuronal differentiation markers such as Tubb3 and Dcx (Fig 4D, E). CCE1 has the least amount of neuronal marker expression and likely are the cells that are going to re-enter cell cycle or enter quiescence. In comparison, the CCE2/CCE3 expression high levels of differentiation markers and thus likely differentiate into neurons. The Beclin1-null and WT clustered differently between CCE 1-3. Specifically, Beclin1-null cells preferentially clustered into

CCE3, while WT cells localized mostly to CCE2 (Fig 4F), suggesting a differential transcriptional fate for the Beclin1-null compared to WT cells during cell cycle exit.

Together these data highlight the power of scRNAseq analysis to identify robust changes in specific sub-populations of cycling cells that cannot be easily resolved through other methods. For example, our histological analysis of aNSCs showed a reduction in aNSCs (Fig 1D-F), yet the scRNAseq data shows the reduction in aNSCs is due to changes in proportion of aNSCs in M phase, rather than S phase. Additionally, our flow cytometry analysis did not detect a significant change in proportion of dividing cells in S-phase (Fig 3C, F), but these results support a significant reduction in specifically the proportion of dividing Beclin1-null NPCs in S-phase of the cell cycle.

Beclin1-null cells regulate cell cycle exit differentially.

To assess what changes in cell fate underlie the preferential clustering of Beclin1-null cells into the CCE3 group, we used scVelo[31] that revealed fate choice vectors of Beclin1-null and WT proliferating cells based on mature and unprocessed RNA dynamics. As expected, the WT mitotic cells entered and largely remained in mitosis followed by entering the CCE1 and CCE2 population (Fig 5A). In contrast, the Beclin1-null cells had little mitotic activity and stronger fate vectors towards CCE3 (Fig 5B). Top 100 cluster-specific genes driving these trajectories were also revealed using scVelo's latent time function (Suppl. Table 1). In accordance with enhanced cell death an reduced mitosis, we observed a loss of regulation of the Beclin1-null mitotic clusters by an apoptosis and DNA damage suppressor Birc5/survivin[32,33] (Suppl. Table 1, Fig 5C). Beclin1-null cells exiting cell cycle showed preferential regulation by genes such as Nfib, a negative regulator of proliferation and positive regulator of cell cycle exit[34,35] (Fig 5D). Beclin1-null mitotic and CCE cells showed regulation by unique transcripts such as Ttc28 that regulates midzone

organization during late mitosis[36] (Fig 5E), and MAPT, a structural protein involved in cell cycle and nuclear maintenance[37] and related to neurodegeneration[38] (Fig 5F). Together this evidence reveals that Beclin1-null mitotic cells follow a differential developmental trajectory accompanied by changes in key players that regulate mitosis and differentiation, and directly activate genes impeding proliferation.

Beclin1-null cells downregulate mitotic genes and upregulate cell stress genes upon cell cycle exit.

There was 223 significantly differentially expressed genes (DEGs) in WT and Beclin1 nKO mice: 49 reduced genes and 174 upregulated (Suppl. Table 2). Corroborating scVelo findings of decreased mitotic transcriptional activity, Beclin1-null cells showed decreased expression in DEGs that were abundantly expressed in the mitotic WT cells. This includes genes that included parts of the mitotic machinery such as Cenpk/m/h [39,40], Kif11 [41], Smc2 [42], that make up the centromere [39], kinesin [43] and condesin I and II [44,45] complexes, respectively, which play roles in the preparation for cell division and in chromatin maintenance [46–48] (Fig 6A; Suppl. Table 2). Furthermore, dysregulation of the kinetochore was evident in Beclin1-null cells by the reduced expression of Kif22 [49], Spc24 and Spc25 [50] (Suppl. Table 2), as well as Ran and RanBP1 that are both required for proper attachment of kinetochores to microtubules [51–53] (Suppl. Table 2). There was also decreased expression of DNA repair genes such as Rrm2 [54] and Ran GTPase [51,55] (Fig 6A) and others such as Top2a [56], Pclaf [57], and Syce2 [58] (Suppl. Table 2). In contrast, the genes that had enhanced expression in Beclin1-null cells were cell stress, metabolism, and neurodevelopment genes, such as Tpt1 [59], Tmxb4x [60], Snapin [61], Nptn [62], Tcf4 [63], and Cplx2 [64] (Fig 6B). Additionally, Beclin1-null cells showed upregulation in cell stress-related transcripts such as reactive oxygen species genes (ROS; e.g., Romo1 [65], Pet100 [66], Ndufa3 [67]; Suppl. Table 2), and P53 targets (e.g.,

Tpt1 [68,69], Cox2 [70], Sesn1 [71]; Suppl. Table 2). These genes also had more enhanced and specific expression in the Beclin1-null cells in the CC3 cluster compared to WT cells.

Gene ontology (GO) term analysis of the upregulated and downregulated differentially expressed genes further revealed that processes relating to cellular processes including cytoplasmic translation, ribonucleoprotein and ribosome generation, oxidative phosphorylation, and p53 signaling were significantly enhanced in Beclin1-null proliferating cells (Fig 6C). The cells also had a decreased expression of processes relating to nonsense-mediated decay of RNA, mitotic cell cycle, chromosome and kinetochore organization, p53 degradation, nuclear maintenance, as well as DNA replication and metabolism (Fig 6C).

In order to observe these pathways during proliferation in relative time, we constructed pseudotime trajectories of WT and Beclin1-null cells (Fig 6D) followed by quantification of pathway activity over time using GO terms. Beclin1-null cells showed a dramatic reduction in the activity of genes necessary for the G2/M transition checkpoint that ensures DNA integrity and cell size (Fig 6E). Further on, mid-mitosis cells also failed to activate genes necessary for the spindle assembly checkpoint (Fig 6F) that ensure proper DNA maintenance in preparation for anaphase and telophase. This did not affect the regulation of cytokinesis (Fig 6G). However, the chromosome segregation genes were significantly inhibited (Fig 6H) in Beclin1-null mitotic cells together with insufficient activation of DNA repair genes (Fig 6I), suggesting that cells may accumulate DNA damage overtime. Lastly, Beclin1-null cells had enhanced p53 signaling at mitotic exit (Fig 6J) which could mediate apoptosis. Together these data corroborate our findings *in/ex vivo* and *in vitro*, and suggest that deficits in chromatin dynamics in Beclin1-null cells reduces the mitotic activity and increases death of the daughter cells upon cell cycle exit leading to the reduction in proliferating.

Beclin1 nKO mice have accumulation of DNA damage and fewer adult-generated granule neurons.

The faulty mitotic checkpoints and DNA maintenance that were seen in Beclin1-null cells can commonly result in DNA damage and chromatin abnormalities such as aneuploidy, genomic instability, micronuclei, and lagging chromosomes in cancer cells [72,73]. To determine if Beclin1-null cells have reduced viability due to DNA damage accumulation, we tested the general levels of fragmented DNA in an alkaline comet assay that is highly sensitive to both double- and single-strand DNA breaks [74]. Sorted Beclin1-null cells had a higher percentage of DNA in the comet tail (Fig 7A, B) suggesting increased DNA fragmentation and supporting the notion that Beclin1-null cells have increased accumulation of DNA damage.

To test if the accumulation of DNA damage results in the reduction in the generation of adult-born cells, we performed lineage-tracing of the Beclin1-null and WT NSCs and NPCs (NSPCs) and their progeny between 14 to 60 dpi. There was a significant reduction in the number of YFP+ cells in the Beclin1 nKO mice compared to WT mice that started at 30 dpi (Fig 7C, D). Since the reduction in number of Beclin1-null cells started 30 days after removal of Beclin1, we tested if Beclin1 was reducing the survival of adult-generated neurons, in addition to reducing proliferation. Through using a retroviral-based approach we have previously published to track the survival of the late-stage dividing NPCs[14], we found no difference in survival of the NPCs at 14, 30, and 60 days after removal of Beclin1, with small but significant overall reduction in survival ratio in the floxed Beclin1 compared to WT mice (Fig S3A, B). Additionally at 60 dpi, there were no significant differences in spine density between the Beclin1-null and WT cells (Fig S3C, D). Given that the overall reduction in survival of floxed Beclin1 late-stage cells was minor, in comparison to the robust reduction proliferation in the Beclin1 nKO, Beclin1 more likely reduces the number

of immature neurons due the reduction in proliferation, which resulted in decreased survival of daughter cells.

To determine if the reduction in the number of Beclin1-null cells in the Beclin1 nKO mice was associated with a reduction, the population of cells expressing the immature neuronal marker DCX and mature neuron marker NeuN was quantified. The Beclin1 nKO mice compared to WT mice had a significant overall reduction in number of DCX+ cells starting at 30 dpi (Fig S4A, B). There was also a significant reduction in the proportion of YFP+ cells that were positive for DCX in the Beclin1 nKO mice compared to controls (Fig 7E-G). Further examination revealed a significant reduction in the proportion of late immature neurons (DCX+) that expressed the mature neuronal marker NeuN (Fig 7H, I), as well as the overall proportion and number of Beclin1-null cell that expressed NeuN (Fig 7H, J, K). Overall, these results support that a lack of Beclin1 induces changes in chromosomal dynamics during mitosis that cause DNA damage and results in the reduction in the generation of adult-born neurons.

DISCUSSION

The results of this study demonstrate that Beclin1 is required cell-autonomously for the proliferation and mitosis of adult NSPCs to sustain adult hippocampal neurogenesis. Our data led to the novel discovery that mitosis in the adult NSPCs is regulated by Beclin1. Mitotic Belcin1-null cells had a dysregulation of genes that are necessary for chromosome maintenance during prophase and metaphase, highlighting that chromatin dynamics during cell cycle in NSPCs is regulated by Beclin1. In addition, dividing Beclin1-null cells have enhanced transcription of genes related to metabolic stress and reduced DNA maintenance that is accompanied by DNA damage that ultimately leads to cell death and a reduction in the number of adult-born granular neurons in the hippocampus.

In vitro live imaging revealed that Beclin1 is required to sustain consecutive mitotic divisions and the survival of NSPCs. This finding parallels our *in vivo* results illustrating deficits in proliferation and mitosis occurring two weeks after Beclin1 was removed and two weeks before deficits in the number of immature neurons and adult-generated neurons. These findings reveal that Beclin1 has a similar requirement in SGZ to that first identified in the SVZ of heterozygous adult Beclin1 knockout mice[12]. Similarly our findings align with the improvement in age-related reductions of NSC the *Becn1*$^{F121A/F121A}$ knockin mice[75]. Our work further extends these findings through the discovery that the deficits can occur independent of loss of Beclin1 during development and are specific to adult NSPCs through its action during mitosis.

Mechanisms that regulate the cell cycle in NSPCs are beginning to be elucidated and our findings reveal Beclin1 as a regulator of mitosis specifically. The ability of our novel analysis to separate the proliferating NSPCs into different stages of the cell cycle revealed the Beclin1 is required in

regulating differential expression of mitotic spindle, centromere, and kinetochore transcripts. For example, Beclin1 loss dysregulated expression of Cenp family genes, chromosomal condensins, and genes sustaining the kinetochore and microtubule attachment. These findings support the work of others that reveals *in vitro* deletion of Beclin1 induces chromatin abnormalities during the cell cycle via the deregulation of the mitotic machinery[10,76,77]. Thus, our findings extend our understanding that Beclin1 can regulate mitosis *in vivo* in the adult brain.

A failure to undergo mitosis can induce DNA damage [73] and there are direct connections between Beclin1 and DNA repair/damage outside of the CNS [78,79]. Beclin1 is also known to directly interact with DNA repair and anti-apoptotic genes [1,9,80,81]. We show that Beclin1 is required in adult NCPSs to regulate transcription of genes involved in metabolic stress, as well as DNA repair and pro-survival genes. Specifically, Beclin1-null proliferating cells had fragmented DNA and showed upregulation of genes underlying reactive oxygen species response, P53 target genes, and a reduction in DNA synthesis and repair genes. For example, neurodevelopmental gene and binding partner of Beclin1 *Birc5/Survivin* [32,82,83] had reduced transcriptional activity in Beclin1 nKO cells, and its deficiency is associated with apoptosis via mitotic deficit and DNA damage in different cell lines[33]. These findings demonstrate that Beclin1 sustains mitosis and DNA maintenance by regulating the expression of DNA repair genes and metabolic stress in the adult neurogenic cells. These findings are also ripe for future investigation to define the precise mechanisms by which these differentially expressed transcripts alter NSPC mitosis and DNA.

In line with the known essential role for Beclin1 in initiation of the autophagosome[1,82], our findings show that the reduction in autolysosomes accompanies the dysregulation of cell cycle and DNA damage that reduces adult neurogenesis. This data aligns with previous publications showing a reduction in autophagy flux following removal of Beclin1 [11,13,84]. While these data suggest that the

actions of Beclin1 in mitosis in NSPCs rely on Beclin1's autophagy-dependent mechanisms, our data does not exclude the possibility that the effects of Beclin1 occur independent of autophagic mechanisms, or through the combination of both autophagy-dependent and -independent mechanisms. Indeed, studies examining different autophagy proteins have highlighted that not all autophagy proteins can regulate neurogenesis in development and the postnatal brain[85]. Notable are three studies that suggested autophagy is not required for adult neurogenesis. These studies include work testing the requirement of proteins involved in the elongation stage of autophagy in naïve conditions through the embryonic removal of Atg16L[86] or embryonic and adult removal of Atg7[86,87]. These studies demonstrated no deficits in proliferation, or the generation of adult born granule neurons. In direct contrast, our previous work and the work of others have suggested that autophagy–dependent mechanisms regulate adult neurogenesis. Our lab showed that retroviral-mediated deletion of Atg5 delayed the survival of adult-generated neurons and reduced autophagic flux, in absence of altering proliferation[14]. Similarly, a significant reduction in survival of adult-generated neurons, as well as depletion of the stem cell pool has been shown following NSPC-specific removal of FoxO3[88], which is involved in the formation of the phagophore. Lastly, studies by the laboratory of Dr. Guan have begun to highlight the hypothesis that a combination of autophagy-dependent and -independent mechanisms may regulate neurogenesis. Following conditional embryonic deletion of the FIP200 (focal adhesion kinase family interacting protein of 200 kD)[89], which recruits the autophagic machinery, deficits in self-renewal and differentiation of NSCs were seen at 4 weeks postnatally. Interestingly, proliferation effects were mechanistically independent of the autophagy pathway[90], whereas the differentiation effect was attributed to a non-cell-autonomous mechanism related to microglia[91]. Thus, these studies highlight the need to

examine the contribution of loss of autophagy to the deficits in mitosis and chromatin maintenance in Beclin1-null cells.

The findings from this study demonstrate the requirement of Beclin1 in the maintenance of mitosis of adult neurogenic cells to ultimately produce granular neurons. Beclin1 removal resulted in a reduction of mitotic cells mediated by transcriptional dysregulation of genes important for genomic maintenance during metaphase and anaphase. These effects were accompanied by increased signatures of cellular stress upon cell cycle exit, and accumulation of DNA damage. Overall, this study links the reduction of Beclin1 in dividing NSPCs with mitotic chromosome maintenance and DNA damage and thus identifies a novel intrinsic regulator of mitosis within the adult hippocampal NSPCs.

Acknowledgements

The authors acknowledge the assistance of Flow Cytometry & Virometry (FCV) Core Facility at the University of Ottawa, and the assistance of the Flow Cytometry & Cell Sorting facility (OHRI; RRID:SCR_023349). In addition, we acknowledge the assistance of StemCore Laboratories Genomics Core Facility at the Ontario Health Research Institute (RRID: SCR_012601). The authors also acknowledge the Cell Biology and Image Acquisition Core (RRID: SCR_021845) funded by the University of Ottawa, Ottawa, Natural Sciences and engineering Research Council of Canada, and the Canada Foundation for Innovation. We thank Dr. Stephen Baird for generously providing us with the help and use of their Opera Phenix imaging system.

Declaration of interests

Authors declare no competing interests.

Figures and figure legends

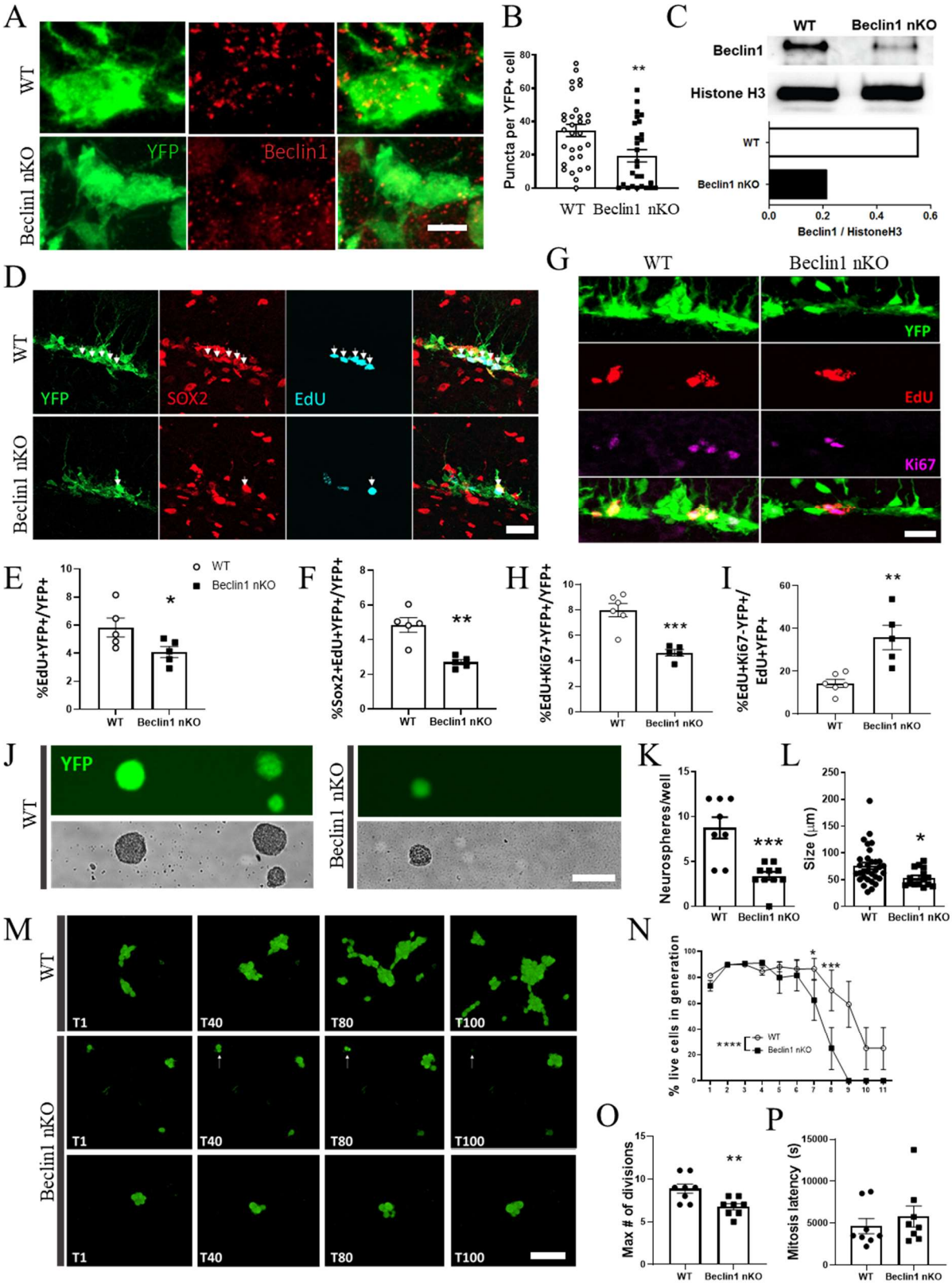

Figure 1. Removal of Beclin1 from adult NSPCs reduces proliferation *in vivo* and *ex vivo*. (A) Representative images and (B) quantification of Beclin1 protein puncta (red) in YFP+ showing a reduction in puncta in Beclin1 nKO mice. (C) Western blot analysis of Beclin1 protein, normalized by Histone H3 in pooled YFP+ cells, showing less Beclin1 protein in Beclin1 nKO mice. (D) Representative images and quantification of YFP+ (green) cells showing a reduction in (E) proliferating NSPCs (EdU+, blue), as well as proliferating NSCs (EdU+ Sox2+(red) in Beclin1 nKO mice. (G) Representative image and quantification (H, I) of YFP+ cells labeled with EdU (red) and Ki67 (violet) showing that of the total number of all YFP+ NSCPs there is a reduction in the (H) activity of cycling (EdU+,Ki67+) cells and (I) increase in cells exiting the cell cycle (EdU+Ki67-) in the Beclin1 nKO mice. (J) Representative images of YFP+ neurospheres (green, top) and brightfield images (bottom) of primary culture made from WT and Beclin1 nKO mice showing a significant reduction in (K) of total numbers of neurospheres per well, and (L) neurosphere size. (M) Representative images from live imaging showing cell division over time (T1-T100) with WT cells growing *in vitro* exponentially, while Beclin1 nKO cells undergoing cell death (white arrow, middle panel) and reduced expansion (lower panel). (N) Percentages of live cells generated via cell division across 11 generations in WT and Beclin1 nKO samples showing a significant drop in generation of cells in Beclin1 nKO samples after generation 6. (O) Beclin1 removal reduced the maximum number of NSPC divisions in the absence of (P) altering mitotic latency. Scale bars represent 5 uM (A), 20 uM (D), 20 uM (G), 100 uM (J), 100 uM (M); For all experiments mice were harvested at 14 dpi with the exception of C (harvested at 35 dpi); All graphed data show individual animals (B, E,F,H, I), or wells/neurospheres/cells (K, L, O, P) as well as the mean ± SEM, with the exception of pooled cell in C; data with 2 groups were analyzed

by unpaired t-test, with exception of (N) analyzed by 2-way repeated ANOVA; * $p \leq 0.05$, ** $p \leq 0.01$, *** $p \leq 0.001$, **** $p \leq 0.0001$.

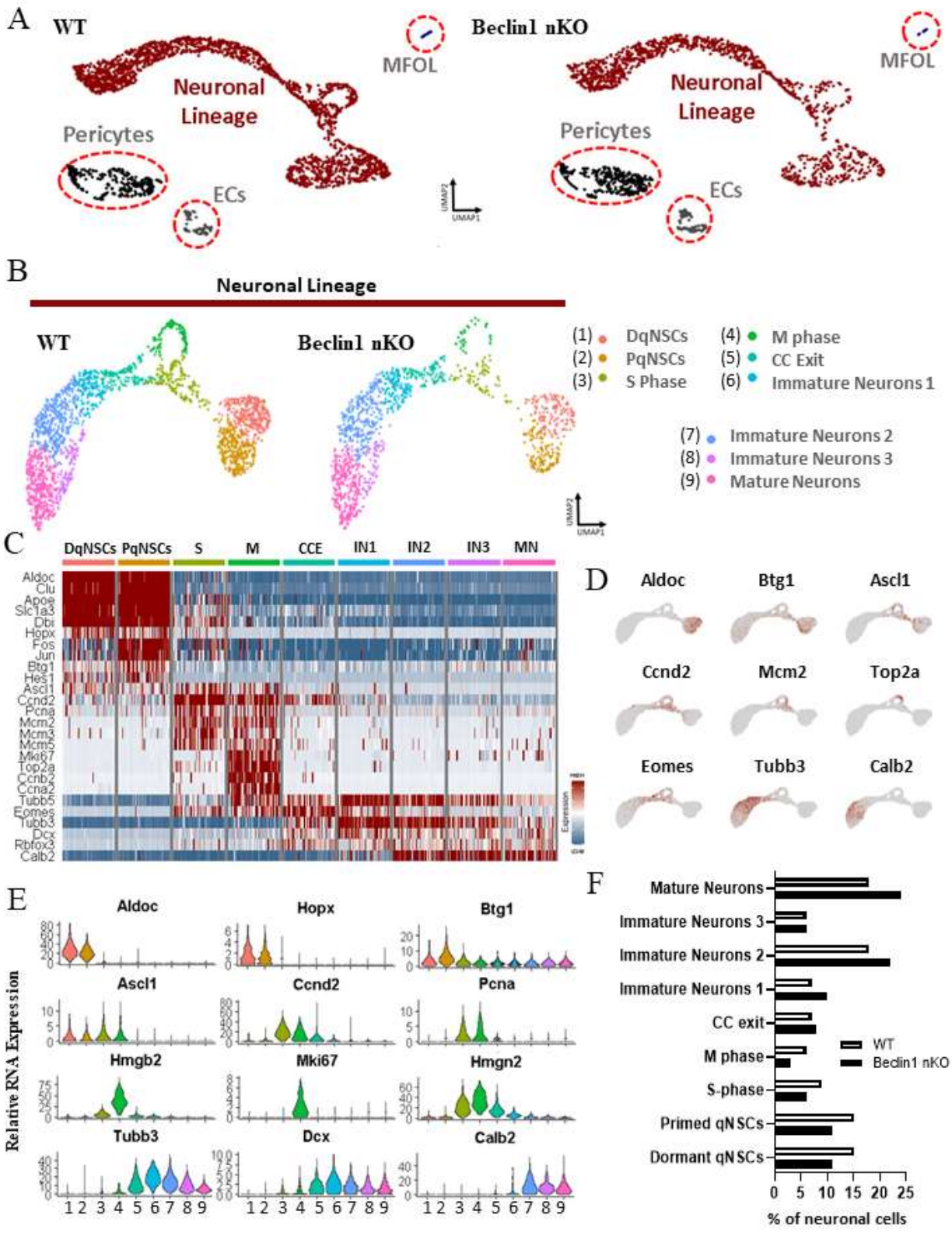

Figure 2. sc-RNAseq of WT and Beclin1 nKO mice highlights heterogeneous neurogenic

populations. (A) UMAP projection of WT and Beclin1 nKO sc-RNAseq samples generated from cells sorted at 14 dpi. (B) UMAP projection of the neuronal lineages without other cell types reveal clusters of dormant quiescent stem cells (DqNSCs), primed qNSCs (PqNSCs), S phase cells, M phase cells, cells exiting cell cycle (CC Exit), immature neurons 1-3, and mature neurons. (C) Heatmap of relative RNA expression of cluster markers within the neurogenic lineage shows high specificity of grouping by cell type and state (blue=low, red=high). (D) Examples of cell markers' expression shown in UMAP projections. (E) Violin plots of relative RNA expression of known markers used to identify different cell types showing Aldoc, Hopx, and Btg expression in dormant and primed qNSCs, Ascl1, Ccnd2, Pcna, Hmgb1, Mki67, Hmgn2 expression in proliferating stem and progenitor cells, and Tubb3, Dcx, and Calb 2 in immature and mature neurons. (F) Percentages of different cell clusters within the neuronal lineage of WT and Beclin1 nKO samples shows a decline in mitotic cells.

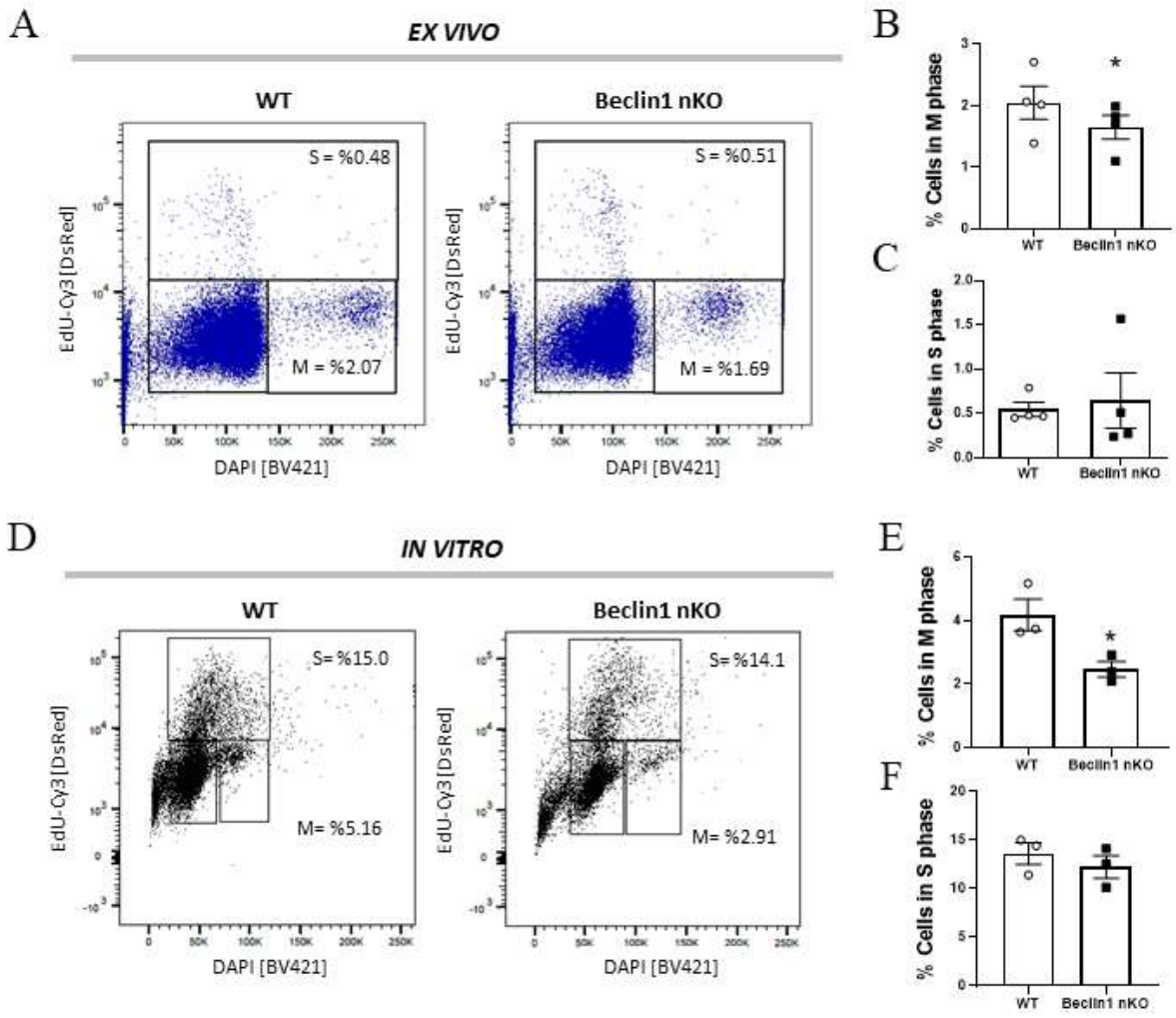

Figure 3. Removal of Beclin1 from adult Nestin NSPCs reduces their mitotic activity *ex vivo* and *in vitro*. (A) Representative images of gating of EdU+ cells in cell cycle flow cytometry graph of EdU-Cy3 (y-axis) and DAPI (x-axis) intensity in flow cytometry analysis of cells from WT and Beclin1 nKO mice shows (B) a significant reduction of the percentage of cells in M phase in Beclin1 mice, in the absence of change in the (C) percentage of cell in S phase. (D) Representative image of gating of EdU+ cells in cell cycle flow cytometry graph of EdU-Cy3 (y-axis) and DAPI (x-axis) intensity in neurospheres cultured from WT and Beclin1 nKO mice show (E) a significant reduction of the percentage of cells in M phase, in the absence of change in the (F) percentage of cell in S phase. Graphs show relative gene expression in 50 randomly selected cells from each cell

cluster (C), relative gene expression values across all individual cells (D), and the distribution of relative gene expression across all cells (E).

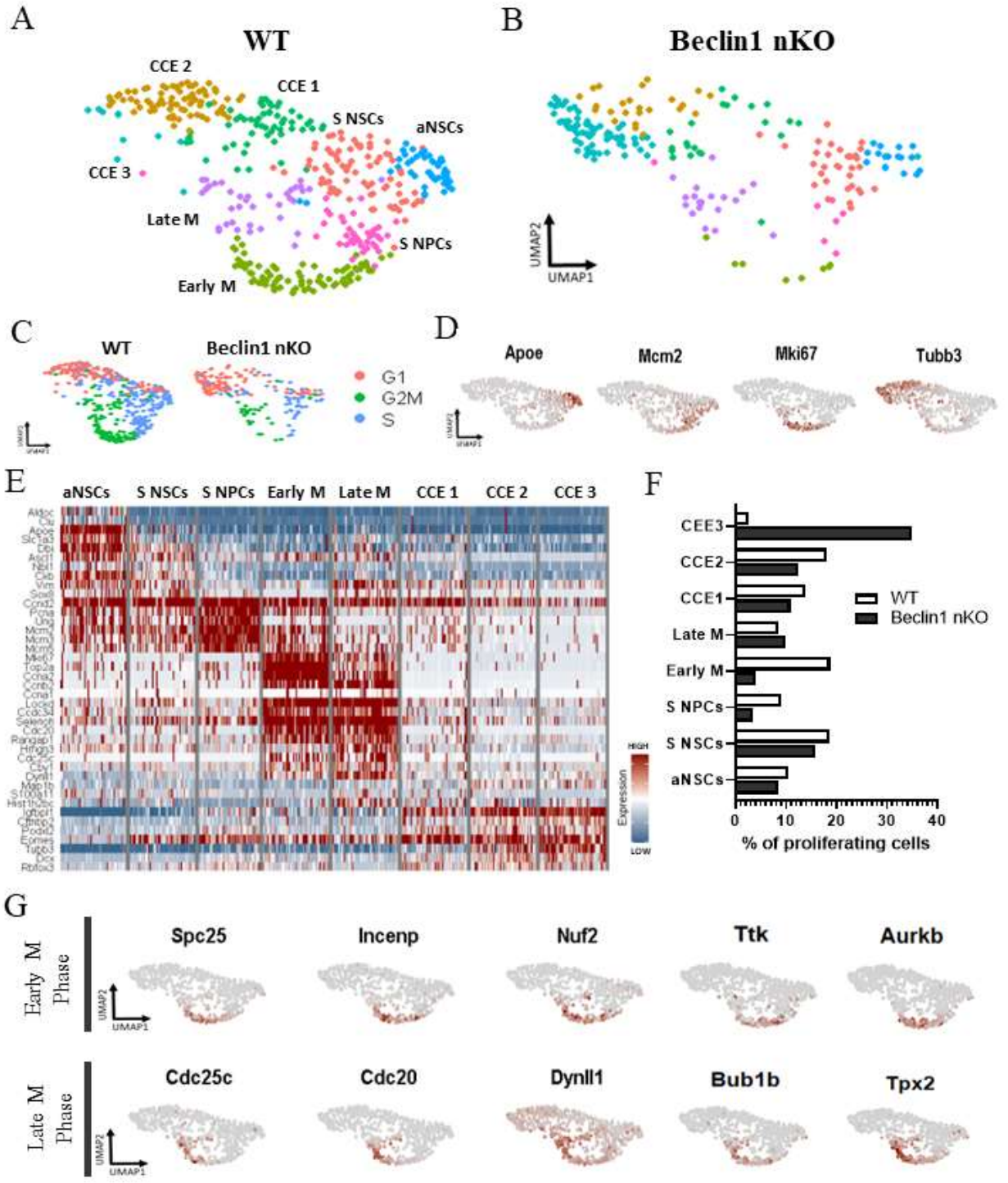

Figure 4. Examination of NSPCs supports differential effect of Beclin1 removal on cell cycle stages. (A, B) Cycling cells (S phase, M phase, and CC exit clusters) were selected for further identification of unique clusters shown in a UMAP projection, including active NSCs (aNSCs)

and S phase NSCs (S NSCs), S phase NPCs (S NPCs),G2 and early M phase cells (early M), late M phase (Late M) and cell cycle exit clusters 1-3 (CCE1-3). (C) UMAP projections of the clusters using cell cycle scoring of WT and Beclin1 nKO cells (S in blue, G2M in green, and G1 in red). (D) UMAP projections of marker RNA expressed in cycling cells with Apoe marking aNSCs, Mcm2 marking S phase, Mki67 marking G2M and Tubb3 marking cells exiting cell cycle. (E) Heatmap of relative RNA expression of genes marking the cell types and states (blue=low, red=high). (F) Percentages of different clusters within the WT and Beclin1 nKO samples. (G) UMAP projections of cycling cells from WT and Beclin1 nKO sc-RNAseq samples showing relative RNA expression of prophase/prometaphase (top) and metaphase/anaphase (bottom) genes.

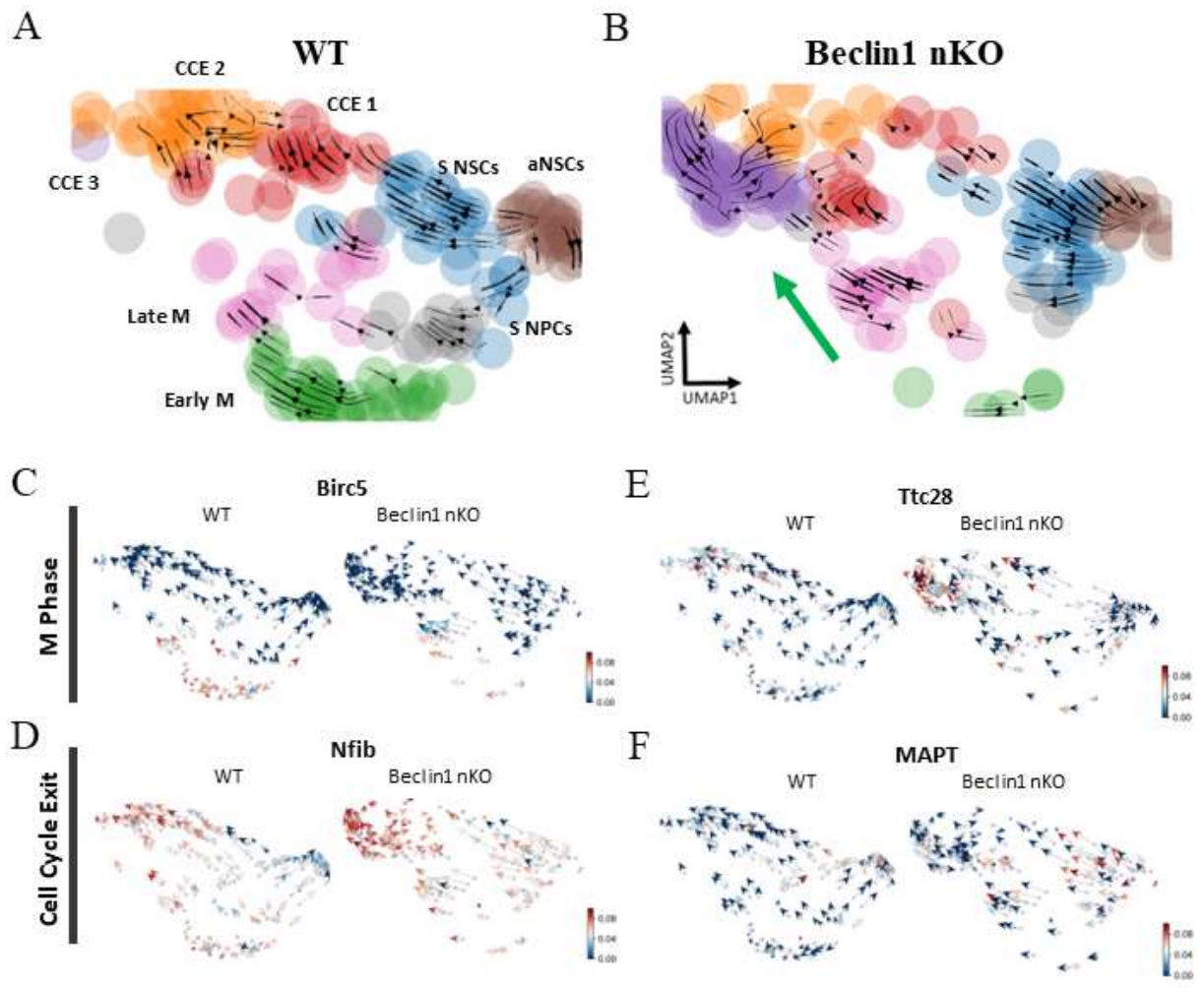

Figure 5. Velocity analysis of WT and Beclin1 nKO proliferating cells identifies differential transcriptional regulation during mitosis and CC exit. (A) WT and Beclin1 nKO cycling cell UMAP projections of cycling clusters with added RNA velocity vectors (black arrows) showing a high propensity of Beclin1 nKO mitotic cells toward exit into CCE3 cluster, while (B) mitotic WT cells show a differential trajectory of highly proliferative state toward CCE1/2 upon exit. M phase and CC exit cells demonstrate reduced transcriptional activity of (C) Birc5 (red arrows high activity, blue arrows low activity), and increased activity of (D) Nfib, (E) Ttc28, and (F) MAPT.

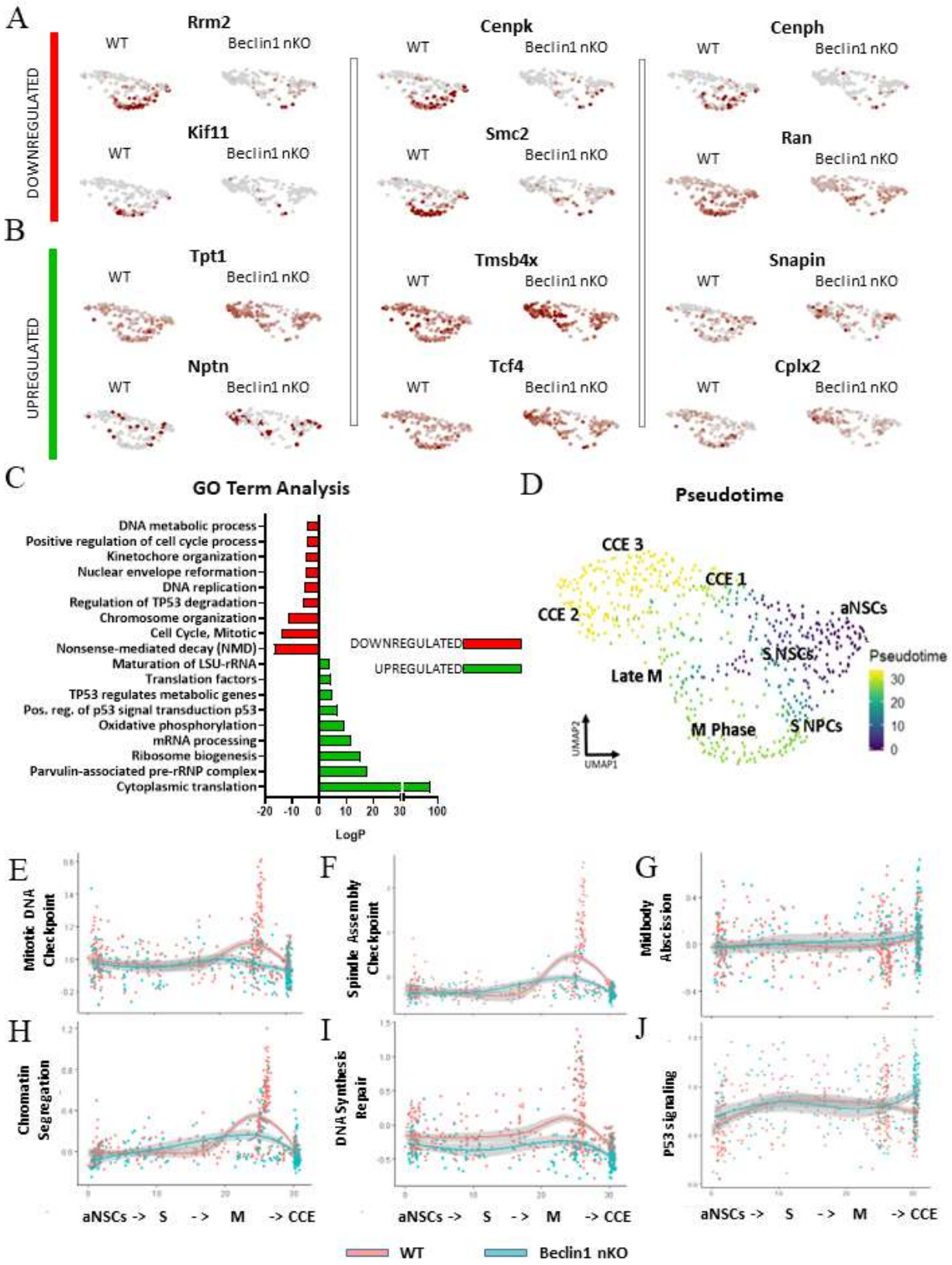
A
DOWNREGULATED
Rrm2
Cenpk
Cenph
Kif11
Smc2
Ran
WT
Beclin1 nKO
B
UPREGULATED
Tpt1
Tmsb4x
Snapin
Nptn
Tcf4
Cplx2
C
GO Term Analysis
DNA metabolic process
Positive regulation of cell cycle process
Kinetochore organization
Nuclear envelope reformation
DNA replication
Regulation of TP53 degradation
Chromosome organization
Cell Cycle, Mitotic
Nonsense-mediated decay (NMD)
Maturation of LSU-rRNA
Translation factors
TP53 regulates metabolic genes
Pos. reg. of p53 signal transduction p53
Oxidative phosphorylation
mRNA processing
Ribosome biogenesis
Parvulin-associated pre-rRNP complex
Cytoplasmic translation
DOWNREGULATED
UPREGULATED
-20 -10 0 10 20 30 100
LogP
D
Pseudotime
CCE 3
CCE 1
CCE 2
aNSCs
S NSCs
Late M
M Phase
S NPCs
Pseudotime
30
20
10
0
UMAP2
UMAP1
E
Mitotic DNA Checkpoint
F
Spindle Assembly Checkpoint
G
Midbody Abscission
H
Chromatin Segregation
I
DNA Synthesis Repair
J
P53 signaling
aNSCs -> S -> M -> CCE
WT
Beclin1 nKO

Figure 6. Beclin1-null NSPCs differentially downregulate mitotic maintenance genes and increase transcription of cell stress signatures. (A) WT and Beclin1 nKO cycling cell UMAP projections of relative RNA expression of genes downregulated in the Beclin1 nKO sample showing localization in mitotic cells. (B) WT and Beclin1 nKO cycling cell UMAP projections of relative RNA expression of genes upregulated in the Beclin1 nKO sample showing localization in cells exiting cell cycle. (C) Gene ontology analysis results shown as LogP values (LogP≥4) for processes upregulated (green) and downregulated (red) in Beclin1 nKO cycling cells. (D) UMAP projection of Pseudotime analysis of cycling WT and Beclin1 nKO cells showing a gradient from relative time 0 (indigo) to relative time 30 (yellow). Combined relative RNA expression of GO Terms along pseudotime showing cell pathways active in WT and Beclin1 nKO cell throughout cell cycle with reduction (E) mitotic DNA checkpoint and (F) spindle assembly checkpoint genes, with (G) no change in midbody abscission. Deficits were also observed in (H) chromatin segregation, (I) DNA synthesis repair, and (J) p53 signaling genes. Individual dots represent cells, lines represent mean calculated expression values for GO Term genes across pseudotime, filled gray line shows standard deviation.

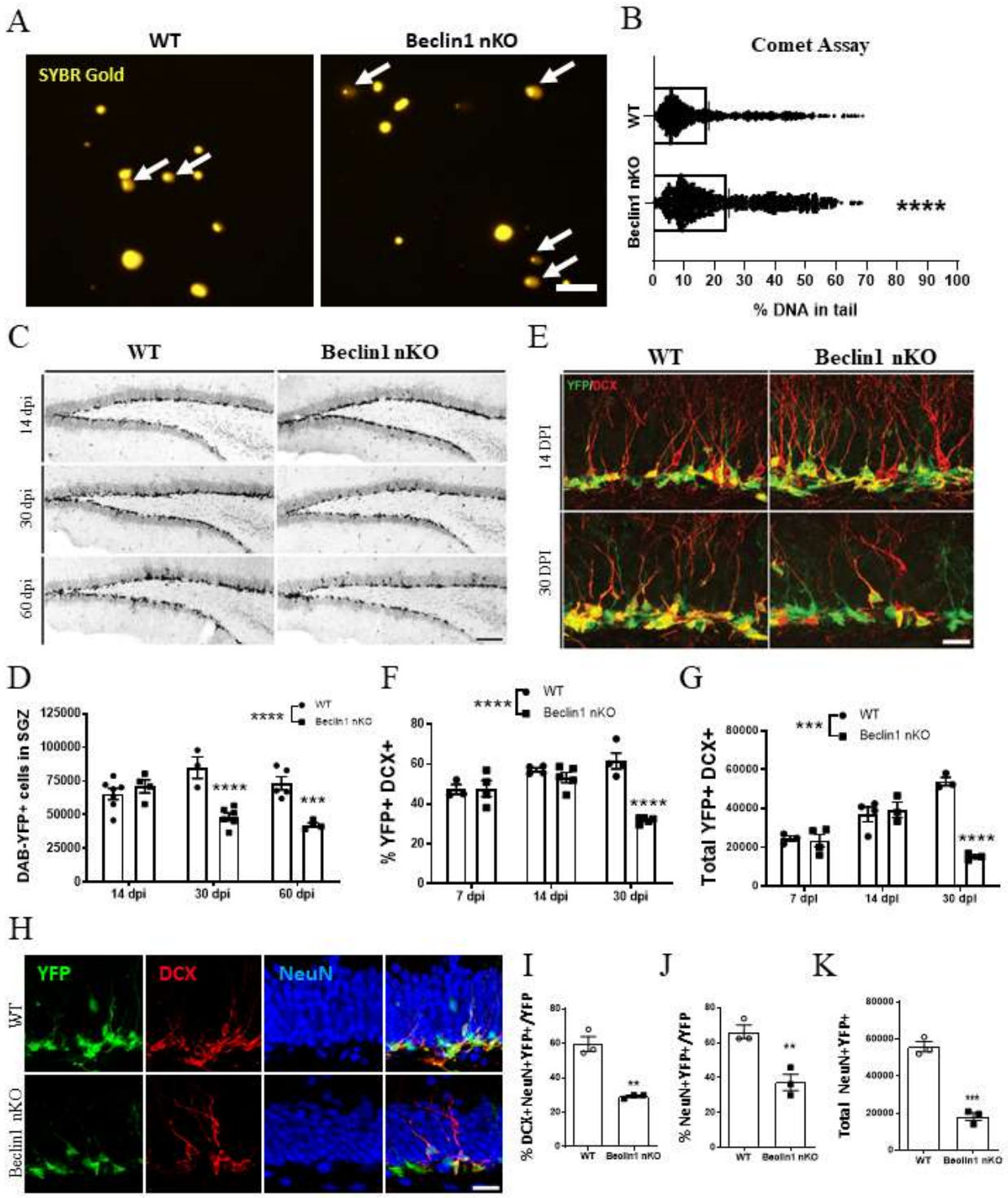

Figure 7. Beclin1 removal increases DNA damage, reduces hippocampal neurogenesis and survival. (A) Representative fluorescent images and quantification (B) of DNA damage visualized using SYBR-Gold (yellow) in WT and Beclin1 nKO recombined cells sorted at 14 dpi showing

fragmented DNA (A, white arrows) and (B) a significant increase of DNA tail percentage in Beclin1 nKO samples. (C) Representative DAB-YFP images and (D) quantification the YFP+ cells (black) in the dentate gyrus in WT and Beclin1 nKO mice showing a reduction YFP+ cells at 30 and 60 dpi (E) Representative images of the immature neuronal marker doublecortin (DCX, red) and YFP+ (green) cells shows a reduction in (F) percentage of YFP+ that expressed DCX and (G) total number of DCX+YFP+ neurons in the Beclin1 nKO mice at 30 dpi. (H) Representative images of the YFP (green), DCX (red) and mature neuronal marker (NeuN). blue) cells shows a reduction in the percentage of (I) maturing (DCX+NeuN+YFP+) and mature neurons (NeuN+,YFP+) as well as (K) total of mature neurons in Beclin1 nKO mice. Scale bars represent 20 uM (A); 500 uM (C), 25 uM (E), 25 uM (H); All graphed data show individual animals (D-G, I-K)), or cells (B), as well as the mean ± SEM; Data with 2 groups were analyzed by unpaired t-test, data with more then 2 groups were analyzed by a 2-way ANOVA; ** $p \leq 0.01$, *** $p \leq 0.001$, **** $p \leq 0.0001$.

STAR Methods

KEY RESOURCES TABLE

REAGENT or RESOURCE	SOURCE	IDENTIFIER
Antibodies		
Chicken Anti-GFP (1:5000)	Aves	GFP-1020
Living Colors Rabbit Anti-DsRed Polyclonal Antibody (1:500)	Clontech	632496
Goat Anti-Doublecortin (C-18) (1:500)	Santa Cruz	SC8066
Rabbit Anti-Ki67 Monoclonal Antibody (1:200)	Cell Marque	275R-14
Mouse anti-BM28 (Mcm2; 1:200)	BD Transduction Laboratories	610701
Mouse Anti-NeuN Clone A60 (1:500)	Millipore	MAB377
Rabbit anti-Aldolase C (1:1000)	Novus Biologicals	NBP1-90954
Goat anti-Sox2 (1:1000)	Neuromics	GT15098
Rabbit anti-Beclin1 (1:250)	Santa Cruz	SC11427
Biotin-SP-AffiniPure Donkey Anti-Chicken IgY (IgG) (1:200)	Jackson Laboratories	703-065-155

Biotin-SP-AffiniPure Donkey Anti-Rabbit IgG (1:200)	Jackson Laboratories	711-065-152
Biotin-SP-AffiniPure Donkey Anti-Goat IgG (1:200)	Jackson Laboratories	705-065-147
Alexa Fluor 488 AffiniPure F(ab')2 Fragment Donkey Anti-Chicken IgY (IgG) (H+L) (1:500)	Jackson Laboratories	703-546-155
Alexa Fluor 594 AffiniPure F(ab')2 Fragment Donkey Anti-Goat IgG (H+L) (1:500)	Jackson Laboratories	705-586-147
DyLight649 AffiniPure F(ab')2 Fragment Donkey Anti-Rabbit IgG (H+L) (1:500)	Jackson Laboratories	711-495-152
Alexa Fluor 647 AffiniPure F(ab')2 Fragment Donkey Anti-Goat IgG (H+L) (1:500)	Jackson Laboratories	705-606-147
Alexa Fluor 594 AffiniPure F(ab')2 Fragment Donkey Anti-Mouse IgG (H+L) (1:500)	Jackson Laboratories	715-586-150
Alexa Fluor 594 AffiniPure F(ab')2 Fragment Donkey Anti-Rabbit IgG (H+L) (1:500)	Jackson Laboratories	711-585-152
Cy3 AffiniPure F(ab')2 Fragment Donkey Anti-Mouse IgG (H+L) (1:500)	Jackson Laboratories	715-165150
Cy5 AffiniPure F(ab')2 Fragment Donkey Anti-Rabbit IgG (H+L) (1:500)	Jackson Laboratories	711-175-152
Chemicals, peptides, and recombinant proteins		
TrypLE Express	Gibco	12604021
Fixation Buffer	Biolegend	420801
Intracellular Staining Permeabilization Wash Buffer (10X)	Biolegend	421002
SYBR™ Gold Nucleic Acid Gel Stain	Invitrogen	S11494
Sulfo-Cyanine3 Azide	Lumiprobe	A1330
Sulfo-Cyanine5 Azide	Lumiprobe	A3330
5-Ethynyl-20-deoxyuridine	Santa Cruz	sc-284628
Tamoxifen	Sigma	T5648-5G
Sunflower seed oil from *Helianthus annuus*	Sigma	S5007-250ML
DMEM-F12 no phenol	Gibco	11039-021
DMEM-F12 with phenol	Gibco	11330032
Penicillin-streptomycin	Multicell	450-201-EL
Ply-d-lysine hydrobromide	Sigma	P0899-10MG
Percoll 100%	GE Healthcare Life Sciences	17-0891-02
Papain	Worthington Biochemical Corp.	LS003126
Fibroblast growth factor (FGF)	Sigma Aldrich	F0291-25UG
Epidermal growth factor (EGF)	Promega	39172901
B-27 Serum-Free Supplement (50X) (10ml)	Gibco	17504044
7-Amino-Actinomycin D (7AAD)	Sigma	A9400-1MG
Critical commercial assays		
Metal Enhanced DAB substrate kit	Thermo Scientific	34065
ABC elite kit	Vector Laboratories	PK-6100
Deposited data		
sc-RNAseq data	This study	GSE247493
Code to analyze sc-RNAseq data	This study	
Software and algorithms		

R software	R Core Team (2021)	
Python	Python Software Foundation	
Seurat	Stuart et al. (2019)[92]	
Monocle	Trapnell et al. (2014)[93]	
scVelo	Bergen et al. (2020)[94]	
FlowJo	Becton, Dickinson and Company	
Zen Blue/Black	GraphPad Software	
ImageJ/Fiji	ImageJ	
GraphPad Prizm	Zeiss group	
Columbus Image Data Storage and Analysis System	Perkin Elmer	

CONTACT FOR REAGENT AND RESOURCE SHARING

Further information and requests for resources and reagents should be directed to and will be fulfilled by the Lead Contact, Dr. Diane Lagace (dlagace@uottawa.ca).

EXPERIMENTAL MODEL AND METHOD DETAILS

Animals

Animal procedures were performed with approval from the University of Ottawa Animal Care Committee and adhered to the Guidelines of the Canadian Council on Animal Care. Beclin1 nestin-inducible knockout transgenic mice (Beclin1 nKO) were created by breeding using: inducible Nestin-CreERT2 mice[95] (line 4.1 obtained from Dr. Ryoichiro Kageyama, Kyoto University, Japan); floxed Beclin1 (fBeclin1) mice (obtained from Dr. Zhenyu Yue, Icahn School of Medicine at Mount Sinai, USA)[13]; and reporter R26R-enhanced Yellow Fluorescent Protein (YFP) mice[96] (Jackson Laboratory). These mice allow for the conditional removal of Beclin1 and expression of YFP from nestin- expressing stem and progenitor cells, as well as all of their progeny following injection of tamoxifen (TAM). Experimental Beclin1 nKO mice were NestinCreERT2^{het};RosaYFP$^{het;}$fBeclin1^{homo} and wild-type (WT) control mice were NestinCreERT2^{het};RosaYFP$^{het;}$fBeclin1^{WT}. Age-, sex- and littermate-matched Beclin1 nKO and

WT mice were randomly used as experimental mice based on their genotype. All strains were obtained and maintained on a C57bl/6J background. Animals were group housed in standard laboratory cages and kept on a 12-hour night/day cycle with ad libitum access to food and water.

Genotyping

Animals were genotyped at 3 weeks of age through DNA samples obtained from ear clippings (~1 mm^2). DNA was extracted using the HotSHOT methodology[97]. Briefly, ear clippings were incubated an Alkaline Lysis Buffer (25 nM NaOH and 0.2 mM Na2EDTA) at 95°C for 30 minutes prior to addition of the Neutralization Solution (40 mM Tris-HCl). Polymerase Chain Reaction (PCR) was completed using primers (Fig S5A) according to previously published protocols for fBeclin1[13], Nestin-CreERT2[95], and R26R-eYFP[96]. The resulting PCR products were resolved by size on a 1% agarose gel using electrophoresis. Size of the PCR products was visualized with ethidium bromide staining under ultraviolet light and estimated by comparison with a 100 base pair (bp) DNA ladder (DM001-R500M; Frogga Inc).

Tamoxifen Administration

Tamoxifen (TAM, T5648-5G; Sigma) was administered via intraperitoneal (IP) injection at a dosage of 160 mg/kg/day for 5 days (dissolved in 10% EtOH and 90% sunflower oil) to 4-8 week-old Beclin1 nKO and control mice, similar to previously published work[98]. For all experimental time points (7, 14, 30, and 60 days post injection of TAM) a minimum of 3 animals per genotype were analyzed.

EdU Administration

5-Ethynyl-2′-Deoxyuridine (EdU; sc-284628; Santa Cruz) was given to the mice through IP injection at a dosage of 50 mg/kg. Mice were injected with EdU four times two hours apart and perfused 8 or 24 hours after the first injection in order to obtain slices for immunohistochemistry (IHC). Similarly, for flow cytometry and cell cycle analyses, mice were injected with EdU four times two hours apart and tissue was harvested 24 hours after the first injection.

Preparation and Stereotaxic Surgical Injection of Retroviruses

To visualize the autolysosome within the brain, the mCherry-EGFP-LC3 retrovirus was created as we have published[14] using the mCherry-EGFP-LC3B plasmid (Addgene, Cambridge, MA, USA, 22418). The retrovirus (1.5µl volume) was injected bilaterally into the dentate gyrus of Beclin1 nKO or WT mice (7–9 weeks old) during stereotaxic surgery 3 days after TAM injections.

To visualize the survival of dividing progenitor cells the *GFP-Cre* and *RFP* retroviruses were created using the retroviral vectors *CAG-GFP-Cre* and *CAG-RFP* and corresponding packing envelopes, that were generously provided from Dr. Fred Gage (Salk Institute of Biological Science). Either *GFP-Cre* and *RFP* retroviruses in a 1:1 ratio mixture (volume 1.5 µl) or *GFP-Cre* (volume 1 µl) retrovirus were injected bilaterally into the dentate gyrus of 7-9 week old floxed Beclin1 (fBeclin1) (homo, or WT control) [13] mice using stereotaxic surgery. The viruses were created using a previously published protocol[99] with minor modifications. Briefly, 293T cells were plated ($8x10^6$ cells/150 mm) and co-transfected using polyethylenimine (PEI; 23966; Polyscience) with either the *CAG-GFP-Cre* or *CAG-RFP* retroviral plasmid combined with the *CMV-Gag-Pol* packing plasmid and *CMV-VSV-G* envelope plasmid in a 3:2:1 ratio, respectively. At 48 and 72 hours post-transfection the supernatant containing the virus was collected and concentrated by two rounds of ultracentrifugation (20,000 RPM for 2 hours at 4°C) with 20% sucrose cushion,

dissolved in phosphate buffered saline (PBS). Virus titre was determined by live tittering through infection of 293T cells plated in a 24-well plate (1.25 x 10^5 cells) with 100 µl of diluted (10^4 dilution) virus. Fluorescence-positive cells were quantified 48 hours post-infection and the number of infectious units (IU) per ml was calculated as the mean of the product of the number of infected cells per viewing field, the well area (243.22 mm2), and the dilution factor (104). Virus titre was approximately 6.7 x 10^8 IU/ml for the *GFP-Cre* virus and 1.7 x 10^9 IU/ml for the *RFP* virus.

During stereotaxic injection, the mice were anesthetized throughout surgery with 2% isoflurane. Viral injections were performed by microinjection using a 33 gauge (0.21 mm diameter) needle (7803-05; Hamilton), into the dentate gyrus using coordinates of -1.7 mm rostrocaudal and ±1.2 mm mediolateral from bregma, and -2.4 mm dorsoventral form the skull surface. The virus was injected using a Nanomite Pump 11 Elite (704507; Harvard Apparatus) at a rate of 0.2 µl/min and the needle was removed 5 minutes after the injection was complete in order to prevent backflow. Post-operation recovery from anesthesia occurred in a 37°C incubator until mice were awake and responsive. Buprenorphine was given to the mice as an analgesic (0.05 mg/kg, subcutaneous injection) one hour before surgery, as well as 6 and 12 hours after viral injection. The mice were sacrificed and perfused at 17 days after viral injection of the mCherry-EGFP-LC3, and after 14, 30, or 60 days after dual *GFP-Cre:RFP* retrovirus delivery.

Western Blot

Tissue from Beclin1 nKO or WT mice were dissected 35 days after Tam treatment. In order to harvest a higher number of cells for proteins lysates the tissue was dissected from adult subventricular zone which contains more YFP+ cells compared to the SGZ[100,101], cells were then incubated in a digestion media containing DMEM/F12 (11039-021; Invitrogen), 1.2 mM EDTA

(E5134-1KG; Sigma), and 20 U/ml papain (LS003126; Worthington Biochemical) at 37°C for 30 min. Cells were triturated followed by centrifugation to obtain a cell pellet that was suspended in media containing DMEM/F12 and 10% Fetal Bovine Serum (FBS; SH3039603; HyClone) to inactivate papain. YFP+ and YFP- cells negative for 7-AAD were then sorted using MoFlo Astriosis (Beckman Coulter). Sorted YFP+ and YFP- cells were lysed in 8 mM urea with 10% sodium dodecyl sulfate (SDS). The lysed samples were mixed with an equal volume of laemmli loading buffer with 10% b-mercaptoethanol, boiled at 95°C, vortexed, and loaded onto a 12% acrylamide gel. The gel was immersed in 1X tris/glycine/SDS (TGS) running buffer and run at 110V for 1.5 hours for optimal band separation. Bands were transferred to a nitrocellulose membrane via a wet transfer in cold 1X Tris/Glycine transfer buffer containing 20% methanol for 1 hour at 110V. The nitrocellulose member was cut into two for detection of Beclin1 (60 kDa) and HistoneH3 (18 kDa). The blots were incubated for 1 hour at room temperature (RT) in a blocking solution containing 5% non-fat dried milk in 1X TBS-T (0.1% Tween-20 in 1X TBS) followed by incubation in blocking solution containing either the primary antibody for Beclin1 (1:1000; sc11427; Santa Cruz) or HistoneH3 (1:1000, ab1791, Abcam) overnight at 4°C. The following day at RT the blots were washed with TBS-T and incubated for 1 hour in blocking solution containing corresponding horseradish peroxidase conjugated secondary antibodies (1:5000). After secondary incubation, the blots were washed in TBS-T incubated in ECL Pierce for 5 minutes to allow chemiluminescence detection. The blot was imaged using a Fuji LAS-4000mini chemiluminescence imager (Thermo Fisher Scientific) and densitometry was performed using Fiji image processing software (ImageJ) to determine relative amounts of protein.

Perfusions and Tissue Collection

Mice were anesthetized with euthanyl (90 mg/kg) and transcardially perfused with cold 1X phosphate buffer solution (PBS, pH 7.4) for 6 minutes and subsequently cold 4% paraformaldehyde (PFA) in 1X PBS (pH 7.4) for 15 minutes at a rate of 7 ml/minute. Brains were removed and postfixed in 4% PFA for 1 hour and then transferred to 30% sucrose in 1X PBS for cryoprotection. Brains were coronally sectioned into 25 or 30 μm slices with a freezing microtome (Leica SM 2000R, Leica Microsystems) and stored in PBS with 0.1% sodium azide.

Antibodies and Immunohistochemistry (IHC)

All primary and secondary antibodies as well as their concentrations used for immunohistochemistry (IHC) are listed in STAR methods table. Notably, a Green Fluorescent Protein (GFP) primary chicken antibody was used to detect both YFP immunoreactive (YFP+) cells in the Beclin1 nKO mice, and GFP-Cre (GFP+) cells in the virally injected fBeclin1 mice.

Slide-mounted IHC was used to detect the total number of YFP+ cells, DCX+ cells, and Ki67+ cells within the SGZ using previously published protocols [98,102]. Briefly, every ninth section through the mouse hippocampus was mounted onto charged slides and allowed to dry overnight. Slides were then pre-treated to enhance antigen retrieval with 0.1M citric acid (pH 6.0) at approximately 95°C for 15 minutes, rinsed in 1X tris-buffer saline (TBS), incubated at RT in 0.1% trypsin for 10 minutes, rinsed in 1X TBS and then incubated with 2N hydrochloric acid (HCl) at RT for 30 minutes. To prevent non-specific binding, the slides were incubated in 3% Normal Donkey Serum (NDS; 017-000-121; Jackson Immuno Research Laboratories Inc) in 0.3% Triton X-100 in 1X TBS for 60 minutes. Sections were then incubated overnight in the primary antibody in 3% NDS in 0.3% Tween20 and 1X TBS. The following day, slides were incubated at RT in: 1) biotinylated attached secondary antibodies in 1.5% NDS in 1X TBS for 60 minutes; 2) 0.3% H2O2

in 1X TBS for 30 minutes to quench endogenous peroxidases; 3) Avidin-Biotin Complex Solution (ABC; PK-6100; Vector Laboratories) for 90 minutes; 4) metal enhanced 3,3'-Diaminobenzidine (1:10, DAB; 34065; Thermo Scientific,) for 10-30 minutes; and 5) fast red nuclear stain (H3403; Vector) to provide a nuclear counterstain. Between all steps, with the exception of after blocking with NDS, the slides were rinsed 3x with 1X TBS. Following staining, slides were dehydrated by consecutively immersing slides in 95% and 100% ethanol for 20 seconds, followed by CitriSolv clearing agent (22-143-975; Fisher) for 20 seconds, 1 minutes, and 5 minutes. Slides were cover-slipped with DPX mounting medium (mixture of Distyrene, Plasticizer, Xylene; 44581; Sigma).

All IHC for the co-labelling of more than one marker was completed using free-floating fluorescent IHC similarly to previously published methods by our laboratory [98,102]. Briefly, sections were washed with 1X PBS three times, and were incubated in a carrier solution (1X PBS, 0.1% TritonX-100, 0.1% Tween20) on a shaker overnight with primary antibody at 4°C, with the exception for staining for Beclin1 protein which used an incubation of 48 hrs. The following day, the sections were incubated at RT in fluorophore-conjugated secondary antibody for 1 hour in carrier solution, washed in 1X PBS. Section being processed for EdU staining were additionally incubated after the secondary antibody in an EdU-staining cocktail containing 1M Tris (pH = 8.5), 200 mM CuSO4*H2O, 4mM of sulfo-Cyanine azide (A3330, A1330; Lumiprobe), and 1M of sodium ascorbate in water for 30 minutes. All sections were counterstained with 4’,6-diamidino-2-phenylindole (1:10000, DAPI; 11836170001; Roche) and the sections were slide mounted and cover-slipped with Immumount mounting media (2860060; Fisher Scientific).

Microscopy and Cellular Quantification

Counts for the number DAB+ cells or immunoreactive fluorescent cells in the SGZ were performed at 40x magnification using an Olympus BX51 fluorescent microscope. Manual counting was completed exhaustively through the SGZ by a blinded experimenter in every 9th section of the hippocampus as previously published[98,102]. Final counts were estimated for the whole SGZ by taking the manual count multiplied by 9, or expressed as a ration of dual-labelled GFP+RFP+ cells over total RFP+ as previously published[99]. Quantification was further verified by an additional blinded experimenter that confirmed less than 10% variation in a minimum of 2 independent animals.

For quantification of the mCherry+ autolysosomes, the YFP+ Beclin1-null or WT cells in the SGZ were imaged with a 63x oil immersion lens with a Zeiss LSM800 AxioObserverZ1 mot Confocal Microscope at emission wavelengths of 517 and 561nm. Autolysosomes were blindly and manually quantified in every YFP+ cell within the section analyzed. Autolysosomes were counted in the cell body and cell processes using ZEN 2012 Blue (Zeiss) image processing software. In order to be counted autolysosomes had to be mCherry+ (red), be circular in shape, and be larger than any observed specs in the background. Quantification was verified by an additional blinded experimenter that confirmed less than 10% variation in 2 independent counts.

For quantification of single- and co-labeled florescent immunoreactive cells was done through imaging the DG at 40x (oil immersion) from bregma matched (positions around -2.06 to -2.30) using either coronal half-brain or full-brain sections. Images were obtained using either a 1) Zeiss LSM 510-META confocal microscope at emission wavelengths of 405, 488, 543, and 633 using either 20x, 0.8 NA, Air, Plan-Apo (DIC II) or 40x, 1.3 NA, Oil, EC Plan-Neofluar (DIC III) objectives; or 2) a Zeiss LSM800 AxioObserverZ1 mot confocal microscope (Zeiss) at emission wavelengths of 405, 488, 561, and 640nm using either 20x, 0.8 NA, Air, Plan-Apo or 40x, 1.3 NA,

Oil, Plan-Apo objectives. ZEN acquisition software (Zeiss) was used for 1-2 μm optical sectioning in the Z-plane. Both single- and co-labeled cells were quantified manually from images visualized through Fiji image processing software (ImageJ) and ZEN Blue (Zeiss) image processing software. The total population of YFP+ cells that co-labeled with another marker was calculated as the product of the absolute YFP counts and the proportion co-labeled per animal.

For quantification of the Beclin1-positive puncta at 14 dpi, the YFP+ Beclin1-null or WT cells in the SGZ were imaged using the Zeiss LSM800 AxioObserverZ1 mot Confocal Microscope at emission wavelengths of 405, 488, and 640nm was used with 63x, 1.4 NA, Oil, Plan-Apo objective and optical sectioning of 0.5 μm in the Z-plane and 16x binning. Images were processed in ZEN Blue (Zeiss) image processing software for single-pixel filtering, and median correction.

For quantification of the spine density in the GFP and RFP co-labeled virally infected cells, the sections were imaged at 63x (oil immersion) with a Quorum Spinning-disk confocal microscope at emission wavelengths of 406, 490, and 561. MetaMorph automation and image acquisition software (Molecular Devices) was used to create a high resolution three-dimensional representation of spines throughout the visible dendritic arbor using 0.5 μm Z-plane optical sectioning in combination with a tile-scan module. Images were subsequently stitched and flattened in MetaMorph and exported to NeuroStudio (CNIC, Ichan School of Medicine at Mount Sinai) to measure neurite length. Spines were manually quantified from a single neurite that spanned the hippocampal molecular layer (top of the granule cell layer to the hippocampal fissure) per cell in Fiji image processing software (ImageJ). Spine density (spines/10 μm) was calculated as the quotient of the number of spines over neurite length multiplied by 10 (methods adapted from Zhao et al.[103])

Neurosphere Culture

For all *in vitro* and *ex vivo* analyses of the DG previously published protocols[104,105] were used to dissect the SGZ from mice 14 days after TAM injections. For neurosphere assay[106,107], the mice were anesthetized with euthanyl (90 mg/kg), decapitated, and their brains were removed and placed in slushy sterile filtered Artificial Cerebrospinal Fluid (aCSF, pH =7.4), consisting of (in mM): 124 NaCl, 5 KCl, 1.3 MgCl2·6H2O, 2 CaCl2·2H2O, 26 NaHCO3, and 1X penicillin-streptomycin (10,000 U/mL; 450-201-EL; Multicell). The dentate gyrus of both hemispheres was dissected out of the brain and placed in aCSF. The tissue was gently broken up with sterile scissors. Tissue was incubated on a thermomixer (30 minutes, 37ºC) in 500 uL/tube of digestion media, containing DMEM/F12 (11039-021; Invitrogen), 1.2 mM EDTA (E5134-1KG; Sigma), and 20 U/ml papain (LS003126; Worthington Biochemical) at 37°C for 30 min. Cells were triturated followed by centrifugation to obtain a cell pellet that was suspended and washed in DMEM/F12 media. Suspension was then transferred in Percoll media, consisting of 19.8% Percoll (17-0891-02; GE Healthcare Life Sciences), 2.2% 10xPBS (311-012-CL; Multicell) and spun down (500 x g, 13 minutes, RT). Cells were again washed with DMEM/F12 and quantified using Countess II (Invitrogen) cell counting charged slides by reconstituting cell suspension with trypan blue at a ratio of 1:1. Cells were then seeded at 20k cells/1ml with growth media containing DMEM/F12, 1X B-27 supplement (17504044; Gibco), 1X Penicillin-Streptomycin, Heparin (H3149-25KU; Sigma), 200 ng/µl of Epidermal Growth Factor (EGF; 39172901; Promega), and 100 ng/µl of Fibroblast Growth Factor (FGF; F0291-25UG; Sigma Aldrich). Neurospheres were quantified live under an inverted Zeiss AxioObserver D1 microscope (Zeiss) using 20x, 0.80 NA, Air, Plan Apochromat (DIC II) objective and AxioCam MRm CCD as a total number of spheres per well and size was calculated using AxioVision 4.8 (Zeiss).

Live *in vitro* imaging

The cells used to perform using live in vitro image were removed, digested, and processed from the Beclin1 nKO and WT mice as described using the same protocol as listed above for the neurosphere assay up to the stage of cell quantification using the Countess II. After counting, for *in vitro* imaging the cells were seeded at a concentration of 40k/ml into 96-well PhenoPlates (6055302, PerkinElmer Health Sciences Canada Inc) pre-coated with Poly-D-lysine hydrobromide (P0899-10MG; Sigma), and cultured in an incubator for 5 days. On day 5 of culture the plate was sealed with Axygen™ Microplate Sealing film (14-222-346, Corning) and imaged using the OperaPhenix Live imaging System (PerkinElmer). The imaging of YFP+ cells occurred at 488 nm every 30 min for 4 days. The data was then analyzed using Harmony's Columbus software with capability to test progeny of the dividing YFP+ cells. Generation information was collected using Columbus' division tracking. Cells dead after division were defined as cells that start with a "split", "cosmos", "merge", or "border" fate and recorded as "cosmos" at the end of their tracking. Cells that were defined as live after division start with "split", "cosmos", "merge", or "border" and end with "split" or "end" at the end of their tracking. In order to calculate latency to mitosis, cells with "split"-"split" fate were considered. To calculate latency to apoptosis, all cells with "cosmos" end fate were considered. Percentages of different groups of cells were calculated and analyzed.

Cell Cycle Flow Cytometry

For *in vivo* cell cycle analysis, 14 dpi WT and Beclin1 nKO mice were injected with EdU four times two hours apart and dentate gyrus was extracted and digested as described above 24 hours after the first injection. After digestion, enzymatic activity was neutralized with media containing DMEM/F12 and 10% Fetal Bovine Serum (FBS; SH3039603; HyClone) and cells were washed

with additional DMEM/F12 to remove excess FBS. The cell suspension was transferred in Percoll media, consisting of 19.8% Percoll (17-0891-02; GE Healthcare Life Sciences), 2.2% 10xPBS (Multicell) and the cells were spun down (500 x g, 12.5 minutes, 4ºC). The cells were re-suspended in 200µL of DMEM:F12 media and counted with trypan blue. The cells were then fixed in a PFA-containing buffer (420801; BioLegend) for 20 min in dark at RT, permeabilized by spinning in 1x wash buffer (421002; Biolegend) twice for 10 min, and passed through 40 µm cell strainer (08-771-1, Fisher). Beclin1 nKO and WT cells were then stained for 20 min in dark with EdU cocktail prepared as described above. The sections were then washed, and resuspended in DAPI/1xPBS. The cells were then accessed using a Fortessa (Beckman Coulter) flow cytometer at 405 nm and 561 nm lasers for DAPI, and EdU-Cy3, respectively.

For *in vitro* cell cycle assessment of WT and Beclin1 nKO cells, neurosphere cultures were prepared as described above. On day 10-12 of culture, EdU was added to culture media at a concentration of 10mM and incubated at 37ºC for 4 hours. Spheres were then dissociated via incubation in TrypLE (12604-013; Gibco) at 37°C followed by trituration. The cells were washed once with phenol-free DMEM-F12 and counted with trypan blue. The cells were then fixed in a PFA-containing buffer (420801; BioLegend) for 20 min in dark at RT, permeabilized by spinning in 1x wash buffer (421002; Biolegend) twice for 10 min, and passed through 40 µm cell strainer (08-771-1; Fisher). Cells were then stained for 20 min in dark with EdU cocktail prepared as described above, washed, and resuspended in DAPI/1xPBS. The cells were then accessed using a Fortessa (Beckman Coulter) flow cytometer at 405 nm and 561 nm lasers for DAPI and EdU-Cy3, respectively.

All visualization and cell counting of flow cytometry data was performed using FlowJo10 and 11 (BD). Values obtained from different experiments using FlowJo were used in t-test with Prism 6.0 (GraphPad).

Single-cell Isolation and Library Preparation

Beclin1 WT and nKO mice were deeply anesthetized and dentate gyrus was extracted and digested as described above. After digestion, cells were washed with media containing DMEM/F12 and 10% Fetal Bovine Serum (FBS; SH3039603; HyClone) to neutralize further enzymatic digestion, then washed with additional DMEM/F12 to remove excess FBS. The cells were transferred in Percoll media, consisting of 19.8% Percoll (17-0891-02; GE Healthcare Life Sciences), 2.2% 10xPBS (Multicell) and spun down (500 x g, 12.5 minutes, 4^{o}C). The cells were re-suspended in 200µL of DMEM:F12 media with 7AAD at a concentration of 50uL/10^6 cells and transferred to the cell sorter on ice. Approximately 60k WT and 40k Beclin1-null YFP+ cells negative for dead marker 7AAD were sorted using a MoFlo Astriosis cell sorter (Beckman Coulter) into DMEM-F12, spun down to concentrate the pellet, resuspended and counted on a Countess Cell Counter. Cells were sequenced by 10x genomics using Chromium's Single Cell 3` v2 chemistry kit. The cDNA libraries were purified, quantified, and then sequenced on the next generation sequencing Illumina NextSeq 500 platform.

Cell Clustering, Visualization, Differential Gene Expression and Go Term Analyses

Prior to data analysis, low quality cells were stringently filtered out based on percentage of mitochondrial genes (<6%), detected RNA counts (500-10,000), and detected RNA features (i.e., genes, 500-3,500). Addition, cells with a high microglial signature of *Fcer1g* (<0.01) and *Csf1r* (<0.001) gene expression were also filtered out. For unsupervised data clustering we used Satija's

R package Seurat v4.0 [92]. WT and Beclin1 nKO samples were merged, split, and SCTransformed. Integration features and anchors were then calculated, and samples were combined for an integrated analysis. Principle component analysis (PCA) was performed and the first 10 PCs were used for Uniform Manifold Approximation and Projection (UMAP) and cluster finding at a clustering resolution of 0.8. After the removal of pericytes, oligodendrocytes, and endothelial cells principal components were calculated again, and reduction was performed on the first 20 components and clustered at a resolution of 0.8. For later analyses on the proliferating clusters, similar steps were performed but increasing the number of PCAs to 30 and clustering resolution to 1.2. Differentially expressed genes (DEGs) were found for the proliferating clusters (adjusted p value < 0.05 and more than 1.5-fold change or p value < 0.05) and the full list is shown in supplementary Table S2.

For GO Term analysis of gross lists of DEGs, DEGs were split into upregulated and downregulated first. The lists were then fed to an online Metascape (metascape.org) for mouse species and resulting GO Terms with LogP>4 are shown in ?.

Analysis of Cell Trajectories and Lineage-driving Transcriptional Regulators

For Pseudotime analysis, Trapnell's Monocle[93] R package was used to pseudotemporally order the cycling clusters, which included aNSCs, S-phase NSCs and NPCs, mitotic cells and cells exiting the cell cycle (CCE1-3). Monocle's differential gene test was also used to confirm DEGs obtained using Seurat. The cells were classified based on expression of quiescence gene *Aldoc* (≥1.5), proliferation genes *Mki67* (>1) and Dynll1 (≥10), and differentiation-related gene *Tubb3* (≥5). Pseudotemporal metadata was then transferred to the original Seurat object to maintain consistent clustering of cycling cell populations. To order cells along the continuum with calculated GO Term

scores for different pathways, first gene sets were obtained from the Mouse Gene Informatics (MGI, informatics.jax.org) using the Gene Ontology browser. GO Term scores were then calculated and added to Seurat metadata, and used along with the pseudotime continuum to determine the timing of activation/expression within the cycling cells.

In order to identify fate trajectories of proliferating neural stem and progenitor cells, single cell RNA velocities were calculated for WT and Beclin1 nKO samples using Bergen's scVelo [94]. Briefly, seurat object containing cycling cells was split into WT and Beclin1 nKO and each processed separately in scVelo using identical code. Spliced and unspliced counts were used to determine RNA velocity and construct cell fate vectors using a dynamical velocity model. Latent time of cell processes was quantified per each cell cluster allowing to determine 100 cluster-specific top-likelihood driver genes that were obtained for WT and Beclin1 nKO. The resulting gene sets were compared to determine the number of same and unique genes regulating WT and Beclin1 nKO cell cycle progression and exit.

Comet Assay

For assessment of DNA damage, dissociated DG cells were sorted from WT and Beclin1 nKO mice at 14 dpi using a Beckman MoFlo Astriosis (Beckman Coulter Canada) for YFP positivity (488-526 nm) and for 7-AAD negativity (571-640nm). Alkaline comet assay was performed according to previously published methods with modifications [74]. Briefly, frosted slides were pre-coated with normal melting point agarose (1% in 1xTBE), dried, and stored at 4°C. 1x TBE (Tris, borate, and EDTA buffer) was cooled before use and kept on ice. Alkaline electrophoresis buffer (300 mM NaOH, 1 mM EDTA, pH>13) was made fresh and cooled before use. On the day of comet assay, low melting point agarose was dissolved in 1xTBE to a final of 1% and kept in 37°C

water bath until use. Sorted cells at a concentration of 10^6 were combined with low melting point agarose as a ratio of 1:10 and applied to pre-coated slides. Cold lysis solution (R&D) was applied to slides and left at 4ºC overnight. Slides were washed with 1x TBE and placed into cold electrophoresis buffer for 30 min to unwind DNA. The current was then applied to slides for 30 min at 1.87 V/cm on ice. Slides were washed and stained with Sybr Gold (S11494; Invitrogen) in 1X PBS for 20 min, partially dried, coverslipped with ImmuMount, and stored flat at 4ºC until imaging. The slides were imaged at 20x on an Olympus BX51 epifluorescent microscope at 561 nm. For comet tail analysis, profile analysis was used in OpenComet plugin in ImageJ with no background correction. Extremely dim cells and cells with percent of DNA in tail higher than 70% were excluded from the analysis.

QUANTIFICATION AND STATISTICAL ANALYSIS

All outcomes are reported as mean ± standard error of the mean (SEM) and were calculated and statistically analyzed using Prism 6.0 (GraphPad). Experiments with two groups were analyzed by a two-tailed student's t-test. Statistical analysis of three or more groups was performed using an ANOVA test, followed by a Bonferroni post hoc. Statistical significance was defined as $p < 0.05$.

DATA AND SOFTWARE AVAILABILITY

All the scRNA-seq data have been deposited in the NCBI Gene Expression Omnibus (GEO) under accession number GEO: GSE247493.

Supplemental Information

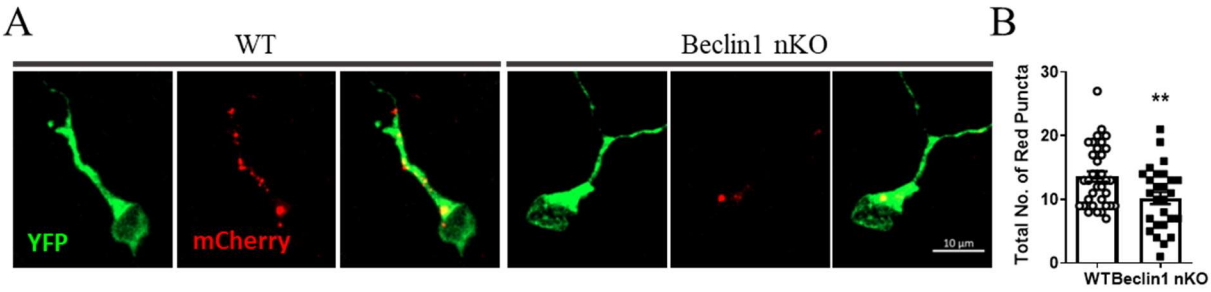

Figure S1. Retroviral assessment of autolysosomes of Beclin1 nKO mice shows reduced autophagy. (A) Representative images of mCherry+ autolysosomes (red) in WT and Beclin1-null YFP+ (green) retrovirally infected cells.. (G) Beclin1 removal is associated with a reduced total number of mCherry+ puncta per cell (mean ± SEM, unpaired t-test). Scale bar represents 5 uM (A); ** $p \leq 0.01$.

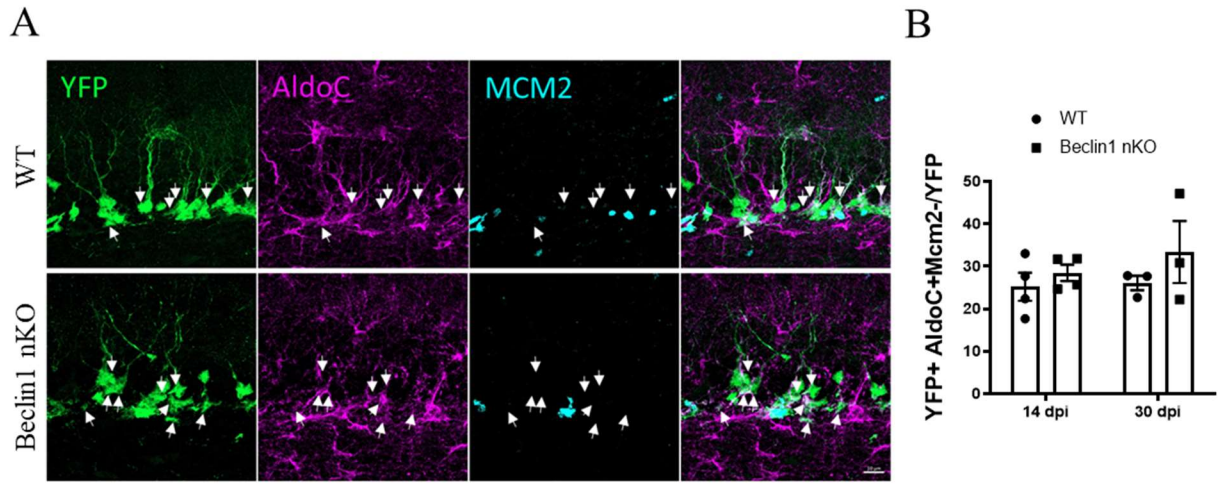

Figure S2. Quantification of quiescent NSCs in WT and Beclin1 nKO mice shows no change. (A) Co-labeling of AldoC (violet) and Mcm2 (blue) with YFP+ (green) recombined WT and Beclin1 nKO in dentate gyrus at 14 dpi shows no change in quiescent NSCs positive for Aldoc and negative for Mcm2 in slices. (B) Removal of Beclin1 resulted in no change in the percentage of YFP+Aldoc+Mcm2- qNSCs at 14 or 30 dpi (mean ± SEM, 2-way ANOVA). Scale bar represents 10 uM.

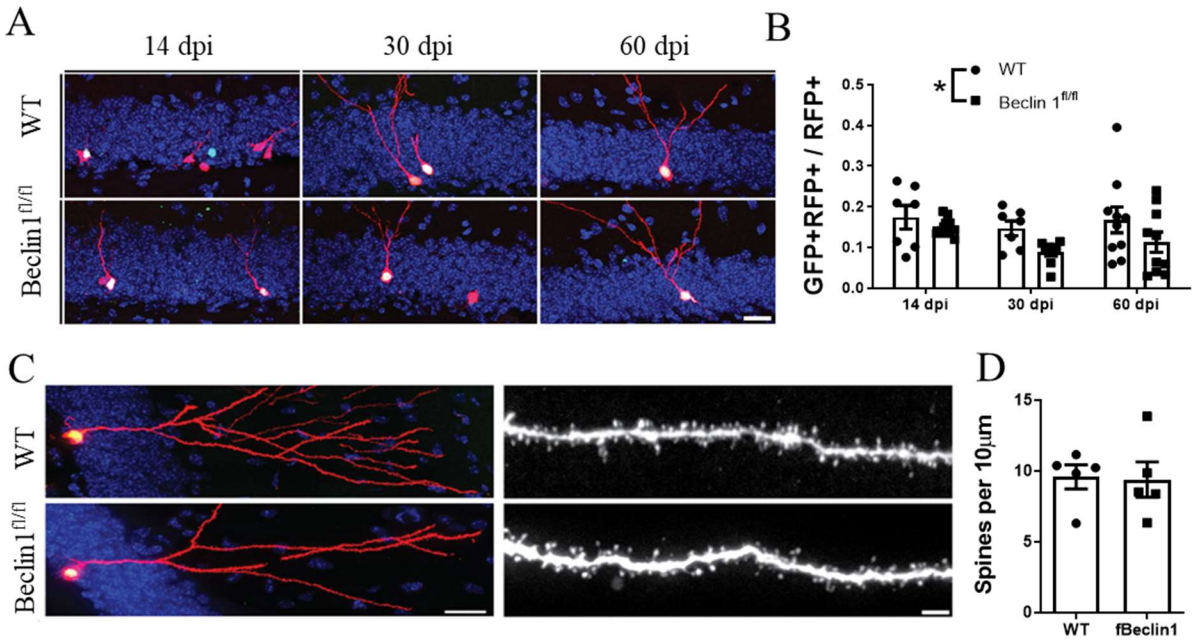

Figure S3. Virus-mediated removal of Beclin1 from dentate gyrus NPCs in WT and Beclin1 fl/fl mice has minor effects. (A) Representative images of GFP+ (green) and RFP+ (red) cells virally infected in the dentate gyrus of WT and Beclin1 fl/fl mice at 14, 30, and 60 dpi. (B) Removal of Beclin1 from dentate gyrus NPCs resulted in an overall modest effect of phenotype on survival of GFP+RFP+ NPCs and their progeny over time (mean ± SEM, 2-way ANOVA). (C) Representative fluorescent images of virally infected WT and Beclin1 fl/fl cells (red and green) at 14 dpi (left) and close-up images of dendritic spines (white) analyzed using Sholl analysis. (D) Sholl analysis results show no difference in the number of spines per 10 uM in WT and Beclin1 fl/fl infected cells (mean ± SEM, unpaired t-test). Scale bars represent 20 uM (A), 10 uM (C left), 5 uM (C right); * $p \leq 0.05$.

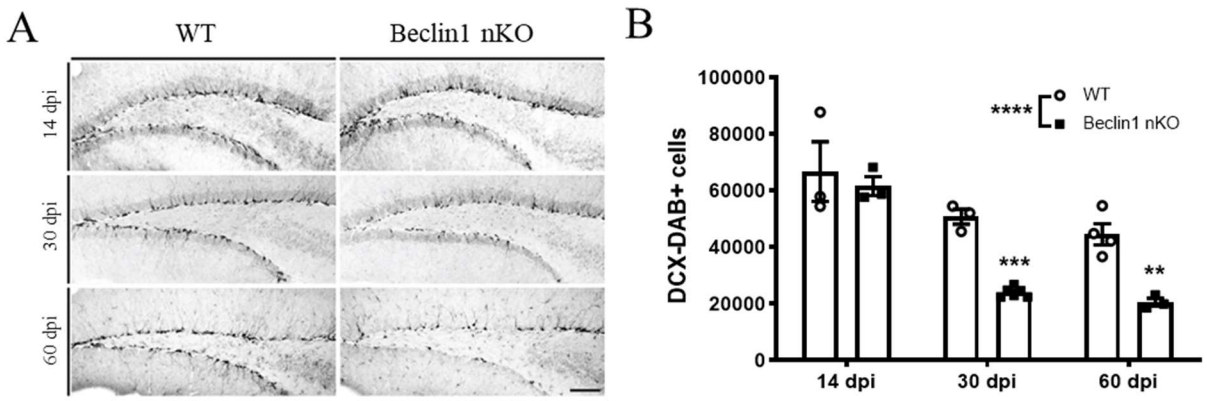

Figure S4. Beclin1 loss results in overall reduction of DG immature neurons. (A) Representative DAB-DCX (black) images of WT and Beclin1 nKO mice at 14, 30, and 60 dpi. (B) Quantification of total DAB-DCX+ cells shows a decrease in Beclin1 nKO mice at 30 and 60 dpi (mean ± SEM, 2-way ANOVA). Scale bar represents 500 uM; ** p≤0.01, *** p≤0.001.

A

Gene		5' Primer	3' Primer	Size (bp)
$CreER^{T2}$	+Control	P26: 5'–CTAGGCCACAGAATTGAAAGATCT–3'	P27: 5'–GTAGGTGGAAATTCTAGCATCATCC–3'	324
	Transgene	P24: 5'–GCGGTCTGGCAGTAAAAACTATC–3'	P25: 5'–GTGAAACAGCATTGCTGTCACTT–3'	100
YFP	WT	P21: 5'–GGAGCGGGAGAAATGGATATG–3'	P20: 5'–GCGAAGAGTTTGTCCTCAACC–3'	560
	Transgene	P21: 5'–GGAGCGGGAGAAATGGATATG–3'	P19: 5'–AAAGTCGCTCTGAGTTGTTAT–3'	310
fBeclin1	WT	P70: 5'–CCACCACCAAGGCAGCGGGTAG–3'	P69: 5'–TCACTGATGGCTCTAACCTCAACTCGTC–3'	650
	Transgene	P70: 5'–CCACCACCAAGGCAGCGGGTAG–3'	P69: 5'–TCACTGATGGCTCTAACCTCAACTCGTC–3'	850

Figure S5. PCR primers. (A) Primers used for the genotyping of WT and Beclin1 nKO mice.

Early M		Late M		CCE1		CCE2		CCE3	
WT	KO	WT	KO	WT	KO	WT	KO	WT	KO
Pclaf	*Kntc1*	*Cdc25c*	*Dbx2*	*Actn1*	*Sstr2*	*Klf3*	*Nfib*	*Igfbpl1*	*Nfib*
Pbk	*Neil3*	*Ptprz1*	*Prdx1*	*Ptprz1*	*Spock2*	*Aplp1*	*Prdm8*	*Nol4*	*Nkain4*
Birc5	*Shcbp1*	*Birc5*	*Notch1*	*Nfib*	*Mt1*	*Eif4g2*	*Mapt*	*Tubb3*	*Sstr2*
Bub1b	*Spc25*	*Ezh2*	*Pdlim4*	*Stmn1*	*Cks2*	*Kctd13*	*Fam174b*	*Lzts1*	*Kcnb2*
Aurka	*Ttc28*	*Igfbpl1*	*Ttc28*	*Lzts1*	*Dusp15*	*1300017J02Rik*	*Kcnb2*	*Stmn1*	*Basp1*
Igfbpl1	*Spag5*	*H2afy*	*Neil3*	*Nol4*	*Fam174b*	*Igfbpl1*	*Dcx*	*1300017J02Rik*	*Cops7a*
Cdca2	*Mapt*	*Spc24*	*Shcbp1*	*Eif4g2*	*Cdk1*	*Atpif1*	*Epha4*	*Aplp1*	*Fam174b*
Spc25	*Zmym1*	*Basp1*	*Nfib*	*Ezh2*	*Fosb*	*Nol4*	*Igfbpl1*	*Palm*	*Mdga1*
Lockd	*Ska1*	*Rgma*	*Cdk1* *Gm10561*	*Chchd10*	*Haus4*	*Elavl4*	*Ttc28*	*Atpif1*	*Polrmt*
Ttk	*Sema3c*	*Sox9*		*Nucks1*	*Pak3*	*Fdft1*	*Sema3c*	*Eif4g2*	*Sccpdh*
Ezh2	*Kif4*	*Stmn1*	*Kntc1*	*Elavl4*	*Nfib*	*Nfasc*	*Nyap1*	*Chmp5*	*Tfap2c*
Iqgap3	*Tuba1c*	*Rad21*	*Sox9*	*Dek*	*Cdh24*	*Mdga1*	*Ap3b2*	*Stmn2*	*Cdh24*
Top2a *Mis18bp1*	*Cdk1*	*Plcd4*	*Mdga1*	*Chmp5*	*Basp1*	*Kif1b*	*Grk6*	*Gm14486*	*Kcnh7*
	Cdkn3	*Ckap2*	*Ska1*	*Aldh2*	*Zmym1*	*Tubb3*	*Eif3f*	*Igsf8*	*Ttc28*
Prr11	*Asf1b*	*Ncapd2*	*Nnat*	*Cklf*	*Prc1*	*Khdrbs2*	*Nrep*	*Fdft1*	*Dcx* *1700025G04Rik*
Cenpe	*Mdga1*	*Eif4g2*	*Basp1*	*Pak7*	*Akap6*	*Srrm4*	*Ccdc28b*	*Hspa14*	
Prc1	*Csrp1*	*Brd8*	*Spag5*	*Mdga1*	*Nr2e1*	*Cttnbp2*	*Fam49a*	*Zfp28*	*Mapt*
Sox9	*Gem*	*Sfxn5*	*Slc1a2*	*Palm*	*Pak7*	*Cenpt*	*Basp1*	*Scrt2*	*Pak7*
Knl1	*Tpcn1*	*Smc2*	*Cks2*	*Cenpt*	*Polrmt*	*Fcgrt*	*Neurod1*	*Calm2*	*Ggta1*
Spc24	*Zfp36l1*	*Cenpp*	*Kif2c*	*Lhx2*	*Serping1*	*Stmn2*	*Gm17750*	*Sh3kbp1*	*Myt1l*
Anln	*Bub1b*	*Gem*	*Bub1b*	*Zfp202*	*Zfp36l1*	*Clybl*	*Rad18*	*Synpr*	*Prkab1*
Kif15	*Sox9*	*Aunip*	*B4galt1*	*Ripk1*	*Mapt* *1700025G04Rik*	*Frmd5*	*Nnat*	*Cenpt*	*Prdm8*
Nol4	*Prdx1*	*Pdik1l*	*Spc25*	*Scrt2*		*Chmp5*	*Id2*	*Pacsin1*	*Epha4*
Cklf	*Igfbpl1*	*Knl1*	*Tcf4*	*Atpif1*	*Atp5b*	*Zfp532*	*Ppp3ca*	*Nfasc*	*Snap25*
Tpx2	*Cdc25c*	*Ptn*	*Myo10*	*Insc*	*Ptprf*	*Nasp*	*Satb1*	*Cep72*	*Nol4*
H2afy	*Cdca2*	*G2e3*	*Drd2*	*Nasp*	*Irf9*	*Mndal*	*Mdga1*	*Nrn1*	*Nrep*
Trip13	*Bcl11a*	*Ckap2l*	*Cttnbp2*	*Epha4*	*Bcl11a*	*Stxbp1*	*Ppp1r14c*	*Lemd1*	*Tubb3*
Ckap2	*Epha4*	*44996*	*Cdca2*	*Nsrp1*	*Hdac4*	*Gipc1*	*Afap1l2*	*Zfp599*	*Clvs1*
	Tcf4	*Gm10561*		*Gsk3b*		*Vbp1*	*Pak3*		

Kif4	*Kifc1*	*Nnat*	*Fosb*	*Poc5*	*Hjurp*	*Apba2*	*Ddx19a*	*Gm17750*	*Nrn1*
Smc2	*Ccdc50*	*Eef2kmt*	*Kifc1*	*Ints12*	*Tfap2c*	*Cenpc1*	*Nol4*	*Ttyh3*	*Pak3*
Smc4	*Cnih3*	*Nedd1*	*Sccpdh*	*Rasgef1b*	*Ccdc34*	*Tnik*	*Tspan12*	*Lhx2*	*Unc5d*
Mki67	*Csad*	*Aldh2*	*Asf1b*	*Tcf4*	*Efhd2*	*Palm*	*Mcrs1*	*Rnf123*	*Igfbpl1*
Cenpq	*Mtfr2*	*Pycard*	*Csrp1*	*Tubb3*	*Dpysl3*	*Zfp28*	*Kcnh7*	*Ugdh*	*Junb*
Tuba1c	*Cep55*	*Vim*	*Cops7a*	*Dopey2*	*Enpp3*	*Lmnb1*	*Atpif1*	*Ptpa*	*Prmt8*
Melk	*Efhd2*	*Mapt*	*Cbs*	*Car11*	*Mcm4*	*Nrn1*	*Chpt1*	*Nnat*	*Scap*
Cdk1	*Notch1*	*Chmp5*	*Dcx*	*Clic1*	*Mgll*	*Slc25a23*	*Ogfod3*	*Pnpla8*	*Ccdc50*
Ccnb2	*Cenpn*	*Appl2*	*Kif4*	*Tmeff1*	*Spc24*	*Gnl2*	*Csad*	*Nptx1*	*Sema3c*
Cenpf	*Prmt8*	*Lzts1*	*Hdac4*	*Epha3*	*Cdk6*	*Rasgef1b*	*Rtn1*	*Cables1*	*St3gal5*
Hjurp	*Melk*	*Tmpo*	*Gfap*	*Rgs20*	*Afap1l2*	*Ncam1*	*Fat1*	*Nsrp1*	*Shb*
Trim59	*Kif11*	*Igdcc3*	*Serping1*	*Myl12b*	*Gm17750*	*Scrt2*	*Rcor2*	*Inpp5b*	*Zfp324*
Kif11	*Nr2e1*	*Cenpc1*	*Bcl11a*	*G2e3*	*Ccdc28b*	*Odf2*	*Plcd1*	*Kcnk1*	*Nnat*
Brd8	*E2f8*	*Ticrr*	*Me3*	*Kif1b*	*Phf19*	*Terf1*	*Serping1*	*Elavl2*	*Chpt1*
Basp1	*Pak3*	*St3gal4*	*Ankrd37*	*Map2k1*	*Eml5*	*Neurod1*	*Agpat4*	*Kif21b*	*Dixdc1*
Kif18a	*Szrd1*	*Synpr*	*Gem*	*Frmd5*	*1810041L15Rik*	*Srgap1*	*Chp1*	*Srrm4*	*Gramd3*
Ncapd2	*Cks2*	*Cmpk1*	*Nr2e1*	*Ranbp9*	*Dixdc1*	*Tspan5*	*Tmem163*	*Cmpk1*	*Gsk3b*
Neil3	*Slc1a2*	*Adk*	*Tacc3*	*Neurod4*	*Amn1*	*Epha4*	*Unc5d*	*Prkcb*	*Rnasel*
Incenp	*Mns1*	*Gpd1*	*Epha4*	*Nsg2*	*Adgrg3*	*Slc6a6*	*Zfpm2*	*Ezh2*	*Elmo1*
Stmn1	*Fosb*	*Pard3b*	*B2m*	*Cyp39a1*	*Kbtbd3*	*Pacsin1*	*2410004B18Rik*	*Nsg2*	*Bcl11a*
H2afv	*Wnt7b*	*Tnfaip8l1*	*Nusap1*	*Plch1*	*Cnih3*	*Cryzl1*	*Nek7*	*Kif1b*	*Serping1*
Tmpo	*B4galt1*	*Clspn*	*Prdm8*	*Tmem159*	*Abcf1*	*Rbms1*	*Rps2*	*Gsk3b*	*Mmp15*
Hmmr	*Mmd2*	*Mad2l1*	*Nol4l*	*Gpd1*	*Psat1*	*Ciapin1*	*Junb*	*Terf1*	*Stmn2*
Ccdc18	*Akap6*	*2810459M11Rik*	*Csmd2*	*Igsf8*	*Pkn2*	*Kif5c*	*Eml5*	*Vbp1*	*Fam208a*
Kif5c	*Cttnbp2*	*Spdl1*	*Ccdc50*	*Rpp30*	*Pbk*	*Lhx2*	*Trim67*	*Ralyl*	*Tmem178*
Kifc5b	*Kif23*	*Ints12*	*Chd1l*	*Hopx*	*Rfx4*	*Cep72*	*Tpd52l2*	*Adk*	*Nyap1*
Rfc4	*2410004B18Rik*	*Sdk2*	*Pak3*	*Ralyl*	*Nol4*	*Epha3*	*Lzts1*	*Neurod1*	*Mpped1*
Shcbp1	*Ppp3ca*	*Kif5c*	*Kif11*	*Gm17750*	*Rps2*	*Pak1*	*Zdhhc18*	*Tnik*	*Syt11*
Ckap5	*Hells*	*Akr7a5*	*Zmym1*	*Ttll1*	*Actb*	*Gm11266*	*Sstr2*	*Stxbp1*	*Khdrbs2*
Apba2	*Nol4*	*Nrp1*	*Lig1*	*Elavl2*	*Ppfia2*	*Josd1*	*Dbn1*	*Ripor1*	*Tspan12*
Sfxn5			*Hspe1*			*Ripor1*		*Jkamp*	*Kctd4*

Myl12b	*B2m*	*Nav1*	*E2f8*	*Dtd1*	*Clstn3*	*Serpini1*	*Vasp*	*Taf1*	*Adck5*
Lzts1	*Chp1*	*Nme7*	*Afap1l2*	*Nr2f1*	*Fam49a*	*Snap25*	*Entpd1*	*Ranbp9*	*Rab11b*
Cdc20	*Dalrd3*	*Kif2c*	*Sptbn1*	*Leprotl1*	*Mtif3*	*Jkamp*	*Kdm5b*	*Pla2g7*	*Cntnap5a*
Tipin	*Nol4l*	*Elavl4*	*Tpx2*	*Clybl*	*Trp53inp2*	*Kif5a*	*Prkab1*	*Cplx2*	*Rbm15*
Nde1	*Siah3*	*Nsrp1*	*Pclaf*	*Khdrbs2*	*Ctnnd2*	*Satb1*	*Clvs1*	*Insc*	*Srrm4*
Nsd2	*Myo10*	*Aif1l*	*Ddx19a*	*S100a10*	*Ttc28*	*Jpt1*	*Zfp324*	*Rbms1*	*Zfpm2*
Klf3	*Tox3*	*Ptprs*	*Cenpn*	*Klf3*	*Kctd4*	*2610035D17Rik*	*Sc5d*	*Slf1*	*Tmem163*
Nucks1	*Knl1*	*Rfc2*	*Cdkn3*	*Rfc2*	*Tspan12*	*Rcor2*	*Ppfia2*	*Gnl2*	*Hspe1*
Lmnb1	*Tacc3*	*H2afv*	*Cntrob*	*Ick*	*Cables1*	*Ttyh3*	*Palm*	*Plch1*	*Ccdc28b*
Cdc25c	*Tfap2c*	*Car11*	*Esco2*	*Snap25*	*Pgm2*	*Slc7a7*	*Tmpo*	*Tmeff1*	*Cnih3*
Nxt1	*Nusap1*	*Dlgap5*	*Nol4*	*Cmpk1*	*Tpd52l2*	*Leprotl1*	*Elmo1*	*Brms1l*	*Satb1*
Nusap1	*Khdrbs2*	*Smc4*	*Slc12a4*	*Stxbp1*	*Prmt8*	*Brms1l*	*Chn2*	*Rbfox3*	*Dopey1*
Cdv3	*Inhbb*	*Cbs*	*Hjurp*	*Nlgn2*	*Mmd2*	*2600014E21Rik*	*Ttc8*	*Dll3*	*Rabggtb*
Dnmt1	*4930558J18Rik*	*Tmem238*	*Stox1*	*Igfbpl1*	*Ralyl*	*Plch1*	*Cttnbp2*	*Usp3*	*Hecw1*
Ube2t	*Uhrf1*	*Cep72*	*Ccdc34*	*Usp3*	*Hat1*	*Rbfox3*	*Ddah2*	*Lims1*	*Chp1*
Sgo2a	*Snap25*	*Tmeff1*	*Rgma*	*Idh1*	*Rassf3*	*Sh3kbp1*	*Cd9*	*Sema3c*	*Glipr2*
Rbfox3	*Pitpnc1*	*Gm11266*	*Trim32*	*Diexf*	*Csmd2*	*Neurod4*	*Fxyd6*	*Kif5a*	*Id2*
Sh3kbp1	*Mipep*	*Kif15*	*Melk*	*Kmt2a*	*Nrn1*	*Rdm1*	*Nav1*	*Snhg10*	*Csad*
Hirip3	*Mcm4*	*Pon2*	*Tuba1c*	*Rps19*	*Spop*	*Syne2*	*Zfp719*	*Ahdc1*	*Ldha*
Ptprs	*Csmd2*	*Itpkb*	*Mki67*	*Ciapin1*	*Pdpn*	*Igsf8*	*Dazap1*	*Mkrn1*	*E2f3*
Nedd1	*Thbs3*	*Me3*	*Top2a*	*Zfp260*	*Tubb3*	*Fdxacb1*	*Galnt17*	*Igdcc3*	*Fam49a*
Pmf1	*Pif1*	*Nucks1*	*Rabggtb*	*Cenpu*	*Hopx*	*Kdm5b*	*Nkain4*	*Rasgef1b*	*Cdk6*
Ect2	*Pdia4*	*Cttnbp2*	*Pdpn*	*Pak1*	*Ppp3ca*	*Kif21b*	*Usp2*	*Pak1*	*Lzts1*
Cenpc1	*Entpd1*	*Frmd5*	*Lhx2*	*Ctnnd2*	*Actn1*	*Snhg10*	*Myt1l*	*Slc25a14*	*Smc4*
Ripk1	*Aftph*	*Hepacam*	*Fam161b*	*Mt2*	*Mxra7*	*Gm17750*	*Bmp1*	*Scarb2*	*Wasf2*
Wee1	*Ago2*	*Gabrb1*	*Rassf3*	*Ipo9*	*Shb*	*Myo19*	*Larp7*	*Ptprd*	*Eml5*
Kif23	*Acot13*	*Apba2*	*Ddah2*	*Hnrnpdl*	*Lsm6*	*Ptprd*	*Gnai2*	*Apba2*	*Dbn1*
Gm4041 8	*Ctnnd2*	*C330027C09Rik*	*Krtcap2*	*Lmnb1*	*Stmn1*	*Sf1*	*Dlgap1*	*Ciapin1*	*Dazap1*
Diaph3	*Top2a*	*Nsg2*	*Mgll*	*Rnf121*	*Prim1*	*Lzts1*	*Aff2*	*Lyrm4*	*Gpd1*
Mdga1	*Trim32*	*Nfib*	*Zfp608*	*Gipc1*	*Pccb*	*Serinc1*	*Ppih*	*Cadm3*	*Ncbp2*
		Lix1		*Atp1b3*	*Klhdc3*		*Wasf2*	*Jam3*	*Dusp14*

Mad2l1	*Ston2*	*Mcm7*	*Oat*	*Cep295*	*Smc4*	*Lyrm4*	*Mdm2*	*Nbdy*	*Actb*
Srrm4	*Ccs*	*Rasgef1b*	*Rab7*	*Jkamp*	*Zfp446*	*Pak7*	*2300009A05Rik*	*Gnai2*	*Kif21b*
Cdk5rap2	*Tedc1*	*Fam210a*	*Naa50*	*Sox8*	*Nt5c2*	*Suclg1*	*Abcf1*	*Rcor2*	*Alcam*
Tbc1d31	*Abcf1*	*Mt3*	*Igfbpl1*	*Tsc22d1*	*Larp7*	*Basp1*	*Dctn5*	*Ick*	*Nuak1*
Arl6ip1	*B3gnt5*	*Ptgds*	*Shroom2*	*Scarb2*	*2410004B18Rik*	*Mtus1*	*Neurod4*	*Klf3*	*Tox3*
Atpif1	*Six5*	*Mgll*	*Eml5*	*Tnik*	*Dopey1*	*Gm40418*	*Trp53inp2*	*Igsf21*	*Dpysl3*
Cep55	*Lig1*	*Gsk3b*	*Ston2*	*Cacybp*	*Lrrc42*	*Zfp91*	*Aco1*	*Mpped1*	*Gap43*
Parpbp	*Atad2*	*Bmper*	*Kif23*	*Aplp1*	*Timeless*	*Ccdc34*	*Retreg3*	*Btbd17*	*Arf2*
Sorbs2	*Rad18*	*Fosb*	*Mtfr2*	*Golph3l*	*Med4*	*Ulk2*	*Bcl11a*	*Sobp*	*Dhtkd1*
Dek	*Cit*	*Dtna*	*Cdc25c*	*Neo1*	*Dusp10*	*Taf1*	*Foxj3*	*Cdk5rap2*	*Gm17750*
Ppwd1	*Lix1*		*Inhbb*		*Nsun4*				

Table S1. Velocity driver genes ranked in each cluster.

Gene Symbol	Avg. Log2FC	% cells expressing in KO	% cells expressing in WT	Adjusted P val
Actb	141.0418358	1	0.995	0.001215059
Nfia	40.01718226	0.94	0.889	0.03936258
Rpl41	39.25991475	1	1	3.06719E-43
Rps28	38.52231195	1	0.988	9.64881E-63
mt-Co3	35.72424248	1	1	6.95577E-06
Tmsb10	34.27146127	0.975	0.968	1.21412E-14
Rps29	30.24485895	1	0.991	4.41471E-70
mt-Co2	28.01218486	0.995	1	3.41695E-05
Rpl37	20.02550813	1	1	5.68425E-40
Nfix	19.65868663	0.985	0.995	2.62951E-07
Tubb2b	18.95963287	0.98	0.961	6.17649E-06
Rpl38	17.20821846	1	0.988	1.77708E-53
Rps8	15.32120367	1	1	3.48911E-15
Rps21	15.32079754	0.99	0.963	6.6741E-42
Rps27rt	15.02318427	0.94	0.524	2.84328E-54
Eef1a1	14.98815654	1	0.998	2.55775E-21
Rplp2	14.76172751	0.995	0.988	5.74198E-36
Rpl27a	13.79412754	1	0.995	6.05228E-10
Fabp5	13.41049647	0.99	0.981	0.000272797
Rpl26	12.81764827	0.995	1	3.06971E-11
Rps4x	12.63788839	1	0.998	5.74944E-06
Hnrnpa1	12.27535054	0.99	0.981	0.005273613
Rpl23a	12.05028499	1	0.998	6.95821E-11
mt-Nd4	11.86931159	0.995	0.998	1.94725E-05
Rpl31	11.32369547	1	0.993	2.1117E-19
Rpl37a	10.91997845	1	1	1.01146E-31
Rpl39	10.51116806	0.995	0.998	2.62597E-39
Rpl35	10.40447418	0.985	0.886	2.72996E-33
Rpl36	10.31303246	1	1	2.26225E-26
Emx1	10.10562343	0.821	0.654	0.000197834
Rplp1	10.06299453	1	0.995	3.27419E-20
Rps15	9.632549968	1	0.998	1.79052E-16
Rpl29	9.581089333	1	0.984	7.62101E-09
Rpl10a	9.488709113	1	0.998	1.05857E-06
Rpl8	9.446857274	1	0.995	2.76532E-09
Rpl36a	8.547739823	0.98	0.893	4.47271E-23
Rps15a	8.438504507	1	0.995	3.44659E-13
Rps23	8.400465717	1	0.998	8.83357E-12
Rpl23	8.303632617	1	0.998	2.11243E-12
Rps24	8.244254083	1	1	5.53872E-16
Eef2	8.235822789	1	0.995	8.07103E-10
Rps3	8.148965538	1	1	1.07234E-09
Rpl6	7.879966882	1	0.998	4.26841E-10
Rpl34	7.434314122	1	0.998	3.63299E-13
H3f3a	7.193964616	0.995	0.998	1.75677E-05
Cox7c	7.156409137	0.985	0.993	0.000436773

Rpl21	6.891325999	1	0.995	4.58971E-15
mt-Nd3	6.819363855	0.92	0.661	8.78086E-36
Rpl7a	6.794636055	0.995	0.954	4.94671E-22
Rps25	6.746804415	1	0.993	2.16376E-12
Comt	6.70735493	0.95	0.631	4.58273E-41
Rps26	6.474601747	1	0.991	1.23859E-12
Rpl5	6.266238972	0.975	0.988	1.69207E-09
Vps37b	6.194100391	0.876	0.784	0.023299943
Elavl4	6.192154923	0.945	0.865	6.42309E-05
Rps10	6.085405014	0.995	0.991	2.4879E-15
Atp5e	5.969673886	0.975	0.958	3.87916E-08
Rps17	5.928377985	1	0.998	7.06753E-15
Rpl7	5.713459154	1	0.998	2.17209E-07
Thra	5.599926537	0.796	0.666	0.002183173
Rpl36a-ps1	5.570432896	0.836	0.471	2.00675E-29
Rpl12	5.485786757	0.985	0.977	1.1207E-13
Cox7a2l	5.482574441	0.95	0.905	1.84766E-05
Ppp1r14b	5.304905991	0.92	0.893	0.014614679
Snrpg	4.932072824	0.925	0.752	6.90527E-31
Cplx2	4.671832627	0.801	0.636	1.27164E-05
Gm11808	4.518792156	0.836	0.487	2.16546E-23
Rpl30	4.364510248	0.99	0.979	2.71614E-09
Cotl1	4.302464665	0.861	0.784	0.000353926
Rpl10-ps3	4.301235865	0.915	0.763	9.60113E-13
Rps20	4.272380437	1	0.991	1.22078E-12
Rpl35a	4.229381517	1	1	4.02884E-14
Rpl11	3.992619172	1	1	1.04213E-09
Rps13	3.958140615	0.99	0.998	3.33992E-07
Rpl36al	3.837838779	0.91	0.701	3.50193E-19
Ptprs	3.714720955	0.9	0.787	0.009554127
Selenow	3.565889794	0.985	0.981	3.64205E-05
Rpl13a	3.510035357	1	0.993	4.30617E-18
Wdr89	3.451223737	0.876	0.529	1.26118E-25
Usmg5	3.428287984	0.935	0.87	3.7618E-09
Rps16	3.336101603	1	1	7.66293E-09
Romo1	3.180218412	0.876	0.715	6.20407E-07
Rpl27-ps3	3.130170452	0.761	0.425	2.50039E-22
Tomm7	2.88730993	0.91	0.782	4.15622E-10
Tspan4	2.858149894	0.368	0.172	0.000215219
Fau	2.84495948	1	0.995	9.08456E-10
Rpl18a	2.818539075	1	1	2.39793E-05
Atp5k	2.806455135	0.9	0.677	1.19653E-18
Eif3f	2.677313227	0.985	0.963	0.004807374
Ptms	2.673218734	0.826	0.719	0.031955269
Ppib	2.541605776	0.985	0.97	0.00454951
Nsg2	2.439697062	0.716	0.585	0.043187101
Uchl1	2.436037432	0.756	0.592	0.002336827
Grcc10	2.417197105	0.677	0.445	2.37931E-07

Rpl28	2.405723713	0.995	0.995	8.74041E-11
Rack1	2.384402583	0.985	0.968	1.91652E-08
Tpt1	2.340895665	1	1	3.56247E-12
Rpl27	2.290171251	0.612	0.206	6.41033E-23
Btbd17	2.212409914	0.692	0.517	0.014736254
Rpl13a-ps1	2.181673474	0.592	0.436	0.004270041
Mrpl52	2.159809699	0.891	0.798	2.29406E-05
Rpl19	2.115860913	1	0.998	3.0385E-08
Uba52	2.08990899	0.612	0.288	9.58929E-15
Rps11	2.089617706	1	0.998	0.003617382
Arrdc3	2.056010881	0.537	0.357	0.04322188
2010107E04Rik	1.920670976	0.97	0.914	2.84561E-09
Ndufa3	1.916293931	0.91	0.747	3.62005E-12
Tmem258	1.842522611	0.886	0.766	0.000332205
Sbk1	1.83832253	0.627	0.466	0.014627565
Cops9	1.777614125	0.856	0.77	0.000558168
Ccni	1.749337828	0.751	0.603	0.003507721
Rps12-ps3	1.731382369	0.582	0.218	1.17149E-18
Npc2	1.705634061	0.95	0.886	0.003484131
Uqcrh	1.644652775	0.98	0.968	0.004258917
Rpl15	1.626770189	1	1	0.000105
Sh3bgrl	1.585286772	0.891	0.773	7.67828E-05
Nhlh1	1.545573526	0.299	0.109	2.12659E-05
Crmp1	1.51629101	0.677	0.531	0.00117554
Rpl24	1.447390987	1	1	8.6103E-05
Cox17	1.43628276	0.612	0.429	0.003109159
Dlgap4	1.413223534	0.612	0.425	0.001272865
Scd2	1.370616036	0.662	0.441	0.000164265
Ywhaz	1.361890531	0.801	0.603	0.000895871
Rpl9-ps6	1.351160268	0.866	0.715	4.15346E-12
Rnf10	1.345021704	0.731	0.578	0.009418733
Pam	1.330019386	0.343	0.179	0.047698896
Bola2	1.318076935	0.826	0.673	0.001279878
Gm2000	1.294188148	0.453	0.158	4.89429E-12
Use1	1.277363045	0.706	0.49	0.002336227
Rab26os	1.244554014	0.378	0.172	2.79773E-05
Snhg6	1.182019716	0.652	0.469	0.010907022
Gm8186	1.162699157	0.652	0.392	3.46571E-08
Srebf2	1.122256955	0.637	0.397	4.46278E-06
Rpl7a-ps5	1.112184867	0.677	0.439	2.93948E-07
Gabarapl1	1.103991257	0.458	0.278	0.016548198
Brk1	1.050147594	0.881	0.752	0.025152671
Pet100	1.018466741	0.537	0.323	0.000159062
Sec61g	0.986599626	0.96	0.947	7.81899E-05
Zmynd8	0.955814997	0.478	0.288	0.001005447
Rtl8a	0.949873564	0.607	0.404	0.002432853
Smoc1	0.949142396	0.234	0.074	9.13687E-05
Rps12	0.927645187	0.368	0.109	4.49925E-11

Ensa	0.924017247	0.517	0.316	0.002969955
Nptn	0.888294721	0.338	0.088	6.22552E-11
mt-Nd2	0.877212796	0.98	0.954	1.98984E-07
Arpc4	0.855830095	0.697	0.517	0.032610824
Rpl17	0.849597003	1	1	1.08514E-06
Map1lc3b	0.830561946	0.955	0.93	0.005213782
Cd164	0.827816363	0.642	0.413	9.06127E-05
Dpysl5	0.81676751	0.338	0.169	0.016715115
Coro2b	0.754214624	0.478	0.29	0.017830353
Eif4b	0.706146962	0.687	0.51	0.006608501
Phf6	0.697499439	0.423	0.218	0.000445898
Atp13a2	0.642012467	0.363	0.179	0.004262007
Vtn	0.637040817	0.313	0.107	1.35315E-06
Igsf8	0.604699186	0.96	0.893	2.98193E-05
Lrrn1	0.597812695	0.294	0.132	0.006281337
Eif4a2	0.554856006	0.955	0.9	0.01264463
Sesn1	0.550603978	0.323	0.125	4.97719E-05
Atf6b	0.54008015	0.537	0.35	0.035644939
Nudcd3	0.532327287	0.458	0.26	0.005664616
Epb41l4aos	0.516834138	0.343	0.174	0.015236716
Nrxn2	0.506343961	0.453	0.258	0.027401379
Ftl1-ps1	0.501978062	0.294	0.09	6.14959E-07
Serinc3	0.478973692	0.229	0.058	2.69803E-06
Pef1	0.452915268	0.383	0.209	0.04850133
Cxcr4	0.404892989	0.154	0.032	0.000440104
Vmn1r13	0.365607172	0.174	0.051	0.006816827
Gm9493	0.339175797	0.771	0.557	4.47573E-06
Gm10269	0.318915826	0.174	0.044	0.000894723
Irgm1	0.303332187	0.144	0.039	0.033621432
Anp32e	0.289871245	0.697	0.845	0.031323668
Rpl22	0.269323078	0.99	0.972	3.07525E-11
Gm12184	0.264676755	0.134	0.026	0.001350013
Cenph	-0.273977195	0.075	0.241	0.011264327
Rplp0	-0.318107768	1	1	2.10529E-05
Igfbpl1	-0.342561342	0.905	0.835	0.036234345
Rpl4	-0.545161334	0.995	0.998	6.88974E-06
Vrk1	-0.594171512	0.219	0.415	0.024172902
Pold3	-0.610635485	0.114	0.288	0.023286114
Gm10073	-0.750570319	0.154	0.355	0.001538538
Mcm3	-0.998378475	0.209	0.418	0.003771888
Marcksl1	-1.126596568	1	0.993	0.005173163
Syce2	-1.404020077	0.204	0.413	0.006767439
Trim2	-1.533234507	0.945	0.803	2.70176E-12
Cenpk	-1.569715974	0.129	0.32	0.003052838
Spc24	-1.631262284	0.154	0.362	0.000371722
Rpsa	-1.659219659	0.995	0.991	1.41605E-07
Kif22	-1.904603563	0.085	0.241	0.023141523
Alyref	-1.949690119	0.433	0.698	2.86151E-11

Rpl32	-2.12036977	1	1	1.19231E-06
Rpa2	-2.175589981	0.303	0.51	0.008799355
Rps27a	-2.478347106	1	1	5.51504E-08
Cenpm	-2.641053969	0.219	0.404	0.011562872
Gmnn	-2.977937689	0.109	0.299	0.001239281
Dnajc9	-3.005071474	0.507	0.664	0.0156821
Ran	-3.063627618	0.985	0.981	0.003754589
Rps3a1	-3.086033921	1	1	4.16732E-10
Ppp2ca	-3.238154723	0.771	0.886	0.004014678
Ccna2	-3.511656919	0.09	0.269	0.002223366
Rpl18	-4.028487228	1	0.998	3.55183E-05
Hat1	-4.337920749	0.239	0.434	0.028626831
Aurkb	-4.477875419	0.06	0.202	0.029431917
Rps7	-4.529381985	1	0.998	1.56726E-05
mt-Co1	-4.6390585	0.995	1	0.002901163
Tcf4	-5.218139683	1	0.993	0.027875776
Top2a	-5.495990571	0.149	0.332	0.005760786
Hnrnpa3	-6.523471177	0.905	0.937	0.019917267
Ranbp1	-7.237605706	0.95	0.956	0.003479533
Rrm2	-7.356246416	0.204	0.432	0.00014781
Rps9	-8.272791442	1	1	4.74153E-07
Rps6	-8.80615625	0.995	1	0.001828364
Rps18	-8.880447022	1	0.998	5.67381E-05
Tmsb4x	-10.43392913	1	1	0.003437858
Rps14	-11.52697252	1	1	9.44096E-11
Pclaf	-11.87769631	0.289	0.469	0.005706332
Pbk	-13.51051462	0.179	0.394	0.000917188
Smc2	-13.91002976	0.299	0.513	0.000166005
mt-Nd1	-14.60887277	1	0.998	0.008387604
Spc25	-15.05749697	0.114	0.276	0.024718886
H1fx	-15.77497643	0.473	0.708	3.30293E-09
Cdk1	-18.42988693	0.129	0.302	0.01550628
H2afz	-57.96940379	0.975	0.984	0.000368803

Table S2. List of genes differentially expressed in Beclin1-nul NSPCs.

References

1. Menon, M.B., and Dhamija, S. (2018). Beclin 1 Phosphorylation – at the Center of Autophagy Regulation. Front. Cell Dev. Biol. *6*.

2. Kang, R., Zeh, H.J., Lotze, M.T., and Tang, D. (2011). The Beclin 1 network regulates autophagy and apoptosis. Cell Death Differ. *18*, 571–580. 10.1038/cdd.2010.191.

3. Funderburk., S.F., Wang, Q.J., and Yue, Z. (2010). Beclin 1-VPS34 complex – At the Crossroads of Autophagy and Beyond. Trends Cell Biol. *20*, 355–362. 10.1016/j.tcb.2010.03.002.

4. Noguchi, S., Honda, S., Saitoh, T., Matsumura, H., Nishimura, E., Akira, S., and Shimizu, S. (2019). Beclin 1 regulates recycling endosome and is required for skin development in mice. Commun. Biol. *2*, 37. 10.1038/s42003-018-0279-0.

5. Konishi, A., Arakawa, S., Yue, Z., and Shimizu, S. (2012). Involvement of Beclin 1 in engulfment of apoptotic cells. J. Biol. Chem. *287*, 13919–13929. 10.1074/jbc.M112.348375.

6. Lemus Silva, E.G., Delgadillo, Y., White, R.E., and Lucin, K.M. (2023). Beclin 1 regulates astrocyte phagocytosis and phagosomal recruitment of retromer. Tissue Cell *82*, 102100. 10.1016/j.tice.2023.102100.

7. Hamurcu, Z., Delibaşı, N., Geçene, S., Şener, E.F., Dönmez-Altuntaş, H., Özkul, Y., Canatan, H., and Ozpolat, B. (2018). Targeting LC3 and Beclin-1 autophagy genes suppresses proliferation, survival, migration and invasion by inhibition of Cyclin-D1 and uPAR/Integrin β1/ Src signaling in triple negative breast cancer cells. J. Cancer Res. Clin. Oncol. *144*, 415–430. 10.1007/s00432-017-2557-5.

8. Park, J.M., Tougeron, D., Huang, S., Okamoto, K., and Sinicrope, F.A. (2014). Beclin 1 and UVRAG Confer Protection from Radiation-Induced DNA Damage and Maintain Centrosome Stability in Colorectal Cancer Cells. PLOS ONE *9*, e100819. 10.1371/journal.pone.0100819.

9. Xu, F., Fang, Y., Yan, L., Xu, L., Zhang, S., Cao, Y., Xu, L., Zhang, X., Xie, J., Jiang, G., et al. (2017). Nuclear localization of Beclin 1 promotes radiation-induced DNA damage repair independent of autophagy. Sci. Rep. *7*, 45385. 10.1038/srep45385.

10. Frémont, S., Gérard, A., Galloux, M., Janvier, K., Karess, R.E., and Berlioz-Torrent, C. (2013). Beclin-1 is required for chromosome congression and proper outer kinetochore assembly. EMBO Rep. *14*, 364–372. 10.1038/embor.2013.23.

11. Yue, Z., Jin, S., Yang, C., Levine, A.J., and Heintz, N. (2003). Beclin 1, an autophagy gene essential for early embryonic development, is a haploinsufficient tumor suppressor. Proc. Natl. Acad. Sci. U. S. A. *100*, 15077–15082. 10.1073/pnas.2436255100.

12. Yazdankhah, M., Farioli-Vecchioli, S., Tonchev, A.B., Stoykova, A., and Cecconi, F. (2014). The autophagy regulators Ambra1 and Beclin 1 are required for adult neurogenesis in the brain subventricular zone. Cell Death Dis. *5*, e1403–e1403. 10.1038/cddis.2014.358.

13. McKnight, N.C., Zhong, Y., Wold, M.S., Gong, S., Phillips, G.R., Dou, Z., Zhao, Y., Heintz, N., Zong, W.X., and Yue, Z. (2014). Beclin 1 Is Required for Neuron Viability and Regulates Endosome Pathways via the UVRAG-VPS34 Complex. PLoS Genet. *10*, 1–18. 10.1371/journal.pgen.1004626.

14. Xi, Y., Dhaliwal, J.S., Ceizar, M., Vaculik, M., Kumar, K.L., and Lagace, D.C. (2016). Knockout of Atg5 delays the maturation and reduces the survival of adult-generated neurons in the hippocampus. Cell Death Dis. *7*, e2127. 10.1038/cddis.2015.406.

15. Furutachi, S., Miya, H., Watanabe, T., Kawai, H., Yamasaki, N., Harada, Y., Imayoshi, I., Nelson, M., Nakayama, K.I., Hirabayashi, Y., et al. (2015). Slowly dividing neural progenitors are an embryonic origin of adult neural stem cells. Nat. Neurosci. *18*, 657–665. 10.1038/nn.3989.

16. Maslov, A.Y., Barone, T.A., Plunkett, R.J., and Pruitt, S.C. (2004). Neural Stem Cell Detection, Characterization, and Age-Related Changes in the Subventricular Zone of Mice. J. Neurosci. *24*, 1726–1733. 10.1523/JNEUROSCI.4608-03.2004.

17. Chaker, Z., Codega, P., and Doetsch, F. (2016). A mosaic world: puzzles revealed by adult neural stem cell heterogeneity. WIREs Dev. Biol. *5*, 640–658. https://doi.org/10.1002/wdev.248.

18. Dulken, B.W., Leeman, D.S., Boutet, S.C., Hebestreit, K., and Brunet, A. (2017). Single-Cell Transcriptomic Analysis Defines Heterogeneity and Transcriptional Dynamics in the Adult Neural Stem Cell Lineage. Cell Rep. *18*, 777–790. 10.1016/j.celrep.2016.12.060.

19. Su, Y.-T., Lau, S.-F., Ip, J.P.K., Cheung, K., Cheung, T.H.T., Fu, A.K.Y., and Ip, N.Y. (2019). α2-Chimaerin is essential for neural stem cell homeostasis in mouse adult neurogenesis. Proc. Natl. Acad. Sci. *116*, 13651–13660. 10.1073/pnas.1903891116.

20. Ellis, P., Fagan, B.M., Magness, S.T., Hutton, S., Taranova, O., Hayashi, S., McMahon, A., Rao, M., and Pevny, L. (2004). SOX2, a Persistent Marker for Multipotential Neural Stem Cells Derived from Embryonic Stem Cells, the Embryo or the Adult. Dev. Neurosci. *26*, 148–165. 10.1159/000082134.

21. Shimozaki, K. (2014). Sox2 transcription network acts as a molecular switch to regulate properties of neural stem cells. World J. Stem Cells *6*, 485–490. 10.4252/wjsc.v6.i4.485.

22. Brazel, C.Y., Limke, T.L., Osborne, J.K., Miura, T., Cai, J., Pevny, L., and Rao, M.S. (2005). Sox2 expression defines a heterogeneous population of neurosphere-forming cells in the adult murine brain. Aging Cell *4*, 197–207. 10.1111/j.1474-9726.2005.00158.x.

23. Kim, J.S., Park, S.W., Hwang, I., Kim, Y.W., Kim, J.H., and Kim, J.H. (2015). Expression of nestin on endothelial cells and pericytes during vascular development in mouse retina. Invest. Ophthalmol. Vis. Sci. *56*, 3403–3403.

24. Almazán, G., Vela, J.M., Molina-Holgado, E., and Guaza, C. (2001). Re-evaluation of nestin as a marker of oligodendrocyte lineage cells. Microsc. Res. Tech. *52*, 753–765. 10.1002/jemt.1060.

25. Shin, J., Berg, D.A., Zhu, Y., Shin, J.Y., Song, J., Bonaguidi, M.A., Enikolopov, G., Nauen, D.W., Christian, K.M., Ming, G., et al. (2015). Single-Cell RNA-Seq with Waterfall Reveals Molecular Cascades underlying Adult Neurogenesis. Cell Stem Cell *17*, 360–372. 10.1016/j.stem.2015.07.013.

26. Basak, O., Krieger, T.G., Muraro, M.J., Wiebrands, K., Stange, D.E., Frias-Aldeguer, J., Rivron, N.C., Wetering, M. van de, Es, J.H. van, Oudenaarden, A. van, et al. (2018). Troy+ brain stem cells cycle through quiescence and regulate their number by sensing niche occupancy. Proc. Natl. Acad. Sci. *115*, E610–E619. 10.1073/pnas.1715911114.

27. Zerjatke, T., Gak, I.A., Kirova, D., Fuhrmann, M., Daniel, K., Gonciarz, M., Müller, D., Glauche, I., and Mansfeld, J. (2017). Quantitative Cell Cycle Analysis Based on an Endogenous All-in-One Reporter for Cell Tracking and Classification. Cell Rep. *19*, 1953–1966. 10.1016/j.celrep.2017.05.022.

28. Pereira, P.D., Serra-Caetano, A., Cabrita, M., Bekman, E., Braga, J., Rino, J., Santus, R., Filipe, P.L., Sousa, A.E., and Ferreira, J.A. (2017). Quantification of cell cycle kinetics by EdU (5-ethynyl-2′-deoxyuridine)-coupled-fluorescence-intensity analysis. Oncotarget *8*, 40514–40532. 10.18632/oncotarget.17121.

29. Yang, C.-P., Gilley, J.A., Zhang, G., and Kernie, S.G. (2011). ApoE is required for maintenance of the dentate gyrus neural progenitor pool. Dev. Camb. Engl. *138*, 4351–4362. 10.1242/dev.065540.

30. Satija, R., Farrell, J.A., Gennert, D., Schier, A.F., and Regev, A. (2015). Spatial reconstruction of single-cell gene expression data. Nat. Biotechnol. *33*, 495–502. 10.1038/nbt.3192.

31. Bergen, V., Lange, M., Peidli, S., Wolf, F.A., and Theis, F.J. (2019). Generalizing RNA velocity to transient cell states through dynamical modeling. bioRxiv, 820936. 10.1101/820936.

32. Jiang, Y., Bruin, A. de, Caldas, H., Fangusaro, J., Hayes, J., Conway, E.M., Robinson, M.L., and Altura, R.A. (2005). Essential Role for Survivin in Early Brain Development. J. Neurosci. *25*, 6962–6970. 10.1523/JNEUROSCI.1446-05.2005.

33. Wiedemuth, R., Klink, B., Töpfer, K., Schröck, E., Schackert, G., Tatsuka, M., and Temme, A. (2014). Survivin safeguards chromosome numbers and protects from aneuploidy independently from p53. Mol. Cancer *13*, 107. 10.1186/1476-4598-13-107.

34. Piper, M., Barry, G., Harvey, T., Mcleay, R., Smith, A., Harris, L., Mason, S., Stringer, B., Day, B., Wray, N., et al. (2014). NFIB-Mediated Repression of the Epigenetic Factor Ezh2 Regulates Cortical Development. J. Neurosci. Off. J. Soc. Neurosci. *34*, 2921–2930. 10.1523/JNEUROSCI.2319-13.2014.

35. Clark, B.S., Stein-O'Brien, G.L., Shiau, F., Cannon, G.H., Davis-Marcisak, E., Sherman, T., Santiago, C.P., Hoang, T.V., Rajaii, F., James-Esposito, R.E., et al. (2019). Single-Cell RNA-Seq Analysis of Retinal Development Identifies NFI Factors as Regulating Mitotic Exit and Late-Born Cell Specification. Neuron *102*, 1111-1126.e5. 10.1016/j.neuron.2019.04.010.

36. Regnell, C.E., Hildrestrand, G.A., Sejersted, Y., Medin, T., Moldestad, O., Rolseth, V., Krokeide, S.Z., Suganthan, R., Luna, L., Bjørås, M., et al. (2012). Hippocampal adult neurogenesis is maintained by Neil3-dependent repair of oxidative DNA lesions in neural progenitor cells. Cell Rep. *2*, 503–510. 10.1016/j.celrep.2012.08.008.

37. Paonessa, F., Evans, L.D., Solanki, R., Larrieu, D., Wray, S., Hardy, J., Jackson, S.P., and Livesey, F.J. (2019). Microtubules Deform the Nuclear Membrane and Disrupt Nucleocytoplasmic Transport in Tau-Mediated Frontotemporal Dementia. Cell Rep. *26*, 582-593.e5. 10.1016/j.celrep.2018.12.085.

38. Leveille, E., Ross, O.A., and Gan-Or, Z. (2021). Tau and MAPT genetics in tauopathies and synucleinopathies. Parkinsonism Relat. Disord. *90*, 142–154. 10.1016/j.parkreldis.2021.09.008.

39. Verdaasdonk, J.S., and Bloom, K. (2011). Centromeres: unique chromatin structures that drive chromosome segregation. Nat. Rev. Mol. Cell Biol. *12*, 320–333.

40. Pesenti, M.E., Raisch, T., Conti, D., Walstein, K., Hoffmann, I., Vogt, D., Prumbaum, D., Vetter, I.R., Raunser, S., and Musacchio, A. (2022). Structure of the human inner kinetochore CCAN complex and its significance for human centromere organization. Mol. Cell *82*, 2113-2131.e8. 10.1016/j.molcel.2022.04.027.

41. Waitzman, J.S., and Rice, S.E. (2014). Mechanism and regulation of kinesin-5, an essential motor for the mitotic spindle. Biol. Cell *106*, 1–12. 10.1111/boc.201300054.

42. Pryzhkova, M.V., and Jordan, P.W. (2016). Conditional mutation of Smc5 in mouse embryonic stem cells perturbs condensin localization and mitotic progression. J. Cell Sci. *129*, 1619–1634. 10.1242/jcs.179036.

43. Cross, R.A., and McAinsh, A. (2014). Prime movers: the mechanochemistry of mitotic kinesins. Nat. Rev. Mol. Cell Biol. *15*, 257–271. 10.1038/nrm3768.

44. Paul, M.R., Hochwagen, A., and Ercan, S. (2019). Condensin action and compaction. Curr. Genet. *65*, 407–415. 10.1007/s00294-018-0899-4.

45. Martin, C.-A., Murray, J.E., Carroll, P., Leitch, A., Mackenzie, K.J., Halachev, M., Fetit, A.E., Keith, C., Bicknell, L.S., Fluteau, A., et al. (2016). Mutations in genes encoding condensin complex proteins cause microcephaly through decatenation failure at mitosis. Genes Dev. *30*, 2158–2172. 10.1101/gad.286351.116.

46. Barra, V., and Fachinetti, D. (2018). The dark side of centromeres: types, causes and consequences of structural abnormalities implicating centromeric DNA. Nat. Commun. *9*, 4340. 10.1038/s41467-018-06545-y.

47. Wu, N., and Yu, H. (2012). The Smc complexes in DNA damage response. Cell Biosci. *2*, 5. 10.1186/2045-3701-2-5.

48. Kim, J.M. (2022). Molecular Link between DNA Damage Response and Microtubule Dynamics. Int. J. Mol. Sci. *23*, 6986. 10.3390/ijms23136986.

49. Thompson, A.F., Blackburn, P.R., Arons, N.S., Stevens, S.N., Babovic-Vuksanovic, D., Lian, J.B., Klee, E.W., and Stumpff, J. (2022). Pathogenic mutations in the chromokinesin KIF22 disrupt anaphase chromosome segregation. eLife *11*, e78653. 10.7554/eLife.78653.

50. McCleland, M.L., Kallio, M.J., Barrett-Wilt, G.A., Kestner, C.A., Shabanowitz, J., Hunt, D.F., Gorbsky, G.J., and Stukenberg, P.T. (2004). The vertebrate Ndc80 complex contains Spc24 and Spc25 homologs, which are required to establish and maintain kinetochore-microtubule attachment. Curr. Biol. CB *14*, 131–137. 10.1016/j.cub.2003.12.058.

51. Cavazza, T., and Vernos, I. (2016). The RanGTP Pathway: From Nucleo-Cytoplasmic Transport to Spindle Assembly and Beyond. Front. Cell Dev. Biol. *3*. 10.3389/fcell.2015.00082.

52. Joseph, J., Liu, S.-T., Jablonski, S.A., Yen, T.J., and Dasso, M. (2004). The RanGAP1-RanBP2 Complex Is Essential for Microtubule-Kinetochore Interactions In Vivo. Curr. Biol. *14*, 611–617. 10.1016/j.cub.2004.03.031.

53. Arnaoutov, A., and Dasso, M. (2003). The Ran GTPase Regulates Kinetochore Function. Dev. Cell *5*, 99–111. 10.1016/S1534-5807(03)00194-1.

54. D'Angiolella, V., Donato, V., Forrester, F.M., Jeong, Y.-T., Pellacani, C., Kudo, Y., Saraf, A., Florens, L., Washburn, M.P., and Pagano, M. (2012). The Cyclin F-Ribonucleotide Reductase M2 axis controls genome integrity and DNA repair. Cell *149*, 1023–1034. 10.1016/j.cell.2012.03.043.

55. Boudhraa, Z., Carmona, E., Provencher, D., and Mes-Masson, A.-M. (2020). Ran GTPase: A Key Player in Tumor Progression and Metastasis. Front. Cell Dev. Biol. *8*.

56. Pommier, Y., Nussenzweig, A., Takeda, S., and Austin, C. (2022). Human topoisomerases and their roles in genome stability and organization. Nat. Rev. Mol. Cell Biol. *23*, 407–427. 10.1038/s41580-022-00452-3.

57. De Biasio, A., de Opakua, A.I., Mortuza, G.B., Molina, R., Cordeiro, T.N., Castillo, F., Villate, M., Merino, N., Delgado, S., Gil-Cartón, D., et al. (2015). Structure of p15(PAF)-PCNA complex and implications for clamp sliding during DNA replication and repair. Nat. Commun. *6*, 6439. 10.1038/ncomms7439.

58. Bolcun-Filas, E., Costa, Y., Speed, R., Taggart, M., Benavente, R., De Rooij, D.G., and Cooke, H.J. (2007). SYCE2 is required for synaptonemal complex assembly, double strand break repair, and homologous recombination. J. Cell Biol. *176*, 741–747. 10.1083/jcb.200610027.

59. Morimoto, Y., Tokumitsu, A., Sone, T., Hirota, Y., Tamura, R., Sakamoto, A., Nakajima, K., Toda, M., Kawakami, Y., Okano, H., et al. (2022). TPT1 Supports Proliferation of Neural Stem/Progenitor Cells and

Brain Tumor Initiating Cells Regulated by Macrophage Migration Inhibitory Factor (MIF). Neurochem. Res. *47*, 2741–2756. 10.1007/s11064-022-03629-6.

60. Gonzalez-Franquesa, A., Stocks, B., Borg, M.L., Kuefner, M., Dalbram, E., Nielsen, T.S., Agrawal, A., Pankratova, S., Chibalin, A.V., Karlsson, H.K.R., et al. (2021). Discovery of thymosin β4 as a human exerkine and growth factor. Am. J. Physiol. Cell Physiol. *321*, C770–C778. 10.1152/ajpcell.00263.2021.

61. Cai, Q., Lu, L., Tian, J.-H., Zhu, Y.-B., Qiao, H., and Sheng, Z.-H. (2010). Snapin-regulated late endosomal transport is critical for efficient autophagy-lysosomal function in neurons. Neuron *68*, 73–86. 10.1016/j.neuron.2010.09.022.

62. Beesley, P.W., Herrera-Molina, R., Smalla, K.-H., and Seidenbecher, C. (2014). The Neuroplastin adhesion molecules: key regulators of neuronal plasticity and synaptic function. J. Neurochem. *131*, 268–283. 10.1111/jnc.12816.

63. Mesman, S., Bakker, R., and Smidt, M.P. (2020). Tcf4 is required for correct brain development during embryogenesis. Mol. Cell. Neurosci. *106*, 103502. 10.1016/j.mcn.2020.103502.

64. Trimbuch, T., and Rosenmund, C. (2016). Should I stop or should I go? The role of complexin in neurotransmitter release. Nat. Rev. Neurosci. *17*, 118–125. 10.1038/nrn.2015.16.

65. Willems, P.H.G.M., Rossignol, R., Dieteren, C.E.J., Murphy, M.P., and Koopman, W.J.H. (2015). Redox Homeostasis and Mitochondrial Dynamics. Cell Metab. *22*, 207–218. 10.1016/j.cmet.2015.06.006.

66. Forsha, D., Church, C., Wazny, P., and Poyton, R.O. (2001). Structure and function of Pet100p, a molecular chaperone required for the assembly of cytochrome c oxidase in Saccharomyces cerevisiae. Biochem. Soc. Trans. *29*, 436–441. 10.1042/bst0290436.

67. Suhane, S., Kanzaki, H., Arumugaswami, V., Murali, R., and Ramanujan, V.K. (2013). Mitochondrial NDUFS3 regulates the ROS-mediated onset of metabolic switch in transformed cells. Biol. Open *2*, 295–305. 10.1242/bio.20133244.

68. Chen, W., Wang, H., Tao, S., Zheng, Y., Wu, W., Lian, F., Jaramillo, M., Fang, D., and Zhang, D.D. (2013). Tumor protein translationally controlled 1 is a p53 target gene that promotes cell survival. Cell Cycle *12*, 2321–2328. 10.4161/cc.25404.

69. Zhang, J., de Toledo, S.M., Pandey, B.N., Guo, G., Pain, D., Li, H., and Azzam, E.I. (2012). Role of the translationally controlled tumor protein in DNA damage sensing and repair. Proc. Natl. Acad. Sci. U. S. A. *109*, E926-933. 10.1073/pnas.1106300109.

70. de Moraes, E., Dar, N.A., de Moura Gallo, C.V., and Hainaut, P. (2007). Cross-talks between cyclooxygenase-2 and tumor suppressor protein p53: Balancing life and death during inflammatory stress and carcinogenesis. Int. J. Cancer *121*, 929–937. 10.1002/ijc.22899.

71. Budanov, A.V., and Karin, M. (2008). p53 Target Genes Sestrin1 and Sestrin2 Connect Genotoxic Stress and mTOR Signaling. Cell *134*, 451–460. 10.1016/j.cell.2008.06.028.

72. Levine, M.S., and Holland, A.J. (2018). The impact of mitotic errors on cell proliferation and tumorigenesis. Genes Dev. *32*, 620–638. 10.1101/gad.314351.118.

73. Hayashi, M.T., and Karlseder, J. (2013). DNA damage associated with mitosis and cytokinesis failure. Oncogene *32*, 4593–4601. 10.1038/onc.2012.615.

74. Nowsheen, S., Xia, F., and Yang, E.S. (2012). Assaying DNA Damage in Hippocampal Neurons Using the Comet Assay. J. Vis. Exp., 50049. 10.3791/50049.

75. Wang, C., Haas, M., Yeo, S.K., Sebti, S., Fernández, Á.F., Zou, Z., Levine, B., and Guan, J.-L. (2021). Enhanced autophagy in Becn1F121A/F121A knockin mice counteracts aging-related neural stem cell exhaustion and dysfunction. Autophagy *0*, 1–14. 10.1080/15548627.2021.1936358.

76. You, S.Y., Park, Y.S., Jeon, H.-J., Cho, D.-H., Jeon, H.B., Kim, S.H., Chang, J.W., Kim, J.-S., and Oh, J.S. (2016). Beclin-1 knockdown shows abscission failure but not autophagy defect during oocyte meiotic maturation. Cell Cycle *15*, 1611–1619. 10.1080/15384101.2016.1181235.

77. Mathew, R., Kongara, S., Beaudoin, B., Karp, C.M., Bray, K., Degenhardt, K., Chen, G., Jin, S., and White, E. (2007). Autophagy suppresses tumor progression by limiting chromosomal instability. Genes Dev. *21*, 1367–1381. 10.1101/gad.1545107.

78. Karantza-Wadsworth, V., Patel, S., Kravchuk, O., Chen, G., Mathew, R., Jin, S., and White, E. (2007). Autophagy mitigates metabolic stress and genome damage in mammary tumorigenesis. Genes Dev. *21*, 1621–1635. 10.1101/gad.1565707.

79. Delaney, J.R., Patel, C.B., Bapat, J., Jones, C.M., Ramos-Zapatero, M., Ortell, K.K., Tanios, R., Haghighiabyaneh, M., Axelrod, J., DeStefano, J.W., et al. (2020). Autophagy gene haploinsufficiency drives chromosome instability, increases migration, and promotes early ovarian tumors. PLoS Genet. *16*, e1008558. 10.1371/journal.pgen.1008558.

80. Tran, S., Fairlie, W.D., and Lee, E.F. (2021). BECLIN1: Protein Structure, Function and Regulation. Cells *10*, 1522. 10.3390/cells10061522.

81. Kaur, S., and Changotra, H. (2020). The beclin 1 interactome: Modification and roles in the pathology of autophagy-related disorders. Biochimie *175*, 34–49. 10.1016/j.biochi.2020.04.025.

82. Wirawan, E., Lippens, S., Vanden Berghe, T., Romagnoli, A., Fimia, G.M., Piacentini, M., and Vandenabeele, P. (2012). Beclin1: A role in membrane dynamics and beyond. Autophagy *8*, 6–17. 10.4161/auto.8.1.16645.

83. Niu, T.-K., Cheng, Y., Ren, X., and Yang, J.-M. (2010). Interaction of Beclin 1 with survivin regulates sensitivity of human glioma cells to TRAIL-induced apoptosis. FEBS Lett. *584*, 3519–3524. 10.1016/j.febslet.2010.07.018.

84. Qu, X., Yu, J., Bhagat, G., Furuya, N., Hibshoosh, H., Troxel, A., Rosen, J., Eskelinen, E.-L., Mizushima, N., Ohsumi, Y., et al. (2003). Promotion of tumorigenesis by heterozygous disruption of the beclin 1 autophagy gene. J. Clin. Invest. *112*, 1809–1820. 10.1172/JCI200320039.

85. Dhaliwal, J., Trinkle-Mulcahy, L., and Lagace, D.C. (2017). Autophagy and Adult Neurogenesis: Discoveries Made Half a Century Ago Yet in their Infancy of being Connected. Brain Plast. *3*, 99–110. 10.3233/BPL-170047.

86. Wang, C., Chen, S., Yeo, S., Karsli-Uzunbas, G., White, E., Mizushima, N., Virgin, H.W., and Guan, J.-L. (2016). Elevated p62/SQSTM1 determines the fate of autophagy-deficient neural stem cells by increasing superoxide. J. Cell Biol. *212*, 545–560. 10.1083/jcb.201507023.

87. Jung, S., Choe, S., Woo, H., Jeong, H., An, H.-K., Moon, H., Ryu, H.Y., Yeo, B.K., Lee, Y.W., Choi, H., et al. (2020). Autophagic death of neural stem cells mediates chronic stress-induced decline of adult hippocampal neurogenesis and cognitive deficits. Autophagy *16*, 512–530. 10.1080/15548627.2019.1630222.

88. Schäffner, I., Minakaki, G., Khan, M.A., Balta, E.-A., Schlötzer-Schrehardt, U., Schwarz, T.J., Beckervordersandforth, R., Winner, B., Webb, A.E., DePinho, R.A., et al. (2018). FoxO Function Is Essential for Maintenance of Autophagic Flux and Neuronal Morphogenesis in Adult Neurogenesis. Neuron *99*, 1188-1203.e6. 10.1016/j.neuron.2018.08.017.

89. Wang, C., Liang, C.-C., Bian, Z.C., Zhu, Y., and Guan, J.-L. (2013). FIP200 is required for maintenance and differentiation of postnatal neural stem cells. Nat. Neurosci. *16*, 532–542. 10.1038/nn.3365.

90. Liu, H., Wang, C., Yi, F., Yeo, S., Haas, M., Tang, X., and Guan, J.-L. (2021). Non-canonical function of FIP200 is required for neural stem cell maintenance and differentiation by limiting TBK1 activation and p62 aggregate formation. Sci. Rep. *11*, 23907. 10.1038/s41598-021-03404-7.

91. Wang, C., Yeo, S., Haas, M.A., and Guan, J.-L. (2017). Autophagy gene FIP200 in neural progenitors non–cell autonomously controls differentiation by regulating microglia. J. Cell Biol. *216*, 2581–2596. 10.1083/jcb.201609093.

92. Stuart, T., Butler, A., Hoffman, P., Hafemeister, C., Papalexi, E., Mauck, W.M., Hao, Y., Stoeckius, M., Smibert, P., and Satija, R. (2019). Comprehensive Integration of Single-Cell Data. Cell *177*, 1888-1902.e21. 10.1016/j.cell.2019.05.031.

93. Trapnell, C., Cacchiarelli, D., Grimsby, J., Pokharel, P., Li, S., Morse, M., Lennon, N.J., Livak, K.J., Mikkelsen, T.S., and Rinn, J.L. (2014). The dynamics and regulators of cell fate decisions are revealed by pseudotemporal ordering of single cells. Nat. Biotechnol. *32*, 381–386. 10.1038/nbt.2859.

94. Bergen, V., Lange, M., Peidli, S., Wolf, F.A., and Theis, F.J. (2020). Generalizing RNA velocity to transient cell states through dynamical modeling. Nat. Biotechnol. *38*, 1408–1414. 10.1038/s41587-020-0591-3.

95. Imayoshi, I., Ohtsuka, T., Metzger, D., Chambon, P., and Kageyama, R. (2006). Temporal regulation of Cre recombinase activity in neural stem cells. genesis *44*, 233–238. 10.1002/dvg.20212.

96. Srinivas, S., Watanabe, T., Lin, C.-S., William, C.M., Tanabe, Y., Jessell, T.M., and Costantini, F. (2001). Cre reporter strains produced by targeted insertion of EYFP and ECFP into the ROSA26 locus. BMC Dev. Biol. *1*, 4. 10.1186/1471-213X-1-4.

97. Truett, G.E., Heeger, P., Mynatt, R.L., Truett, A.A., Walker, J.A., and Warman, M.L. (2000). Preparation of PCR-quality mouse genomic DNA with hot sodium hydroxide and tris (HotSHOT). BioTechniques *29*, 52, 54. 10.2144/00291bm09.

98. Lagace, D.C., Whitman, M.C., Noonan, M.A., Ables, J.L., DeCarolis, N.A., Arguello, A.A., Donovan, M.H., Fischer, S.J., Farnbauch, L.A., Beech, R.D., et al. (2007). Dynamic Contribution of Nestin-Expressing Stem Cells to Adult Neurogenesis. J. Neurosci. *27*, 12623–12629. 10.1523/JNEUROSCI.3812-07.2007.

99. Tashiro, A., Zhao, C., Suh, H., and Gage, F.H. (2015). Purification and Injection of Retroviral Vectors. Cold Spring Harb. Protoc. *2015*, pdb.prot086371. 10.1101/pdb.prot086371.

100. Imayoshi, I., Sakamoto, M., Ohtsuka, T., Takao, K., Miyakawa, T., Yamaguchi, M., Mori, K., Ikeda, T., Itohara, S., and Kageyama, R. (2008). Roles of continuous neurogenesis in the structural and functional integrity of the adult forebrain. Nat. Neurosci. *11*, 1153–1161. 10.1038/nn.2185.

101. Dhaliwal, J., and Lagace, D.C. (2011). Visualization and genetic manipulation of adult neurogenesis using transgenic mice. Eur. J. Neurosci. *33*, 1025–1036. 10.1111/j.1460-9568.2011.07600.x.

102. Lagace, D.C., Donovan, M.H., DeCarolis, N.A., Farnbauch, L.A., Malhotra, S., Berton, O., Nestler, E.J., Krishnan, V., and Eisch, A.J. (2010). Adult hippocampal neurogenesis is functionally important for stress-induced social avoidance. Proc. Natl. Acad. Sci. *107*, 4436–4441. 10.1073/pnas.0910072107.

103. Zhao, C., Teng, E.M., Summers, R.G., Ming, G., and Gage, F.H. (2006). Distinct Morphological Stages of Dentate Granule Neuron Maturation in the Adult Mouse Hippocampus. J. Neurosci. *26*, 3–11. 10.1523/JNEUROSCI.3648-05.2006.

104. Walker, T.L., and Kempermann, G. (2014). One Mouse, Two Cultures: Isolation and Culture of Adult Neural Stem Cells from the Two Neurogenic Zones of Individual Mice. J. Vis. Exp. JoVE. 10.3791/51225.

105. Hagihara, H., Toyama, K., Yamasaki, N., and Miyakawa, T. (2009). Dissection of Hippocampal Dentate Gyrus from Adult Mouse. J. Vis. Exp. JoVE, 1543. 10.3791/1543.

106. Babu, H., Claasen, J.-H., Kannan, S., Rünker, A.E., Palmer, T., and Kempermann, G. (2011). A Protocol for Isolation and Enriched Monolayer Cultivation of Neural Precursor Cells from Mouse Dentate Gyrus. Front. Neurosci. *5*. 10.3389/fnins.2011.00089.

107. Babu, H., Cheung, G., Kettenmann, H., Palmer, T.D., and Kempermann, G. (2007). Enriched Monolayer Precursor Cell Cultures from Micro-Dissected Adult Mouse Dentate Gyrus Yield Functional Granule Cell-Like Neurons. PLOS ONE *2*, e388. 10.1371/journal.pone.0000388.

CHAPTER 4

Beclin1 and Atg5 Differentially Regulate Neural Stem Cells and Adult Hippocampal Neurogenesis

In submission

Contributions of co-authors

Kalinina A. performed all *in vivo*, *in vitro* and *ex vivo* experiments, managed experimental design, analysis and interpretation of data and writing the manuscript

Dhaliwal J. contributed to IHC experiments, prepared samples for EM

Zabek I. contributed to IHC experiments

Riopelle C. contributed to IHC experiments

Xue Y. maintained animal breeding and assisted with tamoxifen treatments

Alkhawaldeh H. contributed to IHC experiments

Lagace D.C. Contributed to the design, analysis, interpretation of results and writing the manuscript

Beclin1 and Atg5 Differentially Regulate Neural Stem Cells and Adult Hippocampal Neurogenesis

Kalinina A.[1], Dhaliwal J.[3], Zabek I. [1], Riopelle C. [1], Xue Y.[1,2], Alkhawaldeh H. [1], & Lagace D.C. [1,2,*]

[1]Department of Cellular and Molecular Medicine, Faculty of Medicine; University of Ottawa; Ottawa, ON, K1H 8M5; Canada.

[2]Brain and Mind Research Institute, Department of Neuroscience, Faculty of Medicine, University of Ottawa; Ottawa, ON, K1H 8M5; Canada.

[3]Hospital for Sick Children; University of Toronto; Toronto, ON, M5G 1X8; Canada.

*Correspondence: dlagace@uottawa.ca

ABSTRACT

Adult hippocampal neurogenesis occurs due to the continued proliferation of adult neural stem and progenitor cells (NSPCs) that generate adult born granule neurons. In a previous study we showed that Beclin1 is required for mitosis and DNA maintenance within Nestin-expressing NSPCs and their progeny to sustain neurogenesis. These finding raise the question if the actions of Beclin1 extrapolate or all types of adult NSPCs, as well as other regulators of autophagy. In this study, we test if Beclin1-mediated effects found in the Nestin-expressing NSPCS and their progeny extend to GLAST+ NSPCs and their progeny by creating an inducible GLAST-dependent Beclin1 knockout mice transgenic mouse (Beclin1 gKO). Beclin1 gKO mice showed loss of mitotic cells, DNA damage and reduction in neurogenesis while no reduction in autophagy was seen. These findings align with our findings in Beclin1 nKO mice and support the notion that Beclin1 affects proliferation and mitosis of NSPCs in an autophagy-independent manner. To test if the effects of Beclin1 occur with other autophagy proteins, Atg5 was removed from GLAST+, Nestin+ and GFAP+ NSPCs and their progeny which resulted in differential phenotypes. Specifically, while loss of autophagy was observed in the GLAST model, neurogenesis defect was transient and was largely dependent on astrocytes, as removing Atg5 from Nestin- and GFAP-expressing NSPCs without affecting astrocytes resulted in little to no cells being lost. As such, this work extends the understanding of autophagy-dependent and -independent contribution of Beclin1 to mitosis and DNA maintenance within adult hippocampal neurogenic cells and sheds more light on the requirement of Atg5 in astrocytes in the development of immature neurons.

INTRODUCTION

The mammalian dentate gyrus of the hippocampus is one of the few areas of the adult brain that maintains a niche of adult neural stem cells (NSCs) throughout the lifespan of an organism, including humans[1–5]. The adult NSCs respond to cues via dynamic fate shifts of quiescent neural stem cells (qNSCs) that give rise to activated NSCs (aNSCs) and neural progenitor cells (NPCs), giving rise to immature neurons[7]. Recent advancements in defining the diversity in types of NSCs and the homeostatic regulation of NSC activity have allowed our lab and others to begin to define the role of autophagy-related genes (Atgs) during adult neurogenesis[9,11,13,15] through the creation of viral and inducible models that target various stages and types of neurogenic cells.

Autophagy is a stepwise catabolic pathway that captures, degrades, and recycles unfolded proteins, expired organelles, and other debris[15], in order to provide the necessary substrates and energy for cellular homeostasis and function. Within this process Beclin1 and Atg5 are well-known to alter different parts of the autophagy pathway and have differential functions in early embryonic development. Specifically, Beclin1 has an essential role in orchestrating the biogenesis of autophagosomes, allowing for the delivery of materials to the lysosomes and endosomes[17]. Lethality in embryonic Beclin1 homozygous knockout mice highlighted first that Beclin1 was indispensable for the proliferation and differentiation of stem cells and supported the requirement of autophagy during development[18]. In contrast, Atg5 is involved in later stages of autophagy and regulates the elongation of the autophagic vacuoles[20]. Furthermore, homozygous loss of Atg5 does not result in embryonic lethality, but induces neonatal lethality via autophagy-dependent mechanisms[22]. Further work removing Atg5 from neural stem cells using the NestinCre conditional model induced a neurodegeneration phenotype associated with aggregate accumulation and loss of adult-born neurons[23]. Together these findings highlight that Beclin1 and

Atg5 may differentially exert their function on cell development and viability. This also raises the possibility that the role of Beclin1 and Atg5 in adult neurogenesis could be via distinct mechanisms that may involve autophagy-dependent or -independent functions, or a combination of both.

Others have also examined autophagy and early postnatal neurogenesis utilizing conditional embryonic knockout mouse models of Atg conjugation proteins. This includes work examining both Atg16L and Atg7, which function mechanistically similar to Atg5 as they participate in the elongation step of autophagy[25,27]. These studies showed that embryonic deletions of Atg16L or Atg7 in a conditional GFAP-Cre mouse line had no deficits in postnatal neurogenesis[25]. In contrast, deletion of FIP200 (focal adhesion kinase family interacting protein of 200 kD), which is more similar to Beclin1 since it activates and induces the autophagy machinery, caused deficits in self-renewal and differentiation of NSCs. These effects were shown to occur at 4 postnatal weeks after the conditional removal of FIP200 in GFAP-expressing cells in the embryo[28]. Moreover, the mechanisms of the deficits in self-renewal and differentiation following the removal of FIP200, were shown in subsequent work to occur specifically through unique mechanisms. In particular, the effects in self renewal were independent of the autophagy pathway[31], whereas the differentiation effect was attributed to a non-cell autonomous mechanism related to autophagy-deficient microglia[32]. These findings underscore that some, but not all, Atg proteins regulate some aspects of embryonic/early postnatal neurogenesis through distinct mechanisms that do not act through the autophagy pathway.

In the adult brain, our lab and others have begun to examine the requirement of autophagy-related proteins and found some, but not all are essential for adult neurogenesis[9]. In support of the pro-survival role of autophagy, heterozygous Beclin1 knockout mice have a significant reduction in the generation of new neurons in the dentate gyrus and the subventricular zone[34]. In mature

neurons, Beclin1 downregulation results in the accumulation of protein aggregates and neurodegeneration[35]. However, Jung et al[27] used an inducible model of deletion of Atg7, which participates in the same step of autophagy as Atg5, from adult hippocampal Nestin-expressing NSPCs and progeny and observed that Atg7 was not required for hippocampal neurogenesis in naïve conditions. In contrast, our lab and others have removed Atg5[37] and FoxO3[39] in NPCs and showed that they were essential for long-term survival of adult-generated neurons. Together these studies highlight that loss of some, but not all autophagy-related proteins alter adult neurogenesis and suggest that the loss of autophagy proteins produces distinct effects within the neurogenic cell lineage likely through unique mechanisms.

In this manuscript we address the role of Beclin1 and Atg5 in the process of adult hippocampal neurogenesis in the adult GLAST, GFAP and Nestin-expressing NSPCs through the creation of four different lineage tracing models. To track the adult GLAST-expressing NSPCs and their progeny after removal of Beclin1 or Atg5, we created inducible tamoxifen-dependent GLAST-CreER^{T2} Beclin1 and Atg5 transgenic mouse models, hereafter referred to as Belcin1 gKO and Atg5 gKO mice, respectively. In addition, we remove Atg5 from Nestin-positive NSPCs and their progeny by creating an inducible NestinCreER^{T2} Atg5 mouse model called Atg5 nKO. Additionally, to remove Atg5 from GFAP+ NSPC, we use an adenovirus that specifically targets the GFAP-expressing qNSCs. Our results demonstrate that 14 days after removal of Beclin1, Beclin1 gKO mice have a significant reduction in proliferation in the SGZ. This loss is accompanied by a significant reduction of mitotic cells, as well as DNA damage, similar to our findings in Beclin1 nKO mice shown in our previous study. In contrast to the findings in the Beclin1 gKO mice, the Atg5 gKO mice, Atg5 nKO, or virally infected Atg5 mice did not alter NSPC proliferation and only transient effects on neurogenesis were observed. Interestingly, the

Atg5 gKO mice had a rapid loss of recombined hippocampal cells. The cell loss in the hippocampus was most pronounced in the GLAST-expressing resident astrocytes and not the different long-term populations of neurogenic cells. Deletion of Atg5 in the Atg5 nKO mice or using the GFAP+ virus with no recombination in resident astrocytes, had mild to no effect on neurogenesis, respectively. These findings suggest that Atg5 gKO mice induced non-cell-autonomous mechanisms via the requirement of Atg5 in astrocytes. Our results also confirm that Beclin1 is required to maintain the proliferation of adult NSPCs in the adult hippocampus during active cell cycle. Furthermore, since Beclin1 removal did not reduce autophagy in gKO mice, our findings suggest that mitotic deficit of Beclin1-null cells mechanistically may be a result of the autophagy-independent function of Beclin1.

RESULTS

Removal of Beclin1 from GLAST+ NSPCs and their progeny reduces adult hippocampal neurogenesis

To determine if deleting Beclin1 would reduce adult neurogenesis in GLAST+ NSPCs and their progeny, we created a Beclin1 GLAST-inducible transgenic mouse model (hereafter referred to as Beclin1 gKO; GLASTCreER^{T2}:CMV-eGFP: Beclin1$^{flox/flox}$) and littermate control wild-type (WT) mice (GLASTCreER^{T2}:CMV-eGFP: fBeclin1$^{WT/WT}$). The Beclin1 gKO mice were used to compare to the Beclin1 nKO mice (Chapter 3), since the GLAST promoter in comparison to the Nestin promoter, allows for recombination in a higher proportion of quiescent NSCs (qNSCs) and thus targets cells earlier in the neurogenic lineage[41,43]. To lineage trace the Beclin1-null cells tamoxifen (TAM) was administered and mice were phenotyped at 3, 14 and 30 dpi (Fig. 1A-C). There were significantly fewer recombined (GFP+) cells in the SGZ of the dentate gyrus in the

Beclin1 gKO mice compared to WT controls ($F=5.034$, $p<0.05$) (Fig 1 C). Post hoc analysis revealed a trend in declining numbers of GFP+ cells at 14 dpi in the Beclin1 gKO mice.

To test if the reduction in neurogenic cells in the Beclin1 gKO mice resulted in a reduction in adult neurogenesis, the number of adult generated immature and mature neurons was assessed at 14 and 30 dpi. As shown by the representative images and quantification of the dentate sections stained with GFP, the immature cell marker doublecortin (DCX), and the mature neuronal nuclei marker (NeuN), the Beclin1 gKO mice had a significant reduction in the proportion of GFP+DCX+ immature neurons (Fig 1D, E) and GFP+NeuN+ mature neurons (Fig 1D, F) at 30 dpi. Together the findings from the Beclin1 gKO, as well as the Beclin1 nKO mice in Chapter 3, both support the requirement of Beclin1 in the maintenance of adult neurogenesis.

To further test if reduced neurogenesis in Beclin1 gKO mice was accompanied by a reduction in autophagy, Beclin1 gKO and WT mice were injected with an mCherry-EGFP-LC3 retrovirus, using our published *in vivo* methodology to identify autophagosomes and autolyosomes[37]. Quantification of the number of autophagosomes and autolysosomes (mCherry+ puncta) revealed no significant reduction in Beclin1-null cells in the Beclin1 gKO mice compared to control cells in the WT mice (Fig 1G, H), suggesting that the Beclin1-null cells had no alteration in autophagy. Overall, these findings support the notion that Beclin1 is necessary for the proper expansion of NSCs in the dentate gyrus and its removal results in decreased production of new cells.

Beclin1 is required for mitotic activity of adult hippocampal NSPCs

To examine whether the removal of Beclin1 from GLAST+ cells and progeny reduces neurogenesis by reducing proliferation, the cycling NSPCs were examined at 14 and 30 dpi. Using IHC to stain for the minichromosome maintenance complex component 2 (Mcm2) in order to label

cycling cells[45], we observed a nearly complete loss of proliferating GFP+Mcm2+ cells at 30 dpi in Beclin1 gKO mice (Fig 2A, B). To further test if the Beclin1 gKO mice had a similar reduction in the proportion of mitotic cells, the *ex vivo* cell cycle assay was repeated using the same EdU paradigm as for the Beclin1 nKO mice. This analysis revealed that the percentage of GFP+EdU+ cells was significantly reduced in Beclin1 gKO mice (Fig 2C, D). Additionally, there was a significant reduction in proportion of the mitotic Beclin1-null cells in the absence of alteration in proportion of the S phase Beclin1- null cells (Fig 2E, F), These findings are congruent with those in the Beclin1 nKO mice and support the notion that the loss of Beclin1 reduces numbers of mitotic cells suggesting that this protein is required for mitotic proliferation of adult NSPCs.

Loss of Beclin1 induces DNA damage in GLAST+ cells and their progeny

The faulty mitotic checkpoints and reduction in DNA maintenance that we discovered in the Beclin1-null cells from the Beclin1 nKO mice (Chapter 3) can commonly result in DNA damage and chromatin abnormalities in cancer cells[47,49]. To analyze the general levels of fragmented DNA, the alkaline comet assay was used, which is highly sensitive to both double- and single- strand DNA breaks[51]. At 14 dpi, sorted Beclin1-null cells in the GLAST gKO mice had a higher percent of DNA in the comet tail and a higher tail moment (Fig 3A, B) suggesting increased DNA fragmentation. These findings thus support that Beclin1-null cells in Beclin1 gKO mice have an increased accumulation of DNA damage.

Next, we tested if Beclin1 gKO mice also had deficits in DNA damage and increased apoptosis activity using flow cytometry to detect the cells expressing ɣH2A histone family member X (ɣH2AX). H2AX is commonly used in assays to detect double-strand breaks in DNA (dsDNA) since it becomes phosphorylated on serine 139, and called ɣH2AX, when dsDNA breaks occur[53,55].

At 14 dpi there was a significant increase in the proportion of Beclin1-null cells that had ɣH2AX activity (Figure 3C, D). Thus, as hypothesized Beclin1-null cells possessed enhanced DNA damage and apoptotic activity, compared to the WT cells.

The comet assay and ɣH2AX findings from the Beclin1 gKO mice both highlight that Beclin1 removal resulted in a substantial curb of mitotic activity and enhanced damage to their DNA. These findings thus corroborate the requirement of Beclin1 in proliferating cells to maintain cell cycle and prevent DNA damage during chromosome maintenance. These results also suggest that Beclin1 is required for chromosomal dynamics during mitosis and the generation of adult-born neurons congruent with the finding in the Beclin1 nKO mice.

Removal of Atg5 from GLAST+ cells and progeny transiently lowers the number of immature neurons and significantly reduces autophagy in Atg5 gKO mice

To test if a reduction in proliferation and neurogenesis would occur with other autophagy proteins, Atg5 was deleted using the same GLAST-inducible transgenic mouse used to delete Beclin1 with the exception that a floxed Atg5 was used during the breeding. The resulting mice were therefore called Atg5 gKO (GLASTCreER^{T2}:CMV-eGFP:Atg5$^{flox/flox}$) and they had corresponding littermate control wild-type (WT) mice (GLASTCreER^{T2}:CMV-eGFP: fAtg5$^{WT/WT}$). Examination of the lineage tracing of the Atg5-null cells (Fig 4A-C) showed that the reduction in the number of cells in the Atg5 gKO mice did not temporally replicate the findings of Beclin1 nKO and gKO models. Unlike the Beclin1 models, the Atg5 nKO had a drastic reduction in number of Atg5-null cells as early as 3 dpi (Fig 4A, C). In addition, while there was a strong reduction of Atg5-null cells at 3 and 14 dpi, the reduction in Atg5-null cells compared to WT cells was transient and not

observed at 30 dpi (Fig 4C). These findings hint at differential mechanisms by which Atg5 and Beclin1 may regulate adult hippocampal neurogenesis.

The effect of removing Atg5 from GLAST cells and their progeny was further assessed through examining the number of Atg5-null cells that expressed markers of immature and mature neurons at 14 and 30 dpi using DCX and NeuN, respectively (Fig 4D). The proportion of immature DCX+ cells in the Atg5 gKO mice was significantly reduced at 30 dpi, but not after 14 days (Fig 4D, E). There was also no difference in the proportion or total number of NeuN+GFP+ cells observed at 30 days (Fig 4F). These results suggest that removal of Atg5 induces only a transient reduction in the neurogenic lineage that may be specific to immature neurons.

To determine whether Atg5 gKO mice had a reduction in autophagy, quantification of autophagic vacuoles was performed using electron microscopy in collaboration with Dr. Marie-Eve Tremblay at University of Victoria. The Atg5 gKO compared to WT mice had a significant reduction in autophagic vacuoles in GFP+ cells in the SGZ, supporting that removal of Atg5 reduced autophagy (Fig 4G, H). These data suggest that Beclin1 and Atg5 are associated with differential temporal effects on adult neurogenesis and the mechanisms altering neurogenesis may be different and involve non-autophagic functions of Beclin1 or Atg5 proteins.

Atg5 removal does not reduce proliferation of adult aNSC or NPCs in the Atg5 gKO mice

To determine if the reduction in Atg5-null cells at 3 dpi and transient reduction in immature neurons at 14 dpi in the Atg5 gKO mice was temporally associated with a reduction in proliferation, a series of experiments were performed to test proliferation at 3 dpi. First, examination of the total number of dividing Ki67-expressing cells showed that Atg5 removal did not modify the number of proliferating cells in the dentate gyrus (Fig 6A, B). Next, an EdU-

labeling paradigm was employed to assess the number of proliferating cells, as well as the proportion of aNSCs, by injecting the mice with EdU four times two hours apart and perfusing two hours after the last injection similar to previously published protocol[57]. Examining the Atg5-null cells that were co-labeled with EdU showed that both the Atg5 gKO and WT mice had a similar number of proliferating GFP+EdU+ cells (Fig 5C, D) corroborating the Ki67 results. To additionally examine the proportion of aNSCs, Sox2, was used to label the NSCs and showed that there was a similar number of aNSCs in the Atg5 gKO and WT mice in the SGZ (Fig 5C, D).

Lastly, to determine if there is a difference in proliferating NPCs, Mcm2 and DCX were used to label proliferating cells and neuroblasts. There was no difference in all proliferating GFP+Mcm2+ cells (Fig 5E, F) as in the previous staining for EdU and Ki67. There was also no significant difference in proliferating Atg5-null DCX+Mcm2+ differentiating progenitors (Fig 5E, F). In conclusion, the large decrease of Atg5-null cells in the Atg5 gKO model at 3 dpi is not accompanied by deficits in proliferating aNSCs, or late NPCs, suggesting that the mechanism of action of Atg5 is distinct from modulation of mitosis as observed in the Beclin1 nKO and Beclin1 gKO mice in the adult neurogenic lineage.

Loss of Atg5 does not modify the proportion of qNSCs or aNCSs in Atg5 gKO mice

Given that there was a reduction in the number of Atg5-null cells at 3 dpi yet no change in proportion of cycling Atg5-null cells, it remained a possibility that loss of Atg5 may increase the number of qNSCs. To test this hypothesis, we used IHC and flow cytometry methodologies to examine qNSCs at 3 dpi which can be difficult to reliably identify.

IHC was used to analyze the percentages of qNSCs positive for aldolase C (AldoC) and negative for proliferating cell nuclear antigen (PCNA-AldoC+) at 3, 14 and 30 dpi. The Atg5-null and WT

mice had similar percentages of proliferating GFP+PCNA+ cells which, as expected, declined over time (Fig 6A, B). The Atg5-null mice had an accompanying significant increase in qNSCs (PCNA-AldocC+) cells compared to the WT mice (genotype main effect) (Fig 6A, C). However, post hoc analysis revealed no significant decline in the percentage of cells at any one time point. As such, while Atg5 loss may enhance NSC quiescence, this mild effect does not align with the large loss of Atg5-null cells at 3 dpi.

Flow cytometry was additionally used to identify NPCs and aNSCs and isolate the qNSCs. Specifically, the membrane-bound epidermal growth factor receptor (EGFR) was used to capture mostly the proliferating NPCs and some aNSCs[58,60], and the membrane-bound Cluster of Differentiation 15 (CD15, also known as Lewis X) was used to capture the NSCs[62] (Fig 6D). Among the GFP+ cells from WT and Atg5 gKO mice, there was no difference in the proportion of proliferating cells (GFP+EGFR+; Fig 6E), aNSCS (GFP+EGFR+CD15+; Fig 6F) or qNSCs (GFP+EGFR-CD15+; Fig 6G). Together with the IHC analysis of the qNSCs, these findings show that Atg5 removal does not alter the proportion of the qNCSs at 3dpi and confirm that the Atg5 gKO have a similar proportion of proliferating aNSCs and NPCs. Thus, these results suggest that differential mechanisms account for the distinctive phenotypes of the Beclin1 versus Atg5 gKO mouse models.

Reduction in astrocytes located in the dentate in the Atg5 gKO mice

A feature of the GLAST model is that it also recombines the GLAST+ resident astrocytes given that GLAST is one of the many proteins expressed in both NSCs and astrocytes[43]. Given some previous findings of autophagy modulating neurogenesis potentially via paracrine effect on resident glia such as astrocytes and microglia[32,39], we tested if Atg5 or Beclin1 from GLAST+ cells

and their progeny modified the number of astrocytes in the dentate gyrus. We quantified the number of recombined GFP+ astrocytes based on phenotypic features in both the Atg5 and Beclin1 gKO mice, specifically, in the hilus and the molecular layer (ML) of the dentate gyrus at 3 and 14 dpi.

The Atg5 gKO mice had a significant reduction in GFP+ astrocytes in the dentate compared to WT mice. There was no significant difference in astrocyte numbers in the hilus of Atg5 gKO mice, however, a significant effect of genotype was observed on the astrocytes in the ML. Post-hoc analysis of astrocytes in the ML showed a near-significant reduction at 3 ($p=0.05$) and 14 dpi ($p=0.09$) (Fig 7A, B). In contrast the Beclin1 mice did not have a significant difference in number of recombined astrocytes compared to their WT control mice in hilus or ML (Fig 7C, D). These results suggest that the reduction in number of recombined neurogenic cells in the SGZ of the Atg5 mice is temporally associated with a reduction in the number of astrocytes in the ML of dentate gyrus. This suggests that the loss of Atg5 in the gKO mice model affecting the astrocyte numbers may non-specifically and transiently reduce total numbers of recombined cells via cell interaction mechanisms.

Viral mediated removal of Atg5 from NSCs and their progeny in vivo

To dissect the contribution of Atg5 within the NSCs and their progeny versus astrocytes in the dentate, we utilized an adenovirus designed with a GFAP promoter that has been shown to infect the qNSCs and their progeny in the absence of infecting astrocytes[64]. Specifically, the rAAV4-GFAP-GFP-Cre virus was injected into $Atg5^{fl/fl}$ and WT mice, then one week after the viral injection EdU was administered to label proliferating NSPCs (Fig 8A). The mice were perfused at 24hr after the last EdU injection (Fig 8B), to align temporally with perfusion at 3 dpi (8 days since

first TAM injection) in the Atg5 gKO mice as shown in Fig 4B. There was no change in the number of virally infected GFP+ cells between WT and $Atg5^{fl/fl}$ mice, suggesting that removal of the Atg5 did not alter the number of NSCs and their progeny (Fig 8C).

To phenotype the virally infected cells, the GFP+ cells were co-labeled with AldoC to quantify the proportion that were qNCS, as well as EdU to quantify the proportion of cells that were proliferating at time of injection and survived 24hrs. As shown in Figure 8D and 8E, more than 60% of infected cells in the Atg5fl/fl mice, as well as in the WT mice, were qNSCs, which aligns with this virus being characterized to mainly infect qNSCs. Similarly, very few (<1%) GFP+ GFP+EdU were labeled (Fig 8D, F) supporting the notion that the virus mainly infects qNSCs[64]. Examination of proliferation using endogenous marker of proliferation PCNA also corroborated that a similar proportion of infected cells (~5-10%) were proliferating in the Atg5fl/fl and WT mice (Fig 8G, H). Lastly, there was a similar proportion of DCX+ neuroblasts and immature neurons (Fig 8G, I). Together these results suggests that removal of Atg5 from the qNSCs in the SGZ did not replicate the reduction in Atg-null cells in the Atg5 gKO mice which supports the hypothesis that removal of Atg5 from the astrocytes in the dentate may mediate the observed reduction in neurogenesis in the Atg5 gKO mice.

Atg5 nKO mice have a mild loss of neurogenesis that does not match the Atg5 gKO mice model

To further test the role of Atg5 in adult neurogenesis we created an Atg5 Nestin-inducible transgenic mouse model (hereafter referred to as Atg5 nKO; $NestinCreER^{T2}$:R26R-eYFP: $Atg5^{flox/flox}$) and littermate control wild-type (WT) mice ($NestinCreER^{T2}$:R26R -eYFP:

fAtg5$^{WT/WT}$). This model thus allowed for the removal of Atg5 in NPCS and their progeny, in the absence of altering Atg5 expression in astrocytes, as previously published[43].

The total numbers of WT and Atg5-null cells were examined at 3, 14 and 30 dpi (Fig 9A, B) which revealed an overall reduction in numbers of recombined (GFP+) cells in the Atg5 nKO compared to WT mice (Fig 9A, C). Post hoc analysis revealed a transient decline in the number of cells at 14 dpi. Although the average number of cells was also lower at 3 and 30 dpi, this effect was not significant. Thus, these findings were more similar to the Beclin1 gKO mice (Fig 1A-C) and did not replicate the dramatic decline in cells in the Atg5 gKO mice at 3 dpi (Fig 4A-C).

The reduction in the number of recombined cells in the Atg5 nKO mice was not associated with any change in proliferating cells, as assessed by the number of Ki67 cells at 14 dpi (Fig 9D, E). There was also a similar percentage of recombined proliferating NSPCs (YFP+PCNA+; Fig 9F, G), aNSCs (YFP+PCNA+Sox2; Fig 9F, H) and qNSCs (YFP+PCNA-Sox2+ Fig 9F, I). These results show that loss of Atg5 in the nKO mice did not alter qNSCs or proliferation and thus corroborate the findings of Atg5 loss in both Atg5 gKO and Atg5$^{flox/flox}$ mice.

The Atg5 nKO mice also had a similar proportion of immature neurons (YFP+DCX+; Fig 9J, K) and adult generated neurons (YFP+NeuN+; Fig 9L) compared to WT mice. While the Atg5 nKO and WT mice had a similar proportion of immature and mature (NeuN) cells, the total number of DCX+YFP+ cells was significantly decreased at 14 dpi in the Atg5 gKO mice (Fig 9M). Thus, removal of Atg5 from nKO mice had a milder effect on recombined cells compared to Atg5 gKO mice and did not produce a significant effect on the proportions of immature and mature neurons at 30 dpi with a transient effect on the total number of recombined immature neurons at 14 dpi.

DISCUSSION

The findings of this study show that Beclin1 and Atg5 autophagy proteins have differential effects on hippocampal neurogenesis. Beclin1 is essential for the generation of adult-born neurons in the hippocampus. Beclin1 loss in the gKO mice resulted in a reduction in proliferation, deficits in mitosis, and DNA damage accumulation. These findings align with the results in the Beclin1 nKO mice shown in Chapter 3 and support the essential role of Beclin1 within two independent KO mouse models that target different populations of NSPCs. In contrast, the Atg5 nKO mice had a transient reduction in neurogenesis, similar to our published work examining Atg5 in the survival of immature neurons[37]. The Atg5 gKO mice, unlike Beclin1 and Atg5 nKO mice, had a distinct striking transient decrease in recombined cells due to Atg5 loss in GLAST-expressing resident astrocytes. These findings therefore revealed that Beclin1 has a cell-intrinsic role in the regulation of proliferation of NSPCs, whereas Atg5 has a role in the maintenance of resident astrocytes.

Our data underpins the novel finding that Beclin1 is required within both GLAST- and Nestin-expressing dividing NSPCs for proliferation and specifically for correct progression through mitosis. These findings are in concert with examination of Beclin1's role in mitosis of cancer and reproductive cells. Specifically, Beclin1 deletion causes a G2/M cell cycle arrest of HeLa cells which is associated with chromatin abnormalities and aberrant spindle and kinetochore assembly[66]. In addition, Beclin1 protein removal from reproductive and cancer cells is related to chromosomal instability, centrosome abnormalities, midbody ring remnants, and cytokinesis failure[68,70,72]. Our *in vivo* findings expand the understanding of the functions of Beclin1 in mitosis, which are yet to be established in other *in vivo* models that target the nervous system. This study supports the involvement of Beclin1 in the regulation of mitotic machinery specifically during adult hippocampal neurogenesis which is yet to be extrapolated to other neurogenic regions.

Since Beclin1 can have autophagy-dependent and -independent roles[17], our findings raise the question whether the observed changes in cell cycle and associated DNA damage occur through an autophagy-dependent mechanism. As discussed in Chapter 3 and the introduction, deficits after embryonic removal of autophagy-associated proteins in NSPCs has been suggested to be due to either autophagy-dependent or–independent mechanisms[11-13]. Specifically, loss of FIP200, a protein in close association with Beclin1[76], in GFAP+ NSPCs and their progeny resulted in a distinct effect on neuronal differentiation which was autophagy-dependent. However loss of FIP200 in the early postnatal GFAP+ NSPCs and their progeny was associated with self-renewal deficits in NSCs that were not dependent on autophagic function of FIP200[28,31]. Since Atg5 loss resulted in both deficient autophagy and neurogenesis in Atg5 gKO mice without proliferation changes, the loss of Beclin1 may lead to the mitotic deficit and DNA damage via independent mechanisms as well. This novel finding is ripe for future delineation of non-autophagic functions of Beclin1 that contribute to the dysregulation in cell cycle and induction of DNA damage in the NSPCs.

The creation of the Atg5 gKO and nKO mouse lines also provides novel insights into the role Atg5 in adult neurogenesis. Both Atg5 gKO and nKO mice had a reduction in Atg5-null cells in the SGZ at 14 dpi that was associated with a reduction in number of recombined cells in the absence of altering proliferation of the NSCPs. The transient reduction in Atg5-null immature neurons is in line with our previous report of reduced immature neurons in adult mice due to a delay in their maturation when removing Atg5 from rapidly dividing NPCs using a retrovirus approach[37]. In the Atg5 gKO, but not Atg5 nKO mice our findings show that the decline in immature neurons was accompanied by a significant decline in the proportion of adult-generated Atg5-null neurons. The reduction of neurogenesis in the Atg5 gKO and not the Atg5 nKO mice we hypothesize is due to

the robust decline in Atg5-null astrocytes and not Atg5 intrinsic effects within the neurogenic lineage per se. In alignment with this hypothesis, embryonic conditional deletion of Atg5 (as well as Atg16L or Atg7) in GFAP+ NSCPs and their progeny does not alter neurogenesis at 3 weeks or 3 months of age[25]. Yet, in embryonic neurogenesis, Atg5 is required for the proliferation and differentiation of NSPCs during cortical development[78]. Thus, our findings support the different functional roles of Atg5 during embryonic, early postnatal and adult neurogenesis. Although one limitation to this work is that it remains unknown how loss of Atg5 in astrocytes reduces adult neurogenesis, it is well known that astrocytes are juxtracrine regulators of adult hippocampal neurogenesis through endocytosis and signaling molecule release that directly target NSPCs[79,81,83,85]. Thus, future studies will be required to elucidate what mediates the reduction in adult neurogenesis in the Atg5 gKO mice.

One of the most unexpected findings found in this study was the discovery that Atg5 is required in GLAST-expressing astrocytes in the adult hippocampus. This was shown in the Atg5 gKO mice that induces recombination and removes Atg5 in astrocytes. The rapid and large reduction of recombined astrocytes occurred began at 3 and persisted at 14 days after the last treatment with tamoxifen. This effect was shown to be specific to Atg5 gKO mice and did not occur in the Beclin1 gKO mice. Wang et al.[87] was the first to discover that Atg5 was essential for the generation of cortical astrocytes during development. In this study, Atg5 knockout induced a robust reduction in both astrocyte generation and maturation, which could be rescued by overexpression of Atg5. Unlike developmental astrogenesis that is initiated by NSCs, astrogenesis in the adult dentate is mediated mainly through the proliferation of local astrocytes[88]. Specifically, *in vivo* two-photon imaging of astrocytes in the hippocampus has shown 2-3 astrocytes can be generated by 1-2 local proliferations. Thus, it will be important for future work to continue to dissect the role of Atg5 in

the astrocyte-derived astrogenesis in the adult dentate and determine if the loss of astrocytes is due to deficits in the proliferation of astrocytes and through what mechanism.

In conclusion, these findings support the notion that Beclin1 and Atg5 have distinct roles in adult neurogenesis. The results of our studies show that Beclin1 is required in GLAST-expressing mitotic NSPCs and their progeny, which aligns with its role in Nestin-expressing NSPCs in Chapter 3. In contrast, Atg5 is involved in the development of immature neurons in the GLAST- and Nestin-expressing NSPCs and their progeny, as characterized by their similar transient reduction in recombined cells. The removal of Atg5 in the GLAST-expressing astrocytes further highlighted a unique requirement of Atg5 in astrogenesis, as characterized by the rapid decline in recombined astrocytes in the dentate gyrus that accompanied an overall reduction in neurogenesis. These findings therefore expand our understanding of the differential role of Beclin1 and Atg5 in adult hippocampal neurogenesis.

Figures and figure Legends

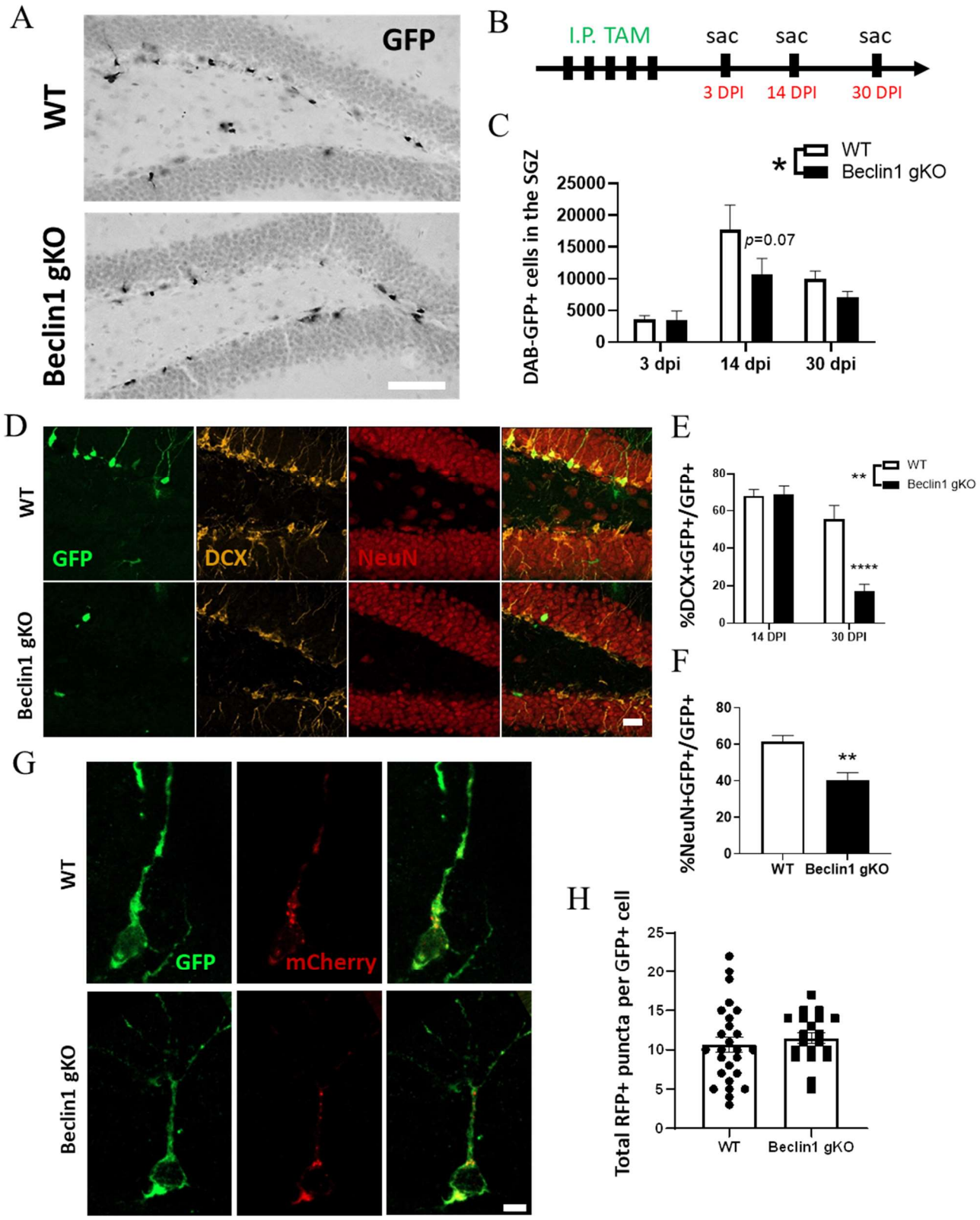

Figure 1. Beclin1 removal reduces neurogenesis in gKO mice. (A) Representative brightfield

images of DAB-GFP+ cells at 14 dpi (B), experimental timeline, and (C) results of quantification of DAB staining in WT and Beclin1 gKO recombined cells. (D) Fluorescent images of recombined (green) immature (gold) and mature neurons (red) at 30 dpi and (E-F) quantification results. (G) Representative images of the virally-infected GFP+ (green) cells with autolysosomes (red) and (H) quantification results. Scale bars represent 250 uM (A); 20 uM (D), 5 uM (G); All graphed data show the mean ± SEM; * $p \leq 0.05$, ** $p \leq 0.01$, **** $p \leq 0.0001$.

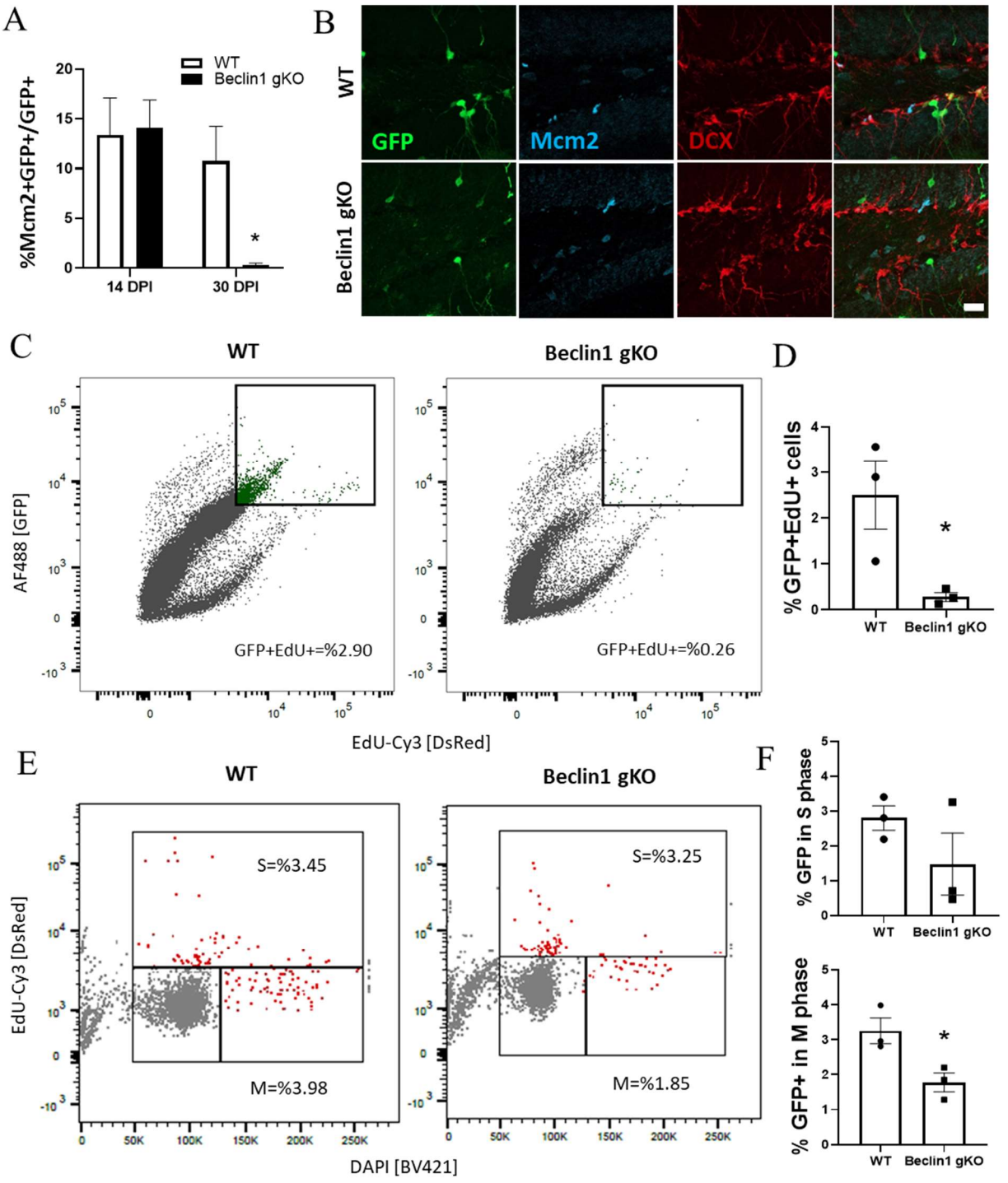

Figure 2. Beclin1 removal reduces proliferation and mitosis in gKO mice. (A) Quantification results of (B) fluorescent images showing recombined (green) proliferating (blue) cells and immature neurons (red). (C) Flow cytometry results showing proliferating EdU-positive recombined cells (green) and (D) quantification results. (E) Flow cytometry results depicting mitotic EdU-positive cells (red) and (D) quantification results showing percentages of cells in S and M phases. Scale bar represents 20 uM (A); All graphed data show the mean ± SEM; * p≤0.05.

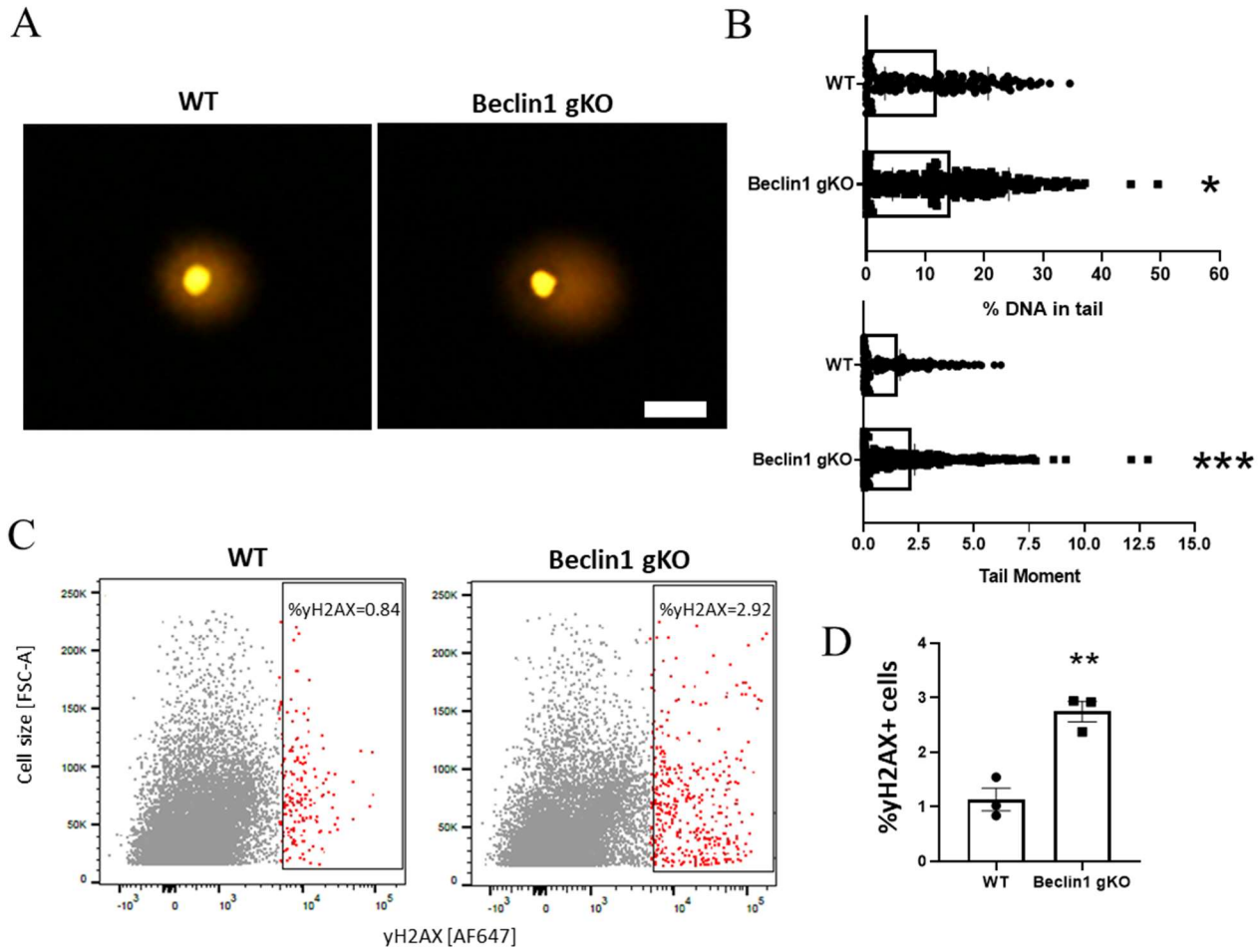

Figure 3. Beclin1 removal results in DNA damage and apoptosis. (A) Representative fluorescent images of GFP+ cells with comet tails (gold), and (B) comet tail and moment quantification results. (C) Flow cytometry results depicting γH2AX+ cells (red) and (D) quantification results. Scale bar represents 20 uM (A); All graphed data show the mean ± SEM; * p≤0.05, ** p≤0.01, *** p≤0.001.

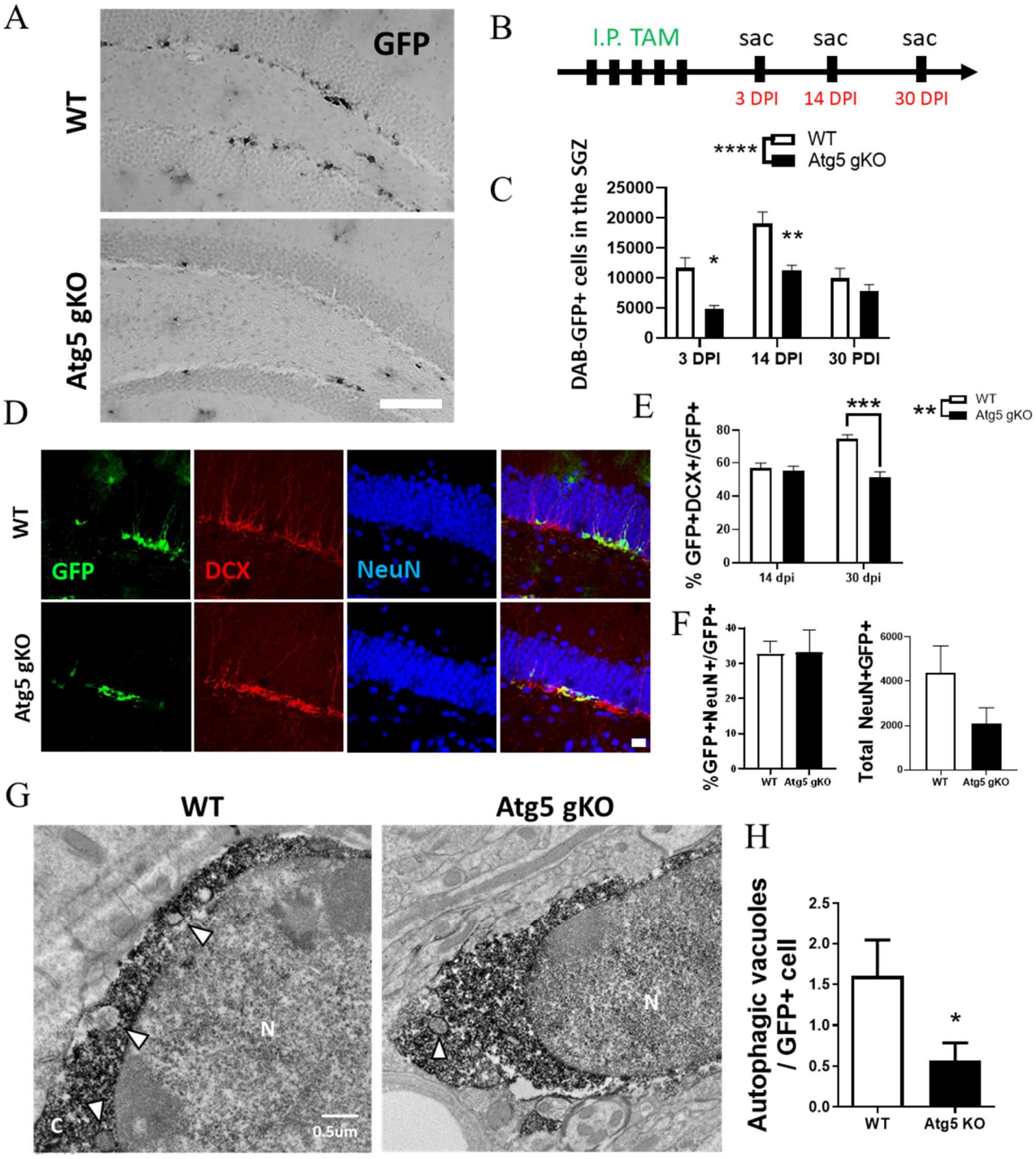

Figure 4. Atg5 removal reduces immature neurons and autophagy in gKO mice. (A) Representative brightfield images of DAB-GFP+ cells at 3 dpi (B), experimental timeline, and (C) results of quantification of DAB staining in WT and Atg5 gKO recombined cells. (D) Fluorescent images of recombined (green) immature (red) and mature neurons (blue) at 30 dpi and (E-F) quantification results. (G) Representative images of the EM-visualized GFP+ (green) cells with autophagosomes (arrowheads) and (H) quantification results. Scale bars represent 250 uM (A); 20

uM (D), 0.5 uM (G); All graphed data show the mean ± SEM; * $p \leq 0.05$, ** $p \leq 0.01$, *** $p \leq 0.001$, **** $p \leq 0.0001$.

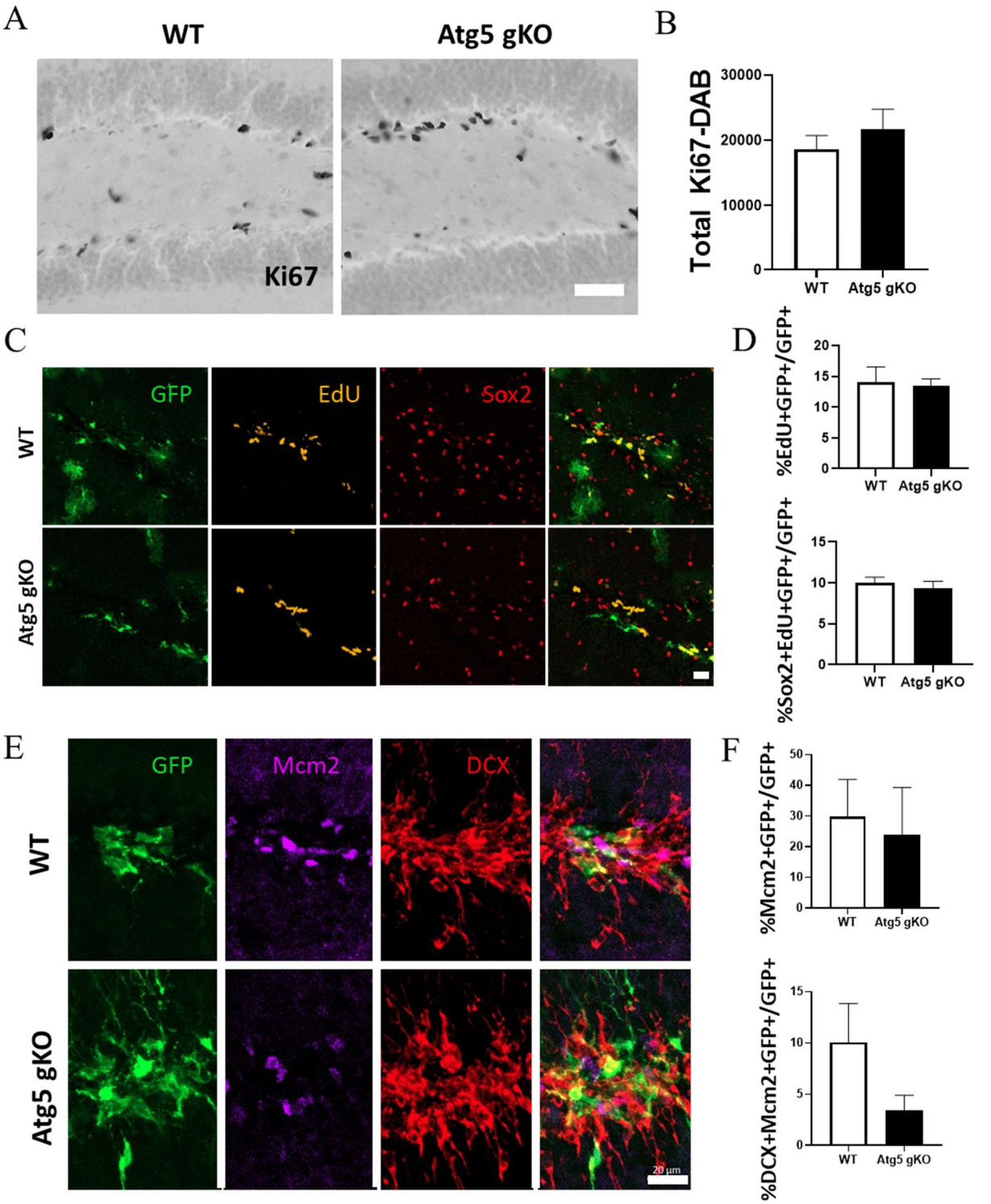

Figure 5. Atg5 loss does not impact proliferation in gKO mice. (A) Representative brightfield images of DAB-Ki67+ cells at 3 dpi and (B) quantification results. (C) Fluorescent images of recombined (green), EdU+ (gold) cells and NSCs (red) at 3 dpi and (D) quantification results. (E) Fluorescent images of recombined (green), proliferating (violet) and immature (red) neurons at 3

dpi and (F) quantification results. Scale bars represent 50 uM (A); 20 uM (C,D); All graphed data show the mean ± SEM.

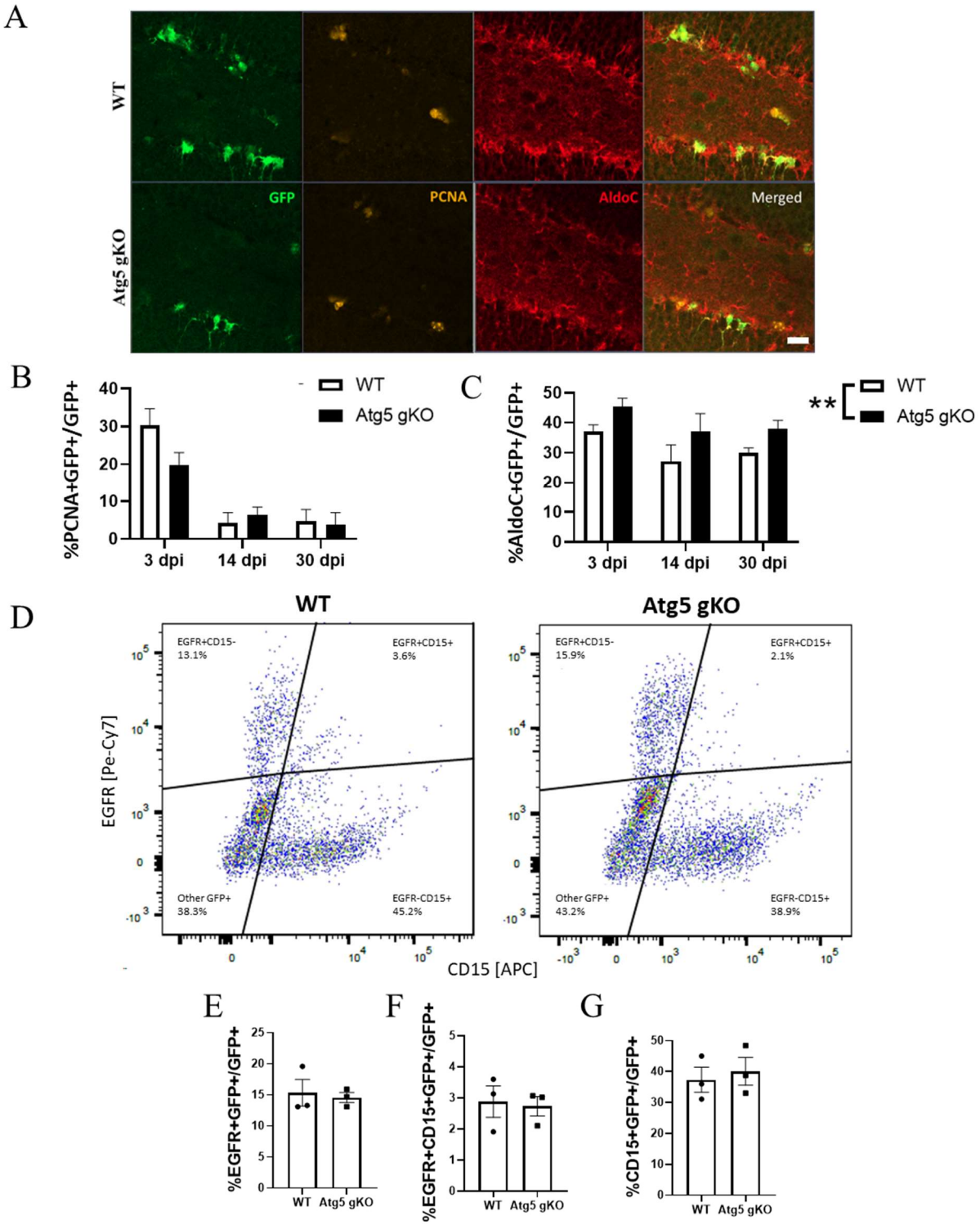

Figure 6. Atg5 removal does not perturb quiescence/activation balance. (A) Representative fluorescent images of recombined (green) proliferating (gold) cells and qNSCs (red) at 14 dpi and (B, C) quantification results. (D) Flow cytometry results showing GFP+ cells split into 4 groups – proliferating cells (top left), proliferating NSCs (top right), qNSCs (bottom right) and other

recombined cells (bottom left) and (E-F) quantification results. Scale bars represent 20 uM (A); All graphed data show the mean ± SEM; ** $p \leq 0.01$.

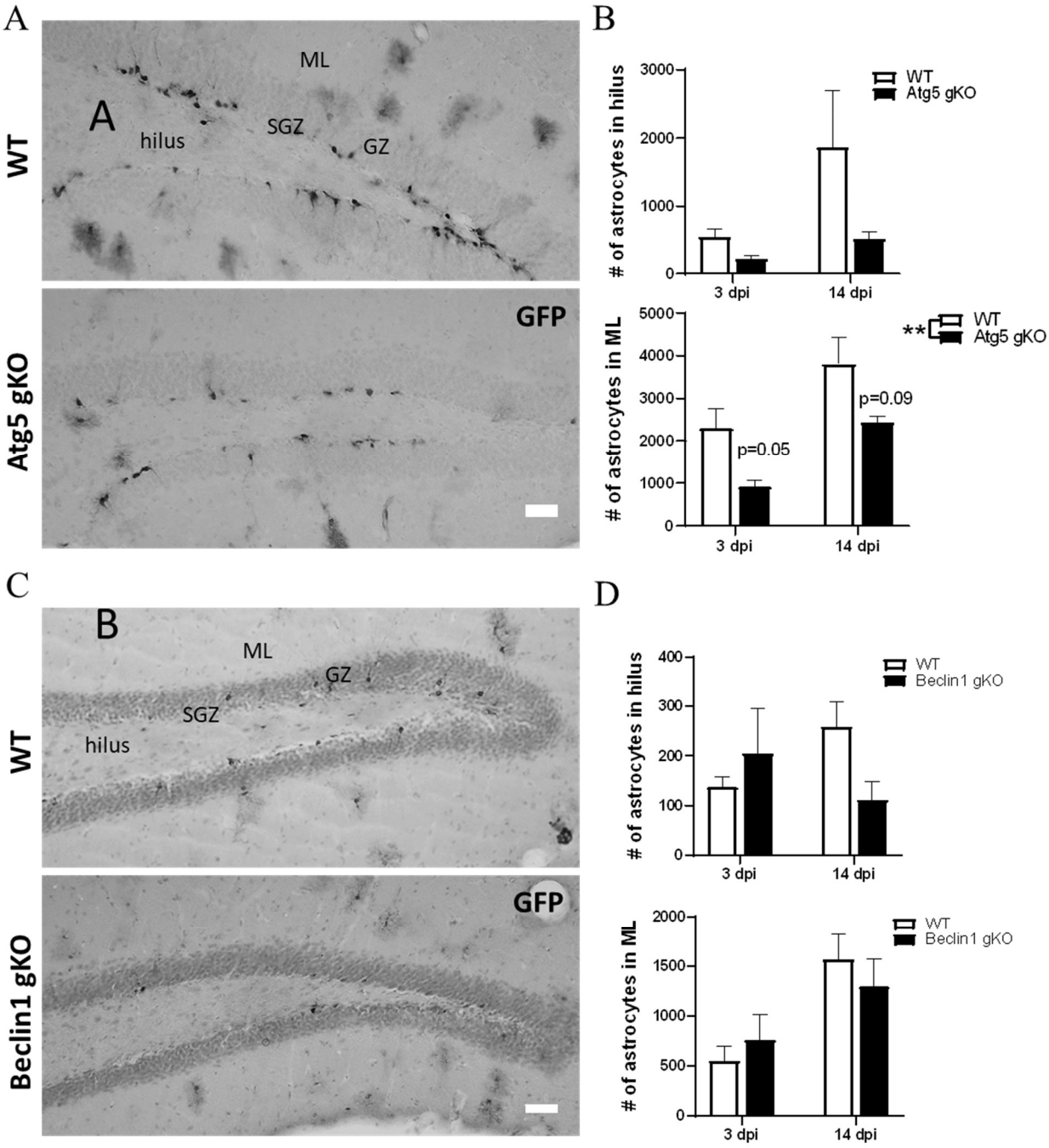

Figure 7. Atg5 but not Beclin1 loss reduces astrocyte numbers in gKO mice. (A) Representative brightfield images of DAB-GFP+ cells at 14 dpi in WT and Atg5 gKO mice and (B) quantification results. (C) Representative brightfield images of DAB-GFP+ cells at 14 dpi in WT and Beclin1 gKO mice and (D) quantification results. Scale bars represent 250 uM (A,D); All graphed data show the mean ± SEM; ** $p \leq 0.01$.

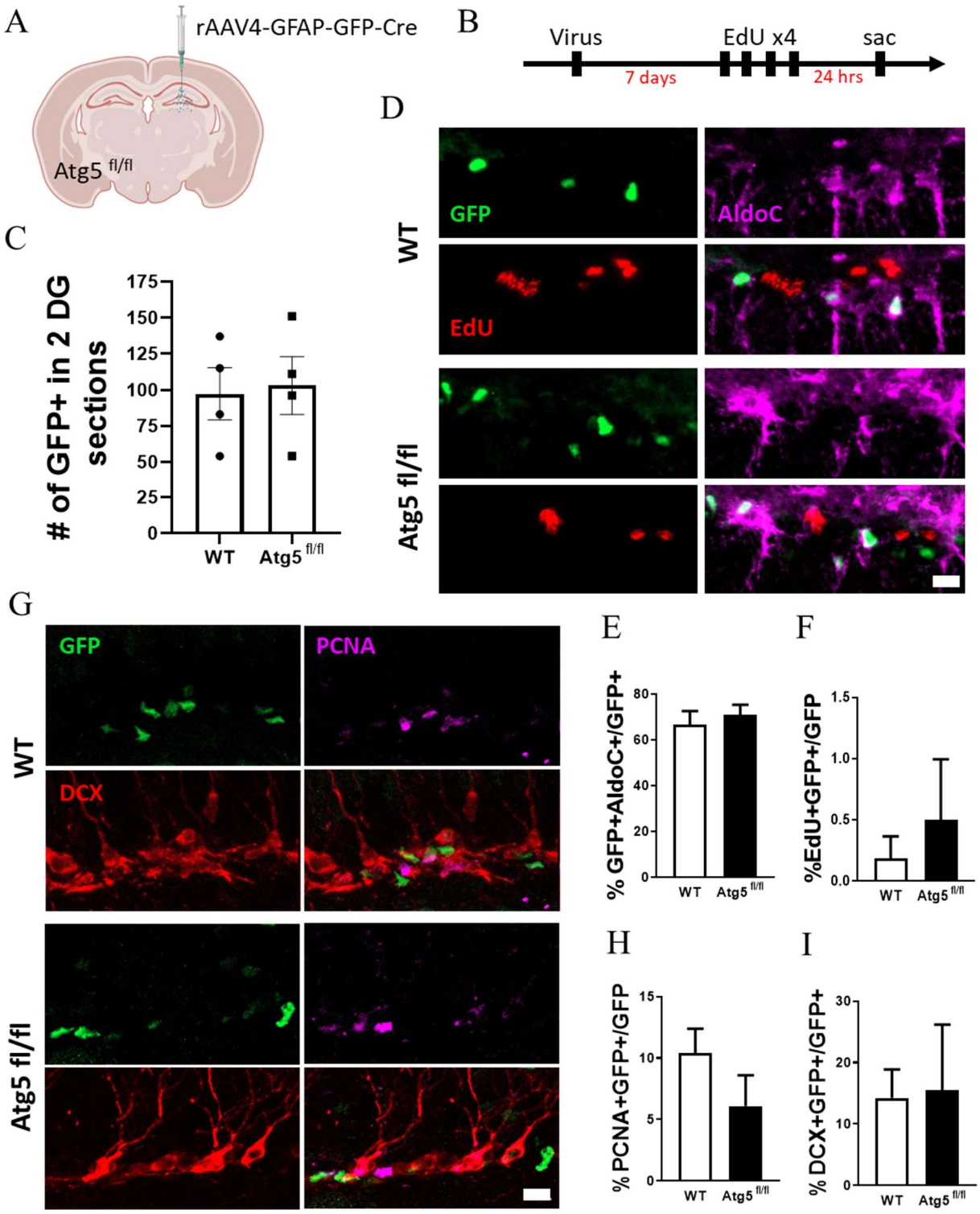

Figure 8. Atg5 loss in GFAP+ cells and progeny doesn't affect proliferation or differentiation. (A) Model and (B) timeline of viral injection experiment. (C) Quantification of GFP+ virally-infected cells in 2 DG sections (D) fluorescent images of recombined (green) proliferating EdU+ (red) cells and qNSCs (violet) and (E, F) quantification results. (G) Fluorescent images of recombined (green), proliferating (violet) and immature (red) neurons and

(H, I) quantification results. Scale bars represent 10 uM (D,G); All graphed data show the mean ± SEM.

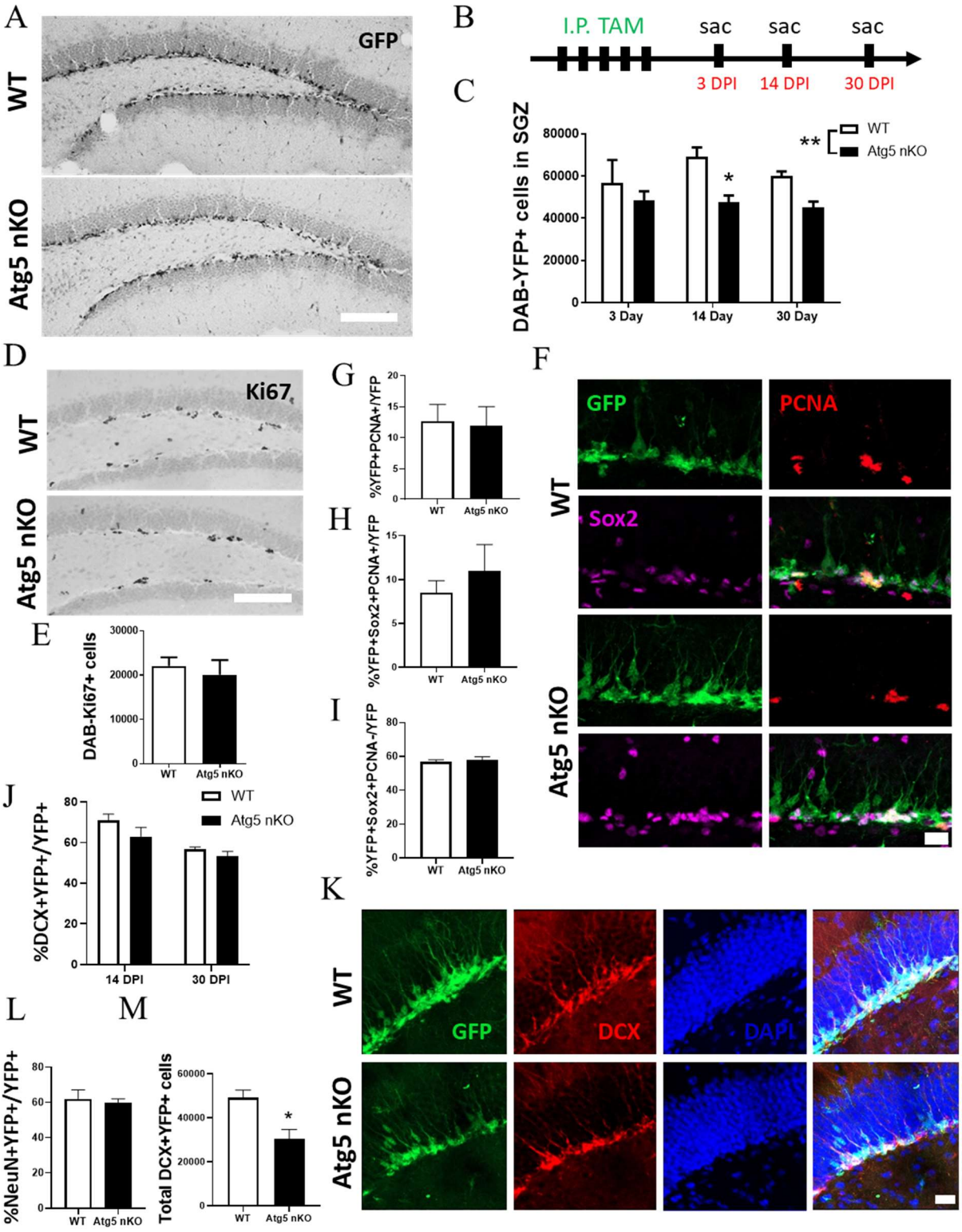

Figure 9. Atg5 loss transiently reduces numbers of immature neurons in nKO mice. (A) Representative brightfield images of DAB-GFP+ cells at 14 dpi with (B) experimental timeline and (C) quantification results. (D) Representative brightfield images of DAB-Ki67+ cells at 14

dpi and (E) quantification results. (F) Fluorescent images of recombined (green), proliferating (red) cells and NSCs (violet) at 14 dpi and (G-I) quantification results. (J) Quantification results of (K) fluorescent images of recombined cells (green) and immature neurons (red) with DAPI (blue) at 30 dpi. Quantification results showing (L) proportion of mature neurons and (M) total numbers of recombined immature neurons. Scale bars represent 500 uM (A, D); 20 uM (G, K); All graphed data show the mean ± SEM; * $p \leq 0.05$, ** $p \leq 0.01$.

MATERIALS AND METHODS

Animals

Animal procedures were performed with approval from the University of Ottawa Animal Care Committee and adhered to the Guidelines of the Canadian Council on Animal Care. Beclin1 nestin-inducible knockout transgenic mice (Beclin1 nKO) were created by breeding NestinCreER^{T2} [91], R26R-eYFP reporter mice [92], and fBeclin1 transgene mice [35], to allow for the conditional removal of Beclin1 from nestin-expressing stem and progenitor cells, as well as all of their progeny following injection of tamoxifen (TAM). Transgenic mouse lines used in this study include: floxed Beclin1 (fBeclin1) mice[35] (obtained from Dr. Zhenyu Yue, Icahn School of Medicine at Mount Sinai); floxed Atg5 (fAtg5) mice[23] (obtained from RIKEN), inducible Nestin-CreERT2 mice[91] (line 4.1 obtained from Paul Frankland, Hospital for Sick Children); inducible GLAST-CreERT2 mice[95] (obtained from Dr. Nicole J. Francis, Montreal Clinical Research Institute), reporter R26R-enhanced Yellow Fluorescent Protein (YFP) mice[92] (obtained from Jackson Laboratory), and reporter CMV-enhanced Green Fluorescent Protein (GFP) mice[96] (obtained from Jackson Laboratory). These mouse lines were crossed to then create the inducible Nestin-CreERT2 Beclin1 and Atg5 knockout mice (Beclin1 nKO and Atg5 nKO), and the inducible GLAST-CreERT2 Beclin1 and Atg5 mice (Beclin1 gKO and Atg5 gKO mice). Control mice were in general NestinCreERT2+ RosaYFP^{het} fBeclin1(WT), NestinCreERT2+ RosaYFP^{het} fAtg5(WT), GLASTCreERT2+ CMVeGFP^{homo} fBeclin1(WT), and GLASTCreERT2+ CMVeGFP^{homo} fAtg5(WT), while experimental mice were NestinCreERT2+ RosaYFP^{het} fBeclin1(homozygote), NestinCreERT2+ RosaYFP^{het} fAtg5(homozygote), GLASTCreERT2+ CMVeGFP^{homo} fBeclin1(homozygote), and GLASTCreERT2+ CMVeGFP^{homo} fAtg5(homozygote). Age-, sex- and littermate-matched control and mutant mice were randomly used as experimental mice based

on their genotype. All strains were obtained and maintained on a C57bl/6J background. Animals were group housed in standard laboratory cages and kept on a 12-hour night/day cycle with ad libitum access to food and water.

Genotyping

Animals were genotyped at 3 weeks of age through DNA samples obtained from ear clippings (~1 mm^2). DNA was extracted using the HotSHOT methodology[98]. Briefly, ear clippings were incubated an Alkaline Lysis Buffer (25 nM NaOH and 0.2 mM Na2EDTA) at 95°C for 30 minutes prior to addition of the Neutralization Solution (40 mM Tris-HCl). Polymerase Chain Reaction (PCR) was completed using primers according to previously published protocols for fBeclin1[35], fAtg5[23], Nestin-CreERT2[91], GLAST-CreERT2[95], CMV-eGFP[96], and R26R-eYFP[92]. The resulting PCR products were resolved by size on a 1% agarose gel for fBeclin1 mice and 2 % agarose for fAtg5 mice using electrophoresis. Size of the PCR products was visualized with ethidium bromide staining under ultraviolet light and estimated by comparison with a 100 base pair (bp) DNA ladder (DM001-R500M; Frogga Inc).

Tamoxifen Administration

Tamoxifen (TAM, T5648-5G; Sigma) was administered via intraperitoneal (IP) injection at a dosage of 160 mg/kg/day for 5 days (dissolved in 10% EtOH and 90% sunflower oil) to 4-8 week-old experimental and control mice, similar to previously published work [99]. For all experimental time points (3, 14, and 30 days post injection of TAM) a minimum of 3 animals per genotype were analyzed.

EdU Administration

In experiments involving cell cycle and proliferation, IP injections of 5-Ethynyl-2′-Deoxyuridine (EdU; sc-284628; Santa Cruz) were given four times two hours apart at a 50 mg/kg to label both the slowly dividing NSCs and rapidly dividing NPCs. For IHC analysis the brains were perfused at 8 or 24 hours after the first injection of EdU, whereas for flow cytometry and cell cycle analyses, the tissue was harvested 24 hours after the first injection.

Immuno-Electron Microscopy

Immuno-EM was performed according to protocols described previously[102] in collaboration with Dr. Marie-Eve Tremblay at University of Victoria. Briefly, mice were transcardially perfused with 4% paraformaldehyde in 0.1 M phosphate buffer (PB) (pH 7.4) at room temperature for 10 min. The brain was removed and postfixed in 4% paraformaldehyde for 48 hours 15 hours after perfusion. Horizontal sections of 50 uM were then cut using a vibratome, cryoprotected in 2% glycerol and 20% DMSO in 0.1 M PB for 20 min, and freeze-thawed eight times in liquid nitrogen. After 0.3% hydrogen peroxide treatment five times five minutes each, and three washes of 10 min in PB + 0.5% bovine serum albumin (BSA-C, Aurion), slices were incubated overnight in the primary antibody (rabbit α-GFP, Chemicon; AB10145) in PB + 0.1% BSA-C at 4 °C. After washing in PB + 0.1% BSA-C, the sections were incubated for 4 hours at room temperature in biotinylated secondary antibody (goat α-rabbit, Jackson Laboratories). Slices were then incubated for 2 hours in avidin biotin peroxidase complex (ABC Elite, Vector Laboratories), then in 3,3′-diaminobenzidine tetrachloride (Vector Laboratories Kit) for 20 min. The sections were fixed overnight in 2.5% glutaraldehyde, followed by osmium tetroxide for 1 hour, dehydrated, and placed in epoxy resin. Serial sections of 40-nm were collected on single-slot grids and contrasted by incubating in 5% uranyl acetate solution for 35 min, followed by 25 min in Reynolds solution. Images of the labeled structures were then serially collected with a digital camera (MegaView III,

SIS) using a JEOL 100 CXII transmission electron microscope at a magnification of 19000× and a filament voltage of 80 kV.

Intracranial Viral Injections

In order to detect autophagic flux in the neurogenic cells, our laboratory has previously published an mCherry-EGFP-LC3 retrovirus[37] that was created using the mCherry-EGFP-LC3B plasmid (Addgene, Cambridge, MA, USA, 22418). Retrovirus was injected bilaterally into the dentate gyrus of mice (7–9 weeks old) during stereotaxic surgery 3 days after TAM injections. Mice were anesthetized throughout surgery with 2% isoflurane and were injected with 1.5uL of the mCherry-EGFP-LC3 retrovirus. Injections were administered by microinjection using a 33 gauge (0.21 mm diameter) needle (7803-05; Hamilton), into the dentate gyrus using coordinates of -1.7 mm rostrocaudal and ±1.2 mm mediolateral from bregma, and -2.4 mm dorsoventral form the skull surface. The virus was injected using a Nanomite Pump 11 Elite (704507; Harvard Apparatus) at a rate of 0.2 µl/min and the needle was removed 5 minutes after the injection was complete in order to prevent backflow. Post-operation recovery from anesthesia occurred in a 37°C incubator until mice were awake and responsive. Buprenorphine was given to the mice as an analgesic (0.05 mg/kg, subcutaneous injection) one hour before surgery, as well as 6 and 12 hours after viral injection. The mice were sacrificed 17 days after viral injection.

The hGFAP-Cre virus was generously prepared and provided by Dr. Song who created and characterized it for the specific infections of qNSCs in the adult dentate gyrus[64]. The adenoviral injections into the dentate gyrus of 7–9-week-old fAtg5 mice were unilateral into the left hemisphere exactly as described above except for the volume of the virus which was 1uL. Mice were injected with EdU the day before perfusion at 8 dpi.

Perfusions and Tissue Collection

Mice were anesthetized with euthanyl (90 mg/kg) and transcardially perfused with cold 1X phosphate buffer solution (PBS, pH 7.4) for 6 minutes and subsequently cold 4% paraformaldehyde (PFA) in 1X PBS (pH 7.4) for 15 minutes at a rate of 7 ml/minute. Brains were removed and postfixed in 4% PFA for 1 hour and then transferred to 30% sucrose in 1X PBS for cryoprotection. Brains were coronally sectioned into 25 or 30 μm slices with a freezing microtome (Leica SM 2000R, Leica Microsystems) and stored in PBS with 0.1% sodium azide.

Antibodies and Immunohistochemistry (IHC)

All primary and secondary antibodies as well as well as their concentrations used for immunohistochemistry (IHC) are listed in methods Table 1. Notably, a Green Fluorescent Protein (GFP) primary chicken antibody was used to detect both YFP immunoreactive (YFP+) cells in the GFP immunoreactive (GFP+) cells in all inducible and virally injected mice.

Slide-mounted IHC was used to detect the total number of YFP+ cells and Ki67+ cells within the SGZ using previously published protocols [99,104]. Briefly, every ninth section through the mouse hippocampus was mounted onto charged slides and allowed to dry overnight. Slides were then pre-treated to enhance antigen retrieval with 0.1M citric acid (pH 6.0) at approximately 95°C for 15 minutes, rinsed in 1X tris-buffer saline (TBS), incubated at RT in 0.1% trypsin for 10 minutes, rinsed in 1X TBS and then incubated with 2N hydrochloric acid (HCl) at RT for 30 minutes. To prevent non-specific binding, the slides were incubated in 3% Normal Donkey Serum (NDS; 017-000-121; Jackson Immuno Research Laboratories Inc) in 0.3% Triton X-100 in 1X TBS for 60 minutes. Sections were then incubated overnight in the primary antibody in 3% NDS in 0.3% Tween20 and 1X TBS. The following day, slides were incubated at RT in: 1) biotinylated attached

secondary antibodies in 1.5% NDS in 1X TBS for 60 minutes; 2) 0.3% H2O2 in 1X TBS for 30 minutes to quench endogenous peroxidases; 3) Avidin-Biotin Complex Solution (ABC; PK-6100; Vector Laboratories) for 90 minutes; 4) metal enhanced 3,3'-Diaminobenzidine (1:10, DAB; 34065; Thermo Scientific,) for 10-30 minutes; and 5) fast red nuclear stain (H3403; Vector) to provide a nuclear counterstain. Between all steps, with exception of after blocking with NDS, the slides were rinsed 3x with 1X TBS. Following staining, slides were dehydrated by consecutively immersing slides in 95% and 100% ethanol for 20 seconds, followed by CitriSolv clearing agent (22-143-975; Fisher) for 20 seconds, 1 minutes, and 5 minutes. Slides were cover-slipped with DPX mounting medium (mixture of Distyrene, Plasticizer, Xylene; 44581; Sigma).

All IHC for the co-labelling of more than one marker was completed using free-floating fluorescent IHC similarly to previously published methods by our laboratory (Lagace et al., 2007; Lagace et al., 2010). Briefly, sections were washed with 1X PBS three times, and were incubated in a carrier solution (1X PBS, 0.1% TritonX-100, 0.1% Tween20) on a shaker overnight with primary antibody at 4°C, with the exception for staining for Beclin1 protein which used an incubation of 48 hrs. The following day, the sections were incubated at room temperature (RT) in fluorophore-conjugated secondary antibody for 1 hour in carrier solution, washed in 1X PBS and counterstained with 4',6-diamidino-2-phenylindole (1:10000, DAPI; 11836170001; Roche). Following staining sections were slide mounted and cover-slipped with Immumount mounting media (2860060; Fisher Scientific). In experiments involving EdU staining, sections were incubated after secondary antibody step in an EdU-staining cocktail containing 1M Tris (pH = 8.5), 200 mM CuSO4*H2O, 4mM of sulfo-Cyanine azide (A3330, A1330; Lumiprobe), and 1M of sodium ascorbate in water for 30 minutes and processed further as above.

Antibodies	Company	Cat #
Chicken Anti-GFP (1:5000)	Aves	GFP-1020
Living Colors Rabbit-Anti-DsRed Polyclonal Antibody (1:500)	Clontech	632496
Goat-Anti-Doublecortin (C-18) (1:500)	Santa Cruz	SC8066
Rabbit-Anti-Ki67 Monoclonal Antibody (1:200)	Cell Marque	275R-14
Mouse anti-BM28 (Mcm2; 1:200)	BD Transduction Laboratories	610701
Mouse anti-PCNA (1:200)	Santa Cruz	sc-56
Mouse-Anti-NeuN Clone A60 (1:500)	Millipore	MAB377
Rabbit anti-Aldolase C (1:1000)	Novus Biologicals	NBP1-90954
Goat anti-Sox2 (1:1000)	Neuromics	GT15098
Rabbit anti-Phospho-Histone (ɣ)H2AX Ser139 (1:200)	Cell Signaling	9718S
PE-Cy7-conugated anti-EGFR (20uL/10^6 cells)	Biolegend	352909
Alexa Fluor 647-conjugated anti-CD15 (20uL/10^6 cells)	BD Bioscience	560120
Biotin-SP-AffiniPure Donkey Anti-Chicken IgY (IgG) (1:200)	Jackson Laboratories	703-065-155
Biotin-SP-AffiniPure Donkey Anti-Rabbit IgG (1:200)	Jackson Laboratories	711-065-152
Biotin-SP-AffiniPure Donkey Anti-Goat IgG (1:200)	Jackson Laboratories	705-065-147
Alexa Fluor 488 AffiniPure F(ab')2 Fragment Donkey Anti-Chicken IgY (IgG) (H+L) (1:500)	Jackson Laboratories	703-546-155
Alexa Fluor 594 AffiniPure F(ab')2 Fragment Donkey Anti-Goat IgG (H+L) (1:500)	Jackson Laboratories	705-586-147
DyLight649 AffiniPure F(ab')2 Fragment Donkey Anti-Rabbit IgG (H+L) (1:500)	Jackson Laboratories	711-495-152
Alexa Fluor 647 AffiniPure F(ab')2 Fragment Donkey Anti-Goat IgG (H+L) (1:500)	Jackson Laboratories	705-606-147
Alexa Fluor 594 AffiniPure F(ab')2 Fragment Donkey Anti-Mouse IgG (H+L) (1:500)	Jackson Laboratories	715-586-150
Alexa Fluor 594 AffiniPure F(ab')2 Fragment Donkey Anti-Rabbit IgG (H+L) (1:500)	Jackson Laboratories	711-585-152
Cy3 AffiniPure F(ab')2 Fragment Donkey Anti-Mouse IgG (H+L) (1:500)	Jackson Laboratories	715-165150
Cy5 AffiniPure F(ab')2 Fragment Donkey Anti-Rabbit IgG (H+L) (1:500)	Jackson Laboratories	711-175-152

Table 1. Primary and secondary antibodies used in preparation of data for Chapter 4.

Microscopy and Cellular Quantification

All counts of DAB+ cells were performed at 40x magnification using an Olympus BX51 fluorescent microscope and recorded with a manual counter by a blinded experimenter in every 9th DG section and the number was multiplied by 9 to approximate numbers of DAB+ cells in the

entire DG. Quantification was further verified by an additional blinded experimenter that confirmed less than 10% variation in 2 independent counts. The number of immunoreactive cells in the SGZ of the dentate gyrus were manually quantified in every ninth coronal brain section using stereological methods as previously published [99,104].

For analysis of autolysosomes, YFP+ recombined cells in the SGZ cells expressing mCherry+ autolysosomes were blindly imaged with a 63x oil immersion lens with a Zeiss LSM800 AxioObserverZ1 mot Confocal Microscope at emission wavelengths of 517 and 561nm. Autolysosomes were blindly manually quantified in every YFP+ cell. Autolysosomes were counted in the cell body and cell processes using ZEN 2012 Blue (Zeiss) image processing software. To be counted autolysosomes had to be mCherry+ (red), be circular in shape, and be larger than any observed specs in the background. Quantification was verified by an additional blinded experimenter that confirmed less than 10% variation in 2 independent counts.

For analysis of florescent immunoreactive cells, the DG was imaged at either 20x or 40x (oil immersion) from bregma matched (positions around -2.06 to -2.30) coronal half-brain or full-brain sections. Imaging was performed using a Zeiss LSM 510-META confocal microscope at emission wavelengths of 405, 488, 543, and 633 using either 20x, 0.8 NA, Air, Plan-Apo (DIC II) or 40x, 1.3 NA, Oil, EC Plan-Neofluar (DIC III) objectives; or a Zeiss LSM800 AxioObserverZ1 mot confocal microscope (Zeiss) at emission wavelengths of 405, 488, 561, and 640nm using either 20x, 0.8 NA, Air, Plan-Apo or 40x, 1.3 NA, Oil, Plan-Apo objectives. ZEN acquisition software (Zeiss) was used for 1-2 μm optical sectioning in the Z-plane. Both single- and co-labeled cells were quantified manually from images visualized through Fiji image processing software (ImageJ) and ZEN Blue (Zeiss) image processing software. The total population of YFP+ cells that co-

labeled with another marker was calculated as the product of the absolute YFP counts and the proportion co-labeled per animal.

EGRF-CD15 Flow Cytometry

For all *ex vivo* analyses previously published protocols[105,107] were used to dissect the dentate gyrus from WT and Beclin1 gKO mice 3 days after TAM injections. The mice were anesthetized with euthanyl (90 mg/kg), decapitated, and their brains were removed and placed in slushy Artificial Cerebrospinal Fluid (aCSF, pH =7.4), consisting of (in mM): 124 NaCl, 5 KCl, 1.3 MgCl2·6H2O, 2 CaCl2·2H2O, 26 NaHCO3, and 1X penicillin-streptomycin (10,000 U/mL; 450-201-EL; Multicell). The dentate gyrus of both hemispheres was dissected out of the brain and placed in aCSF. The tissue was gently broken up with sterile scissors. Tissue was incubated on a thermomixer (30 minutes, 37oC) in 500 uL/tube of digestion media, containing DMEM/F12 (11039-021; Invitrogen), 1.2 mM EDTA (E5134-1KG; Sigma), and 20 U/ml papain (LS003126; Worthington Biochemical) at 37°C for 30 min. Cells were triturated followed by centrifugation to obtain a cell pellet that was suspended and washed in DMEM/F12 media. Suspension was then transferred in Percoll media, consisting of 19.8% Percoll (17-0891-02; GE Healthcare Life Sciences), 2.2% 10xPBS (311-012-CL; Multicell) and spun down (500 x g, 13 minutes, RT). Cells were again washed with DMEM/F12 and quantified using Countess II (Invitrogen) cell counting charged slides by reconstituting cell suspension with trypan blue at a ratio of 1:1. Cells were co-incubated in human anti-EGFR (Biolegend) and anti-CD15 (BD Biosciences) antibodies for 30 minutes in dark on ice. After one wash, cells were resuspended with 4′,6-diamidino-2-phenylindole (DAPI; 11836170001; Roche) at a concentration of 1:1000.

ɣH2AX Flow Cytometry

The mouse dentate gyrus tissue was prepared in the same fashion as for the EGFR-CD15 staining. After counting, the cells were fixed in a PFA-containing buffer (420801; BioLegend) for 20 min in dark at RT, permeabilized by spinning in 1x wash buffer (421002; Biolegend) twice for 10 min. Beclin1 gKO and WT cells were then stained with γH2AX antibody overnight and next morning washed with PBS and stained with secondary fluorescent Cy5 antibody. The sections were then washed and resuspended in DAPI/1xPBS. The cells were then accessed using a Fortessa (Beckman Coulter) flow cytometer at 405 nm and 640 nm lasers for DAPI, and γH2AX -Cy5, respectively.

Cell Cycle Flow Cytometry

For *in vivo* cell cycle analysis, 14 dpi WT and Beclin1 gKO mice were injected with EdU four times two hours apart and dentate gyrus was extracted and digested as described above 24 hours after the first injection. After counting, the cells were fixed in a PFA-containing buffer (420801; BioLegend) for 20 min in dark at RT, permeabilized by spinning in 1x wash buffer (421002; Biolegend) twice for 10 min, and passed through 40 μm cell strainer (08-771-1, Fisher). Beclin1 gKO and WT cells were then stained with YFP antibody overnight and next morning washed with PBS and stained with secondary fluorescent AF488 antibody. Beclin1 gKO and WT cells were then stained for 20 min in dark with EdU cocktail prepared as described above. The sections were then washed and resuspended in DAPI/1xPBS. The cells were then accessed using a Fortessa (Beckman Coulter) flow cytometer at 405 nm and 561 nm lasers for DAPI, and EdU-Cy3, respectively.

All visualization and cell counting of flow cytometry data was performed using FlowJo10 and 11 (BD). Values obtained from different experiments using FlowJo were used in t-test with Prism 6.0 (GraphPad).

Comet Assay

For assessment of DNA damage, dissociated DG cells were sorted from 2 WT and 3 Beclin1 gKO mice at 14 dpi using a Beckman MoFlo Astriosis (Beckman Coulter Canada) for YFP positivity (488-526 nm) and for 7-AAD negativity (571-640nm) and prepared in the same fashion as the Beclin1 nKO and WT mice in Chapter 3. For comet tail analysis, comet assay software project tool (CASP, v1.2.3b1) was used. Extremely dim cells and cells with percent of DNA in tail higher than 70% were excluded from the analysis, analyzing a final total of 165 WT and 288 Beclin1 gKO cells. Percent of DNA in comet tail and comet tail moment were compared for all cells in a t-test using Prism 6.0 (GraphPad).

Statistical Analysis

All outcomes are reported as mean ± standard error of the mean (SEM) and were calculated and statistically analyzed using Prism 6.0 (GraphPad). Experiments with two groups were analyzed by a two-tailed student's t-test. Statistical analysis of three or more groups was performed using an ANOVA test, followed by a Bonferroni post hoc. Statistical significance was defined as $p < 0.05$.

CHAPTER 5: GENRAL DISCUSSION

1. Thesis summary

This thesis has examined the role of autophagy-related proteins Beclin1 and Atg5 in adult hippocampal neurogenesis. A multitude of methods has been applied to determine the role of these proteins in the production of adult-generated granule neurons from NSPCs. In chapter 2, a cell sorting technique was tested for detection and extraction of NSCs from live cell suspensions which led to the discovery of a novel method of isolating brain endothelial cells instead of NSCs from the hippocampus and subventricular zone[109]. In chapter 3, Beclin1 is determined to be required within the adult NSPCs for proper progression through mitosis and DNA maintenance during the cell cycle through lineage tracing and isolation of the different neurogenic cells in the Beclin1 nKO mice. Similarly, in chapter 4, different mechanisms by which Beclin1 and Atg5 regulate adult hippocampal neurogenesis are discovered. Like the findings in the Beclin1 nKO mice, the Beclin1 gKO mice reveal that Beclin1 is required for mitosis and DNA maintenance highlighting that its requirement in the dividing cells derived from Nestin and GLAST NPSCs. On the contrary, creation of the Atg5 nKO or Atg5 gKO mice showed that Atg5 was not required for proliferation of NSPCs. Both Atg5 inducible mouse models revealed that Atg5 has a transient effect on reducing the number of immature neurons. The Atg5 gKO mice also revealed a striking role of Atg5 in regulating the number of GLAST+ resident astrocytes which accompanied a significant decline in the generation of adult-born neurons. Thus, these findings highlight that Beclin1 and Atg5 have distinct effects during the dynamic process of adult hippocampal neurogenesis.

2. Beclin1 is required in mitosis of adult NSPCs

The results of this study demonstrate that loss of Beclin1 from the adult Nestin+ and GLAST+ NSPCs and their progeny results in a cell-autonomous reduction in proliferation and mitosis of

NSPCs *ex vivo* and *in vitro*. Our data in Chapter 3 support that Beclin1 mediates the proliferation of NSPCs by regulating chromosomal maintenance during mitosis, as highlighted by the differential expression of mitotic spindle, centromere, and kinetochore components in our sc-RNAseq analysis. Specifically the Beclin1-null cells had a significant reduction of centromere genes Cenpk, Cenpm and Cenph[111]. Additionally condensin I and II encoded by the Smc2 gene[113] which maintain the condensed state of the chromosomes before and during chromosome segregation, were depleted. Furthermore, dysregulation of the kinetochore was evident in Beclin1-null cells by the reduced expression of Kif22[115], Spc24 and Spc25[117], as well as Ran and RanBP1 that are both required for proper attachment of kinetochores to microtubules[119,121,123]. These data align with findings reported in HeLa cells that show that Beclin1 deletion induces G2/M arrest and chromatin abnormalities via the deregulation of spindle and kinetochore assembly[66]. Similarly, in both reproductive and cancer cells, Beclin1 protein removal is related to chromosomal instability via centrosome abnormalities, midbody ring remnants, and cytokinesis failure[68,70,72]. Thus, our *in vivo* findings add to a growing appreciation of the functions of Beclin1 in regulating mitosis, which has been mainly identified *in vitro* and outside of the CNS. Our study shows a clear link between Beclin1 removal and the transcriptional dysregulation of mitotic machinery in the context of adult hippocampal neurogenesis which is yet to be explored in other adult neurogenic regions.

3. Beclin1 is necessary for chromatin health during cell cycle

The results of Chapter 3 show that mitotic Belcin1-null cells had a dysregulation of genes that are necessary for chromosome maintenance during prophase and metaphase, suggesting that Beclin1 is important for proper chromatin dynamics during cell cycle. In addition, dividing Beclin1-null cells regulated their fate choice differentially, with enhanced transcription of genes related to metabolic stress and reduced DNA maintenance that ultimately caused cell death and reduces adult

hippocampal neurogenesis. Removal of Beclin1 form both adult Nestin+ and GLAST+ neurogenic cells in the hippocampus has resulted in the accumulation of damaged DNA and cell death. The loss of Beclin1 provoked an enhanced transcription of p53 target genes involved in metabolic stress and DNA damage response. There is a great deal of cross-talk between p53 signaling, DNA damage response, and proliferation outcomes in the context of adult neurogenesis[124,126,128,130], while direct links have also been made between p53 and autophagy in other models[132,134]. The defects of the Beclin1-null cells to undergo mitosis were accompanied by the enhanced transcription of genes involved in metabolic stress, as well as a reduction of expression of DNA repair and pro-survival genes. For example, the Beclin1-null proliferating cells showed upregulation in cell stress-related transcripts such as reactive oxygen species genes (ROS; e.g., Romo1[135], Pet100[137], Ndufa3[139]), and P53 targets (e.g., Tpt1[141,143], Cox2 [145], Sesn1[147]). Beclin1 nKO cells also showed a reduction in DNA synthesis and repair genes, such as Top2a[148], Pclaf[150], and Syce2[152]. These findings were accompanied by the Beclin1-null cells having enhanced fragmentation of DNA *ex vivo.* This is in line with literature showing that a failure to undergo mitosis can induce DNA damage[49], as well as direct connections between Beclin1 and DNA repair/damage outside of the CNS. Specifically, haploinsufficiency of Beclin1 is linked to damaged DNA in mammary cells[154] and chromosomal instability in ovarian cells[156]. In support of this, haploinsufficiency of Beclin1 also resulted in enhanced DNA damage in experiments targeting DNA in subventricular zone cells[158]. Beclin1 is also known to directly interact with DNA repair and anti-apoptotic genes[160,161,163,165]. For example, neurodevelopmental gene and binding partner of Beclin1 Birc5/Survivin[167,169,171], which had reduced transcriptional activity in Beclin1 nKO cells, is associated with apoptosis via mitotic deficit and DNA damage in different cell lines when its activity is reduced[173]. Overall, these findings suggest that the deficits of Beclin1-null cells

during mitosis resulted in metabolic stress and reduced DNA repair in the adult neurogenic cells, which resulted in DNA damage and cell death.

4. Atg5 is required in astrocytes in the dentate gyrus

One of the most interesting discoveries of this thesis is that Atg5 is not required in NSPCs but is required in astrocytes for the proper expansion of the neurogenic niche in the early time points. The effect of Atg5 in the resident astrocytes was observed in the Atg5 gKO mice since this model, since this model recombines GLAST+ resident astrocytes unlike the GFAP-targeted viral infection of NSCs, or the Atg5 nKO mice[43,95]. The loss of Atg5 resulted fewer resident hippocampal astrocytes as soon as 3 days after the last dosage of tamoxifen and lasted for 2 weeks. This finding is in contrast to Beclin1 gKO mice which had no loss of resident astrocytes and also did not show a reduction of recombined cells at 3 days after last tamoxifen treatment. These results highlight that Atg5 but not Beclin1 is required for the maintenance of the astrocytic population in the hippocampus. During embryonic cortical development, Atg5 is required for the expansion and differentiation of cortical astrocytes via degradation of Sox2 *in vivo* and *in vitro*[87]. Whether Atg5 has a similar role on expansion of the resident astrocytes remains unknow, and it would be important to use methodologies in the future to test if the reduced number of resident astrocytes is associated with a reduction in the proliferative capacity or cell death in the Atg5-null astrocytes. Unlike the findings during cortical development, Atg5 in the adult resident astrocytes did not appear to regulate the differentiation or morphological characteristics of the resident astrocytes at a gross level (unquantified) that were found in the Atg5 gKO compared to WT mice. However, to fully explore this, future work would also require careful phenotyping of the astrocytes temporally following removal of Atg5.

Astrocytes have been previously shown to play an important role in the paracrine regulation of NSC and neuron activity[79,81,83,85]. Atg5 specifically functions in cellular pathways that encompass cellular communication and involve vesicle maturation and exchange, as well as membrane dynamics, such as autophagy, exocytosis, and antigen presentation, respectively[20,175,177]. It is plausible that Atg5 may regulate the numbers of neurogenic cells in the dentate gyrus via astrocyte-dependent mechanisms. As such, the relationship between astrocyte loss after Atg5 removal and reduction in other recombined cells at 3 dpi needs to be further explored.

5. Are roles of Beclin1 and Atg5 dependent on autophagy?

Given the growing appreciation that autophagy-related proteins such as Beclin1 and Atg5 have roles beyond their canonical effects on regulating autophagy[20,169,175], our work begs the question of whether the phenotypes we found in our mouse models are dependent on autophagy. This is not a simple question to answer given that it is not easy to measure autophagic flux *in vivo* and we have not used the same outcome measure in all our models to examine autophagy. In addition, our analyses utilized one method per mouse model. As per our previous lab publication[37] we used the LC3-GFP-mCherry virus to look at autophagic flux, but since we were using it in transgenic mice, it was only possible to measure autolysosomes. In the Atg5 gKO mice, we used EM to quantify autophagosomes which is a different method from the fluorescence-based assessment of autolysosomes limiting our ability to answer this question directly. This raises the need for future studies to clarify the dynamics of the autophagy pathway in knockout models through combining these and other methods. However, the differential effects between these models and data still allow for hypotheses about whether some of our main findings appear to be due to autophagy-dependent or -independent effects of Beclin1 and or Atg5.

For example, we hypothesize that the effect of Beclin1 in the regulation of proliferation appears to occur independently of its autophagic functions based on our data and support from the literature outside of the CNS. The strongest support for this hypothesis comes from two independent findings in our study. One that the Beclin1 gKO and nKO mice have deficits in mitosis yet only the nKO model and not the gKO model had a reduction in autolysomes. The second finding is that the removal of Atg5 in three independent mouse models in chapter 4 did not alter proliferation and was shown to have a reduction in autophagy in the gKO model. Indeed, most other autophagy proteins do not cause proliferation deficits while successfully inhibiting the autophagy process. For example, removal of Atg7 from Nestin+ NSPCs and their progeny resulted in the loss of autophagy but no change in neurogenesis or proliferation of NSPCs in naïve conditions[179]. Similarly, removal of Atg5, Atg7 and Atg16L in embryonic GFAP+ NSPCs and their progeny resulted in reduced autophagy but no change in proliferation or neurogenesis in the early postnatal SGZ[181]. Lastly, work from our lab virally removing Atg5 from the neurogenic cells from adult NPCs in the dentate gyrus, while resulting in reduced autophagy and delayed maturation of neurons, had no effect on proliferation[37]. Thus, it could be that removing proteins involved in the elongation stage of autophagy (such as Atg5) has differential effects on neurogenesis compared to proteins involved in autophagy initiation (such as Beclin1) due to their more conserved role within the process of vesicle formation, which includes autophagy, endocytosis and other related pathways[169,175]. In support of differential requirement of elongation autophagy proteins, removal of FIP200 and FoxO3, which are involved in autophagy initiation, from GFAP+ and GLAST+ NSPCs and progeny, respectively, resulted in both decreased autophagy, reduced neurogenesis, and proliferation deficits[182,184].the function of FIP200 within proliferating NSPCs was specifically independent of the autophagy pathway as well[31]. Overall, these novel findings open the door for

future work to continue to elucidate the cellular mechanisms regulating the autophagy-dependent and -independent reduction in adult neurogenesis.

The hypothesis that supports Beclin1's action occurs independently of autophagy does not align with the some literature that connects the autophagy pathway with proliferation, and cell cycle regulation outside of the CNS[185,186,189]. Indeed, a large number of autophagy-dependent mechanisms that have been identified to regulate cell division[186] and DNA repair[181,191,193]. For example, autophagic degradation of growth factors and cell cycle components, cytokinesis, and "cell division clean-up" have been previously demonstrated as direct autophagy-dependent cell cycle regulators[186]. Autophagy has also been shown to indirectly negatively regulate DNA damage during proliferation by maintaining proper cell homeostasis during replication stress through degradation and substrate availability[191,193,195,197], but also via direct involvement in the nucleotide-excision repair pathway[199]. Beclin1's effect on proliferation has been shown but the exact mechanisms of its regulation of cell cycle remain vastly unclear. For instance, *Becn1*$^{F121A/F121A}$ knockin mice, that have enhanced levels of autophagy, have a reversal in age-related reductions in both autophagy and NSC function in the subventricular zone. These data suggest an association between autophagy and NSC function, but do not provide evidence that Beclin1 acts through an autophagy-dependent role. Our findings also support the notion that actions of Beclin1 in dividing NSPCs do not involve the autophagy-independent role of Beclin1 in endo/exocytosis or cytokinesis, which is known to regulate the cell cycle outside of the CNS[35,163,169,201–203]. Specifically, the proliferation deficits observed *in vitro* highlight the cell-autonomous role of Beclin1 which does not support Beclin1-mediated endo/exocytosis. Interestingly, effects of autophagy protein deletion on the specific stages of the cell cycle and cell cycle exit/arrest can vary based on the experimental conditions and may be differentially

established in unalike cell types[186] which may further suggest engagement of either autophagy-dependent and –independent mechanisms, or a combination of both.

The interactome of the Beclin1 protein and gene have been described[160,161,165] and contain contenders that could underlie the direct regulation of the cell cycle process and mitosis by Beclin1 independent of autophagy. For example, Hmgb1 protein has been shown to interact with the Beclin1 protein[205] but is also a known regulator of neural stem and progenitor cell proliferation and differentiation[207,209]. Recently, a Beclin1 interaction with the Hippo pathway has been found which controls proliferation in a cancer cell model[211] suggesting another link between Beclin1 and proliferation. Additionally, haploinsufficiency of Beclin1 has been linked to damaged DNA in epithelial mammary cells[154] and chromosomal instability in ovarian cells[156]. Thus, a strong link between Beclin1 removal and genomic instability has been demonstrated in the context of p53 signaling and metabolic stress with the advancing ability to distinguish between individual pathway effects. However, this topic and the specific biochemical effects exerted by Beclin1 in the context of neurogenesis require further exploration. The involvement of these non-canonical functions of Beclin1 could therefore be tested in future work through examining for example the involvement of Beclin1 in membrane dynamics, and/or direct regulation of phosphoinositide synthesis.

6. Concluding remarks

In conclusion, the findings from this thesis demonstrate the requirement of Beclin1 in the maintenance of proliferation of adult neurogenic hippocampal cells. Removal of Beclin1 resulted in a significant reduction of mitotic cells and accumulation of DNA damage in progeny likely in an autophagy-independent manner. These effects were mediated via transcriptional dysregulation

of genes important for genomic maintenance during metaphase and anaphase, and increased signatures of cellular stress upon cell cycle exit. Overall, this work links the reduction of Beclin1 in dividing NPCs with mitotic chromosome maintenance and DNA damage mechanisms and thus identifies a novel intrinsic regulator of proliferation within the adult NSPCs. Alternatively, loss of Atg5 transiently reduces neurogenesis not via an effect on proliferation of adult hippocampal NSPCs but through the reduction in astrocyte numbers. This supports the unique autophagy-independent role of Beclin1 in mitosis and DNA health during neurogenesis. In addition, these data highlight a unique requirement of Atg5 but not Beclin1 in resident hippocampal astrocytes. The findings also highlight the role of Atg5 within immature neurons, however, future studies will delineate whether this is directly dependent on the autophagic roles of Atg5. These studies provide an important benchmark for neurogenesis research and expand our understanding of the nuanced regulation of this process by autophagy-related players which can further their therapeutic potential in health and disease.

References

1. Wang, W., Wang, M., Yang, M., Zeng, B., Qiu, W., Ma, Q., Jing, X., Zhang, Q., Wang, B., Yin, C., et al. (2022). Transcriptome dynamics of hippocampal neurogenesis in macaques across the lifespan and aged humans. Cell Res., 1–15. 10.1038/s41422-022-00678-y.

2. Zhou, Y., Su, Y., Li, S., Kennedy, B.C., Zhang, D.Y., Bond, A.M., Sun, Y., Jacob, F., Lu, L., Hu, P., et al. (2022). Molecular landscapes of human hippocampal immature neurons across lifespan. Nature *607*, 527–533. 10.1038/s41586-022-04912-w.

3. Spalding, K.L., Bhardwaj, R.D., Buchholz, B.A., Druid, H., and Frisén, J. (2005). Retrospective birth dating of cells in humans. Cell *122*, 133–143. 10.1016/j.cell.2005.04.028.

4. Eriksson, P.S., Perfilieva, E., Björk-Eriksson, T., Alborn, A.M., Nordborg, C., Peterson, D.A., and Gage, F.H. (1998). Neurogenesis in the adult human hippocampus. Nat. Med. *4*, 1313–1317. 10.1038/3305.

5. Pilz, G.A., Bottes, S., Betizeau, M., Jörg, D.J., Carta, S., Simons, B.D., Helmchen, F., and Jessberger, S. (2018). Live imaging of neurogenesis in the adult mouse hippocampus. Science *359*, 658–662. 10.1126/science.aao5056.

6. Shin, J., Berg, D.A., Zhu, Y., Shin, J.Y., Song, J., Bonaguidi, M.A., Enikolopov, G., Nauen, D.W., Christian, K.M., Ming, G., et al. (2015). Single-Cell RNA-Seq with Waterfall Reveals Molecular Cascades underlying Adult Neurogenesis. Cell Stem Cell *17*, 360–372. 10.1016/j.stem.2015.07.013.

7. Kalinina, A., and Lagace, D. (2022). Single-Cell and Single-Nucleus RNAseq Analysis of Adult Neurogenesis. Cells *11*, 1633. 10.3390/cells11101633.

8. Enikolopov, G., Overstreet-Wadiche, L., and Ge, S. (2015). Viral and Transgenic Reporters and Genetic Analysis of Adult Neurogenesis. Cold Spring Harb. Perspect. Biol. *7*. 10.1101/cshperspect.a018804.

9. Dhaliwal, J., Trinkle-Mulcahy, L., and Lagace, D.C. (2017). Autophagy and Adult Neurogenesis: Discoveries Made Half a Century Ago Yet in their Infancy of being Connected. Brain Plast. *3*, 99–110. 10.3233/BPL-170047.

10. Imayoshi, I., Sakamoto, M., and Kageyama, R. (2011). Genetic Methods to Identify and Manipulate Newly Born Neurons in the Adult Brain. Front. Neurosci. *5*.

11. Khacho, M., Clark, A., Svoboda, D.S., Azzi, J., MacLaurin, J.G., Meghaizel, C., Sesaki, H., Lagace, D.C., Germain, M., Harper, M.E., et al. (2016). Mitochondrial Dynamics Impacts Stem Cell Identity and Fate Decisions by Regulating a Nuclear Transcriptional Program. Cell Stem Cell *19*, 232–247. 10.1016/j.stem.2016.04.015.

12. Mori, T., Tanaka, K., Buffo, A., Wurst, W., Kühn, R., and Götz, M. (2006). Inducible gene deletion in astroglia and radial glia--a valuable tool for functional and lineage analysis. Glia *54*, 21–34. 10.1002/glia.20350.

13. Su, Y.-T., Lau, S.-F., Ip, J.P.K., Cheung, K., Cheung, T.H.T., Fu, A.K.Y., and Ip, N.Y. (2019). α2-Chimaerin is essential for neural stem cell homeostasis in mouse adult neurogenesis. Proc. Natl. Acad. Sci. *116*, 13651–13660. 10.1073/pnas.1903891116.

14. Griffin, J.M., Fackelmeier, B., Fong, D.M., Mouravlev, A., Young, D., and O'Carroll, S.J. (2019). Astrocyte-selective AAV gene therapy through the endogenous GFAP promoter results in robust transduction in the rat spinal cord following injury. Gene Ther. *26*, 198–210. 10.1038/s41434-019-0075-6.

15. Casares-Crespo, L., Calatayud-Baselga, I., García-Corzo, L., and Mira, H. (2018). On the Role of Basal Autophagy in Adult Neural Stem Cells and Neurogenesis. Front. Cell. Neurosci. *12*. 10.3389/fncel.2018.00339.

16. DeCarolis, N.A., Mechanic, M., Petrik, D., Carlton, A., Ables, J.L., Malhotra, S., Bachoo, R., Götz, M., Lagace, D.C., and Eisch, A.J. (2013). In vivo contribution of nestin- and GLAST-lineage cells to adult hippocampal neurogenesis. Hippocampus *23*, 708–719. 10.1002/hipo.22130.

17. Wirawan, E., Lippens, S., Vanden Berghe, T., Romagnoli, A., Fimia, G.M., Piacentini, M., and Vandenabeele, P. (2012). Beclin1: A role in membrane dynamics and beyond. Autophagy *8*, 6–17. 10.4161/auto.8.1.16645.

18. Yue, Z., Jin, S., Yang, C., Levine, A.J., and Heintz, N. (2003). Beclin 1, an autophagy gene essential for early embryonic development, is a haploinsufficient tumor suppressor. Proc. Natl. Acad. Sci. U. S. A. *100*, 15077–15082. 10.1073/pnas.2436255100.

19. Dhaliwal, J., Trinkle-Mulcahy, L., and Lagace, D.C. (2017). Autophagy and Adult Neurogenesis: Discoveries Made Half a Century Ago Yet in their Infancy of being Connected. Brain Plast. *3*, 99–110. 10.3233/BPL-170047.

20. Codogno, P., and Meijer, A.J. (2006). Atg5: more than an autophagy factor. Nat. Cell Biol. *8*, 1045–1047. 10.1038/ncb1006-1045.

21. Wang, C.-L., Ohkubo, R., Mu, W.-C., Chen, W., Fan, J.L., Song, Z., Maruichi, A., Sudmant, P.H., Pisco, A.O., Dubal, D.B., et al. (2023). The mitochondrial unfolded protein response regulates hippocampal neural stem cell aging. Cell Metab. 10.1016/j.cmet.2023.04.012.

22. Kuma, A., Hatano, M., Matsui, M., Yamamoto, A., Nakaya, H., Yoshimori, T., Ohsumi, Y., Tokuhisa, T., and Mizushima, N. (2004). The role of autophagy during the early neonatal starvation period. Nature *432*, 1032–1036. 10.1038/nature03029.

23. Hara, T., Nakamura, K., Matsui, M., Yamamoto, A., Nakahara, Y., Suzuki-Migishima, R., Yokoyama, M., Mishima, K., Saito, I., Okano, H., et al. (2006). Suppression of basal autophagy in neural cells causes neurodegenerative disease in mice. Nature *441*, 885–889. 10.1038/nature04724.

24. Xi, Y., Dhaliwal, J.S., Ceizar, M., Vaculik, M., Kumar, K.L., and Lagace, D.C. (2016). Knockout of Atg5 delays the maturation and reduces the survival of adult-generated neurons in the hippocampus. Cell Death Dis. *7*, e2127. 10.1038/cddis.2015.406.

25. Wang, C., Chen, S., Yeo, S., Karsli-Uzunbas, G., White, E., Mizushima, N., Virgin, H.W., and Guan, J.-L. (2016). Elevated p62/SQSTM1 determines the fate of autophagy-deficient neural stem cells by increasing superoxide. J. Cell Biol. *212*, 545–560. 10.1083/jcb.201507023.

26. Velloso, F.J., Shankar, S., Parpura, V., Rakic, P., and Levison, S.W. (2022). Neural Stem Cells in Adult Mammals are not Astrocytes. ASN NEURO *14*, 17590914221134739. 10.1177/17590914221134739.

27. Jung, S., Choe, S., Woo, H., Jeong, H., An, H.K., Moon, H., Ryu, H.Y., Yeo, B.K., Lee, Y.W., Choi, H., et al. (2020). Autophagic death of neural stem cells mediates chronic stress-induced decline of adult hippocampal neurogenesis and cognitive deficits. Autophagy *16*, 512–530. 10.1080/15548627.2019.1630222.

28. Wang, C., Liang, C.-C., Bian, Z.C., Zhu, Y., and Guan, J.-L. (2013). FIP200 is required for maintenance and differentiation of postnatal neural stem cells. Nat. Neurosci. *16*, 532–542. 10.1038/nn.3365.

29. Berg, D.A., Su, Y., Jimenez-Cyrus, D., Patel, A., Huang, N., Morizet, D., Lee, S., Shah, R., Ringeling, F.R., Jain, R., et al. (2019). A Common Embryonic Origin of Stem Cells Drives Developmental and Adult Neurogenesis. Cell *177*, 654-668.e15. 10.1016/j.cell.2019.02.010.

30. Furutachi, S., Miya, H., Watanabe, T., Kawai, H., Yamasaki, N., Harada, Y., Imayoshi, I., Nelson, M., Nakayama, K.I., Hirabayashi, Y., et al. (2015). Slowly dividing neural progenitors are an embryonic origin of adult neural stem cells. Nat. Neurosci. *18*, 657–665. 10.1038/nn.3989.

31. Liu, H., Wang, C., Yi, F., Yeo, S., Haas, M., Tang, X., and Guan, J.-L. (2021). Non-canonical function of FIP200 is required for neural stem cell maintenance and differentiation by limiting TBK1 activation and p62 aggregate formation. Sci. Rep. *11*, 23907. 10.1038/s41598-021-03404-7.

32. Wang, C., Yeo, S., Haas, M.A., and Guan, J.-L. (2017). Autophagy gene FIP200 in neural progenitors non–cell autonomously controls differentiation by regulating microglia. J. Cell Biol. *216*, 2581–2596. 10.1083/jcb.201609093.

33. Radecki, D.Z., and Samanta, J. (2022). Endogenous Neural Stem Cell Mediated Oligodendrogenesis in the Adult Mammalian Brain. Cells *11*, 2101. 10.3390/cells11132101.

34. Yazdankhah, M., Farioli-Vecchioli, S., Tonchev, A.B., Stoykova, A., and Cecconi, F. (2014). The autophagy regulators Ambra1 and Beclin 1 are required for adult neurogenesis in the brain subventricular zone. Cell Death Dis. *5*, e1403–e1403. 10.1038/cddis.2014.358.

35. McKnight, N.C., Zhong, Y., Wold, M.S., Gong, S., Phillips, G.R., Dou, Z., Zhao, Y., Heintz, N., Zong, W.X., and Yue, Z. (2014). Beclin 1 Is Required for Neuron Viability and Regulates Endosome Pathways via the UVRAG-VPS34 Complex. PLoS Genet. *10*, 1–18. 10.1371/journal.pgen.1004626.

36. Dulken, B.W., Leeman, D.S., Boutet, S.C., Hebestreit, K., and Brunet, A. (2017). Single-Cell Transcriptomic Analysis Defines Heterogeneity and Transcriptional Dynamics in the Adult Neural Stem Cell Lineage. Cell Rep. *18*, 777–790. 10.1016/j.celrep.2016.12.060.

37. Xi, Y., Dhaliwal, J.S., Ceizar, M., Vaculik, M., Kumar, K.L., and Lagace, D.C. (2016). Knockout of Atg5 delays the maturation and reduces the survival of adult-generated neurons in the hippocampus. Cell Death Dis. *7*, e2127. 10.1038/cddis.2015.406.

38. Daynac, M., Chicheportiche, A., Pineda, J.R., Gauthier, L.R., Boussin, F.D., and Mouthon, M.A. (2013). Quiescent neural stem cells exit dormancy upon alteration of GABAAR signaling following radiation damage. Stem Cell Res. *11*, 516–528. 10.1016/j.scr.2013.02.008.

39. Schäffner, I., Minakaki, G., Khan, M.A., Balta, E.-A., Schlötzer-Schrehardt, U., Schwarz, T.J., Beckervordersandforth, R., Winner, B., Webb, A.E., DePinho, R.A., et al. (2018). FoxO Function Is Essential for Maintenance of Autophagic Flux and Neuronal Morphogenesis in Adult Neurogenesis. Neuron *99*, 1188-1203.e6. 10.1016/j.neuron.2018.08.017.

40. Leeman, D.S., Hebestreit, K., Ruetz, T., Webb, A.E., McKay, A., Pollina, E.A., Dulken, B.W., Zhao, X., Yeo, R.W., Ho, T.T., et al. (2018). Lysosome activation clears aggregates and enhances quiescent neural stem cell activation during aging. Science *359*, 1277–1283. 10.1126/science.aag3048.

41. Chaker, Z., Codega, P., and Doetsch, F. (2016). A mosaic world: puzzles revealed by adult neural stem cell heterogeneity. WIREs Dev. Biol. *5*, 640–658. https://doi.org/10.1002/wdev.248.

42. Morizur, L., Chicheportiche, A., Gauthier, L.R., Daynac, M., Boussin, F.D., and Mouthon, M.A. (2018). Distinct Molecular Signatures of Quiescent and Activated Adult Neural Stem Cells Reveal Specific Interactions with Their Microenvironment. Stem Cell Rep. *11*, 1–13. 10.1016/j.stemcr.2018.06.005.

43. DeCarolis, N.A., Mechanic, M., Petrik, D., Carlton, A., Ables, J.L., Malhotra, S., Bachoo, R., Götz, M., Lagace, D.C., and Eisch, A.J. (2013). In vivo contribution of nestin- and GLAST-lineage cells to adult hippocampal neurogenesis. Hippocampus *23*, 708–719. 10.1002/hipo.22130.

44. Borrett, M.J., Tahmasian, N., Innes, B.T., Bader, G.D., Kaplan, D.R., and Miller, F.D. (2022). A Shared Transcriptional Identity for Forebrain and Dentate Gyrus Neural Stem Cells from Embryogenesis to Adulthood. eneuro, ENEURO.0271-21.2021. 10.1523/ENEURO.0271-21.2021.

45. Maslov, A.Y. (2004). Neural Stem Cell Detection, Characterization, and Age-Related Changes in the Subventricular Zone of Mice. J. Neurosci. *24*, 1726–1733. 10.1523/JNEUROSCI.4608-03.2004.

46. Shimozaki, K. (2014). Sox2 transcription network acts as a molecular switch to regulate properties of neural stem cells. World J. Stem Cells *6*, 485–490. 10.4252/wjsc.v6.i4.485.

47. Levine, M.S., and Holland, A.J. (2018). The impact of mitotic errors on cell proliferation and tumorigenesis. Genes Dev. *32*, 620–638. 10.1101/gad.314351.118.

48. Miller, I., Min, M., Yang, C., Tian, C., Gookin, S., Carter, D., and Spencer, S.L. (2018). Ki67 is a Graded Rather than a Binary Marker of Proliferation versus Quiescence. Cell Rep. *24*. 10.1016/j.celrep.2018.06.110.

49. Hayashi, M.T., and Karlseder, J. (2013). DNA damage associated with mitosis and cytokinesis failure. Oncogene *32*, 4593–4601. 10.1038/onc.2012.615.

50. Niu, W., Zou, Y., Shen, C., and Zhang, C.-L. (2011). Activation of Postnatal Neural Stem Cells Requires Nuclear Receptor TLX. J. Neurosci. *31*, 13816–13828. 10.1523/JNEUROSCI.1038-11.2011.

51. Nowsheen, S., Xia, F., and Yang, E.S. (2012). Assaying DNA Damage in Hippocampal Neurons Using the Comet Assay. J. Vis. Exp., 50049. 10.3791/50049.

52. Pereira, P.D., Serra-Caetano, A., Cabrita, M., Bekman, E., Braga, J., Rino, J., Santus, R., Filipe, P.L., Sousa, A.E., and Ferreira, J.A. (2017). Quantification of cell cycle kinetics by EdU (5-ethynyl-2′-deoxyuridine)-coupled-fluorescence-intensity analysis. Oncotarget *8*, 40514–40532. 10.18632/oncotarget.17121.

53. Mah, L.-J., El-Osta, A., and Karagiannis, T.C. (2010). γH2AX: a sensitive molecular marker of DNA damage and repair. Leukemia *24*, 679–686. 10.1038/leu.2010.6.

54. Kee, N., Sivalingam, S., Boonstra, R., and Wojtowicz, J.M. (2002). The utility of Ki-67 and BrdU as proliferative markers of adult neurogenesis. J. Neurosci. Methods *115*, 97–105. 10.1016/s0165-0270(02)00007-9.

55. Solier, S., and Pommier, Y. (2014). The Nuclear γ-H2AX Apoptotic Ring: Implications for Cancers and Autoimmune Diseases. Cell. Mol. Life Sci. CMLS *71*, 2289–2297. 10.1007/s00018-013-1555-2.

56. Nouruzi, S., Ganguli, D., Tabrizian, N., Kobelev, M., Sivak, O., Namekawa, T., Thaper, D., Baca, S.C., Freedman, M.L., Aguda, A., et al. (2022). ASCL1 activates neuronal stem cell-like lineage programming through remodeling of the chromatin landscape in prostate cancer. Nat. Commun. *13*, 2282. 10.1038/s41467-022-29963-5.

57. Kuhn, H.G., Eisch, A.J., Spalding, K., and Peterson, D.A. (2016). Detection and Phenotypic Characterization of Adult Neurogenesis. Cold Spring Harb. Perspect. Biol. *8*, a025981. 10.1101/cshperspect.a025981.

58. Codega, P., Silva-Vargas, V., Paul, A., Maldonado-Soto, A.R., DeLeo, A.M., Pastrana, E., and Doetsch, F. (2014). Prospective identification and purification of quiescent adult neural stem cells from their in vivo niche. Neuron *82*, 545–559. 10.1016/j.neuron.2014.02.039.

59. Llorens-Bobadilla, E., Zhao, S., Baser, A., Saiz-Castro, G., Zwadlo, K., and Martin-Villalba, A. (2015). Single-Cell Transcriptomics Reveals a Population of Dormant Neural Stem Cells that Become Activated upon Brain Injury. Cell Stem Cell *17*, 329–340. 10.1016/j.stem.2015.07.002.

60. Pastrana, E., Cheng, L.-C., and Doetsch, F. (2009). Simultaneous prospective purification of adult subventricular zone neural stem cells and their progeny. Proc. Natl. Acad. Sci. *106*, 6387–6392. 10.1073/pnas.0810407106.

61. Fabra-Beser, J., Alves Medeiros de Araujo, J., Marques-Coelho, D., Goff, L.A., Costa, M.R., Müller, U., and Gil-Sanz, C. (2021). Differential Expression Levels of Sox9 in Early Neocortical Radial Glial Cells Regulate the Decision between Stem Cell Maintenance and Differentiation. J. Neurosci. *41*, 6969–6986. 10.1523/JNEUROSCI.2905-20.2021.

62. Hennen, E., and Faissner, A. (2012). LewisX: A neural stem cell specific glycan? Int. J. Biochem. Cell Biol. *44*, 830–833. 10.1016/j.biocel.2012.02.019.

63. Stevanovic, M., Drakulic, D., Lazic, A., Ninkovic, D.S., Schwirtlich, M., and Mojsin, M. (2021). SOX Transcription Factors as Important Regulators of Neuronal and Glial Differentiation During Nervous System Development and Adult Neurogenesis. Front. Mol. Neurosci. *14*.

64. Crowther, A.J., Lim, S.-A., Asrican, B., Albright, B.H., Wooten, J., Yeh, C.-Y., Bao, H., Cerri, D.H., Hu, J., Ian Shih, Y.-Y., et al. (2018). An Adeno-Associated Virus-Based Toolkit for Preferential Targeting and Manipulating Quiescent Neural Stem Cells in the Adult Hippocampus. Stem Cell Rep. *10*, 1146–1159. 10.1016/j.stemcr.2018.01.018.

65. Zhang, R., Boareto, M., Engler, A., Louvi, A., Giachino, C., Iber, D., and Taylor, V. (2019). Id4 Downstream of Notch2 Maintains Neural Stem Cell Quiescence in the Adult Hippocampus. Cell Rep. *28*, 1485-1498.e6. 10.1016/j.celrep.2019.07.014.

66. Frémont, S., Gérard, A., Galloux, M., Janvier, K., Karess, R.E., and Berlioz-Torrent, C. (2013). Beclin-1 is required for chromosome congression and proper outer kinetochore assembly. EMBO Rep. *14*, 364–372. 10.1038/embor.2013.23.

67. Kaltezioti, V., Kouroupi, G., Oikonomaki, M., Mantouvalou, E., Stergiopoulos, A., Charonis, A., Rohrer, H., Matsas, R., and Politis, P.K. (2010). Prox1 Regulates the Notch1-Mediated Inhibition of Neurogenesis. PLOS Biol. *8*, e1000565. 10.1371/journal.pbio.1000565.

68. You, S.Y., Park, Y.S., Jeon, H.-J., Cho, D.-H., Jeon, H.B., Kim, S.H., Chang, J.W., Kim, J.-S., and Oh, J.S. (2016). Beclin-1 knockdown shows abscission failure but not autophagy defect during oocyte meiotic maturation. Cell Cycle *15*, 1611–1619. 10.1080/15384101.2016.1181235.

69. Artegiani, B., Lyubimova, A., Muraro, M., van Es, J.H., van Oudenaarden, A., and Clevers, H. (2017). A Single-Cell RNA Sequencing Study Reveals Cellular and Molecular Dynamics of the Hippocampal Neurogenic Niche. Cell Rep. *21*, 3271–3284. 10.1016/j.celrep.2017.11.050.

70. Mathew, R., Kongara, S., Beaudoin, B., Karp, C.M., Bray, K., Degenhardt, K., Chen, G., Jin, S., and White, E. (2007). Autophagy suppresses tumor progression by limiting chromosomal instability. Genes Dev. *21*, 1367–1381. 10.1101/gad.1545107.

71. Dhaliwal, J., and Lagace, D.C. (2011). Visualization and genetic manipulation of adult neurogenesis using transgenic mice. Eur. J. Neurosci. *33*, 1025–1036. 10.1111/j.1460-9568.2011.07600.x.

72. Pohl, C., and Jentsch, S. (2009). Midbody ring disposal by autophagy is a post-abscission event of cytokinesis. Nat. Cell Biol. *11*, 65–70. 10.1038/ncb1813.

73. Schmid, R.S., Yokota, Y., and Anton, E.S. (2006). Generation and characterization of brain lipid-binding protein promoter-based transgenic mouse models for the study of radial glia. Glia *53*, 345–351. 10.1002/glia.20274.

74. Wang, C., Yeo, S., Haas, M.A., and Guan, J.-L. (2017). Autophagy gene FIP200 in neural progenitors non–cell autonomously controls differentiation by regulating microglia. J. Cell Biol. *216*, 2581–2596. 10.1083/jcb.201609093.

75. Kim, E.J., Leung, C.T., Reed, R.R., and Johnson, J.E. (2007). In Vivo Analysis of Ascl1 Defined Progenitors Reveals Distinct Developmental Dynamics during Adult Neurogenesis and Gliogenesis. J. Neurosci. *27*, 12764–12774. 10.1523/JNEUROSCI.3178-07.2007.

76. Funderburk., S.F., Wang, Q.J., and Yue, Z. (2010). Beclin 1-VPS34 complex – At the Crossroads of Autophagy and Beyond. Trends Cell Biol. *20*, 355–362. 10.1016/j.tcb.2010.03.002.

77. Wang, X. (2009). Cre transgenic mouse lines. Methods Mol. Biol. Clifton NJ *561*, 265–273. 10.1007/978-1-60327-019-9_17.

78. Lv, X., Jiang, H., Li, B., Liang, Q., Wang, S., Zhao, Q., and Jiao, J. (2014). The Crucial Role of Atg5 in Cortical Neurogenesis During Early Brain Development. Sci. Rep. *4*, 6010. 10.1038/srep06010.

79. Wilhelmsson, U., Faiz, M., Pablo, Y. de, Sjöqvist, M., Andersson, D., Widestrand, Å., Potokar, M., Stenovec, M., Smith, P.L.P., Shinjyo, N., et al. (2012). Astrocytes Negatively Regulate Neurogenesis Through the Jagged1-Mediated Notch Pathway. STEM CELLS *30*, 2320–2329. 10.1002/stem.1196.

80. Semerci, F., and Maletic-Savatic, M. (2016). Transgenic mouse models for studying adult neurogenesis. Front. Biol. *11*, 151–167. 10.1007/s11515-016-1405-3.

81. Asrican, B., Wooten, J., Li, Y.-D., Quintanilla, L., Zhang, F., Wander, C., Bao, H., Yeh, C.-Y., Luo, Y.-J., Olsen, R., et al. (2020). Neuropeptides Modulate Local Astrocytes to Regulate Adult Hippocampal Neural Stem Cells. Neuron *108*, 349-366.e6. 10.1016/j.neuron.2020.07.039.

82. Bedbrook, C.N., Deverman, B.E., and Gradinaru, V. (2018). Viral Strategies for Targeting the Central and Peripheral Nervous Systems. Annu. Rev. Neurosci. *41*, 323–348. 10.1146/annurev-neuro-080317-062048.

83. Ashton, R.S., Conway, A., Pangarkar, C., Bergen, J., Lim, I.K., Shah, P., Bissell, M., and Schaffer, V.D. (2012). Astrocytes regulate adult hippocampal neurogenesis through ephrin-B signaling. Nat. Neurosci. *15*, 1399–1406. 10.1038/nn.3212.

84. Haggerty, D.L., Grecco, G.G., Reeves, K.C., and Atwood, B. (2019). Adeno-Associated Viral Vectors in Neuroscience Research. Mol. Ther. Methods Clin. Dev. *17*, 69–82. 10.1016/j.omtm.2019.11.012.

85. Song, H., Stevens, C.F., and Gage, F.H. (2002). Astroglia induce neurogenesis from adult neural stem cells. Nature *417*, 39–44. 10.1038/417039a.

86. Reynolds, B.A., and Weiss, S. (1992). Generation of neurons and astrocytes from isolated cells of the adult mammalian central nervous system. Science *255*, 1707–1710. 10.1126/science.1553558.

87. Wang, S., Li, B., Qiao, H., Lv, X., Liang, Q., Shi, Z., Xia, W., Ji, F., and Jiao, J. (2014). Autophagy-related gene Atg5 is essential for astrocyte differentiation in the developing mouse cortex. EMBO Rep. *15*, 1053–1061. 10.15252/embr.201338343.

88. Schneider, J., Weigel, J., Wittmann, M.-T., Svehla, P., Ehrt, S., Zheng, F., Elmzzahi, T., Karpf, J., Paniagua-Herranz, L., Basak, O., et al. (2022). Astrogenesis in the murine dentate gyrus is a life-long and dynamic process. EMBO J., e110409. 10.15252/embj.2021110409.

89. Soares, R., Ribeiro, F.F., Lourenço, D.M., Rodrigues, R.S., Moreira, J.B., Sebastião, A.M., Morais, V.A., and Xapelli, S. (2021). The neurosphere assay: an effective in vitro technique to study neural stem cells. Neural Regen. Res. *16*, 2229–2231. 10.4103/1673-5374.310678.

90. Rust, R., and Walker, T.L. (2022). Isolation and Culture of Adult Hippocampal Precursor Cells as Free-Floating Neurospheres. Methods Mol. Biol. Clifton NJ *2389*, 33–44. 10.1007/978-1-0716-1783-0_3.

91. Imayoshi, I., Ohtsuka, T., Metzger, D., Chambon, P., and Kageyama, R. (2006). Temporal regulation of Cre recombinase activity in neural stem cells. genesis *44*, 233–238. 10.1002/dvg.20212.

92. Srinivas, S., Watanabe, T., Lin, C.-S., William, C.M., Tanabe, Y., Jessell, T.M., and Costantini, F. (2001). Cre reporter strains produced by targeted insertion of EYFP and ECFP into the ROSA26 locus. BMC Dev. Biol. *1*, 4. 10.1186/1471-213X-1-4.

93. Walker, T.L., White, A., Black, D.M., Wallace, R.H., Sah, P., and Bartlett, P.F. (2008). Latent Stem and Progenitor Cells in the Hippocampus Are Activated by Neural Excitation. J. Neurosci. *28*, 5240–5247. 10.1523/JNEUROSCI.0344-08.2008.

94. Deleyrolle, L., Rietze, R., and Reynolds, B. (2008). The neurosphere assay, a method under scrutiny. Acta Neuropsychiatr. *20*. 10.1111/j.1601-5215.2007.00251.x.

95. Mori, T., Tanaka, K., Buffo, A., Wurst, W., Kühn, R., and Götz, M. (2006). Inducible gene deletion in astroglia and radial glia—A valuable tool for functional and lineage analysis. Glia *54*, 21–34. 10.1002/glia.20350.

96. Ganat, Y.M., Silbereis, J., Cave, C., Ngu, H., Anderson, G.M., Ohkubo, Y., Ment, L.R., and Vaccarino, F.M. (2006). Early Postnatal Astroglial Cells Produce Multilineage Precursors and Neural Stem Cells *In Vivo*. J. Neurosci. *26*, 8609–8621. 10.1523/JNEUROSCI.2532-06.2006.

97. Boesch, M., Zeimet, A.G., Fiegl, H., Wolf, B., Huber, J., Klocker, H., Gastl, G., Sopper, S., and Wolf, D. (2016). High prevalence of side population in human cancer cell lines. Oncoscience *3*, 85–87. 10.18632/oncoscience.300.

98. Truett, G.E., Heeger, P., Mynatt, R.L., Truett, A.A., Walker, J.A., and Warman, M.L. (2000). Preparation of PCR-quality mouse genomic DNA with hot sodium hydroxide and tris (HotSHOT). BioTechniques *29*, 52, 54. 10.2144/00291bm09.

99. Lagace, D.C., Whitman, M.C., Noonan, M.A., Ables, J.L., DeCarolis, N.A., Arguello, A.A., Donovan, M.H., Fischer, S.J., Farnbauch, L.A., Beech, R.D., et al. (2007). Dynamic Contribution of Nestin-Expressing Stem Cells to Adult Neurogenesis. J. Neurosci. *27*, 12623–12629. 10.1523/JNEUROSCI.3812-07.2007.

100. Boesch, M., Wolf, D., and Sopper, S. (2015). Optimized Stem Cell Detection Using the DyeCycle-Triggered Side Population Phenotype. Stem Cells Int. *2016*, e1652389. https://doi.org/10.1155/2016/1652389.

101. Golebiewska, A., Brons, N.H.C., Bjerkvig, R., and Niclou, S.P. (2011). Critical Appraisal of the Side Population Assay in Stem Cell and Cancer Stem Cell Research. Cell Stem Cell *8*, 136–147. 10.1016/j.stem.2011.01.007.

102. Jessberger, S., Aigner, S., Jr, G.D.C., Toni, N., Lie, D.C., Karalay, Ö., Overall, R., Kempermann, G., and Gage, F.H. (2008). Cdk5 Regulates Accurate Maturation of Newborn Granule Cells in the Adult Hippocampus. PLOS Biol. *6*, e272. 10.1371/journal.pbio.0060272.

103. Barnum, K.J., and O'Connell, M.J. (2014). Cell Cycle Regulation by Checkpoints. Methods Mol. Biol. Clifton NJ *1170*, 29–40. 10.1007/978-1-4939-0888-2_2.

104. Lagace, D.C., Donovan, M.H., DeCarolis, N.A., Farnbauch, L.A., Malhotra, S., Berton, O., Nestler, E.J., Krishnan, V., and Eisch, A.J. (2010). Adult hippocampal neurogenesis is functionally important for stress-induced social avoidance. Proc. Natl. Acad. Sci. *107*, 4436–4441. 10.1073/pnas.0910072107.

105. Walker, T.L., and Kempermann, G. (2014). One Mouse, Two Cultures: Isolation and Culture of Adult Neural Stem Cells from the Two Neurogenic Zones of Individual Mice. J. Vis. Exp. JoVE. 10.3791/51225.

106. Urbach, A., and Witte, O.W. (2019). Divide or Commit – Revisiting the Role of Cell Cycle Regulators in Adult Hippocampal Neurogenesis. Front. Cell Dev. Biol. *7*.

107. Hagihara, H., Toyama, K., Yamasaki, N., and Miyakawa, T. (2009). Dissection of Hippocampal Dentate Gyrus from Adult Mouse. J. Vis. Exp. JoVE, 1543. 10.3791/1543.

108. Borrett, M.J., Innes, B.T., Jeong, D., Tahmasian, N., Storer, M.A., Bader, G.D., Kaplan, D.R., and Miller, F.D. (2020). Single-Cell Profiling Shows Murine Forebrain Neural Stem Cells Reacquire a Developmental State when Activated for Adult Neurogenesis. Cell Rep. *32*, 108022. 10.1016/j.celrep.2020.108022.

109. Kalinina, A., Gnyra, C., Tang, V., Xue, Y., and Lagace, D.C. (2022). Isolation of the side population from neurogenic niches enriches for endothelial cells. PLOS ONE *17*, e0250752. 10.1371/journal.pone.0250752.

110. Farioli-Vecchioli, S., and Tirone, F. (2015). Control of the Cell Cycle in Adult Neurogenesis and its Relation with Physical Exercise. Brain Plast. *1*, 41–54. 10.3233/BPL-150013.

111. Pesenti, M.E., Raisch, T., Conti, D., Walstein, K., Hoffmann, I., Vogt, D., Prumbaum, D., Vetter, I.R., Raunser, S., and Musacchio, A. (2022). Structure of the human inner kinetochore CCAN complex and its significance for human centromere organization. Mol. Cell *82*, 2113-2131.e8. 10.1016/j.molcel.2022.04.027.

112. Peco, E., Escude, T., Agius, E., Sabado, V., Medevielle, F., Ducommun, B., and Pituello, F. (2012). The CDC25B phosphatase shortens the G2 phase of neural progenitors and promotes efficient neuron production. Development *139*, 1095–1104. 10.1242/dev.068569.

113. Martin, C.-A., Murray, J.E., Carroll, P., Leitch, A., Mackenzie, K.J., Halachev, M., Fetit, A.E., Keith, C., Bicknell, L.S., Fluteau, A., et al. (2016). Mutations in genes encoding condensin complex proteins cause microcephaly through decatenation failure at mitosis. Genes Dev. *30*, 2158–2172. 10.1101/gad.286351.116.

114. Arai, Y., Pulvers, J.N., Haffner, C., Schilling, B., Nüsslein, I., Calegari, F., and Huttner, W.B. (2011). Neural stem and progenitor cells shorten S-phase on commitment to neuron production. Nat. Commun. *2*, 154. 10.1038/ncomms1155.

115. Thompson, A.F., Blackburn, P.R., Arons, N.S., Stevens, S.N., Babovic-Vuksanovic, D., Lian, J.B., Klee, E.W., and Stumpff, J. (2022). Pathogenic mutations in the chromokinesin KIF22 disrupt anaphase chromosome segregation. eLife *11*, e78653. 10.7554/eLife.78653.

116. Marlier, Q., Verteneuil, S., Renaud, V., Nicolas, C., Kaldis, P., Nguyen, L., and Malgrange, B. (2015). Unraveling the role of Cdk1 in postnatal neurogenesis. Front. Neurosci. *9*. 10.3389/conf.fnins.2015.89.00069.

117. McCleland, M.L., Kallio, M.J., Barrett-Wilt, G.A., Kestner, C.A., Shabanowitz, J., Hunt, D.F., Gorbsky, G.J., and Stukenberg, P.T. (2004). The vertebrate Ndc80 complex contains Spc24 and Spc25 homologs, which are required to establish and maintain kinetochore-microtubule attachment. Curr. Biol. CB *14*, 131–137. 10.1016/j.cub.2003.12.058.

118. Li, Y.-Q., and Wong, C.S. (2018). Effects of p21 on adult hippocampal neuronal development after irradiation. Cell Death Discov. *4*, 1–12. 10.1038/s41420-018-0081-2.

119. Cavazza, T., and Vernos, I. (2016). The RanGTP Pathway: From Nucleo-Cytoplasmic Transport to Spindle Assembly and Beyond. Front. Cell Dev. Biol. *3*. 10.3389/fcell.2015.00082.

120. Micheli, L., D'Andrea, G., Ceccarelli, M., Ferri, A., Scardigli, R., and Tirone, F. (2019). p16Ink4a Prevents the Activation of Aged Quiescent Dentate Gyrus Stem Cells by Physical Exercise. Front. Cell. Neurosci. *13*.

121. Joseph, J., Liu, S.-T., Jablonski, S.A., Yen, T.J., and Dasso, M. (2004). The RanGAP1-RanBP2 Complex Is Essential for Microtubule-Kinetochore Interactions In Vivo. Curr. Biol. *14*, 611–617. 10.1016/j.cub.2004.03.031.

122. Kowalczyk, A., Filipkowski, R.K., Rylski, M., Wilczynski, G.M., Konopacki, F.A., Jaworski, J., Ciemerych, M.A., Sicinski, P., and Kaczmarek, L. (2004). The critical role of cyclin D2 in adult neurogenesis. J. Cell Biol. *167*, 209–213. 10.1083/jcb.200404181.

123. Arnaoutov, A., and Dasso, M. (2003). The Ran GTPase Regulates Kinetochore Function. Dev. Cell *5*, 99–111. 10.1016/S1534-5807(03)00194-1.

124. Beukelaers, P., Vandenbosch, R., Caron, N., Nguyen, L., Moonen, G., and Malgrange, B. (2012). Cycling or not cycling: cell cycle regulatory molecules and adult neurogenesis. Cell. Mol. Life Sci. *69*, 1493–1503. 10.1007/s00018-011-0880-6.

125. Johnson, C.A., Wright, C.E., and Ghashghaei, H.T. (2017). Regulation of cytokinesis during corticogenesis: focus on the midbody. FEBS Lett. *591*, 4009–4026. 10.1002/1873-3468.12676.

126. Gil-Perotin, S., Haines, J.D., Kaur, J., Marin-Husstege, M., Spinetta, M.J., Kim, K.-H., Duran-Moreno, M., Schallert, T., Zindy, F., Roussel, M.F., et al. (2011). Roles of p53 and p27 Kip1 in the regulation of neurogenesis in the murine adult subventricular zone. Eur. J. Neurosci. *34*, 1040–1052. 10.1111/j.1460-9568.2011.07836.x.

127. Ryu, J.R., Hong, C.J., Kim, J.Y., Kim, E.-K., Sun, W., and Yu, S.-W. (2016). Control of adult neurogenesis by programmed cell death in the mammalian brain. Mol. Brain *9*, 43. 10.1186/s13041-016-0224-4.

128. Mfossa, A.-C.M., Verslegers, M., Verreet, T., Fida, H. bin, Mysara, M., IJcken, W.F.J.V., Vos, W.H.D., Moons, L., Baatout, S., Benotmane, M.A., et al. (2020). p53 drives premature neuronal differentiation in response to radiation-induced DNA damage during early neurogenesis. Preprint at bioRxiv, 10.1101/2020.06.26.171132 10.1101/2020.06.26.171132.

129. Engeland, K. (2022). Cell cycle regulation: p53-p21-RB signaling. Cell Death Differ. *29*, 946–960. 10.1038/s41418-022-00988-z.

130. Li, Y.-Q., Cheng, Z.-C., Liu, S.-W., Aubert, I., and Wong, C.S. (2016). P53 regulates disruption of neuronal development in the adult hippocampus after irradiation. Cell Death Discov. *2*, 1–10. 10.1038/cddiscovery.2016.72.

131. Caneus, J., Granic, A., Rademakers, R., Dickson, D.W., Coughlan, C.M., Chial, H.J., and Potter, H. (2018). Mitotic defects lead to neuronal aneuploidy and apoptosis in frontotemporal lobar degeneration caused by MAPT mutations. Mol. Biol. Cell *29*, 575–586. 10.1091/mbc.E17-01-0031.

132. White, E. (2016). Autophagy and p53. Cold Spring Harb. Perspect. Med. *6*, a026120. 10.1101/cshperspect.a026120.

133. Blagosklonny, M.V. (2007). Mitotic Arrest and Cell Fate: Why and How Mitotic Inhibition of Transcription Drives Mutually Exclusive Events. Cell Cycle *6*, 70–74. 10.4161/cc.6.1.3682.

134. Broz, D.K., Mello, S.S., Bieging, K.T., Jiang, D., Dusek, R.L., Brady, C.A., Sidow, A., and Attardi, L.D. (2013). Global genomic profiling reveals an extensive p53-regulated autophagy program contributing to key p53 responses. Genes Dev. *27*, 1016–1031. 10.1101/gad.212282.112.

135. Willems, P.H.G.M., Rossignol, R., Dieteren, C.E.J., Murphy, M.P., and Koopman, W.J.H. (2015). Redox Homeostasis and Mitochondrial Dynamics. Cell Metab. *22*, 207–218. 10.1016/j.cmet.2015.06.006.

136. D'Angiolella, V., Donato, V., Forrester, F.M., Jeong, Y.-T., Pellacani, C., Kudo, Y., Saraf, A., Florens, L., Washburn, M.P., and Pagano, M. (2012). The Cyclin F-Ribonucleotide Reductase M2 axis controls genome integrity and DNA repair. Cell *149*, 1023–1034. 10.1016/j.cell.2012.03.043.

137. Forsha, D., Church, C., Wazny, P., and Poyton, R.O. (2001). Structure and function of Pet100p, a molecular chaperone required for the assembly of cytochrome c oxidase in Saccharomyces cerevisiae. Biochem. Soc. Trans. *29*, 436–441. 10.1042/bst0290436.

138. Gomez Godinez, V., Kabbara, S., Sherman, A., Wu, T., Cohen, S., Kong, X., Maravillas-Montero, J.L., Shi, Z., Preece, D., Yokomori, K., et al. (2020). DNA damage induced during mitosis undergoes DNA repair synthesis. PLoS ONE *15*, e0227849. 10.1371/journal.pone.0227849.

139. Suhane, S., Kanzaki, H., Arumugaswami, V., Murali, R., and Ramanujan, V.K. (2013). Mitochondrial NDUFS3 regulates the ROS-mediated onset of metabolic switch in transformed cells. Biol. Open *2*, 295–305. 10.1242/bio.20133244.

140. di Pietro, F., Echard, A., and Morin, X. (2016). Regulation of mitotic spindle orientation: an integrated view. EMBO Rep. *17*, 1106–1130. 10.15252/embr.201642292.

141. Chen, W., Wang, H., Tao, S., Zheng, Y., Wu, W., Lian, F., Jaramillo, M., Fang, D., and Zhang, D.D. (2013). Tumor protein translationally controlled 1 is a p53 target gene that promotes cell survival. Cell Cycle *12*, 2321–2328. 10.4161/cc.25404.

142. Musacchio, A. (2015). The Molecular Biology of Spindle Assembly Checkpoint Signaling Dynamics. Curr. Biol. *25*, R1002–R1018. 10.1016/j.cub.2015.08.051.

143. Zhang, J., de Toledo, S.M., Pandey, B.N., Guo, G., Pain, D., Li, H., and Azzam, E.I. (2012). Role of the translationally controlled tumor protein in DNA damage sensing and repair. Proc. Natl. Acad. Sci. U. S. A. *109*, E926-933. 10.1073/pnas.1106300109.

144. Konstantinidis, G., and Tavernarakis, N. (2022). Autophagy of the Nucleus in Health and Disease. Front. Cell Dev. Biol. *9*.

145. de Moraes, E., Dar, N.A., de Moura Gallo, C.V., and Hainaut, P. (2007). Cross-talks between cyclooxygenase-2 and tumor suppressor protein p53: Balancing life and death during inflammatory stress and carcinogenesis. Int. J. Cancer *121*, 929–937. 10.1002/ijc.22899.

146. Ma, H.T., and Poon, R.Y.C. (2020). Aurora kinases and DNA damage response. Mutat. Res. *821*, 111716. 10.1016/j.mrfmmm.2020.111716.

147. Budanov, A.V., and Karin, M. (2008). p53 Target Genes Sestrin1 and Sestrin2 Connect Genotoxic Stress and mTOR Signaling. Cell *134*, 451–460. 10.1016/j.cell.2008.06.028.

148. Pommier, Y., Nussenzweig, A., Takeda, S., and Austin, C. (2022). Human topoisomerases and their roles in genome stability and organization. Nat. Rev. Mol. Cell Biol. *23*, 407–427. 10.1038/s41580-022-00452-3.

149. Kinner, A., Wu, W., Staudt, C., and Iliakis, G. (2008). γ-H2AX in recognition and signaling of DNA double-strand breaks in the context of chromatin. Nucleic Acids Res. *36*, 5678–5694. 10.1093/nar/gkn550.

150. De Biasio, A., de Opakua, A.I., Mortuza, G.B., Molina, R., Cordeiro, T.N., Castillo, F., Villate, M., Merino, N., Delgado, S., Gil-Cartón, D., et al. (2015). Structure of p15(PAF)-PCNA complex and implications for clamp sliding during DNA replication and repair. Nat. Commun. *6*, 6439. 10.1038/ncomms7439.

151. Gregan, J., Polakova, S., Zhang, L., Tolić-Nørrelykke, I.M., and Cimini, D. (2011). Merotelic kinetochore attachment: causes and effects. Trends Cell Biol. *21*, 374–381. 10.1016/j.tcb.2011.01.003.

152. Bolcun-Filas, E., Costa, Y., Speed, R., Taggart, M., Benavente, R., De Rooij, D.G., and Cooke, H.J. (2007). SYCE2 is required for synaptonemal complex assembly, double strand break repair, and homologous recombination. J. Cell Biol. *176*, 741–747. 10.1083/jcb.200610027.

153. Sazonova, E.V., Petrichuk, S.V., Kopeina, G.S., and Zhivotovsky, B. (2021). A link between mitotic defects and mitotic catastrophe: detection and cell fate. Biol. Direct *16*, 25. 10.1186/s13062-021-00313-7.

154. Karantza-Wadsworth, V., Patel, S., Kravchuk, O., Chen, G., Mathew, R., Jin, S., and White, E. (2007). Autophagy mitigates metabolic stress and genome damage in mammary tumorigenesis. Genes Dev. *21*, 1621–1635. 10.1101/gad.1565707.

155. Akagawa, R., Nabeshima, Y., and Kawauchi, T. (2021). Alternative Functions of Cell Cycle-Related and DNA Repair Proteins in Post-mitotic Neurons. Front. Cell Dev. Biol. *9*.

156. Delaney, J.R., Patel, C.B., Bapat, J., Jones, C.M., Ramos-Zapatero, M., Ortell, K.K., Tanios, R., Haghighiabyaneh, M., Axelrod, J., DeStefano, J.W., et al. (2020). Autophagy gene haploinsufficiency drives chromosome instability, increases migration, and promotes early ovarian tumors. PLoS Genet. *16*, e1008558. 10.1371/journal.pgen.1008558.

157. Cecchini, M.J., Amiri, M., and Dick, F.A. (2012). Analysis of Cell Cycle Position in Mammalian Cells. J. Vis. Exp. JoVE. 10.3791/3491.

158. Yazdankhah, M., Farioli-Vecchioli, S., Tonchev, A.B., Stoykova, A., and Cecconi, F. (2014). The autophagy regulators Ambra1 and Beclin 1 are required for adult neurogenesis in the brain subventricular zone. Cell Death Dis. *5*, e1403–e1403. 10.1038/cddis.2014.358.

159. Smith, P.J. (2016). EdU and BrdU incorporation resolve their differences. Cell Cycle *15*, 1527–1528. 10.1080/15384101.2016.1171654.

160. Tran, S., Fairlie, W.D., and Lee, E.F. (2021). BECLIN1: Protein Structure, Function and Regulation. Cells *10*, 1522. 10.3390/cells10061522.

161. Kaur, S., and Changotra, H. (2020). The beclin 1 interactome: Modification and roles in the pathology of autophagy-related disorders. Biochimie *175*, 34–49. 10.1016/j.biochi.2020.04.025.

162. Etienne, O., Bery, A., Roque, T., Desmaze, C., and Boussin, F.D. (2014). Assessing Cell Cycle Progression of Neural Stem and Progenitor Cells in the Mouse Developing Brain after Genotoxic Stress. J. Vis. Exp. JoVE. 10.3791/51209.

163. Xu, F., Fang, Y., Yan, L., Xu, L., Zhang, S., Cao, Y., Xu, L., Zhang, X., Xie, J., Jiang, G., et al. (2017). Nuclear localization of Beclin 1 promotes radiation-induced DNA damage repair independent of autophagy. Sci. Rep. *7*, 45385. 10.1038/srep45385.

164. Yoon, K.-J., Ringeling, F.R., Vissers, C., Jacob, F., Pokrass, M., Jimenez-Cyrus, D., Su, Y., Kim, N.-S., Zhu, Y., Zheng, L., et al. (2017). Temporal Control of Mammalian Cortical Neurogenesis by m6A Methylation. Cell *171*, 877-889.e17. 10.1016/j.cell.2017.09.003.

165. Menon, M.B., and Dhamija, S. (2018). Beclin 1 Phosphorylation – at the Center of Autophagy Regulation. Front. Cell Dev. Biol. *6*.

166. Yang, C.-P., Gilley, J.A., Zhang, G., and Kernie, S.G. (2011). ApoE is required for maintenance of the dentate gyrus neural progenitor pool. Dev. Camb. Engl. *138*, 4351–4362. 10.1242/dev.065540.

167. Jiang, Y., Bruin, A. de, Caldas, H., Fangusaro, J., Hayes, J., Conway, E.M., Robinson, M.L., and Altura, R.A. (2005). Essential Role for Survivin in Early Brain Development. J. Neurosci. *25*, 6962–6970. 10.1523/JNEUROSCI.1446-05.2005.

168. Carosso, G.A., Boukas, L., Augustin, J.J., Nguyen, H.N., Winer, B.L., Cannon, G.H., Robertson, J.D., Zhang, L., Hansen, K.D., Goff, L.A., et al. (2019). Precocious neuronal differentiation and disrupted oxygen responses in Kabuki syndrome. JCI Insight *4*. 10.1172/jci.insight.129375.

169. Wirawan, E., Lippens, S., Vanden Berghe, T., Romagnoli, A., Fimia, G.M., Piacentini, M., and Vandenabeele, P. (2012). Beclin1: A role in membrane dynamics and beyond. Autophagy *8*, 6–17. 10.4161/auto.8.1.16645.

170. Abe, T., Sakaue-Sawano, A., Kiyonari, H., Shioi, G., Inoue, K., Horiuchi, T., Nakao, K., Miyawaki, A., Aizawa, S., and Fujimori, T. (2013). Visualization of cell cycle in mouse embryos with Fucci2 reporter directed by Rosa26 promoter. Development *140*, 237–246. 10.1242/dev.084111.

171. Niu, T.-K., Cheng, Y., Ren, X., and Yang, J.-M. (2010). Interaction of Beclin 1 with survivin regulates sensitivity of human glioma cells to TRAIL-induced apoptosis. FEBS Lett. *584*, 3519–3524. 10.1016/j.febslet.2010.07.018.

172. Aimone, J.B., Li, Y., Lee, S.W., Clemenson, G.D., Deng, W., and Gage, F.H. (2014). Regulation and Function of Adult Neurogenesis: From Genes to Cognition. Physiol. Rev. *94*, 991–1026. 10.1152/physrev.00004.2014.

173. Wiedemuth, R., Klink, B., Töpfer, K., Schröck, E., Schackert, G., Tatsuka, M., and Temme, A. (2014). Survivin safeguards chromosome numbers and protects from aneuploidy independently from p53. Mol. Cancer *13*, 107. 10.1186/1476-4598-13-107.

174. Basak, O., Krieger, T.G., Muraro, M.J., Wiebrands, K., Stange, D.E., Frias-Aldeguer, J., Rivron, N.C., Wetering, M. van de, Es, J.H. van, Oudenaarden, A. van, et al. (2018). Troy+ brain stem cells cycle through quiescence and regulate their number by sensing niche occupancy. Proc. Natl. Acad. Sci. *115*, E610–E619. 10.1073/pnas.1715911114.

175. Subramani, S., and Malhotra, V. (2013). Non-autophagic roles of autophagy-related proteins. EMBO Rep. *14*, 143–151. 10.1038/embor.2012.220.

176. Winkelman, M.A., Koppes, A.N., Koppes, R.A., and Dai, G. (2021). Bioengineering the neurovascular niche to study the interaction of neural stem cells and endothelial cells. APL Bioeng. *5*, 011507. 10.1063/5.0027211.

177. Codogno, P., Mehrpour, M., and Proikas-Cezanne, T. (2012). Canonical and non-canonical autophagy: variations on a common theme of self-eating? Nat. Rev. Mol. Cell Biol. *13*, 7–12. 10.1038/nrm3249.

178. Moss, J., Gebara, E., Bushong, E.A., Sánchez-Pascual, I., O'Laoi, R., El M'Ghari, I., Kocher-Braissant, J., Ellisman, M.H., and Toni, N. (2016). Fine processes of Nestin-GFP–positive radial glia-like stem cells in the adult dentate gyrus ensheathe local synapses and vasculature. Proc. Natl. Acad. Sci. *113*, E2536–E2545. 10.1073/pnas.1514652113.

179. Jung, S., Choe, S., Woo, H., Jeong, H., An, H.-K., Moon, H., Ryu, H.Y., Yeo, B.K., Lee, Y.W., Choi, H., et al. (2020). Autophagic death of neural stem cells mediates chronic stress-induced decline of adult hippocampal neurogenesis and cognitive deficits. Autophagy *16*, 512–530. 10.1080/15548627.2019.1630222.

180. Cassé, F., Richetin, K., and Toni, N. (2018). Astrocytes' Contribution to Adult Neurogenesis in Physiology and Alzheimer's Disease. Front. Cell. Neurosci. *12*. 10.3389/fncel.2018.00432.

181. Hewitt, G., Carroll, B., Sarallah, R., Correia-Melo, C., Ogrodnik, M., Nelson, G., Otten, E.G., Manni, D., Antrobus, R., Morgan, B.A., et al. (2016). SQSTM1/p62 mediates crosstalk between autophagy and the UPS in DNA repair. Autophagy *12*, 1917–1930. 10.1080/15548627.2016.1210368.

182. Wang, C., Liang, C.-C., Bian, Z.C., Zhu, Y., and Guan, J.-L. (2013). FIP200 is required for maintenance and differentiation of postnatal neural stem cells. Nat. Neurosci. *16*, 532–542. 10.1038/nn.3365.

183. Bond, A.M., Peng, C.-Y., Meyers, E.A., McGuire, T., Ewaleifoh, O., and Kessler, J.A. (2014). BMP signaling regulates the tempo of adult hippocampal progenitor maturation at multiple stages of the lineage. Stem Cells Dayt. Ohio *32*, 2201–2214. 10.1002/stem.1688.

184. Schäffner, I., Minakaki, G., Khan, M.A., Balta, E.-A., Schlötzer-Schrehardt, U., Schwarz, T.J., Beckervordersandforth, R., Winner, B., Webb, A.E., DePinho, R.A., et al. (2018). FoxO Function Is Essential for Maintenance of Autophagic Flux and Neuronal Morphogenesis in Adult Neurogenesis. Neuron *99*, 1188-1203.e6. 10.1016/j.neuron.2018.08.017.

185. Mizushima, N., and Levine, B. (2010). Autophagy in mammalian development and differentiation. Preprint at Nature Publishing Group, 10.1038/ncb0910-823 10.1038/ncb0910-823.

186. Mathiassen, S.G., De Zio, D., and Cecconi, F. (2017). Autophagy and the Cell Cycle: A Complex Landscape. Front. Oncol. *7*.

187. Qu, Q., Sun, G., Murai, K., Ye, P., Li, W., Asuelime, G., Cheung, Y.-T., and Shi, Y. (2013). Wnt7a Regulates Multiple Steps of Neurogenesis. Mol. Cell. Biol. *33*, 2551–2559. 10.1128/MCB.00325-13.

188. Gonzalez-Reyes, L.E., Chiang, C.-C., Zhang, M., Johnson, J., Arrillaga-Tamez, M., Couturier, N.H., Reddy, N., Starikov, L., Capadona, J.R., Kottmann, A.H., et al. (2019). Sonic Hedgehog is expressed by hilar mossy cells and regulates cellular survival and neurogenesis in the adult hippocampus. Sci. Rep. *9*, 17402. 10.1038/s41598-019-53192-4.

189. Almacellas, E., and Mauvezin, C. (2022). Emerging roles of mitotic autophagy. J. Cell Sci. *135*, jcs255802. 10.1242/jcs.255802.

190. Spampinato, S.F., Bortolotto, V., Canonico, P.L., Sortino, M.A., and Grilli, M. (2019). Astrocyte-Derived Paracrine Signals: Relevance for Neurogenic Niche Regulation and Blood–Brain Barrier Integrity. Front. Pharmacol. *10*.

191. Cecconi, F. (2020). Autophagy, replication stress and DNA synthesis, an intricate relationship. Cell Death Differ. *27*, 829–830. 10.1038/s41418-019-0479-2.

192. Khacho, M., Harris, R., and Slack, R.S. (2019). Mitochondria as central regulators of neural stem cell fate and cognitive function. Nat. Rev. Neurosci. *20*, 34–48. 10.1038/s41583-018-0091-3.

193. Ambrosio, S., and Majello, B. (2020). Autophagy Roles in Genome Maintenance. Cancers *12*, 1793. 10.3390/cancers12071793.

194. Khacho, M., Clark, A., Svoboda, D.S., MacLaurin, J.G., Lagace, D.C., Park, D.S., and Slack, R.S. (2017). Mitochondrial dysfunction underlies cognitive defects as a result of neural stem cell depletion and impaired neurogenesis. Hum. Mol. Genet. *26*, 3327–3341. 10.1093/hmg/ddx217.

195. Guo, J.Y., Teng, X., Laddha, S.V., Ma, S., Van Nostrand, S.C., Yang, Y., Khor, S., Chan, C.S., Rabinowitz, J.D., and White, E. (2016). Autophagy provides metabolic substrates to maintain energy charge and nucleotide pools in Ras-driven lung cancer cells. Genes Dev. *30*, 1704–1717. 10.1101/gad.283416.116.

196. Delgado-Esteban, M., García-Higuera, I., Maestre, C., Moreno, S., and Almeida, A. (2013). APC/C-Cdh1 coordinates neurogenesis and cortical size during development. Nat. Commun. *4*, 2879. 10.1038/ncomms3879.

197. Kataura, T., Sedlackova, L., Otten, E.G., Kumari, R., Shapira, D., Scialo, F., Stefanatos, R., Ishikawa, K., Kelly, G., Seranova, E., et al. (2022). Autophagy promotes cell survival by maintaining NAD levels. Dev. Cell *57*, 2584-2598.e11. 10.1016/j.devcel.2022.10.008.

198. Piper, M., Barry, G., Harvey, T., Mcleay, R., Smith, A., Harris, L., Mason, S., Stringer, B., Day, B., Wray, N., et al. (2014). NFIB-Mediated Repression of the Epigenetic Factor Ezh2 Regulates Cortical Development. J. Neurosci. Off. J. Soc. Neurosci. *34*, 2921–2930. 10.1523/JNEUROSCI.2319-13.2014.

199. Qiang, L., Zhao, B., Shah, P., Sample, A., Yang, S., and He, Y.-Y. (2016). Autophagy positively regulates DNA damage recognition by nucleotide excision repair. Autophagy *12*, 357–368. 10.1080/15548627.2015.1110667.

200. Rolando, C., Erni, A., Grison, A., Beattie, R., Engler, A., Gokhale, P.J., Milo, M., Wegleiter, T., Jessberger, S., and Taylor, V. (2016). Multipotency of Adult Hippocampal NSCs In Vivo Is Restricted by Drosha/NFIB. Cell Stem Cell *19*, 653–662. 10.1016/j.stem.2016.07.003.

201. Kang, R., Zeh, H.J., Lotze, M.T., and Tang, D. (2011). The Beclin 1 network regulates autophagy and apoptosis. Cell Death Differ. *18*, 571–580. 10.1038/cdd.2010.191.

202. Luo, H., Huang, D., Tang, X., Liu, Y., Luo, Q., Liu, C., Huang, H., Chen, W., and Qi, Z. (2022). Beclin-1 exerts protective effects against cerebral ischemia-reperfusion injury by promoting DNA damage repair through a non-autophagy-dependent regulatory mechanism. Int. J. Mol. Med. *49*, 1–11. 10.3892/ijmm.2022.5117.

203. Thoresen, S.B., Pedersen, N.M., Liestøl, K., and Stenmark, H. (2010). A phosphatidylinositol 3-kinase class III sub-complex containing VPS15, VPS34, Beclin 1, UVRAG and BIF-1 regulates cytokinesis and degradative endocytic traffic. Exp. Cell Res. *316*, 3368–3378. 10.1016/j.yexcr.2010.07.008.

204. Zheng, K., Lin, L., Jiang, W., Chen, L., Zhang, X., Zhang, Q., Ren, Y., and Hao, J. (2022). Single-cell RNA-seq reveals the transcriptional landscape in ischemic stroke. J. Cereb. Blood Flow Metab. *42*, 56–73. 10.1177/0271678X211026770.

205. Kang, R., Livesey, K.M., Zeh, H.J., Loze, M.T., and Tang, D. (2010). HMGB1: a novel Beclin 1-binding protein active in autophagy. Autophagy *6*, 1209–1211. 10.4161/auto.6.8.13651.

206. Bar-Yosef, T., Damri, O., and Agam, G. (2019). Dual Role of Autophagy in Diseases of the Central Nervous System. Front. Cell. Neurosci. *13*. 10.3389/fncel.2019.00196.

207. Wang, L., Yu, L., Zhang, T., Wang, L., Leng, Z., Guan, Y., and Wang, X. (2014). HMGB1 enhances embryonic neural stem cell proliferation by activating the MAPK signaling pathway. Biotechnol. Lett. *36*, 1631–1639. 10.1007/s10529-014-1525-2.

208. Malik, B.R., Maddison, D.C., Smith, G.A., and Peters, O.M. (2019). Autophagic and endo-lysosomal dysfunction in neurodegenerative disease. Mol. Brain *12*, 100. 10.1186/s13041-019-0504-x.

209. Zhao, X., Rouhiainen, A., Li, Z., Guo, S., and Rauvala, H. (2020). Regulation of Neurogenesis in Mouse Brain by HMGB1. Cells *9*, 1714. 10.3390/cells9071714.

210. Arano, T., Imai, Y., Arano, T., and Imai, Y. (2015). Mitophagy Regulated by the PINK1-Parkin Pathway. In Cell Death - Autophagy, Apoptosis and Necrosis (IntechOpen). 10.5772/61284.

211. Tang, F., and Christofori, G. (2020). LATS1-Beclin1 mediates a non-canonical connection between the Hippo pathway and autophagy. Mol. Cell. Oncol. *7*, 1757378. 10.1080/23723556.2020.1757378.

212. Casares-Crespo, L., Calatayud-Baselga, I., García-Corzo, L., and Mira, H. (2018). On the Role of Basal Autophagy in Adult Neural Stem Cells and Neurogenesis. Front. Cell. Neurosci. *12*. 10.3389/fncel.2018.00339.

213. Levine, B., and Klionsky, D.J. (2017). Autophagy wins the 2016 Nobel Prize in Physiology or Medicine: Breakthroughs in baker's yeast fuel advances in biomedical research. Proc. Natl. Acad. Sci. *114*, 201–205. 10.1073/pnas.1619876114.

214. Beese, C.J., Brynjólfsdóttir, S.H., and Frankel, L.B. (2020). Selective Autophagy of the Protein Homeostasis Machinery: Ribophagy, Proteaphagy and ER-Phagy. Front. Cell Dev. Biol. *7*.

215. Peker, N., and Gozuacik, D. (2020). Autophagy as a Cellular Stress Response Mechanism in the Nervous System. J. Mol. Biol. *432*, 2560–2588. 10.1016/j.jmb.2020.01.017.

216. Johansen, T., and Lamark, T. (2011). Selective autophagy mediated by autophagic adapter proteins. Autophagy *7*, 279–296. 10.4161/auto.7.3.14487.

217. Kang, R., Zeh, H.J., Lotze, M.T., and Tang, D. (2011). The Beclin 1 network regulates autophagy and apoptosis. Cell Death Differ. *18*, 571–580. 10.1038/cdd.2010.191.

218. Kang, R., Zeh, H.J., Lotze, M.T., and Tang, D. (2011). The Beclin 1 network regulates autophagy and apoptosis. Cell Death Differ. *18*, 571–580. 10.1038/cdd.2010.191.

219. Niu, T.-K., Cheng, Y., Ren, X., and Yang, J.-M. (2010). Interaction of Beclin 1 with survivin regulates sensitivity of human glioma cells to TRAIL-induced apoptosis. FEBS Lett. *584*, 3519–3524. 10.1016/j.febslet.2010.07.018.

220. Lindmo, K., and Stenmark, H. (2006). Regulation of membrane traffic by phosphoinositide 3-kinases. J. Cell Sci. *119*, 605–614. 10.1242/jcs.02855.

221. Balla, T. (2013). Phosphoinositides: Tiny Lipids With Giant Impact on Cell Regulation. Physiol. Rev. *93*, 1019–1137. 10.1152/physrev.00028.2012.

222. Marat, A.L., and Haucke, V. (2016). Phosphatidylinositol 3-phosphates—at the interface between cell signalling and membrane traffic. EMBO J. *35*, 561–579. 10.15252/embj.201593564.

223. Matthew-Onabanjo, A.N., Janusis, J., Mercado-Matos, J., Carlisle, A.E., Kim, D., Levine, F., Cruz-Gordillo, P., Richards, R., Lee, M.J., and Shaw, L.M. (2020). Beclin 1 promotes endosome recruitment of hepatocyte growth factor tyrosine kinase substrate to suppress tumor proliferation. Cancer Res. *80*, 249–262. 10.1158/0008-5472.CAN-19-1555.

224. Noguchi, S., Honda, S., Saitoh, T., Matsumura, H., Nishimura, E., Akira, S., and Shimizu, S. (2019). Beclin 1 regulates recycling endosome and is required for skin development in mice. Commun. Biol. *2*, 1–10. 10.1038/s42003-018-0279-0.

225. Frémont, S., Gérard, A., Galloux, M., Janvier, K., Karess, R.E., and Berlioz-Torrent, C. (2013). Beclin-1 is required for chromosome congression and proper outer kinetochore assembly. EMBO Rep. *14*, 364–372. 10.1038/embor.2013.23.

226. Xu, F., Fang, Y., Yan, L., Xu, L., Zhang, S., Cao, Y., Xu, L., Zhang, X., Xie, J., Jiang, G., et al. (2017). Nuclear localization of Beclin 1 promotes radiation-induced DNA damage repair independent of autophagy. Sci. Rep. *7*, 45385. 10.1038/srep45385.

227. Tougeron, D., Park, J.M., Okamoto, K., Huang, S., and Sinicrope, F.A. (2014). Use of the essential autophagy protein beclin 1 to regulate DNA damage response and predict response to chemoradiation in rectal cancer. J. Clin. Oncol. *32*, 492–492. 10.1200/jco.2014.32.3_suppl.492.

228. Park, J.M., Tougeron, D., Huang, S., Okamoto, K., and Sinicrope, F.A. (2014). Beclin 1 and UVRAG Confer Protection from Radiation-Induced DNA Damage and Maintain Centrosome Stability in Colorectal Cancer Cells. PLOS ONE *9*, e100819. 10.1371/journal.pone.0100819.

229. Thoresen, S.B., Pedersen, N.M., Liestøl, K., and Stenmark, H. (2010). A phosphatidylinositol 3-kinase class III sub-complex containing VPS15, VPS34, Beclin 1, UVRAG and BIF-1 regulates cytokinesis and degradative endocytic traffic. Exp. Cell Res. *316*, 3368–3378. 10.1016/j.yexcr.2010.07.008.

230. Shimizu, S. (2018). Biological Roles of Alternative Autophagy. Mol. Cells *41*, 50–54. 10.14348/molcells.2018.2215.

231. Chen, D., Fan, W., Lu, Y., Ding, X., Chen, S., and Zhong, Q. (2012). A Mammalian Autophagosome Maturation Mechanism Mediated by TECPR1 and the Atg12-Atg5 Conjugate. Mol. Cell *45*, 629–641. 10.1016/j.molcel.2011.12.036.

232. Yamamoto, H., Zhang, S., and Mizushima, N. (2023). Autophagy genes in biology and disease. Nat. Rev. Genet. *24*, 382–400. 10.1038/s41576-022-00562-w.

233. Ye, X., Zhou, X.-J., and Zhang, H. (2018). Exploring the Role of Autophagy-Related Gene 5 (ATG5) Yields Important Insights Into Autophagy in Autoimmune/Autoinflammatory Diseases. Front. Immunol. *9*.

234. Honda, S., Arakawa, S., Yamaguchi, H., Torii, S., Tajima Sakurai, H., Tsujioka, M., Murohashi, M., and Shimizu, S. (2020). Association Between Atg5-independent Alternative Autophagy and Neurodegenerative Diseases. J. Mol. Biol. *432*, 2622–2632. 10.1016/j.jmb.2020.01.016.

235. Yang, J., He, Y., Zhai, N., Ding, S., Li, J., and Peng, Z. (2018). MicroRNA-181a inhibits autophagy by targeting Atg5 in hepatocellular carcinoma. Front. Biosci. Landmark Ed. *23*, 388–396. 10.2741/4596.

236. Nguyen, H.Q., Zada, S., Lai, T.H., Pham, T.M., Hwang, J.S., Ahmed, M., and Kim, D.R. (2019). Calpain-dependent Beclin1 cleavage stimulates senescence-associated cell death in HT22 hippocampal cells under the oxidative stress conditions. Neurosci. Lett. *701*, 106–111.

237. Russo, R., Berliocchi, L., Adornetto, A., Varano, G.P., Cavaliere, F., Nucci, C., Rotiroti, D., Morrone, L.A., Bagetta, G., and Corasaniti, M.T. (2011). Calpain-mediated cleavage of Beclin-1 and autophagy deregulation following retinal ischemic injury in vivo. Cell Death Dis. *2*, e144. 10.1038/cddis.2011.29.

238. Lee, H.K., Mattei, L.M., Steinberg, B.E., Alberts, P., Lee, Y.H., Chervonsky, A., Mizushima, N., Grinstein, S., and Iwasaki, A. (2010). In vivo requirement for Atg5 in antigen presentation by dendritic cells. Immunity *32*, 227–239. 10.1016/j.immuni.2009.12.006.

239. Oh, D.S., and Lee, H.K. (2019). Autophagy protein ATG5 regulates CD36 expression and anti-tumor MHC class II antigen presentation in dendritic cells. Autophagy *15*, 2091–2106. 10.1080/15548627.2019.1596493.

240. Liu, E., Van Grol, J., and Subauste, C.S. (2015). Atg5 but not Atg7 in dendritic cells enhances IL-2 and IFN-γ production by Toxoplasma gondii-reactive CD4+ T cells. Microbes Infect. *17*, 275–284. 10.1016/j.micinf.2014.12.008.

241. Baerga, R., Zhang, Y., chen, po-H., Goldman, scott, and Jin, shengkan (2009). Targeted deletion of autophagy-related 5 (atg5) impairs adipogenesis in a cellular model and in mice. Autophagy *5*, 1118–1130.

242. Tian, Y., Wang, M.-L., and Zhao, J. (2019). Crosstalk between Autophagy and Type I Interferon Responses in Innate Antiviral Immunity. Viruses *11*, 132. 10.3390/v11020132.

243. Wang, C., Haas, M., Yeo, S.K., Sebti, S., Fernández, Á.F., Zou, Z., Levine, B., and Guan, J.-L. (2021). Enhanced autophagy in Becn1F121A/F121A knockin mice counteracts aging-related neural stem cell exhaustion and dysfunction. Autophagy *0*, 1–14. 10.1080/15548627.2021.1936358.

244. Au, A.K., Bayir, H., Kochanek, P.M., and Clark, R.S.B. (2010). Evaluation of autophagy using mouse models of brain injury. Biochim. Biophys. Acta BBA - Mol. Basis Dis. *1802*, 918–923. 10.1016/j.bbadis.2009.10.010.

245. Zhao, Q., Liu, K., Zhang, L., Li, Z., Wang, L., Cao, J., Xu, Y., Zheng, A., Chen, Q., and Zhao, T. (2022). BNIP3-dependent mitophagy safeguards ESC genomic integrity via preventing oxidative stress-induced DNA damage and protecting homologous recombination. Cell Death Dis. *13*, 1–10. 10.1038/s41419-022-05413-4.

246. Matsui, A., Kamada, Y., and Matsuura, A. (2013). The Role of Autophagy in Genome Stability through Suppression of Abnormal Mitosis under Starvation. PLoS Genet. *9*. 10.1371/journal.pgen.1003245.

247. Holdgaard, S.G., Cianfanelli, V., Pupo, E., Lambrughi, M., Lubas, M., Nielsen, J.C., Eibes, S., Maiani, E., Harder, L.M., Wesch, N., et al. (2019). Selective autophagy maintains centrosome integrity and accurate mitosis by turnover of centriolar satellites. Nat. Commun. *10*, 4176. 10.1038/s41467-019-12094-9.

248. Gomes, L.R., Menck, C.F.M., and Leandro, G.S. (2017). Autophagy Roles in the Modulation of DNA Repair Pathways. Int. J. Mol. Sci. *18*, 2351. 10.3390/ijms18112351.

249. Ambrosio, S., and Majello, B. (2020). Autophagy Roles in Genome Maintenance. Cancers *12*, 1793. 10.3390/cancers12071793.

250. Rocchi, A., Carminati, E., De Fusco, A., Kowalska, J.A., Floss, T., and Benfenati, F. (2021). REST/NRSF deficiency impairs autophagy and leads to cellular senescence in neurons. Aging Cell *20*, e13471. 10.1111/acel.13471.

251. Komatsu, M., Waguri, S., Ueno, T., Iwata, J., Murata, S., Tanida, I., Ezaki, J., Mizushima, N., Ohsumi, Y., Uchiyama, Y., et al. (2005). Impairment of starvation-induced and constitutive autophagy in Atg7-deficient mice. J. Cell Biol. *169*, 425–434. 10.1083/jcb.200412022.

252. Sou, Y., Waguri, S., Iwata, J., Ueno, T., Fujimura, T., Hara, T., Sawada, N., Yamada, A., Mizushima, N., Uchiyama, Y., et al. (2008). The Atg8 conjugation system is indispensable for proper development of autophagic isolation membranes in mice. Mol. Biol. Cell *19*, 4762–4775. 10.1091/mbc.e08-03-0309.

253. Saitoh, T., Fujita, N., Jang, M.H., Uematsu, S., Yang, B.-G., Satoh, T., Omori, H., Noda, T., Yamamoto, N., Komatsu, M., et al. (2008). Loss of the autophagy protein Atg16L1 enhances endotoxin-induced IL-1β production. Nature *456*, 264–268. 10.1038/nature07383.

254. Hara, T., Takamura, A., Kishi, C., Iemura, S., Natsume, T., Guan, J.-L., and Mizushima, N. (2008). FIP200, a ULK-interacting protein, is required for autophagosome formation in mammalian cells. J. Cell Biol. *181*, 497–510. 10.1083/jcb.200712064.

255. Wang, C., Chen, S., Yeo, S., Karsli-Uzunbas, G., White, E., Mizushima, N., Virgin, H.W., and Guan, J.-L. (2016). Elevated p62/SQSTM1 determines the fate of autophagy-deficient neural stem cells by increasing superoxide. J. Cell Biol. *212*, 545–560. 10.1083/jcb.201507023.

256. Liu, H., Wang, C., Yi, F., Yeo, S., Haas, M., Tang, X., and Guan, J.-L. (2021). Non-canonical function of FIP200 is required for neural stem cell maintenance and differentiation by limiting TBK1 activation and p62 aggregate formation. Sci. Rep. *11*, 23907. 10.1038/s41598-021-03404-7.

257. Audesse, A.J., Dhakal, S., Hassell, L.-A., Gardell, Z., Nemtsova, Y., and Webb, A.E. (2019). FOXO3 directly regulates an autophagy network to functionally regulate proteostasis in adult neural stem cells. PLoS Genet. *15*, e1008097. 10.1371/journal.pgen.1008097.

258. Calatayud-Baselga, I., Casares-Crespo, L., Franch-Ibáñez, C., Guijarro-Nuez, J., Sanz, P., and Mira, H. (2023). Autophagy drives the conversion of developmental neural stem cells to the adult quiescent state. Nat. Commun. *14*, 7541. 10.1038/s41467-023-43222-1.

APPENDIX I – Review Paper by Kalinina A. and Lagace D.C. (2022)

Review

Single-cell and Single-nucleus RNAseq Analysis of Adult Neurogenesis

Alena Kalinina and Diane Lagace

Department of Cellular and Molecular Medicine, Neuroscience Program, Ottawa Hospital Research Institute, Brain and Mind Research Institute, University of Ottawa, Ottawa, Canada

*Corresponding author

Diane Lagace

E-mail: dlagace@uottawa.ca

Abstract:

The complexity of adult neurogenesis is becoming increasingly apparent as we learn more about cellular heterogeneity and diversity of the neurogenic lineages and stem cell niches within the adult brain. This complexity has been unraveled in part due to single-cell and single-nucleus RNA sequencing (sc-RNAseq and sn-RNAseq) studies that have focused on adult neurogenesis. This review summarizes 33 published studies in the field of adult neurogenesis that have used sc- or sn-RNAseq methods to answer questions about the three main regions that host adult neural stem cells (NSCs): the subventricular zone (SVZ), the dentate gyrus (DG) of the hippocampus, and the hypothalamus. The review explores the similarities and differences in methodology between these studies and provides an overview of how these studies have advanced the field and expanded possibilities for the future.

Keywords:

Adult neurogenesis, single-cell/single-nucleus RNA sequencing, single-nucleus, subventricular zone, dentate gyrus, hypothalamus

Single-cell and single-nucleus RNA sequencing (sc-RNAseq and sn-RNAseq) studies have provided unparalleled insight into the transcriptional programs of different cellular states during the process of adult neurogenesis by measuring the transcriptomes of thousands of individual cells. This review summarizes 33 studies examining adult neurogenesis that have either created or used sc- or sn-RNAseq datasets from the subventricular zone (SVZ) (Table 1, n=17), dentate gyrus (DG) of the hippocampus (Table 2, n=17) and hypothalamus [1–3]. Given the larger number of studies performed in the SVZ and DG, the review first summarizes the methodological variations between these studies in terms of the species and types of models used; differences in dissection, isolation, purification of the single cells and nuclei protocols; as well as the variety of platforms and analysis pipelines utilized. This is followed by a review of the number and type of cells identified, the transcriptional dynamics within the SVZ, DG, and hypothalamus, as well as insights gained on neurogenesis within the aging and injured brain.

Methodology: Species Demographics

Mice were used in all the reviewed studies, with the exception of four publications in the hippocampus. Cynomolgus macaques were used by Zhang et al. [4] in 2021 and provided the first snRNA analysis of frozen post-mortem hippocampus samples from eight young (4-6 years old) and eight aged (18-21 years old) primate animals. Sn-RNA analysis was first published in human samples in 2017 by Habib et al. [5], followed by 2021 by Tran et al. [6] and Ayhan et al. [7], and most recently in 2022 by Franjic et al. [8]. The work by Habib et al. [5] utilized human samples from four non-diseased donors aged 40-65 that were obtained from the Genotype-Tissue Expression (GTEx) project. This dataset was also reanalyzed by Sorrels et al. in 2021 [9]. The work by Tran et al. used hippocampus from three neurotypical donors with an age range of 40-69 [6], which is in contrast to Ayhan et al. [7], that isolated hippocampus from 5 patients aged 24-60 that were undergoing surgical treatment for epilepsy. In 2022, the first examination of the neurogenic lineage cells in the adult human hippocampus-entorhinal system was performed by Franjic et al. [8]. This study included six clinically unremarkable human donors with a mean age of 52 years old and used sn-RNAseq analysis in the adult rhesus macaques, young adult pigs, and previously published mouse data [10] that reveal species-specific differences.

In addition to the comparison done in young and old cynomolgus macaques [4], within the mouse literature there are four studies that have compared different ages directly (n=3, SVZ, Table 1; n=2, DG Table 2). This work has identified aging-specific difference for example, when analyzing mice across different life stages at 2 weeks, 2,6, and 12 months [11], 3 and 28-29 months [12], in 2, 22-23 month-old animals [13], and in 2 and 14 month-old animals [14]. Aside from these few studies that examined more than one age, the vast majority of studies, in both the SVZ and SGZ have focused on relatively young mice of less than 12 weeks of age, which impacts the ability to make generalizations about the findings obtained.

Between the studies there is also diversity in terms of whether both sexes were used, and how sex-based difference were tested. More specifically, the datasets have included either the use of male

or female samples; combined males and females into a pooled sample; kept the two sexes unpooled; or pooled the sexes and used Multi-seq barcodes to identify the males and females. For the SVZ datasets, 45% were created using male mice, and the remaining studies used either female mice (n=1), both sexes (n=3), both sexes unpooled (n=2), or multiplexed pooled samples (n=1). Of the studies that analyzed unpooled samples, only one reported sexual dimorphism, which showed that male mice have a higher number of oligodendrocyte progenitors within the septal SVZ wall [15]. In contrast, a later study that multiplexed pooled samples with high success did not identify sexual dimorphisms in the neurogenic transcriptome within the SVZ [16]. The hippocampal datasets generated from mice included male mice (n=3), female mice (n=1), both sexes pooled (n=4), or both sexes pooled but separated later for downstream analyses (n=1). The study performing downstream sex-based analyses in the mouse DG examined the sum expression of sex-specific genes like Ddx3y and Xist [10], however, sex-based differences in adult neurogenesis could not be adequately addressed using this method. Similarly, the hippocampal datasets generated from primates included males [5,6], as well as females and males separately [4,7,8], with one study citing direct comparisons [4]. Male and female cynomolgus monkeys showed no sex differences in the cell distributions, but suggested that the male hippocampus maybe more susceptible to aging based on a larger number of differentially expressed genes in male compared to female groups across almost all cell types [4]. Given the successful use of multiplexed pooled female and male samples, it is only a matter of time before other researchers use this technique with high success in the DG. Furthermore it will be important for researchers, reviewers, and editors to continue to ensure the sex of the animals used and method for combining samples and any sex-based analysis is published to increase the rigor and reproducibility of this work.

Methodology: Sample Collection

Approximately an equal number of studies have been published using samples collected from the SVZ (Table 1, n=17) and the DG (Table 2, n=17). The open-source availability of the high-throughput single-cell datasets associated with these papers have paved the way for other researchers to use these datasets to enrich their own analyses. Datasets have often been used in subsequent studies to obtain new result based on testing new hypotheses, or to compare results for consistency and cross-referencing. For example, the most commonly used SVZ dataset comes from the early work by Llorens-Bobadilla et al. [17], which has been subsequently utilized in five studies. Similarly, the seminal work of Hochgerner et al. [10] in the DG, has been subsequently utilized in six studies. In addition, seven studies (n=2 in SVZ; n=5 in DG) did not create new datasets but performed an additional analysis, and/or used already published datasets to refine methodology. Included in this group is the work by Sorrells et. al [9] who reanalyze the neural stem cells (NSCs) identified in the human postmortem DG sample by Habib et al. [5]. Given the continuous development of new analysis pipelines, it seems likely that the use of published datasets will continue to become more prevalent in the future.

The areas of microdissection for either the SVZ or hippocampus have vastly varied between the studies. For the dissection of the SVZ, the vast majority of papers (n=9) dissected the lateral wall

of the ventricle (Table 1). However over time there is a trend for different subregions of the SVZ to be examined. This includes analysis of the septal and lateral SVZ [15], the SVZ and corresponding OB [18], the dorsal and ventral region [19], and, most recently, examination of the anterior-dorsal, posterior-dorsal, anterior-ventral, and posterior-ventral regions [16]. For dissection of the mouse hippocampus, there are three seminal studies that used microdissected DG and two studies used hippocampal anatomical subregions (DG, CA1, CA2, and CA3) [6,19]. Within the paper examining primates, three studies included the hippocampus [4–6], whereas Ayhan et al. [7] used anterior and posterior hippocampus, and Franjic et al. [8] included five microdissected subregions (SGZ, CA2-CA4), CA1, Sub, and EC). This variability in dissected regions in both the SVZ and hippocampus thus allows for a rich number of datasets for future data mining, as well as reveals spatial differences in cell types residing within the SVZ and DG.

A critical component of the protocol for sc- and sn-RNAseq is the isolation of high-fidelity single cells or nuclei and the generation of single-cell suspensions. The use of sc-RNAseq compared to sn-RNAseq in adult brain studies appears to provide better results, capturing more transcripts per cell, as well as resulting in more successful mapping of the transcriptome [16,21,22]. However, some cells require freezing, fixation, staining, or harsher and more extended treatments that may impact their viability or transcriptomic integrity, which supports the use of sn-RNAseq [3]. Likely due to the fairly short procedure for dissociation of live cells from the brain, and later development of sn-RNAseq, studies have utilized sc-RNAseq more extensively than sn-RNAseq in the SVZ and DG. Indeed only two studies have isolated single nuclei in the SVZ, and six studies in the DG, including in this are all five of the datasets generated from primates [4–8]. The work with human samples notably had a large range in postmortem intervals (PMI). The shortest PMI was 12 minutes with the samples being removed from patients with epilepsy undergoing surgery treatment using an *en bloc* resection technique that allowed the hippocampus to be dissected from its vascular pedicle immediately prior to tissue process [7]. This is in contrast to the others that included an average PMI of 12.5 hours [5], 20-38 hours [6]. and 9-12 hours [8]. To control for possible confounding effects of PMI, Franjic et al. [8] also subjected their young adult pig samples to a 30 minutes, 1 hour, and 7 hours of warm ischemic PMI and found no effect of duration. However, questions remain whether this shorter time period in the pig was sufficient to recapitulate the possible effect that occurred in human samples that had a PMI of 9-12 hours [23].

The collection, dissociation and storage methods of cells or nuclei from the brain also varied within the studies (Tables 1 and 2). For example, within the SVZ Zywitza et al. [24] used papain digestion and methanol fixation, Llorens-Bobadilla et al. [17] used trypsin digestion and FACS of cells that were subsequently frozen, and Mizrak et al. [15] processed the cells live. One paper also provided a comparison of datasets using papain versus trypsin for digestion, which revealed that the transcriptional dynamics of NSC regulators were very similar with respect to the expression of key dynamically regulated genes [26]. In contrast to this variability, the work in humans has commonly used either sucrose gradient centrifugation [5,8], or the “Frankenstein” method of nuclei isolation [5–7]. The latter method is highly utilized and includes the use of FACS to identify cell subpopulations based on ploidy to ensure isolation of single nuclei and removal of debris and ambient RNA to help reduce background [25]. Given the diversity of methods utilized, researchers should be aware of biases and benefits of different dissociation and storage methods for cell

preparation that may confound outcomes. Thus, publishing work that addresses this concern in the future, even as part of larger studies, will aid the field greatly.

After the generation of single-cell suspensions, 70% of studies have enriched and purified the samples to isolate the cell types of interest prior to analysis. Purification has been performed most often in both the SVZ and DG using isolation for fluorescence-tagged cells from reporter mice, conditional or inducible transgenic mice, or virus-injected mice. This is in comparison to fewer studies using immunofluorescent staining of live or fixed cell/nuclei suspensions. In the SVZ there are four datasets that used reporter mice, including two that used the GFAP promoter, and one that used both the Ki67 promoter and the CGD promoter. In contrast, in the DG there are four datasets that used reporter mice, with two using the Nestin promoter and two using the GFAP promoter. Conditional (n=3) and inducible (n=6) Cre transgenic mouse models with a variety of promoters have also been used in creating datasets in the SVZ, yet have not been used to create datasets in the DG. One of the strengths of the conditional or inducible mice is that these models label the cell type of interest and all their progeny, thus providing a robust way to track lineage, but make it sometimes more difficult to identify when temporal changes occur within cell populations. This limitation can be overcome through the use of more animals at varying time points, or by combining different mouse models. For example, Magnusson et al. [27] used the Cre-inducible transgenic model and AAV-Cre virus-mediated recombination to label different cell populations and compare the datasets. There are also concerns that treatment with tamoxifen in Cre-inducible mice may have confounding effects. This was in part addressed in a sc-RNAseq study by Lee et al. [28] which showed that prenatal treatments of tamoxifen alters cortical neurogenesis. This paper also found that in 3-4 week old adult mice tamoxifen treatment reduces proliferation as measured by immunohistochemical methods, whereas others have not found such effects in mice at 4-7 weeks [29] or 5 months of age [30] using similar methods. It is possible that these differences are due to strain-, age-, or dosage- dependent effects and thus the use of sc-RNAseq in the future could help address the long-lasting debate about the potential effect of tamoxifen on adult neurogenesis.

Methodology: Plate- versus Droplet-based Methods and Number of Cells Obtained

While both plate-based and droplet-based methods are used in the SVZ and DG, droplet-based methods are chosen predominantly. Specifically in the SVZ and SGZ, there were 60% and 60% of studies that used droplet-based methods, respectively. For the plate-based methods, such as Smart-Seq2, individual cells are directly sorted into a well-plate either using a FACS procedure, with each well containing lysing reagents and barcoded primers bound to a microbead, or a fluorescence-based selection with a microscope. For the more commonly used droplet-based methods, such as the Chromium's 10x Genomics, microfluidics are used to isolate each cell into a droplet containing the same reagents. The microbeads have unique well- or droplet-specific barcodes as well as unique molecular identifiers for each transcript. This procedure allows for precise tagging and identification of individual templates for each cell. The microbeads are isolated and pulled RNA is reverse-transcribed and amplified by PCR, followed by addition of adapters for library preparation and sequencing. Both droplet- and plate-based sc-RNAseq protocols require sequencing of obtained libraries, such as NextSeq or HiSeq platforms by Illumina.

The more common use of droplet-based methods within the field of adult neurogenesis is not surprising since it is well known to allow for a higher throughput study of single-cell transcriptomes and more resolution of the rare populations within heterogeneous niches, which is the case in the study of adult neurogenesis. Indeed as summarized in Table 1 and 2, droplet-based methods allowed to capture transcripts of several thousands to tens of thousands of cells [e.g., 5,7,19], whereas plate-based methods rarely reached a quantity above a few thousand cells [e.g., 9,20,21]. In addition, multiplexing of samples which has been noted to be successful to identify male and female mice in SVZ samples [16], also provides the benefits of more comparisons to be made while reducing the cost and number of animals required.

Methodology: Analysis Pipelines

Once the data matrices are obtained, machine learning algorithms are used to analyze the information in a high-dimensional space. A large variety of pipelines has been used to manipulate sc-RNAseq data for clustering by cell type and to analyze differential gene expression, pathway dynamics, lineage tracing, pseudotemporal resolution, and RNA splicing. In general, the most common platforms for cell clustering and differential gene expression are R-based, such as Seurat developed by Satija lab [31] and Monocle developed by Trapnell lab [32]. In addition to these popular methods, python- and Matlab-based analyses have also been used. Specifically, in the SVZ, 2/3rd (n=10) used Seurat and 1/3rd (n=5) used Monocle. In the DG, ten used Seurat and three used Monocle, while others relied on a few other methods ranging from Waterfall to Matlab-based analyses. There are many studies that have combined a few pipelines to maximize the information that can be obtained from the dataset, which also allows to verify results across platforms and enhance interpretation (Tables 1 and 2). For instance, python-based scVelo [33] or Velocyto [34] are often used to analyze induction and repression of genes via RNA velocity estimation together with Seurat or Monocle's Pseudotime for complete developmental trajectory inference. In fact, a whole array of tools is being developed to study cell fate and regulation of gene expression based on leveraging the information about spliced and unspliced RNA counts alone [35,36].

Variability in Methodology in Examination of SVZ and DG

Summarizing these methodological variations highlighted that the studies in both the SVZ and DG vastly differ in types of mice utilized, methodologies for dissection, isolation, purification of the single cells or nuclei, and can be used in either plate-based or droplet-based methods and analyzed via a wide array of pipelines. Although these differences in the utilized methodologies may seem somewhat overwhelming, they enhance the robustness of datasets to answer new questions in the field of adult neurogenesis. It is also striking that despite this variability, there are many similarities in outcomes and take-home messages from this large body of work. Included in these similarities are the various cell types that are commonly identified in the dissected areas, pseudotemporal resolution of developmental trajectories of adult-born cells, and the differences between reciprocal cell types. Furthermore, these studies provide some common findings and challenges left to solve in regards to the dynamic process of adult neurogenesis in the SVZ and DG.

Identification of Cell Types within the SVZ

One significant development resulting from sc- and sn-RNAseq analyses in adult neurogenesis studies was the generation of cell atlases. Zywitza et al. [24] was the first to study unsorted live and fixed cells from whole SVZ and resolved 17 clusters of cells including: endothelial cells, pericytes, smooth muscle cells, microglia, perivascular macrophages, ependymal cells, medium spiny neurons (two types), oligodendrocyte (four types), astrocytes, neuroblasts (early and late), transient amplifying neural progenitors (NPCs, mitotic and not), and NSCs. Using FAC-sorted cells, Dulken et al. [4] also found similar cell types in their study, except for some differences in resolution of oligodendrocytes, the absence of ependymal cells, and no distinction between astrocytes and quiescent NSCs (qNSCs). The absence of ependymal cells may be due to their similarity to NSCs, which were subsequently found to be distinct using sc-RNAseq analysis of the a SMACre^{ERT2} ependymal inducible mouse model [37]. Chen et al. [38] used homogenized frozen tissue chunks and identified 19 instead of 17 clusters with similar resolution to Zywitza et al. [24]. Specifically, they found all the same cell types except for macrophages, and got a larger number of clusters due to higher resolution of neuronal subtypes. This included identifying early versus late activated NSCs (aNSCs), as well as better resolution between qNSCs and astrocytes. Thus, overall there has been a large consensus, with up to 19 distinct subtypes of cells residing in the adult SVZ.

Mizrak et al. [15,18] performed a deeper analysis of SVZ heterogeneity by examining the ventral and septal walls of the SVZ as sources of variation between different cell types and their frequencies. One of the most striking findings of this analysis is that the lineage residing in the ventral wall is more biased towards giving rise to cells of neuronal fate, and that the septal wall has a gliogenic bias. In addition, heterogeneity of ventral and septal astrocytes correlated with NPCs and oligodendrocyte progenitor cells (OPCs), respectively. They have identified several clusters of astrocytes, some of which were positive for qNSC markers like Id2 and Hopx, as well as transition cells positive for aNSC markers Ascl1 and Egfr, although the classification of qNSCs was not separate from astrocytes. This led to the seminal finding that regional differences between septal and ventral NSCs and astrocytes contribute to the phenotypical heterogeneity of the SVZ.

Identification of Cell Types within the Dentate

The most extensive characterization of the cell types residing within the dentate at different developmental stages has been performed using hGFAP^{GFP} reporter mice by Hochgerner et al. [10]. This dataset encompasses perinatal, juvenile, and adult animals and analyzed 24,000 cells resulting in the identification of 23 cell clusters in the adult mice. This included a large number of different neuronal cell types including: two types of granule neurons (mature and immature), two types of neuroblasts, NPCs, Cajal-Retizus cells, three types of excitatory mossy cells, and three types of inhibitory neurons. There was also a large number of different types of glial cells,

including astrocytes, oligodendrocytes (mature, precursors, newly formed), microglia, and radial glia-like NSCs. Mature astrocytes separated from RG-like NSCs (also known as qNSCs), but the cycling RG NSCs (also known as aNSCs) had to be separated from NPCs manually. Lastly, the dataset identified a number of vascular-associated cells including endothelial cells, microglia, perivascular macrophages, as well as vascular leptomeningeal cells.

When comparing the hippocampus to SVZ, it is likely more difficult to isolate the relatively small populations of proliferating NSCs and NPCs given the overwhelming number of mature neurons. Artegiani et al. [39], therefore, took the approach to purify all non-neuronal cell types in the DG by negative sorting (GluR1-/CD24-), arguably, to reduce the selection bias of the experiment. This resulted in the identification of 11 clusters of non-neuronal cells, including microglia, pericytes, interneurons, oligodendrocyte precursor cells, myelin-forming oligodendrocyte cells, endothelial cells, NPCs and NSCs. This study also showed that NSCs and NPCs exist on a continuum of states in mice, which can be seen using Pseudotime and examining expression of quiescence, cell cycle, and neuronal specification genes.

In the human hippocampus, use of sn-RNAseq to identify adult-generated NSCs and NPCs has suggested that that very few, if any, exist in the adult. Habib et al. [5] first observed a cluster of 201 cells that were identified as NSCs in the human hippocampus based on putative NSC marker genes. Ayhan et al. [7] later demonstrated that the human hippocampus did not have glial cells with a stem cells identity, which was inconsistent with Habib et al. [5]. Similarly, Tran et al. [6] only observed clusters of astrocytes in the DG. Sorrells et al. [9] performed a reanalysis of Habib et al. [5] dataset combined with an enrichment analysis of ependymal markers and identified that the labelled NSCs in Habib et al. [5] were ependymal cells. In addition, they analyzed DCX expression in the same dataset and found scattered DCX expression in various cell types, with only 1.1% of the hippocampal cells expressing extremely low levels. These data led the authors to conclude that if any neurogenesis continues in the adult human DG, it is a rare phenomenon. In 2022, Franjic et al. [8] used Seurat and Monocle integration of all DG cells, but also performed a reintegrated analysis with only the granule cell lineage across the mouse, pig, macaque, and human. This reintegration analysis allowed for the identification of five clusters of cells including astrocytes/RG-like qNSCs, activated RGL cells (aNSCs), neural intermediate progenitor cells (NPCs), neuroblasts and granule cells. RNA velocity further provided progenitor and neuroblast trajectories for adult neurogenesis in the mouse, pig and macaque, in the absence of any clear trajectory in humans. In the human, a total of 20 cells were found to have an identity resembling NPCs, and only two astrocyte/RG-like cells showed high velocity toward a neuron fate. As such, this data supports findings of previous research [6,7,9] and contributes to the different methodological approaches fueling the debate on the existence of human neurogenesis [23].

Distinguishing Astrocytes and Neural Stem Cells (NSCs) in the SVZ and DG

The use of sc- and sn-RNAseq has allowed researchers to transcriptionally distinguish populations of cells involved in adult neurogenesis. This has been especially important in the separation of astrocytes and NSCs within the SVZ and DG. In 2018, Zywitza et al. [24] were the first to

distinguish between astrocytes and qNSCs in the SVZ based on the lack of Aqp4 expression in qNSCs. Moreover, qNSCs and aNSCs were resolved on the basis of Ascl1. More transcriptional differences between the astrocytes and NSC populations in the SVZ were subsequently identified by Borrett et al. [19,40] in their analysis of whole live cells from Emx1::Cre;R26^{EYFP} mice and Nkx2.1::Cre-R26^{EYFP} mice. They proposed a considerable list of genes that can be examined together in order to distinguish between these populations, such as the use of Nestin, Dbi, Thbs4, Meg3, Vim for identification of qNSCs, and Aqp4, Agt, S100b, Hbegf, Htra1 for astrocytes. Similar genes were also identified in Redmond et al. [16] to be differentially expressed between astrocyte and qNSC clusters from the analysis of sorted whole cells and single nuclei from hGFAP^{GFP} mice. These studies are in contrast to the work of others in the SVZ, that did not find separate clusters for the astrocytes and NSCs [12,15,18,25,41]; or alternatively, developed rescue strategies to separate astrocytes and qNSCs on the basis of a Thbs4 and CD9 likelihood ratio [24].

Separating astrocytes from NSCs in the DG was shown in some, but not all studies. Hochgerner et al. [10] was the first to separate qNSCs and astrocytes in cells isolated from the DG of the hGFAP^{GFP} reporter mice based on their transcriptional differences. Additionally, Batiuk et al. [42] sorted Atp1b2+ cells from the adult C57BL/6J mouse hippocampus to study regional astrocyte heterogeneity, which allowed for the separation between the astrocytes and aNSCs. Alternatively, some transgenic models using CGD, Sox2 or Nestin promoters allow for the isolation of qNSCs in the absence of astrocytes as demonstrated in sc-RNAseq SVZ studies [11,37]. These studies highlight how the commonly used approach of presorting cells using either transgenic mice or immunofluorescent markers can aid in separating similar population of cells.

The four primate datasets from the DG [4,8] were unable to separate astrocytes from qNSC, as has been achieved in DG mouse dataset [10], which may in part be due to not presorting the cells. One dataset using the monkey failed to detect clusters with an astrocyte signature [4], whereas the first dataset generated from human hippocampus identified two clusters of astrocytes and one cluster of NSCs, which were later identified as ependymal and not NSCs upon reanalysis by other researchers [9]. The integrated mouse, pig, monkey and human datasets were able to resolve aNSCs and astrocytes [8], but did not provide resolution to differentiate astrocytes from the qNSCs. The astrocyte clusters in this dataset also had high heterogeneity in transcriptional signatures and RNA velocity, thus additional analysis pipelines, or additional studies enriching for subpopulations are ripe for use in future exploration in primate samples.

Distinguishing Neural Stem and Progenitor Cells (NSCs and NPCs) in the SVZ and DG

Distinguishing qNSCs, aNSCs, and NPCs has been less of a challenge for samples obtained from the SVZ. when compared the hippocampus. In the adult mouse SVZ, NPCs and neuroblasts have strong transcriptional signatures that make them easy to separate from NSCs, as demonstrated in many of the reviewed publications [e.g., 11,12,38]. Priming of NSCs from a quiescent state has been extensively described in Borrett et al. [19] who showed decreased expression of Mt1, Glul, Cst3 and increased expression of Hmgb3, H2afz and other proliferation-related genes in primed NSCs during this process. Upon activation, aNSCs acquire expression of Ascl1 and Egfr as they

move toward NPC or neuroblast fate where they start to show high expression of pro-neural Sox11 and Dlx genes [41]. In addition, signatures of stemness, such as glycolysis pathway activity and lipid metabolism decrease while providing room for increased ribogenesis and neuronal differentiation, both peaking at the NPC stage [24]. These signatures can be used together with pseudotemporal ordering of cell neurogenesis to truly distinguish NSCs from NPCs.

It has been more difficult to distinguish NSCs and NPCs in the adult mouse DG. Shin et al. [43] were the first to perform sc-RNAseq and provide a comprehensive examination of NSC transitional states using a Nestin^{CFP} reporter mouse. The Waterfall analysis method they developed showed a distinction between qNSCs, aNSCs and NPCs based on the expression of Aldoc, Hopx, and Stmn1 with the former two declining as the NSCs become primed and activated. Artegiani et al. [39] did not corroborate this finding using naïve and Nestin^{GFP} mice, as they did not find many NSCs that were activated and expressing proliferation markers. They, however, identified two stages of NPCs using Waterfall, early and late, which differed in their expression of neural fate choice markers. In comparison, Habib et al. [20] used a procedure called Div-Seq to study proliferating cells in the adult DG in a more isolated and controlled fashion. They combined sn-RNAseq with an EdU pulse and sorted the EdU+ cells at different chase times. Although they did not show the clustering of EdU-labeled cells by identity and, therefore, never confirmed the separation between aNSCs and NPCs, the expression pattern of Sox9 and Notch1 in their dataset is clearly distributed along the cell cycle / differentiation continuum. This suggests that the technique has the potential to separate aNSCs from NPCs by varying the EdU injection pulses and chases, and in the future this can be achieved by coupling the procedure to FACS analysis of cell cycle via DNA content. Some of this disagreement among the studies may be due to differences in defining primed NSCs versus aNSCs versus NPCs based on gene expression. The difficulty in reaching consensus reflects the dispersed and heterogeneous nature of hippocampal NSCs and NPCs that is difficult to assess even with such high-resolution analysis as sc-RNAseq. Therefore, combining sc-RNAseq with transgenic models, as well as other cell labeling methods (e.g., EdU, immunolabeling), may aid in the resolution of qNSCs, aNSCs, and NPCs.

Identification of the hypothalamic tanycytes

Literature examining neurogenesis in the hypothalamic area is growing, and includes two sc-RNAseq [1,2] studies, and one sn-RNAseq [3] study, that have all identified the hypothalamic NSCs called tanycytes. Chen et al. [1] described hypothalamic diversity in adult mice detailing 34 glutamatergic and GABAergic neuronal and 11 non-neuronal sub-types. The study had a high level of transcriptional resolution and identified two types of hypothalamic stem cells: Rax+ tanycytes that were also positive for vimentin and nestin, and Ccdc153+ ependymocytes. This study also provides a few genes that can be used to identify tanycytes, such as Col23a1, Slc16a2, Lhx2, and Ptn, as well as specific markers to be able to distinguish subtypes of tanycytes based on their dorsoventral position. This data was nicely complemented by Kim et al. [2], who used pseudotime and RNA velocity algorithms to describe the developmental trajectory of tanycytes, from early embryo to adult. Using SCENIC to examine the spatial regulators of patterning of hypothalamic subregions, they identified that the expansion and patterning of tanycytes and progenitors in the

ventral hypothalamus was governed by Nkx2, and thus may be of interest for examination in adult hypothamic neurogenesis. Hajdarovic et al. [3] further described regulation of the tanycytes during aging using differential gene expression, SCENIC and pseudotime analysis in single nuclei to determine that tanycytes are regulated by FoxO factors. They also show that gene expression is more stable with age in tanycytes compared to astrocytes, neurons, or oligodendrocytes, yet also is sexually dimorphic. Unlike the studies in the SVZ and dentate, these studies were able to separate the astrocytes from NSCs, however, in the hypothalamus there is overlap in gene expression between endocytes, ependymal cells, and tanycytes. Albeit few in number, overall these comprehensive studies have helped classify the stem cells in the hypothalamus and provide novel leads to determine their functional dynamics and how they generate mature hypothalamic cells.

The transcriptional dynamics of upregulation of the neurogenic program in the SVZ

The sc- and sn-RNAseq studies in the SVZ have provided a consensus for the pseudotemporal ordering of genes involved in the qNSC and aNSC transition, despite of the different cell isolation, various RNAseq protocols, and varying cell cluster resolution. The studies have highlighted important steps in the NSC activation, which include upregulation of translation and ribogenesis, and downregulation of astrocytic/stemness genes upon transition from qNSCs to early aNSCs state, followed by cell cycle and proliferation-related gene upregulation during transition from early to mid-late aNSC stage [24,26]. Lastly, upon transition to later aNSC stages, neuronal differentiation genes become upregulated and astrocyte/NSC identity genes are suppressed. The genetic program of NSC activation and differentiation is governed by Clu, Ccnd2, Dlx2, Dcx, and other genes, including the earlier described Ascl1: all defining distinct molecular signatures of qNSC-like, aNSC-early, aNSC-mid, aNSC-late, and NPC-like populations [26]. This advancement was made due to analysis pipelines like Monocle and its Pseudotime function, which were paramount for lineage inference and pseudotemporal ordering of cell processes across the neurogenic continuum [e.g. 8,9,23]. These were also crucial for the discovery of novel regulators of SVZ neurogenesis, such as Troy, which is important in NSC activation and proliferation [41], Lrig1 [44], and Notum, which controls NSC activity and division together with niche occupancy sensing [18].

Unlike the consensus pseudotemporal ordering of genes during the qNSC/aNSC transition, there has been disagreement about which population of cells first upregulates the transcriptional neurogenic program. For instance, early work by Llorens-Bobadilla et al. [17] performed a series of experiments that captured the transcriptomes of $Glast^{+}Prom1^{+}$ NSCs and $Glast^{-}Prom1^{-}Egfr^{+}$ NPCs. This analysis unearthed a primed qNSC population, while also discovering evidence of a differentiation program at the aNSC stage. In contrast, Dulken et al. [26] found that late aNSCs lacked expression of neuronal specification markers like Dcx, Nrxn3, Sp8, etc., which allowed for their separation from NPCs. This study also compared *in vitro* neurospheres with *in vivo* FACS-ed aNSCs and suggested the neurospheres separated from their *in vivo* counterparts due to increased signatures of inflammation and a lack of expression of differentiation markers in

neurospheres relative to aNSCS/NPCs. These findings align with previous literature that identified inherent differences between *in vivo* and *in vitro* stem and progenitor cell behavior [45]. Additionally, this work supports the proposition that *in vivo* aNSCs, may possess some level of expression of differentiation markers, even if it is less prominent compared to *in vivo* NPCs.

The transcriptional dynamics defining hippocampal neurogenesis

Shin et al. [43] provided the first sc-RNAseq analysis of adult DG using the Nestin^{CFPnuc} reporter mice to describe the transcriptional mechanisms of adult NSC activation and neurogenesis using their analysis pipeline Waterfall, which incorporated pseudotime and gene expression analyses. This study was paramount in that it did not support the notion of qNSCs as a passive and dormant cell niche: instead adult qNSCs continuously integrate various signals from their microenvironment using functional receptors and signaling pathway activity. Upon activation of NSCs, a metabolic shift occurs in qNSCs from lipid and glutathione metabolism (e.g., Spot14, Ascl3 and 6, Acsbg1) as well as glycolysis (aldolase A and C, Ldhb), to oxidative phosphorylation and upregulated expression of mitochondrial genes in NSCs undergoing cell cycle entry. Other hallmarks of NSC activation and proliferation involved transcripts related to, or directly regulating cell cycle, DNA replication, and spindle formation. During the transition between G0 to G1, a marked activation of protein synthesis was observed that also preceded each cell cycle stage transition. These findings have been replicated by others, although all these studies differ in their cluster labels. For example, Hochgerner et al. [10] had similar findings, although they report the qNSCs, aNSCs, and NPCs as individual clusters. Artegiani et al. [39] also report similar pathways of activation in the clusters of qNSCs, and early and late NPCs.

Various additional methods were used by others on datasets from the DG, which allowed for a more in-depth evaluation of the transcriptional temporal dynamics occurring in hippocampal neurogenesis. Bergen et al. [33] used the dataset in Hochgerner et al. [10] to demonstrate that developmental trajectories can be inferred using RNA velocity information, which results in determining the fate of the cell seconds to hours ahead. In addition, Zhang and Zhang [36] developed CellPath, a tool that uses RNA velocity data to construct smaller accurate trajectories, or paths, which was shown to be better than the commonly used Pseudotime and Slingshot. This analysis showed that astrocytes arise from qNSCs, as well as resolved novel regulators of neurogenesis: Camk2a and Rasl10a. They have also found a trajectory resembling de-differentiation of adult granule cells, which may involve expression of Tmsb10. Among other tools that have been recently optimized for trajectory inference in the hippocampus is the VeTra tool that has shown promising resolution of lineages compared to Slingshot and other methods [35]. Overall, the abundance of current methods has defined important aspects of dynamic signal integration by qNSCs, as well reveal the different trajectories of the subpopulations of NSCs and NPCs.

Effects of Aging and Injury on Adult Neurogenesis

The vast majority of the reviewed studies examine neurogenesis in a naïve state and the use of sc- and sn-RNAseq has only begun to be used to define the transcriptional changes and mechanisms that induce or sustain the reduction or increase in adult neurogenesis in physiological and pathological conditions. For example, four studies have used sc-RNAseq to address how aging reduces production of new cells in the SVZ [11–13,46], two studies have been completed in the hippocampus [14,39], and one in the hypothalamus [3]. Shi et al [46] using sc-RNAseq analysis demonstrated that aging overall reduced cell proliferation, altered cell cycle regulation, and an induced inflammatory SVZ microenvironment. This is consistent with the findings in the dentate that aged adult mice had a smaller ratio of NSCs to dividing NPCs [39]. Quiescent NSCs from the aging SVZ were further shown by Kalamakis et al. [13] to be more resistant to becoming aNSCs, with an accompanying increase in the qNSC population to preserve the small pool of NSCs. The proposed mechanism for the reduction in transition from qNSC to aNCSs was hypothesized by Dulken et al. [12] due to the infiltration by immune cells and increased gamma-interferon signaling in the aging SVZ. Most recently, Xie et al. [11] additionally explored the role of aging utilizing a CGD^{GFP} reporter mouse and found seven distinguishable subgroups of NSCs and NPCs. Using this higher level of specificity to separate their cell populations, they confirm that aging is associated with the failure of qNSC to transition to progenitors. They additionally show the transcriptional down-regulation of cell cycle, protein and macromolecular catabolism pathways, as well as master regulator genes, such as Myc, Sp1, Srebf2, E2f1. Taken together these studies, have opened up new avenues for future data mining to identify more mechanisms by which the balance between quiescence and activation of NSCs is perturbed in aging.

The use of sc-RNAseq in the SVZ has also addressed pertinent questions relating to the increase in NSCs and NPCs within the SVZ niche to various types of injury. The first sc-RNAseq study of adult SVZ cells which described the local neurogenic niche and its transcriptional response to ischemic injury in adult mice [17] showed that ischemic injury triggers the entry of qNSCs into a state primed for activation via gamma-interferon signaling. Similarly, mild traumatic brain injury is associated with the entry of resident astrocytes into a neurogenic program and the subsequent expansion of the qNSC and aNSC pools [38]. Importantly, in this study there was direct evidence of differentiation of aNSCs into neuroblasts, supporting the notion that aNSCs possess differentiation signals to commit to neurogenesis.

The Future

Single-cell and -nucleus RNA sequencing has significantly advanced our understanding of the molecular features and dynamics of stem cells housed in the adult murine SVZ, DG, and hypothalamus. There is no doubt that continuous use of this technology will make it more widely available to unravel novel regulators and pathways that allow for the generation of neurons from NSCs in the adult brain. Given the rapidly evolving abundance of new pipelines and analyses being continuously generated, the future is also bright to resolve specific trajectories of development and

transcriptional networks of different cellular subtypes and allow for optimal resolution of cells with similar transcriptional signatures. For instance, with increased availability of sc-RNAseq data, neural networks can be used for cell type assignment [47] and for uncovering complex gene networks [48] which will enhance our interpretation of these datasets. Furthermore it is exciting to imagine how combining sc-RNAseq with chromatin analysis in scATACseq [49], glycan analysis in scGRseq [50], or spatial sc-RNAseq technologies [51] will provide more high-throughput information from individual cells and more depth to our understanding of how neurons are generated in the adult brain.

Acknowledgements

We would like to thank Dr. Pierre Mattar, Dr. Jing Wang, Dr. Ruth Slack, David Cook, Bensun Fong, and Mohamed Ariff Iqbal, members of the StemCore Laboratories (Ottawa Hospital Research Institute) for fruitful discussions, the reviewers for feedback, as well as all members of the Lagace lab, especially Yingben Xue for continued valued feedback.

Author Contributions

Conceptualization, AK and DL.; data curation AK; writing—original draft preparation AK; writing—review and editing, AK and DL. Both authors have read and agreed to the published version of the manuscript.

Funding

This research was funded by NSERC Discovery Grant and CIHR Project Grant to DCL.

Institutional Review Board Statement

Not applicable.

Informed Consent Statement

Not applicable.

Data Availability Statement

Not applicable.

Conflicts of Interest

The authors declare no conflict of interest.

References

1. Chen, R.; Wu, X.; Jiang, L.; Zhang, Y. Single-Cell RNA-Seq Reveals Hypothalamic Cell Diversity. *Cell Reports* **2017**, *18*, 3227–3241, doi:10.1016/j.celrep.2017.03.004.

2. Kim, D.W.; Washington, P.W.; Wang, Z.Q.; Lin, S.H.; Sun, C.; Ismail, B.T.; Wang, H.; Jiang, L.; Blackshaw, S. The Cellular and Molecular Landscape of Hypothalamic Patterning and Differentiation from Embryonic to Late Postnatal Development. *Nat Commun* **2020**, *11*, 4360, doi:10.1038/s41467-020-18231-z.

3. Hajdarovic, K.H.; Yu, D.; Hassell, L.-A.; Evans, S.; Neretti, N.; Webb, A.E. Single Cell Analysis of the Aging Hypothalamus. *bioRxiv* **2021**, 2021.03.07.434282, doi:10.1101/2021.03.07.434282.

4. Zhang, H.; Li, J.; Ren, J.; Sun, S.; Ma, S.; Zhang, W.; Yu, Y.; Cai, Y.; Yan, K.; Li, W.; et al. Single-Nucleus Transcriptomic Landscape of Primate Hippocampal Aging. *Protein Cell* **2021**, doi:10.1007/s13238-021-00852-9.

5. Habib, N.; Avraham-Davidi, I.; Basu, A.; Burks, T.; Shekhar, K.; Hofree, M.; Choudhury, S.R.; Aguet, F.; Gelfand, E.; Ardlie, K.; et al. Massively Parallel Single-Nucleus RNA-Seq with DroNc-Seq. *Nat Methods* **2017**, *14*, 955–958, doi:10.1038/nmeth.4407.

6. Tran, M.N.; Maynard, K.R.; Spangler, A.; Huuki, L.A.; Montgomery, K.D.; Sadashivaiah, V.; Tippani, M.; Barry, B.K.; Hancock, D.B.; Hicks, S.C.; et al. Single-Nucleus Transcriptome Analysis Reveals Cell-Type-Specific Molecular Signatures across Reward Circuitry in the Human Brain. *Neuron* **2021**, *109*, 3088-3103.e5, doi:10.1016/j.neuron.2021.09.001.

7. Ayhan, F.; Kulkarni, A.; Berto, S.; Sivaprakasam, K.; Douglas, C.; Lega, B.C.; Konopka, G. Resolving Cellular and Molecular Diversity along the Hippocampal Anterior-to-Posterior Axis in Humans. *Neuron* **2021**, *109*, 2091-2105.e6, doi:10.1016/j.neuron.2021.05.003.

8. Franjic, D.; Skarica, M.; Ma, S.; Arellano, J.I.; Tebbenkamp, A.T.N.; Choi, J.; Xu, C.; Li, Q.; Morozov, Y.M.; Andrijevic, D.; et al. Transcriptomic Taxonomy and Neurogenic Trajectories of Adult Human, Macaque, and Pig Hippocampal and Entorhinal Cells. *Neuron* **2022**, *110*, 452-469.e14, doi:10.1016/j.neuron.2021.10.036.

9. Sorrells, S.F.; Paredes, M.F.; Zhang, Z.; Kang, G.; Pastor-Alonso, O.; Biagiotti, S.; Page, C.E.; Sandoval, K.; Knox, A.; Connolly, A.; et al. Positive Controls in Adults and Children Support That Very Few, If Any, New Neurons Are Born in the Adult Human Hippocampus. *J. Neurosci.* **2021**, *41*, 2554–2565, doi:10.1523/JNEUROSCI.0676-20.2020.

10. Hochgerner, H.; Zeisel, A.; Lönnerberg, P.; Linnarsson, S. Conserved Properties of Dentate Gyrus Neurogenesis across Postnatal Development Revealed by Single-Cell RNA Sequencing. *Nature Neuroscience* **2018**, *21*, 290–299, doi:10.1038/s41593-017-0056-2.

11. Xie, X.P.; Laks, D.R.; Sun, D.; Poran, A.; Laughney, A.M.; Wang, Z.; Sam, J.; Belenguer, G.; Fariñas, I.; Elemento, O.; et al. High-Resolution Mouse Subventricular Zone Stem-Cell Niche Transcriptome Reveals Features of Lineage, Anatomy, and Aging. *Proc Natl Acad Sci USA* **2020**, *117*, 31448–31458, doi:10.1073/pnas.2014389117.

12. Dulken, B.W.; Buckley, M.T.; Navarro Negredo, P.; Saligrama, N.; Cayrol, R.; Leeman, D.S.; George, B.M.; Boutet, S.C.; Hebestreit, K.; Pluvinage, J.V.; et al. Single-Cell Analysis Reveals T Cell Infiltration in Old Neurogenic Niches. *Nature* **2019**, *571*, 205–210, doi:10.1038/s41586-019-1362-5.

13. Kalamakis, G.; Brüne, D.; Ravichandran, S.; Bolz, J.; Fan, W.; Ziebell, F.; Stiehl, T.; Catalá-Martinez, F.; Kupke, J.; Zhao, S.; et al. Quiescence Modulates Stem Cell Maintenance and Regenerative Capacity in the Aging Brain. *Cell* **2019**, *176*, 1407-1419.e14, doi:10.1016/j.cell.2019.01.040.

14. Schneider, J.; Weigel, J.; Wittmann, M.-T.; Svehla, P.; Ehrt, S.; Zheng, F.; Elmzzahi, T.; Karpf, J.; Paniagua-Herranz, L.; Basak, O.; et al. Astrogenesis in the Murine Dentate Gyrus Is a Life-Long and Dynamic Process. *EMBO J* **2022**, e110409, doi:10.15252/embj.2021110409.

15. Mizrak, D.; Levitin, H.M.; Delgado, A.C.; Crotet, V.; Yuan, J.; Chaker, Z.; Silva-Vargas, V.; Sims, P.A.; Doetsch, F. Single-Cell Analysis of Regional Differences in Adult V-SVZ Neural Stem Cell Lineages. *Cell Reports* **2019**, *26*, 394-406.e5, doi:10.1016/j.celrep.2018.12.044.

16. Cebrian-Silla, A.; Nascimento, M.A.; Redmond, S.A.; Mansky, B.; Wu, D.; Obernier, K.; Romero Rodriguez, R.; Gonzalez-Granero, S.; García-Verdugo, J.M.; Lim, D.A.; et al. Single-Cell Analysis of the Ventricular-Subventricular Zone Reveals Signatures of Dorsal and Ventral Adult Neurogenesis. *eLife* **2021**, *10*, e67436, doi:10.7554/eLife.67436.

17. Llorens-Bobadilla, E.; Zhao, S.; Baser, A.; Saiz-Castro, G.; Zwadlo, K.; Martin-Villalba, A. Single-Cell Transcriptomics Reveals a Population of Dormant Neural Stem Cells That Become Activated upon Brain Injury. *Cell Stem Cell* **2015**, *17*, 329–340, doi:10.1016/j.stem.2015.07.002.

18. Mizrak, D.; Bayin, N.S.; Yuan, J.; Liu, Z.; Suciu, R.; Niphakis, M.J.; Ngo, N.; Lum, K.M.; Cravatt, B.F.; Joyner, A.L.; et al. Single-Cell Profiling and SCOPE-Seq Reveal the Lineage Dynamics of Adult Neurogenesis and NOTUM as a Key V-SVZ Regulator. *bioRxiv* **2019**, 770610, doi:10.1101/770610.

19. Borrett, M.J.; Innes, B.T.; Jeong, D.; Tahmasian, N.; Storer, M.A.; Bader, G.D.; Kaplan, D.R.; Miller, F.D. Single-Cell Profiling Shows Murine Forebrain Neural Stem Cells Reacquire a Developmental State When Activated for Adult Neurogenesis. *Cell Reports* **2020**, *32*, 108022, doi:10.1016/j.celrep.2020.108022.

20. Habib, N.; Li, Y.; Heidenreich, M.; Swiech, L.; Avraham-Davidi, I.; Trombetta, J.J.; Hession, C.; Zhang, F.; Regev, A. Div-Seq: Single Nucleus RNA-Seq Reveals Dynamics of Rare Adult Newborn Neurons. *Science* **2016**, *353*, 925–928, doi:10.1126/science.aad7038.

21. Bakken, T.E.; Hodge, R.D.; Miller, J.A.; Yao, Z.; Nguyen, T.N.; Aevermann, B.; Barkan, E.; Bertagnolli, D.; Casper, T.; Dee, N.; et al. Single-Nucleus and Single-Cell Transcriptomes Compared in Matched Cortical Cell Types. *PLOS ONE* **2018**, *13*, e0209648, doi:10.1371/journal.pone.0209648.

22. Ding, J.; Adiconis, X.; Simmons, S.K.; Kowalczyk, M.S.; Hession, C.C.; Marjanovic, N.D.; Hughes, T.K.; Wadsworth, M.H.; Burks, T.; Nguyen, L.T.; et al. Systematic Comparison of Single-Cell and Single-Nucleus RNA-Sequencing Methods. *Nat Biotechnol* **2020**, *38*, 737–746, doi:10.1038/s41587-020-0465-8.

23. Nano, P.R.; Bhaduri, A. Mounting Evidence Suggests Human Adult Neurogenesis Is Unlikely. *Neuron* **2022**, *110*, 353–355, doi:10.1016/j.neuron.2022.01.004.

24. Zywitza, V.; Misios, A.; Bunatyan, L.; Willnow, T.E.; Rajewsky, N. Single-Cell Transcriptomics Characterizes Cell Types in the Subventricular Zone and Uncovers Molecular Defects Impairing Adult Neurogenesis. *Cell Reports* **2018**, *25*, 2457-2469.e8, doi:10.1016/j.celrep.2018.11.003.

25. Dulken, B.W.; Leeman, D.S.; Boutet, S.C.; Hebestreit, K.; Brunet, A. Single-Cell Transcriptomic Analysis Defines Heterogeneity and Transcriptional Dynamics in the Adult Neural Stem Cell Lineage. *Cell Reports* **2017**, *18*, 777–790, doi:10.1016/j.celrep.2016.12.060.

26. Martelotto, L. 'Frankenstein' Protocol for Nuclei Isolation from Fresh and Frozen Tissue for Sn-RNAseq Available online: https://www.protocols.io/view/frankenstein-protocol-for-nuclei-isolation-from-f-3eqgjdw.

27. Magnusson, J.P.; Zamboni, M.; Santopolo, G.; Mold, J.E.; Barrientos-Somarribas, M.; Talavera-Lopez, C.; Andersson, B.; Frisén, J. Activation of a Neural Stem Cell Transcriptional Program in Parenchymal Astrocytes. *eLife* **2020***, 9*, e59733, doi:10.7554/eLife.59733.

28. Lee, C.-M.; Zhou, L.; Liu, J.; Shi, J.; Geng, Y.; Liu, M.; Wang, J.; Su, X.; Barad, N.; Wang, J.; et al. Single-Cell RNA-Seq Analysis Revealed Long-Lasting Adverse Effects of Tamoxifen on Neurogenesis in Prenatal and Adult Brains. *PNAS* **2020**, *117*, 19578–19589, doi:10.1073/pnas.1918883117.

29. Lagace, D.C.; Whitman, M.C.; Noonan, M.A.; Ables, J.L.; DeCarolis, N.A.; Arguello, A.A.; Donovan, M.H.; Fischer, S.J.; Farnbauch, L.A.; Beech, R.D.; et al. Dynamic Contribution of Nestin-Expressing Stem Cells to Adult Neurogenesis. *J Neurosci* **2007**, *27*, 12623–12629, doi:10.1523/JNEUROSCI.3812-07.2007.

30. Rotheneichner, P.; Romanelli, P.; Bieler, L.; Pagitsch, S.; Zaunmair, P.; Kreutzer, C.; König, R.; Marschallinger, J.; Aigner, L.; Couillard-Després, S. Tamoxifen Activation of Cre-Recombinase Has No Persisting Effects on Adult Neurogenesis or Learning and Anxiety. *Front Neurosci* **2017**, *11*, 27, doi:10.3389/fnins.2017.00027.

31. Satija, R.; Farrell, J.A.; Gennert, D.; Schier, A.F.; Regev, A. Spatial Reconstruction of Single-Cell Gene Expression Data. *Nat Biotechnol* **2015**, *33*, 495–502, doi:10.1038/nbt.3192.

32. Trapnell, C.; Cacchiarelli, D.; Grimsby, J.; Pokharel, P.; Li, S.; Morse, M.; Lennon, N.J.; Livak, K.J.; Mikkelsen, T.S.; Rinn, J.L. The Dynamics and Regulators of Cell Fate Decisions Are Revealed by Pseudotemporal Ordering of Single Cells. *Nat Biotechnol* **2014**, *32*, 381–386, doi:10.1038/nbt.2859.

33. Bergen, V.; Lange, M.; Peidli, S.; Wolf, F.A.; Theis, F.J. Generalizing RNA Velocity to Transient Cell States through Dynamical Modeling. *bioRxiv* **2019**, 820936, doi:10.1101/820936.

34. La Manno, G.; Soldatov, R.; Zeisel, A.; Braun, E.; Hochgerner, H.; Petukhov, V.; Lidschreiber, K.; Kastriti, M.E.; Lönnerberg, P.; Furlan, A.; et al. RNA Velocity of Single Cells. *Nature* **2018**, *560*, 494–498, doi:10.1038/s41586-018-0414-6.

35. Weng, G.; Kim, J.; Won, K.J. VeTra: A Tool for Trajectory Inference Based on RNA Velocity. *Bioinformatics* **2021**, *37*, 3509–3513, doi:10.1093/bioinformatics/btab364.

36. Zhang, Z.; Zhang, X. Inference of High-Resolution Trajectories in Single Cell RNA-Seq Data from RNA Velocity. *bioRxiv* **2021**, 2020.09.30.321125, doi:10.1101/2020.09.30.321125.

37. Shah, P.T.; Stratton, J.A.; Stykel, M.G.; Abbasi, S.; Sharma, S.; Mayr, K.A.; Koblinger, K.; Whelan, P.J.; Biernaskie, J. Single-Cell Transcriptomics and Fate Mapping of Ependymal Cells Reveals an Absence of Neural Stem Cell Function. *Cell* **2018**, *173*, 1045-1057.e9, doi:10.1016/j.cell.2018.03.063.

38. Chen, X.; Cao, S.; Wang, Y.; Li, M.; Guo, Y.; Ye, Y.; Wang, Z.; Dai, H.; Yang, W.; Sun, Y.; et al. Single-Cell Profiling Resolved Transcriptional Alterations and Lineage Dynamics of Subventricular Zone after Mild Traumatic Brain Injury. *bioRxiv* **2021**, 2021.05.31.446381, doi:10.1101/2021.05.31.446381.

39. Artegiani, B.; Lyubimova, A.; Muraro, M.; van Es, J.H.; van Oudenaarden, A.; Clevers, H. A Single-Cell RNA Sequencing Study Reveals Cellular and Molecular Dynamics of the Hippocampal Neurogenic Niche. *Cell Reports* **2017**, *21*, 3271–3284, doi:10.1016/j.celrep.2017.11.050.

40. Borrett, M.J.; Tahmasian, N.; Innes, B.T.; Bader, G.D.; Kaplan, D.R.; Miller, F.D. A Shared Transcriptional Identity for Forebrain and Dentate Gyrus Neural Stem Cells from Embryogenesis to Adulthood. *eNeuro* **2022**, ENEURO.0271-21.2021, doi:10.1523/ENEURO.0271-21.2021.

41. Basak, O.; Krieger, T.G.; Muraro, M.J.; Wiebrands, K.; Stange, D.E.; Frias-Aldeguer, J.; Rivron, N.C.; Wetering, M. van de; Es, J.H. van; Oudenaarden, A. van; et al. Troy+ Brain Stem Cells Cycle through

Quiescence and Regulate Their Number by Sensing Niche Occupancy. *PNAS* **2018**, *115*, E610–E619, doi:10.1073/pnas.1715911114.

42. Batiuk, M.Y.; Martirosyan, A.; Wahis, J.; de Vin, F.; Marneffe, C.; Kusserow, C.; Koeppen, J.; Viana, J.F.; Oliveira, J.F.; Voet, T.; et al. Identification of Region-Specific Astrocyte Subtypes at Single Cell Resolution. *Nat Commun* **2020**, *11*, 1220, doi:10.1038/s41467-019-14198-8.

43. Shin, J.; Berg, D.A.; Zhu, Y.; Shin, J.Y.; Song, J.; Bonaguidi, M.A.; Enikolopov, G.; Nauen, D.W.; Christian, K.M.; Ming, G.L.; et al. Single-Cell RNA-Seq with Waterfall Reveals Molecular Cascades Underlying Adult Neurogenesis. *Cell Stem Cell* **2015**, *17*, 360–372, doi:10.1016/j.stem.2015.07.013.

44. Nam, H.; Capecchi, M.R. Lrig1 Expression Prospectively Identifies Stem Cells in the Ventricular-Subventricular Zone That Are Neurogenic throughout Adult Life. *Neural Development* **2020**, *15*, 3, doi:10.1186/s13064-020-00139-5.

45. Jensen, J.B.; Parmar, M. Strengths and Limitations of the Neurosphere Culture System. *Mol Neurobiol* **2006**, *34*, 153–161, doi:10.1385/MN:34:3:153.

46. Shi, Z.; Geng, Y.; Liu, J.; Zhang, H.; Zhou, L.; Lin, Q.; Yu, J.; Zhang, K.; Liu, J.; Gao, X.; et al. Single-Cell Transcriptomics Reveals Gene Signatures and Alterations Associated with Aging in Distinct Neural Stem/Progenitor Cell Subpopulations. *Protein Cell* **2017**, doi:10.1007/s13238-017-0450-2.

47. Li, Z.; Feng, H. A Neural Network-Based Method for Exhaustive Cell Label Assignment Using Single Cell RNA-Seq Data. *Sci Rep* **2022**, *12*, 910, doi:10.1038/s41598-021-04473-4.

48. Shrivastava, H.; Zhang, X.; Song, L.; Aluru, S. GRNUlar: A Deep Learning Framework for Recovering Single-Cell Gene Regulatory Networks. *Journal of Computational Biology* **2022**, *29*, 27–44, doi:10.1089/cmb.2021.0437.

49. Ji, Z.; Zhou, W.; Hou, W.; Ji, H. Single-Cell ATAC-Seq Signal Extraction and Enhancement with SCATE. *Genome Biology* **2020**, *21*, 161, doi:10.1186/s13059-020-02075-3.

50. Odaka, H.; Ozaki, H.; Tateno, H. ScGR-Seq: Integrated Analysis of Glycan and RNA in Single Cells. *STAR Protoc* **2022**, *3*, 101179, doi:10.1016/j.xpro.2022.101179.

51. Longo, S.K.; Guo, M.G.; Ji, A.L.; Khavari, P.A. Integrating Single-Cell and Spatial Transcriptomics to Elucidate Intercellular Tissue Dynamics. *Nat Rev Genet* **2021**, *22*, 627–644, doi:10.1038/s41576-021-00370-8.

52. Lisi, V.; Luna, G.; Apostolaki, A.; Giroux, M.; Kosik, K.S. *Cell Population Effects in a Mouse Tauopathy Model Identified by Single Cell Sequencing*; Cell Biology, 2019;

Author (year)	Species	Age	Sex	Models	Method	Platform	Analysis	Number of cells
Llorens-Bobadilla et al. (2015) [17]	Mouse	8 -12 wk	M	C57BL/6 mice	SVZ wholemount digested with trypsin, whole cells sorted and frozen	Smart-seq2	FactoMineR, Monocle, likelihood-ratio	<100 - 1,000
Dulken et al. (2017) [26]	Mouse	3 mo	M	$GFAP^{GFP}$ reporter mice, datasets Llorens-Bobadilla et al. (2015) & Shin et al. (2015)	SVZ microdissected, digested with papain, whole cells sorted and processed live	Fluidigm C1	GBM modeling, Monocle, SCDE, GSEA	329
Basak et al. (2018) [41]	Mouse	2 d - 1 yr	F	$Troy^{GFPiresCreER}$ and $Ki67^{RFP}$ reporter mice	SVZ wholemount enzymatically digested, whole cells sorted and processed live	CEL-seq	RaceID2, Descan, Pseudotime in TSCAN	1,465
Shi et al. (2017) [46]	Mouse	1, 24 mo	F+M	C57BL/6 mice, dataset Llorens-Bobadilla et al. (2015)	SVZ microdissected, digested with papain, cultured as neurospheres, whole cells sorted and frozen	Smart-Seq2	t-SNE, WGCNA, DESeq2, GO	22
Zywitza et al. (2018) [24]	Mouse	2-4 mo	M, F, F+M	C57BL/6N mice Lrp2 KO mice, dataset Artegiani et al (2017)	SVZ microdissected digested with papain, whole cells processed live or methanol-fixed	Drop-seq	Seurat, SNN-cliq, Velocyto	9,804
Shah et al. (2018) [37]	Mouse	2-6 mo	F+M	aSMA::$CreER^{T2}$; $R26^{tdTomato}$/$Sox2^{GFP}$ mice	SVZ microdissected, digested with papain, whole cells sorted and processed live	10x Genomics	Seurat, SCDE	1,200 6,000
Kalamakis et al. (2019) [13]	Mouse	2, 22, 23 mo	M	C57BL/6J mice and dataset from Llorens-Bobadilla et al. (2015)	SVZ wholemount digested with trypsin, whole cells sorted and frozen	Smart-Seq2	Seurat, Monocle, clusterProfiler, DESeq2	>2,000
Mizrak et al. (2019) [15]	Mouse	8 -10 wk	M, F	hGFAP::$CreER^{T}$;$R26^{tdTomato}$ mice and datasets from Llorens-Bobadilla et al. (2015), Dulken et al. (2017)	Lateral and septal SVZ wholemounts digested with papain, whole cells processed live	Drop-seq	Phenograph, GSEA, SCDE	41,000
Dulken et al. (2019) [12]	Mouse	3, 28- 29 mo	M	C57BL/6NIA mice	SVZ microdissected, digested with papain, whole cells sorted and processed live	10x Genomics	Seurat, Enrichr	14,685
Mizrak et al. (2020) [18]	Mouse	8 -10 wk	M	hGFAP::$CreER^{T}$;$R26^{tdTomato}$ mice ratNes::FLPOER;$R26^{TdTomato}$ mice	Lateral and septal SVZ wholemounts digested with papain, whole cells processed live	Drop-seq	Phenograph, SCDE	56,000
Magnusson et al. (2020) [27]	Mouse	>2 mo	M, F	Cx3::CreER;$Rbpj^{fl/fl}$;$R26^{tdTomato/YFP}$ mice, AAV-Cre injection into $Rbpj^{fl/fl}$;$R26^{tdTomato}$ mice, datasets from Zywitza et al. (2018), and Hochgerner et al. (2018)	Microdissected striatum digested with papain, whole cells sorted and frozen	Smart-Seq2, 10x Genomics	Seurat, Monocle	1,393 203
Borrett et al. (2020) [19]	Mouse	E - 2 mo	F+M	Emx1::Cre;$R26^{EYFP}$ mice Nkx2.1::Cre;$R26^{EYFP}$ mice	Dorsal and lateral SVZ microdissected, digested enzymatically, whole cells sorted and processed live	10x Genomics	Seurat	>6,000

Nam and Capecchi (2020) [44]				Mizrak et al. (2020) dataset			Seurat	
Xie et al. (2020) [11]	Mouse	2 wo - 15 mo	F+M	CGD^{GFP} reporter mice, datasets from Dulken et al. (2017), Llorens-Bobadilla et al. (2015), Codega et al. (2014)	Wholemount SVZ digested with papain, whole cells sorted and processed live	Drop-seq	Seurat, Pseudotime, TFactS, String	5,600
Chen et al. (2021) [38]	Mouse	8-10 wo	M	C57BL/6J mice	Microdissected SVZ frozen, homogenized, and nuclei processed after sucrose gradient centrifugation	10x Genomics	Seurat, GO, CellPhoneDB, Monocle	15,754
Cebrian-Silla et al. (2021) [16]	Mouse	4-5 wo	M, F	$hGFAP^{GFP}$ reporter mice	Microdissected SVZ digested with papain, whole cells multiplexed, processed live	10x Genomics	Seurat, scVelo, GO	30,897
				CD1-elite mice	Anterior/posterior-dorsal/ventral SVZ microdissected SVZ frozen, homogenized, and nuclei processed after sucrose gradient centrifugation			45,820
Borrett et al. (2022) [40]				Datasets from Hochgerner et al. (2018) , Borrett et al. (2020)			Seurat, Monocle, GSEA	

Table 1. Primary literature using sc-RNAseq or sn-RNAseq assessing adult neurogenesis in the SVZ.

Abbreviations: F=female M=male, F+M= female and male samples pooled; nr= sex not reported; E= embryonic; d=days; w=weeks, mo=months; yr=years.

Author (year)	Species	Age	Sex	Model	Method	Platform	Analysis	Number of cells
Shin et al. (2015) [43]	Mouse	8-12 wk	M	Nestin^{CFPnuc} reporter mice	Microdissected DG digested with papain, whole live cells sorted and frozen	Smart-seq2	Waterfall	<200
Habib et al. (2016) [20]	Mouse	<2 yr	M	AAV1/2 injection into vGAT-Cre mice	Microdissected DG and other hippocampal subregions digested, fixed, sorted, nuclei frozen and processed with "Frankenstein" method [25]	Smart-seq2	Seurat	1,367
Habib et al. (2017) [5]	Mouse, Human	10-14 wk mice, 40-65 yr human	M	C57Bl/6 mice and humans	Frozen hippocampus dissected and nuclei were processed using the sucrose gradient centrifugation or the "Frankenstein" method [25]	Drop-seq, DroNc-seq	Seurat	Mouse: 13,313 Human: 14,963
Artegiani et al. (2017) [39]	Mouse	6 & 10 wk, >1 yr	F+M	C57BL/6 mice Nestin^{GFP} reporter mice	Microdissected DG digested with papain, whole cells sorted and frozen	SORT-seq	RaceID2, StemID, Waterfall	1,408
Hochgerner et al. (2018) [10]	Mouse	2-5 wk	F+M	C57BL/6 mice hGAFP^{GFP} reporter mice	Microdissected DG digested with papain, sorted, whole cells sorted and processed live	Fluidigm C1, 10x Genomics	Matlab	24,185
Lisi et al. (2019) [52]	Mouse	4-6 wk, 32-40 wk	F	rTg4510 tauopathy mouse model	Dissected hippocampus digested with papain, whole cells processed live	Drop-seq	Seurat, Monocle	>3,000
Bergen et al. (2019) [33]				Dataset from Hochgerner et al. (2018)			scVelo	
Batiuk et al. (2020) [42]	Mouse	2 mo	F+M	C57BL/6J mice	Dissected hippocampus digested with papain, whole cells sorted and frozen	Smart-seq2	Seurat, GO	2,015
Zhang and Zhang (2021) [36]				Dataset from Hochgerner et al. (2018)			scVelo, Velocyto, CellPath, Slingshot, Vdpt, reCAT	
Zhang et al. (2021) [4]	Macaque	4-6 yr, 18-21 yr	M, F	Cynomolgus macaques	Frozen hippocampus is homogenized, nuclei sorted, and processed	10x Genomics	Seurat, Monocle, GO, SCENIC, CellPhoneDB, Pseudotime	>8,000
Weng et al. (2021) [35]				Dataset from Hochgerner et al. (2018)			VeTra	
Tran et al. (2021) [6]	Human	40-69 yr	M	Human	Frozen hippocampus dissected and nuclei were processed using the "Frankenstein" method [25]	10x Genomics	Bioconductor, MAGMA	70,615
Ayhan et al. (2021) [7]	Human	24-60 yr	M, F	Human and datasets from Habib et al. (2016, 2017), and Batiuk et al. (2020)	Frozen anterior and posterior hippocampus dissected and nuclei were processed using the "Frankenstein" method [25]	10x Genomics	Seurat, GO, MAST	129,908

Sorrells et al. (2021) [9]				Dataset from Habib et al. (2017)			Seurat	
Franjic et al. (2022) [8]	Human, Macaque, Pig	48-58 yr human 8-14 yr macaque 3 mo pig	M, F	Human, rhesus macaques, pig, and datasets from Ayhan et al. (2021), Hochgerner et al. (2018) and Zhong et al. (2020)	Frozen DG and other hippocampal regions microdissected, homogenized, nuclei processed after sucrose gradient centrifugation	10x Genomics	Seurat, Velocyto, scVelo	Human: 139,187 Macaque: 36,107 Pig: 38,851
Borrett et al. (2022) [40]				Datasets from Hochgerner et al. (2018) and Borrett et al. (2020)			Seurat, Monocle, GSEA	
Schneider et al. (2022) [14]	Mouse	2-14 mo	F+M	hGAFP^{eGFP} reporter mice	Microdissected DG digested with trypsin, whole cells processed live	10x Genomics	Seurat, GO	>5,000

Table 2. Primary literature using sc-RNAseq or sn-RNAseq assessing adult neurogenesis in the hippocampus.

Abbreviations: F=female M=male, F+M= female and male samples pooled; nr= sex not reported; E= embryonic; d=days; w=weeks, mo=months; yr=years.